METAL CATHODES AND HYDROGEN

PART 1: LEAD DISINTEGRATION

PART 2: HYDROGEN ADSORPTION ON SILVER

ABBAS ALI ROSTAMI

METAL CATHODES AND HYDROGEN

PART 1 LEAD DISINTEGRATION

PART 2 HYDROGEN ADSORPTION ON SILVER

by

Abbas Ali Rostami, B.Sc., M.Sc.

A thesis submitted in partial fulfillment
of the requirements for the degree of
Doctor of Philosophy

Department of Chemistry
Memorial University of Newfoundland
March 1979

St. John's Newfoundland
Canada

TO

MY WIFE

PARVANEH

ABSTRACT

In Part 1 of the thesis the disintegration of lead cathodes in aqueous perchloric and sulphuric acids at room temperature is considered. Electrochemical methods of analysis (differential pulse anodic stripping voltammetry and differential pulse polarography) of the Pb^{2+} concentrations generated by lead disintegration has enabled it to be detected at lower rates and hence at lower current densities than hitherto. Periodic sampling has enabled observations to continue during several hours of cathodisation.

Lead disintegration rates in aqueous H_2SO_4 were found to be 10-25 times those observed by Gastwirt and Salzberg in 1957, probably because of the exclusion of air, other precautions against impurities and because of the use of more sensitive techniques for measuring disintegration. Disintegration rates in aqueous $HClO_4$ are comparable to those in H_2SO_4, in both cases decreasing with increase in $[H_3O^+]$ because of the inhibiting effects of hydronium ions on disintegration.

As found by Gastwirt and Salzberg, threshold current densities also increase with $[H_3O^+]$, continuous disintegration being unobservable at lower current densities. Nevertheless, disintegration of a different type does occur below threshold current densities, in this case being a discontinuous process. This previously unknown phenomenon is attributed to accumulation of atomic hydrogen in the lead, combining within the lattice to H_2 and exerting such pressures that particles of lead are ejected.

Cathodic disintegration of lead is thought to involve chemical and mechanical processes simultaneously. The chemical process is proposed to be formation and decomposition of surface PbH_x where $x \leq 2$, while the mechanical process involves bulk diffusion of H atoms and their subsequent combination to H_2 resulting in Pb ejection.

In Part 2 of the thesis, studies of the diffusion of electrolytically generated hydrogen through silver are described, together with the results of overvoltage and capacitance measurements at silver cathodes in aqueous perchloric acid at room temperature. Capacitances were deduced from open-circuit potential decay measurements. The increase of overvoltage and the growth of the measured capacitances in the course of electrolysis are attributed to a growing pseudocapacitance component. This is analysed in terms of an increasing coverage, θ_H, of the cathode by adsorbed hydrogen atoms. The increase in surface coverage from the beginning up to several days of cathodisation ranged up to 2% of a monolayer for silver in 0.1 mol ℓ^{-1} $HClO_4$ and up to 0.9% of a monolayer in 1 mol ℓ^{-1} $HClO_4$.

The increase of overvoltage at constant current density and the increase of electrode capacitance at constant overvoltage with the logarithm of the cathodic charge (-Q) were both linear up to Q values of about -60 C cm^{-2}. This increase of overvoltage and pseudocapacitance might be attributed to the adsorption and absorption of hydrogen atoms by silver cathodes.

ACKNOWLEDGEMENTS

I wish to express my sincere gratitude to my supervisor, Dr. Frank R. Smith, for his guidance, constructive criticism and support during various stages of this thesis.

My special thanks are due to Dr. Michael D. Mackey for his many helpful discussions during the course of this study.

Thanks are also extended to the doctoral committee members, Dr. Michael J. Newlands and Dr. Earle K. Ralph for their critical reading of the manuscript. I am also grateful to Dr. Newlands, Head of the Chemistry Department, for his understanding and good-will throughout my graduate work at Memorial University.

The good friendship of my colleague, Mr. Terry Wadden, is highly appreciated.

The assistance of the personnel of the Glassblowing, Electronics and Machine Shop Section of Technical Services, Memorial University is gratefully acknowledged.

Special thanks are due to Memorial University for providing financial assistance.

I extend my sincere thanks to Miss Teresa Barker for patiently typing this thesis. Thanks are also due to Mrs. Cathy Chen for drawing the figures.

I owe my most cordial and special thanks to my wife and my son, Ali, for their patience and deep understanding. Last but no means least, I express my high regards and deep indebtedness to my respected mother and brothers whose blessings and inspirations have brought me to a stage where this work is possible.

CONTENTS

LIST OF TABLES ix

LIST OF FIGURES xi

LIST OF SYMBOLS xv

THEORETICAL INTRODUCTION TO PARTS 1 AND 2

A. Hydrogen Overvoltage 1

I Types of Overvoltage 3

(a) Charge-Transfer Overvoltage 4

(b) Reaction Overvoltage 4

(c) Mass-Transport or Diffusion Overvoltage 5

(d) iR Drop Overvoltage 6

II The Structure of the Electrical Double-Layer 7

III Charge-Transfer Steps in the h.e.r. 12

IV Double-Layer Effects on Charge-Transfer 21

B. Adsorption of Hydrogen by Metals 25

I The Adsorption Pseudocapacitance 25

II Determination of Adsorption Pseudocapacitance Involving Open Circuit Decay 28

III Evaluation of Hydrogen Coverage 30

C. Permeation of Hydrogen Atoms Through Metals 32

I Methods of Measuring Diffusion Coefficients of Hydrogen in Metals 36

(a) Time-Lag Method 36

(b) Rise-Time Method 36

(c) Breakthrough time 39

(d) Decay time constant 39

(e) Alternating Current Method 40

II Diffusivity and Solubility of Hydrogen in Metals . 41

PART 1. CATHODIC DISINTEGRATION OF LEAD

CHAPTER 1. INTRODUCTION 45

CHAPTER 2. EXPERIMENTAL METHODS AND PROCEDURE 52

I Materials 52

II Preparation of Lead Electrodes 55

(a) Electropolishing and Comments concerning its Mechanism 55

(b) Method and Solutions Used in the Present Work 57

III Procedure 60

IV Electrical Measurements 63

V Lead Analysis 64

(a) Preparation of Calibration Curves for Pb^{2+} 66

(i) Differential Pulse Anodic Stripping Voltammetry 66

(ii) Differential Pulse Polarography . . . 71

(b) Evaluation of Calibration Curves . . . 75

(i) Differential Pulse Polarography . . . 75

(ii) Differential Pulse Anodic Stripping Voltammetry 77

CHAPTER 3. RESULTS 80

I Perchloric Acid Solutions at High Current Densities 81

II Perchloric Acid Solutions at Low Current Densities 95

III Sulphuric Acid Solutions 100

IV Alkaline Solutions 113

V Dependence of Lead Disintegration Rate on Cathodic Current Densities in Acid Solutions 119

CHAPTER 4. DISCUSSION 129

PART 2. HYDROGEN ADSORBED ON AND ABSORBED BY SILVER CATHODES IN ACID SOLUTIONS

CHAPTER 1. INTRODUCTION 142

I Diffusion of Gas Phase Hydrogen Through Silver 144

II Hydrogen Overvoltage Measurements on Silver 146

III Capacitance Measurements on Silver and Adsorption of Hydrogen by Silver in Aqueous Solution 152

CHAPTER 2. EXPERIMENTAL METHODS AND PROCEDURE 157

A. Experimental Methods and Procedure for Electrolytic Hydrogen Diffusion Through Silver and Hydrogen Overvoltage Measurements on Silver . . . 157

I Materials 157

II Purification of Solutions 160

(a) Pre-electrolytic Purification . . . 160

(b) Adsorptive Purification 162

III Apparatus 163

IV Procedure and Instrumentation 166

B. Experimental Methods and Procedure for Capacitance Measurements 171

CHAPTER 3. RESULTS 181

I Electrolytic Hydrogen Diffusion Through Silver 183

II Hydrogen Overvoltage Measurements . . . 189

(a) Overvoltage as a Function of Total Cathodic Charge 189

(b) Overshoot Hysteresis 196

(c) Tafel Plots 201

III Capacitance Measurements at Silver Cathodes 209

(a) Preliminary Experiment 209

(b) Experiments with Charcoal-cleaned pre-electrolysed solutions . 209

IV Calculations of Hydrogen Coverage 225

CHAPTER 4. DISCUSSION 233

SUMMARIZING CONCLUSIONS 244

REFERENCES 247

LIST OF TABLES

1. Calibration data for differential pulse anodic stripping voltammetry and differential pulse polarography analysis of Pb^{2+} in 0.01 mol ℓ^{-1} $HClO_4$ 72

2. Analysis for standard Pb^{2+} solutions using differential pulse polarography and DPASV with different concentrations of $HClO_4$ and H_2SO_4 as supporting electrolyte 78

3. Data for lead disintegration in a preliminary experiment. . . 82

4. Data for lead disintegration in 0.01 mol ℓ^{-1} $HClO_4$ at i = -200 mA cm^{-2} 89

5. Data for lead disintegration in 0.1 mol ℓ^{-1} $HClO_4$ at i = -115 mA cm^{-2} 93

6. Data for a discontinuous disintegration of lead in 1 mol ℓ^{-1} $HClO_4$ at i = -10 mA cm^{-2} 97

7. Lead disintegration in 0.001 mol ℓ^{-1} H_2SO_4 at i = -20 mA cm^{-2} 101

8. Lead disintegration in 0.005 mol ℓ^{-1} H_2SO_4 at i = -60 mA cm^{-2} 105

9. Lead disintegration in 1 mol ℓ^{-1} NaOH at i = -16 mA cm^{-2} . . 116

10. Initial disintegration rate as a function of acid concentration and cathodic current density 120

11. Mole ratios Pb:H as a function of acid concentration for c.d.'s above threshold (present work) 125

12. Mole ratios Pb:H as a function of electrolyte and pH for c.d.'s above threshold (Salzberg's work) 126

13. Mole ratios Pb:H as a function of electrolyte composition for c.d.'s above threshold (Gastwirt and Salzberg's work) 127

14. Water activity as a function of electrolyte concentration and slope of rate-current density curve 136

15. Summary of the results of Tafel slopes and exchange current density on silver in acid by various investigators 150

16. Calibration data for the differential galvanostatic method 177

17. Hydrogen overvoltage for silver cathodes in 1 mol ℓ^{-1} $HClO_4$ in expt. A1 to A6 190

18. Hydrogen overvoltage for silver cathodes in 1 mol ℓ^{-1} $HClO_4$ at constant i = -1.16 mA/cm^{-2} in expt. A8 to A10 193

19. Variation of exchange c.d.'s with total cathodic charge passed 208

20. Electrode capacitance of a silver electrode B1 in unpurified 1 mol ℓ^{-1} $HClO_4$ 210

21. Electrode capacitance of a silver electrode B2 in purified 1 mol ℓ^{-1} $HClO_4$ 213

22. Electrode capacitance of a silver electrode B3 in purified 1 mol ℓ^{-1} $HClO_4$ 214

23. Electrode capacitance of a silver electrode B4 in purified 0.1 mol ℓ^{-1} $HClO_4$ 215

24. Electrode capacitance of a silver electrode B5 in purified 0.1 mol ℓ^{-1} $HClO_4$ 216

25. Increase of hydrogen coverage for electrode B2 in 1 mol ℓ^{-1} $HClO_4$ 226

26. Increase of hydrogen coverage for electrode B3 in 1 mol ℓ^{-1} $HClO_4$ 227

27. Increase of hydrogen coverage for electrode B4 in 0.1 mol ℓ^{-1} $HClO_4$ 228

28. Increase of hydrogen coverage for electrode B5 in 0.1 mol ℓ^{-1} $HClO_4$ 229

LIST OF FIGURES

1. Stern-Grahame model of the electrical double layer 9

2. Potential energy diagram for Volmer reaction 16

3. Equivalent circuit for system exhibiting an adsorption pseudocapacitance 27

4. Simplest scheme of apparatus for studying diffusion 33

5. Hydrogen permeation transient 37

6. Sectional drawing of electropolishing cell for lead rod . . 58

7. Sectional drawing of main reservoir cell for studies of lead disintegration 61

8. Stripping analysis cell 67

9. Analysis of standard Pb^{2+} solutions using DPASV (concentration range: 1.0 to 50 ppm) 70

10. Calibration curve for Pb^{2+} analysis by DPASV (concentration range: 1 to 140 ppb) 73

11. Calibration curve for Pb^{2+} analysis by differential pulse polarography (concentration range: 0.1 to 60 ppm). . . 76

12. Quantity of lead disintegrated vs time in a preliminary experiment 83

13. Quantity of lead disintegrated vs time in 0.003 mol ℓ^{-1} $HClO_4$ at -30 mA cm^{-2} 85

14. Quantity of lead disintegrated vs time in 0.003 mol ℓ^{-1} $HClO_4$ at -50 mA cm^{-2} 87

15. Quantity of lead disintegrated vs time in 0.01 mol ℓ^{-1} $HClO_4$ at -60 mA cm^{-2} 88

16. Quantity of lead disintegrated vs time in 0.01 mol ℓ^{-1} $HClO_4$ at -200 mA cm^{-2} 90

17. Quantity of lead disintegrated vs time in 0.1 mol ℓ^{-1} $HClO_4$ at -54 mA cm^{-2} 92

32. Disintegration rate of lead cathode vs current density in 0.1 mol ℓ^{-1} $HClO_4$ and 0.1 mol ℓ^{-1} H_2SO_4 123

33. Pre-electrolysis cell 161

34. Main cell for studies at silver foils 164

35. Sectional drawing of electropolishing cell for silver foils 167

36. The electrical circuit for diffusion studies of silver foils 170

37. Schematic of transistor switch 172

38. Differentiating circuit 173

39. Linear relation between $\frac{dV}{dt}$ of calibration (saw-tooth signal) and $\frac{dV}{dt}$ calculated using differentiated voltage signal (log scales) 178

40. Overvoltage decay signal and its differentiated signal 179

41. Chronopotentiogram for dissolution of oxide film on silver in KOH solution 184

42. Plots of rising transients for hydrogen permeation through 0.1 mm thick silver 187

43. Semilogarithmic plot of overvoltage vs total charge passed for electrodes A8 to A10 195

44. Time dependence of overvoltage at 1.16 mA cm^{-2} after decreasing current from 11.6 mA cm^{-2} for electrode A7 197

45. Time dependence of overvoltage at 11.6 mA cm^{-2} after increasing current from 1.16 mA cm^{-2} for electrode A9 198

46. Time dependence of overvoltage at 0.116 mA cm^{-2} after decreasing current from 11.6 mA cm^{-2} for electrode A10 199

47. Semilogarithmic plot of overvoltage vs time using data from Figures 45 and 46 200

48. Typical Tafel plots for electrode A1 in unpurified 1 mol ℓ^{-1} $HClO_4$ 202

18. Quantity of lead disintegrated vs time in 0.1 mol ℓ^{-1} $HClO_4$ at -115 mA cm^{-2} 94

19. Moles of Pb^{2+} in solution vs time in 0.1 mol ℓ^{-1} $HClO_4$ at -1 mA cm^{-2} 96

20. Moles of Pb^{2+} in solution vs time in 1 mol ℓ^{-1} $HClO_4$ at -10 mA cm^{-2} 99

21. Quantity of lead disintegrated vs time in 0.01 mol ℓ^{-1} H_2SO_4 at -20 mA cm^{-2} 102

22. Quantity of lead disintegrated vs time in 0.001 mol ℓ^{-1} H_2SO_4 at -94 mA cm^{-2} 103

23. Quantity of lead disintegrated vs time in 0.005 mol ℓ^{-1} H_2SO_4 at -60 mA cm^{-2} 107

24. Quantity of lead disintegrated vs time in 0.005 mol ℓ^{-1} H_2SO_4 at -115 mA cm^{-2} 108

25. Quantity of lead disintegrated vs time in 0.01 mol ℓ^{-1} H_2SO_4 at -115 mA cm^{-2} 110

26. Quantity of lead disintegrated vs time in 0.01 mol ℓ^{-1} H_2SO_4 at -190 mA cm^{-2} 111

27. Quantity of lead disintegrated vs time in 0.1 mol ℓ^{-1} H_2SO_4 at -350 mA cm^{-2} 112

28. Quantity of lead disintegrated vs time in contaminated 0.01 mol ℓ^{-1} $HClO_4$ at -200 mA cm^{-2} 114

29. Quantity of lead disintegrated vs time in 1 mol ℓ^{-1} NaOH at -16 mA cm^{-2} 118

30. Disintegration rate of lead cathode vs current density in 0.003 and 0.01 mol ℓ^{-1} $HClO_4$ 121

31. Disintegration rate of lead cathode vs current density in 0.001, 0.005 and 0.01 mol ℓ^{-1} H_2SO_4 122

49. Typical Tafel plots for electrode A2 in 1 mol ℓ^{-1} $HClO_4$ contaminated with Ag^+ ions 203

50. Tafel plots for electrode A5 in purified 1 mol ℓ^{-1} $HClO_4$ 205

51. Tafel plots for electrode A6 in purified 1 mol ℓ^{-1} $HClO_4$ 206

52. Variation of electrode capacitance with overvoltage and total charge for electrode B1 in unpurified 1 mol ℓ^{-1} $HClO_4$ 211

53. Variation of electrode capacitance with overvoltage and total charge for electrode B2 in purified 1 mol ℓ^{-1} $HClO_4$ 217

54. Variation of electrode capacitance with overvoltage and total charge for electrode B3 in purified 1 mol ℓ^{-1} $HClO_4$ 218

55. Variation of electrode capacitance with overvoltage total charge for electrode B4 in purified 0.1 mol ℓ^{-1} $HClO_4$ 219

56. Variation of electrode capacitance with overvoltage and total charge for electrode B5 in purified 0.1 mol ℓ^{-1} $HClO_4$ 220

57. Relationship between electrode capacitances at constant overvoltage and $\log_{10}$ (-Q) for electrode B3 222

58. Relationship between electrode capacitances at constant overvoltage and $\log_{10}$ (-Q) for electrode B4 223

59. Relationship between electrode capacitances at constant overvoltage and $\log_{10}$ (-Q) for electrode B5 224

60. Linear relationship between overvoltage and logarithm of increase of hydrogen coverages in experiments B2 to B5 230

LIST OF SYMBOLS

a	Tafel constant
a_{H_2O}	Water activity
A	Quantity defined in equation 30
b	Tafel slope
C	Coulomb
C_d	Diffuse layer capacitance
C_G	Gouy-Chapman capacitance
C_H	Helmholtz capacitance
$C_{d.l.}$	Double layer capacitance
$C_{expt.}$	Experimentally measured electrode capacitance
C_{in}	Inner layer capacitance
C_{ps}	Hydrogen adsorption pseudocapacitance
ΔC_{ps}	Increase in adsorption pseudocapacitance
C_f	Feed-back capacitor
C_i	Input capacitor
C_{H_3O}	Concentration of H_3O^+ ions in the bulk of the solution.
$C^*_{H_3O}$	Concentration of H_3O^+ ions at the pre-electrode state.
C_{ion}	Concentration of cations or anions in the solution.
C_o	Concentration of absorbed H atoms just beneath the cathodic surface.
C_L	Concentration of absorbed H atoms on diffusion side of a membrane.
$C_{(x,t)}$	Concentration of H atom at a point x in the membrane of time t.
c.d.	Current density

D_H	Diffusion coefficient of hydrogen atom in the metal.
D_{H^+}	Diffusion coefficient of hydronium ion.
DME	Dropping mercury electrode
DPASV	Differential pulse anodic stripping voltammetry
e	Charge on the electron
E	Electrode potential
E_o	Equilibrium electrode potential
E(M-H)	Binding energy of adsorbed hydrogen atoms
f	Frequency
F	Faraday
$\Delta \underline{G}^{\rightleftharpoons\ddagger}$ and $\Delta \underline{G}^{\rightleftharpoons\ddagger}$	Standard electrochemical free energies of activation for forward and backward reaction (1)
$\Delta G^{\rightleftharpoons\ddagger}$ and $\Delta G^{\rightleftharpoons\ddagger}$	Standard chemical free energies of activation for forward and backward reaction (1) at zero electrical potential difference
h	Plank's constant
i	Anodic current density
-i	Cathodic current density
$\vec{i}$ and $\overleftarrow{i}$	Partial current densities for the forward and backward steps of the Volmer reaction (1)
i_{lim}^-	Limiting cathodic current density
$\lvert I_a \rvert$	Amplitude of the alternating current for hydrogen oxidation
i_o	Apparent exchange current density
i_o^t	True exchange current density
J_∞	Steady-state permeation current for hydrogen atoms
J_t	Permeation current for hydrogen atoms at any time t
k	Boltzmann's constant

k'	Total charge required to form a monolayer of adsorbed hydrogen atoms
k_H	Rate constant for the Heyrovsky reaction
k_V	Rate constant for the Volmer reaction
K	Kelvin scale temperature
L	Thickness of the metal membrane
m	Molality of solute
n	Number of adsorption sites cm^{-2}
N	Avogadro's number
pH	$-\log_{10}$ of hydrogen ion concentration
P	Pressure
P_{H_2}	Partial pressure of hydrogen molecule
$[Pb^{2+}]$	Concentration of Pb^{2+} ions in the solution
q_H	Charge equivalent to adsorbed hydrogen on the metal per unit area
Δq_H	Increase in charge equivalent to adsorbed hydrogen on the metal per unit area
q_m	Charge on the metal per unit area
$-Q$	Total charge passed during extended cathodic electrolysis
$-\Delta Q$	Additional charge passed during extended cathodic electrolysis
R	Gas constant
R_f	Feed-back resistor
R_{F_1}	Reaction resistance for charging step (Fig. 3)
R_i	Input resistor
SCE	Saturated KCl calomel electrode
t	Time

t_o	Rise time constant
$t_{0.5}$	Half-rise time
t_b	Breakthrough time
t_{lag}	Time lag
t_r	Relaxation time
t_{H^+}	Transference number of hydronium ion
T	Absolute temperature
Z	Defined in equation (48)
α	Cathodic transfer coefficient
$(1-\alpha)$	Anodic transfer coefficient
β_1 and β_2	Angles of inclination of energy surfaces for H_{ads} and H_3O^+aq (Fig. 2)
γ	Activity coefficient of solute
δ	Thickness of diffusion layer
ε	Dielectric constant in the diffuse layer
$-\eta$	Cathodic hydrogen overvoltage
η_m	Mass-transport or diffusion overvoltage
η_r	Reaction overvoltage
η_t	Charge-transfer overvoltage
η_Ω	iR Drop overvoltage
η_{meas}	The total measured overvoltage $(\eta_t + \eta_r + \eta_m + \eta_\Omega)$
$(\frac{d\eta}{dt})_{t=o}$	Initial rate of overvoltage decay with time t=o, the time of current interruption
$(\frac{d\eta}{dt})_t$	Rate of variation of overvoltage with time at t, the time elapsed after the current interruption

$\Delta\eta$	Change in overvoltage with ϕ^* or with the time of cathodic polarisation
θ_H	Surface hydrogen atom coverage
$\Delta\theta_H$	Increase in surface hydrogen atom coverage
μ	Chemical potential of the electrolyte
ν	Total number of ions in the solution
τ	Dimensionless parameter in equation (43)
ϕ_m	Inner potential of the electrode metal
ϕ_s	Inner potential of the bulk solution
ϕ_1	Potential in the inner Helmholtz plane
ϕ_2	Potential in the outer Helmholtz plane
ϕ^*	Potential at the pre-electrode state
ϕ^*_o	Constant in equation (10)
$\Delta\phi^*$	Change in ϕ^*
ω	Angular frequency

THEORETICAL INTRODUCTION TO PARTS 1 AND 2

This thesis is divided into two parts. In the first part, cathodic disintegration of lead in acid solutions is examined and in the second part, the adsorption and absorption of hydrogen by silver in acid solutions are described. Since these two topics are sufficiently similar to have a common theoretical introduction, theoretical considerations are given before Part 1 for the understanding of the physical basis of the phenomena encountered in this thesis. The Theoretical Introduction contains three different sections:

A. Hydrogen Overvoltage.

B. Adsorption Pseudocapacitance.

C. Permeation of Hydrogen Atoms Through Metals.

A. Hydrogen Overvoltage

There is a long history to the study of the hydrogen evolution reaction (h.e.r.), dating from the beginning of this century. Many reaction steps have been proposed as part of the overall process. However, only two reaction paths involving three possible steps are regarded as likely. The principal steps of the h.e.r. in acid solution probably occur through the following partial reactions:

Discharge (Volmer)

$$H_3O^+_{aq} + e^- + M = H_2O + M\text{-}H_{ads} \qquad (1)$$

Combination (Tafel)

$$M\text{-}H_{ads} + H_{ads}\text{-}M = 2M + H_2 \qquad (2)$$

Ion + Atom (Heyrovsky)

$$H_3O^+_{aq} + M\text{-}H_{ads} + e^- = H_2O + M + H_2 \qquad (3)$$

$\Delta\eta$	Change in overvoltage with ϕ^* or with the time of cathodic polarisation
θ_H	Surface hydrogen atom coverage
$\Delta\theta_H$	Increase in surface hydrogen atom coverage
μ	Chemical potential of the electrolyte
ν	Total number of ions in the solution
τ	Dimensionless parameter in equation (43)
ϕ_m	Inner potential of the electrode metal
ϕ_s	Inner potential of the bulk solution
ϕ_1	Potential in the inner Helmholtz plane
ϕ_2	Potential in the outer Helmholtz plane
ϕ^*	Potential at the pre-electrode state
ϕ^*_o	Constant in equation (10)
$\Delta\phi^*$	Change in ϕ^*
ω	Angular frequency

however, that the reverse velocities of all steps are negligible compared with the forward velocities. Under these conditions, the overall reaction is said to be a coupled reaction. In a simple unbranched consecutive reaction, e.g. (1) followed by (2) or (3), all steps must proceed at the same net velocity in the steady state, otherwise the surface coverage of the intermediate will change continuously with time.

I. Types of Overvoltage

It is well known that the hydrogen overvoltage depends on electrode material as first shown experimentally at the beginning of this century by Tafel (1). The relationship between overvoltage and cathodic current density could be satisfactorily expressed in the form:

$$-\eta = a - b \log_{10} (-i)$$

where the Hydrogen overvoltage, $-\eta$, is the difference of electrical potential between the working cathode and a reversible hydrogen electrode in the same solution, and $-i$ is cathodic current density (current density is defined as c.d.), with a and b constants. The slope of the Tafel plot, $\frac{\partial \eta}{\partial \log_{10} i}$, gives the value of b, while the intercept of $\eta = 0$ gives the value of a. The numerical value of the Tafel slope depends on the mechanism of the electrode reaction and the experimental determination of this parameter is one of the important approaches to the evaluation of reaction mechanisms. Since $\eta = 0$ at the reversible potential when the net current is zero, the parameter a can be written as $a = b \log_{10} (i_o)$ giving the value of the exchange current density i_o.

The overall reaction may be completed by two routes which are (1) followed by (2):

$$2H^+_{aq} + 2e^- + 2M = 2M\text{-}H_{ads} = 2M + H_2$$

or (1) followed by (3):

$$2H^+_{aq} + 2e^- + 2M = M\text{-}H_{ads} + H^+_{aq} + e^- = M + H_2$$

In solutions of pH $\geq$ 8, reactions analogous to reaction (1) and (3) occur, but with H_2O as the main proton source, i.e.

$$H_2O + e^- + M = M\text{-}H_{ads} + OH^- \qquad (1a)$$

$$H_2O + M\text{-}H_{ads} + e^- = M + H_2 + OH^- \qquad (3a)$$

In multistep consecutive reactions, the rate determining step (r.d.s.) controls the overall reaction rate. The condition for the existence of a single r.d.s. is that the activated state corresponding to the r.d.s. is higher in free energy (by ca. 12.5 kJ mol^{-1} for a hundred fold decrease in rate at 298 K with respect to the initial rate for the overall reaction) than the activated state corresponding to any other step. For two steps which have activated states of almost the same level of energy with respect to initial state, the two steps will exercise dual control over the rate of the overall reaction. In such a case, the overall reaction is said to have a dual mechanism. Steps other than the r.d.s. are considered always to be in quasi-equilibrium, meaning that their forward and reverse velocities are taken to be high relative to that of the r.d.s. and virtually equal. Suppose,

Overvoltage may arise from a number of causes, each of which may effect a retardation of the overall process. Depending on the origin, overvoltage can be divided into a number of additive parts (2).

(a) Charge-Transfer Overvoltage

The charge-transfer overvoltage, η_t, arises from a barrier to charge transfer across the electrode-electrolyte interface, e.g. reactions (1) or (3). Charge-transfer reactions are of fundamental importance in the h.e.r., since they are the only reactions directly affected by the electrode potential.

The charge-transfer overvoltage is frequently called activation overvoltage. However, this expression is ambiguous as noted by Vetter (2), because partial control of an electrode process by a chemical reaction also corresponds to an activation process associated with a significant activation energy. The charge-transfer overvoltage will be considered in detail in Section III below.

(b) Reaction Overvoltage

Reaction overvoltage, η_r, arises from a slow chemical reaction, e.g. reaction (2), producing a reactant or removing a product of the charge-transfer step, which is indirectly retarded because of depletion or accumulation of reactants or products.

Following the experimental observation of a b value of $\frac{2.3\ RT}{2\ F} \simeq 29$ mV at 298 K, Tafel (1) suggested that the slow recombination of hydrogen atoms step (2) would be the r.d.s. Many subsequent investigators (3,4,5) supported the view that the slow recombination of hydrogen atoms is the most likely r.d.s. on catalytically active

metals such as Pt, Au, causing occurrence of a Tafel slope of $\frac{2.3\ RT}{2\ F}$. However, this view has been criticised by Ives (6), Knorr (6a) and Lewis (7). Ives found it hard to believe that at the catalytically active Pt electrodes atom recombination (2) is very fast, but is rate limiting, while at the inactive Hg it is very slow but is not rate limiting. In fact, the Tafel slope of $\frac{2.3\ RT}{2\ F}$ is not unique for slow hydrogen atom recombination because it is also found when H_2 transport is rate limiting (6a).

(c) Mass-Transport or Diffusion Overvoltage

Mass-transport overvoltage, η_m, arises when a slow transport process is responsible for depletion or accumulation of reactants or products, respectively, once again resulting in indirect retardation of charge transfer, e.g.

$$H_3O^+_{aq}\ (\text{bulk solution}) \overset{\text{slow}}{=} H_3O^+_{aq}\ (\text{interface}) \quad \text{and}$$

$$H_{2aq}\ (\text{interface}) \overset{\text{slow}}{=} H_{2aq}\ (\text{bulk solution}).$$

Mass-transport processes play an important role in the h.e.r. at catalytically active metals such as Pt, Ir, Rh and Pd (7) where the rate of hydrogen ion discharge, i.e. reaction 1, or of hydrogen generation, i.e. reactions 2 and 3, can be significantly greater than the rate at which H_2 is transported to or from the interface.

The transport of $H_3O^+_{aq}$ ions from the bulk solution to the solution electrode interface may be rate determining at pH $\geq$ 3 at quite small cathodic currents and at lower pH at sufficiently high cathodic currents. However, calculated values of η_m (8,9) in 0.1 and 1 mol ℓ^{-1}

II. The Structure of the Electrical Double-Layer

The interphase between a metallic electrode and an aqueous solution of an electrolyte behaves like an electrical capacitor and is generally known as the electrical double layer. This fact was realized by Helmholtz (10) almost a century ago. To account for this phenomenon, Helmholtz proposed a model of the interphase, in which all the excess charge on the metal is located at its surface and there exists in the solution a rigidly held layer of oppositely charged ions in a plane parallel to the surface of the electrode and very close to it, leading to the development of a potential difference across the interphase. This potential changes sharply from its value in the electrode to that at the centre of the ionic layer. This is the Helmholtz parallel-plate-capacitor model of the ionic double layer. Accurate measurements of the numerical value of the double layer capacitance showed that the interphase can never be represented by a parallel-plate-capacitor as proposed by Helmholtz.

An alternative to Helmholtz's model proposed independently by Gouy (11) and Chapman (12) predicts a dependence of the measured capacitance both on potential and on electrolyte concentrations. This model came to be known as the diffuse-double layer model. The Gouy-Chapman theory leads to a one dimensional Debye Hückel ionic atmosphere type of distribution with the potential falling off more gradually through the diffuse layer.

The Gouy-Chapman model is not very suitable for the case of real ions and Stern (13) suggested that a satisfactory theory of the double layer must take into account both the finite size of the adsorbed

acid solutions bubbled rapidly by gas are less than 4 mV up to $i = -50$ mA cm^{-2} (the maximum current density of the present work on silver cathodes). Even though it does not seem possible to eliminate η_m entirely by extremely vigorous stirring of the catholyte, it seems that the contribution of η_m to the total apparent overvoltage can be made very small in stirred solution. To diminish it still further one would have to use a rotating disc electrode or similar mechanical device.

(d) iR Drop Overvoltage, η_Ω.

Another contribution to the experimentally observed overvoltage is that due to a potential drop between working and reference electrodes. This is not caused by any slow process in the overall reaction but is a function of the effective electrical resistance between the reference electrode and the cathode, and of the current flowing between the cathode and the anode during electrolysis. Attempts are made to minimize the effect of this potential drop in practice by placing the reference electrode (or generally the tip of a connection to it, designated a Luggin capillary) close to the cathode or using oscilloscopic techniques to measure the open-circuit electrode potential immediately subsequent to the interruption of the current flow. The measured overvoltage will be exclusive of η_Ω.

Thus the total measured overvoltage, η_{meas}, is the sum of individual overvoltages, i.e.

$$\eta_{meas} = \eta_t + \eta_r + \eta_m + \eta_\Omega \qquad (4)$$

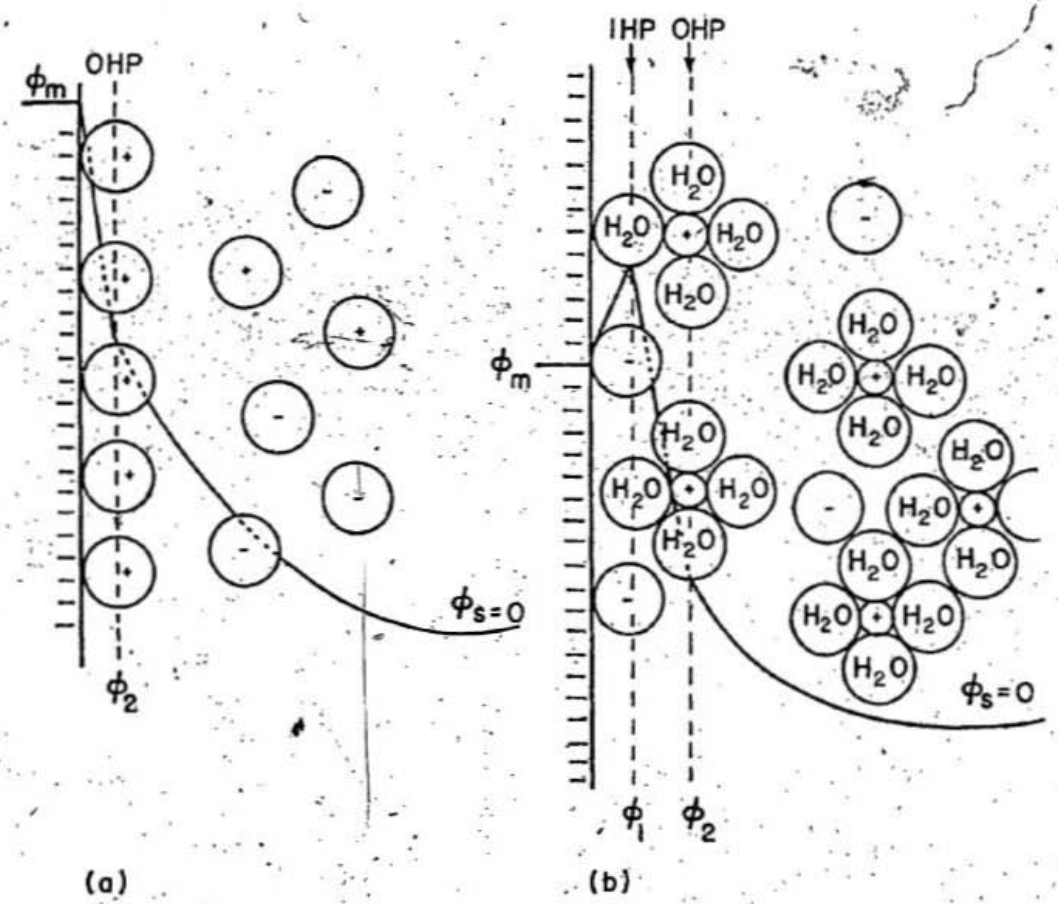

Fig. 1. The charge and potential distribution in the electrical double layer, (a) according to Stern and (b) according to Grahame with negative polarisation of the metal. ϕ_m, ϕ_1, ϕ_2 and ϕ_s are inner potential of electrode, potential in the inner Helmholtz plane, potential in the outer Helmholtz plane and inner potential of the bulk of solution, respectively. As shown ϕ_m, ϕ_1, and ϕ_2 are negative with respect to $\phi_s = 0$.

ions and any specific chemisorption interaction they may suffer with the electrode surface. He considered that in the case of, e.g. a negatively charged surface, a layer of positive ions is held at the interface by chemisorptive or electrostatic attractions. The double layer region from the surface to the centre of the first layer of positive ions is referred to as the compact or Helmholtz layer; there is a sharp potential drop in the Helmholtz part of the double layer. Outside the Helmholtz layer, there is a diffuse or Gouy-Chapman layer over which the potential drops gradually to that in the bulk of the solution (see Fig. 1a). Stern's model of the double layer is actually a combination of the two previous models and the total capacitance of this model can be derived in the following way. The potential difference between the electrode, ϕ_m, and the bulk of the solution, ϕ_s, may be written as

$$\phi_m - \phi_s = (\phi_m - \phi_2) + (\phi_2 - \phi_s) \qquad (5)$$

The potential at the outer Helmholtz plane (OHP) is denoted by ϕ_2, and since it is assumed that ϕ_s is equal to zero (by convention) then

$$\phi_m = (\phi_m - \phi_2) + \phi_2 \qquad (6)$$

Differentiation of equation (6) with respect to the charge on the electrode, q_m, gives

$$\frac{\partial\phi_m}{\partial q_m} = \frac{\partial(\phi_m - \phi_2)}{\partial q_m} + \frac{\partial\phi_2}{\partial q_m} \qquad (7)$$

$$\text{or} \quad \frac{1}{C_{d.l.}} = \frac{1}{C_H} + \frac{1}{C_G} = \frac{1}{C_{in}} + \frac{1}{C_d} \qquad (8)$$

lateral repulsion between neighbouring ions of the same sign. In the work of Levine et al, image energy resulting from the image forces-interaction between the test (the adsorbed ion) and induced charges was suggested as the origin of specific adsorption in contrast with Grahame's view which suggested that the specific adsorption is due to the formation of a covalent bond superimposed upon electrostatic interaction. Grahame and Levine et al's proposal was criticised by Bockris, Devanathan and Muller (16). Bockris et al compared the bond strengths for mercury-halide bonds with the adsorbability. The bond strength decreased from F^- to I^-, while the adsorbability increased from F^- to I^-. It was further proposed by Bockris et al that image energy should not be considered as the origin of the specific adsorption. Because this would influence specific adsorption in the wrong direction, e.g. for the halide ions, the adsorbability increases roughly according to the cube of the ionic radius, while image energy would change by a negligible amount. Also, specific adsorption is not a phenomenon restricted to anions, sufficiently large cations showing similar phenomena. However, Bockris et al advocated that the specific adsorption is a function of the degree and type of hydration. The model of the double layer proposed by Bockris et al was similar to that proposed by Grahame but it takes into account the predominant existence of the solvent in the interphase, held by charge-dipole forces at the electrode surface. If ions have sufficiently stable primary hydration shells - those which are associated during transport with a definite number of water molecules, - they remain in the outer layer, and are not specifically adsorbed.

where $C_{d.l.}$ is the experimentally determined capacitance and C_H or C_{in} is the capacitance of Helmholtz or inner layer and C_G or C_d is the capacitance of the Gouy-Chapman or diffuse layer.

Subsequent to Stern's model there have been a number of further proposals which refine the model in various details. Strong specific adsorption (specific adsorption appears to have a chemical as distinct from an electrostatic origin, dependent on the nature of the metal and the ions involved) of, in particular, halide ions on mercury, led Grahame (14) to develop a model of the interphase which consists of three regions (see Fig. 1b), although it is still commonly referred to as the double layer. The first region in Grahame's model extends from the electrode to a plane passing through the centres of the specifically adsorbed ions. This is the inner Helmholtz plane (IHP) and its potential is denoted by ϕ_1. Next is the outer Helmholtz plane (OHP) which passes through the centres of the hydrated ions at distance of closest approach to the electrode. Beyond the OHP lies the diffuse double layer. Figure 1b illustrates a negative polarisation of the metal at which there is a sharp change in potential, from the electrode of potential ϕ_m, to the plane corresponding to the centres of a layer of specifically adsorbed ions (IHP), at which the potential is ϕ_1. Then, there is a sharp potential drop to the plane corresponding to the centres of the layer of hydrated ions (OHP) and finally, there is a gradual potential drop from the OHP into the bulk of the solution at a potential $\phi_s = 0$.

The model, developed by Levine, Bell and Calvert (15), LBC model, describes the interaction between adsorbate particles in terms of a

neutralized. Butler's theory originated in ideas of Gurney, but Butler allowed for the adsorption of atomic hydrogen on the electrode, in keeping with the suggestion of Horiuti et al, and applied this additional factor as a correction to the Gurney theory.

Electron tunnelling is of great significance to electron transfer reactions at a metal-solution interface. Indeed, it is the central act in the theory of the electrochemical reactions. Matthews (22) pointed out that the r.d.s. and reaction path remain the same, but the mode of achieving electron tunnelling may vary with the potential, e.g. bond bending, bond stretching, stretching of different bonds or solvent libration etc. According to Matthews, at any potential, the favoured mode will be that which tends to give the value of symmetry factory of 0.5 to satisfy the electron tunnelling condition (i.e. minimum activation energy which is related to the symmetry factor). Later Bockris and Matthews (23) suggested that tunnelling is possible <u>only</u> if the $H^+ - H_2O$ bond stretches until the electron can be accepted into an empty level of suitable energy. Tunnelling is a radiationless transition. In other words, if electrons tunnel through the barrier at the surface of a metal, they come out with the same energy as they had in the metal.

The interfacial potential difference at the electrode-electrolyte interface influences the h.e.r. rate due to (a) its effect on the concentration of $H_3O^+_{aq}$ ions at the pre-electrode state, the plane from which reactants embark upon the activation step, and (b) its influence on the activation energy of the charge-transfer step. The pre-electrode state of potential, ϕ^*, is thought to be located at the OHP (i.e. $\phi^* = \phi_2$)

Such adsorption may be called equivalent (equal charges on the electrode and in the solution part of the double layer). If ions possess no primary hydration water, they can gain energy by replacing the surrounding water dielectric by the (infinite dielectric constant) metal, and move out of the solution into contact with the metal. The tendency to do so is not dependent (primarily) upon the charge on the metal and occurs against electrostatic forces, if sufficient energy is to be gained. Such adsorption is termed super-equivalent adsorption.

III. Charge-Transfer Steps in the h.e.r.

The charge transfer across an electrode-electrolyte interface consists essentially of the exchange of electrons, either from the electrode to an electron acceptor (e.g. $H_3O^+_{aq}$) or from an electron donor (e.g. hydrogen) to the electrode, on the solution side of the interface and such charge transfer proceeds at rates slower than electronic transitions within the ions or molecules involved, probably because of the slow rearrangement of the solvation sheath around the ions or slow bond stretching between ions and solvent. Reactions (1) and (3), previously considered, are important charge-transfer steps in the h.e.r. in acid solutions.

The foundations of the subject were laid in particular by Butler (17), Gurney (18), Frumkin (19), Volmer and Erdey-Gruz (20) and Horiuti and Polanyi (21). Butler suggested that the discharge process takes place in either electron escape from the metal to become attached to a nearby hydronium ion in the solution or a proton of a hydronium ion comes into contact with, or is adsorbed on, the metal and is then

e.g. 1 mol ℓ^{-1} KCl, to HCl, maintains ϕ^* essentially constant and independent of C_{H_3O} (24), so that the double layer effect on the h.e.r. may be neglected.

More important is the kinetic effect (b). We assume that the potential that is applied in excess of the reversible potential, i.e. the overvoltage, operates across the region between the electrode and the pre-electrode state, not including the diffuse layer, and aids or opposes charge-transfer across the interface by modifying the electrochemical free energy of activation. The effect of the electrode potential on the charge-transfer process can be studied by considering a simple two dimensional potential energy-reaction coordinate diagram of the type used by Butler (17) or Horiuti and Polanyi (21) as shown in Figure 2. The solid curve at the right shows the potential energy of the initial state ($H_3O^+_{aq}$ in solution + e^- in the metal) and the solid curve at the left shows the potential energy of the final state (M-H_{ads} + H_2O molecule), respectively, plotted against the distance from the electrode surface in the absence of the electrical potential difference, i.e. $\phi_m - \phi^* = 0$. By increasing the metal-solution potential difference from zero to $\phi_m - \phi^*$, i.e. applying an electrical potential to the metal, the whole initial state curve ($H_3O^+_{aq}$ + e^-) is shifted by an amount $(\phi_m - \phi^*)$ F to the dashed right hand line, without change of its shape, with a consequent decrease of the activation free energy of $H_3O^+_{aq}$ discharge by some fraction α of the total potential energy change resulting from the potential difference, i.e. by $\alpha(\phi_m - \phi^*)F$. Simultaneously, the activation free energy for hydrogen ionisation increases by an amount $(1-\alpha)(\phi_m - \phi^*)F$. The fraction

or, if the reactant is a solvent molecule or if the hydronium ions are specifically adsorbed, at the IHP (i.e. $\phi^* = \phi_1$).

Consider first effect (a). If there is a potential difference between the bulk solution and the OHP, the $H_3O^+_{aq}$ ions have to do work to climb this potential hill to reach the pre-electrode state. Assuming that there is an equilibrium distribution between the concentration of $H_3O^+_{aq}$ ions at the pre-electrode state, $C^*_{H_3O}$, and the bulk concentration of $H_3O^+_{aq}$ ions, C_{H_3O}, one can use the Boltzmann distribution law to relate the two concentrations

$$C^*_{H_3O} = C_{H_3O} \exp\left(-\frac{F\phi^*}{RT}\right) \qquad (9)$$

where $F\phi^*$ is the electrical work required to carry a unit charge through the potential difference from the bulk solution to the pre-electrode state and R and T have their usual meaning. If $H_3O^+_{aq}$ ions are the only cations present in the solution, the potential at the pre-electrode state will be concentration dependent.

Under some simple limiting conditions, Frumkin (24) showed from the theory of the electrical double layer that

$$\phi^* = \phi^*_o + \frac{RT}{F} \ln C_{H_3O} \qquad (10)$$

where ϕ^*_o is a constant. Substituting (10) into (9) one would obtain an expression in which $C^*_{H_3O}$ = constant. The independence of potential (at constant c.d.) on the concentration in dilute acid solutions, in the absence of a supporting electrolyte, was confirmed with a high degree of precision for HCl concentrations not exceeding 0.1 mol ℓ^{-1} in the h.e.r. at Hg (24). Adding excess inert supporting electrolyte,

α depends on the relative slopes of the two intersecting potential-energy curves given by the geometrical equation $\alpha = \frac{\tan \beta_1}{\tan \beta_1 + \tan \beta_2}$ where β_1 and β_2 are angles of inclination of the energy surfaces for H_{ads} and $H_3O^+_{aq}$, respectively (see Fig. 2). Using this simple geometric concept, it is easy to see that $0<\alpha<1$ and that if the slopes are equal then $\alpha = 0.5$ (a value which is often found in practice).

In the presence of an electrode potential E, shifting the initial state ($H_3O^+_{aq}$ in solution + e^- in metal) to favour the discharge of $H_3O^+_{aq}$ ions, the standard electrochemical free energy of activation for the forward reaction (1) $\Delta\underline{G}^{\ddagger}_{\rightarrow}$ becomes

$$\Delta\underline{G}^{\ddagger}_{\rightarrow} = \Delta G^{\ddagger}_{\rightarrow} - \alpha FE \qquad (11)$$

where α is the cathodic transfer coefficient. Correspondingly, the standard electrochemical free energy of activation for ionisation of H_{ads} {reverse reaction of (1)} $\Delta\underline{G}^{\ddagger}_{\leftarrow}$, will be

$$\Delta\underline{G}^{\ddagger}_{\leftarrow} = \Delta G^{\ddagger}_{\leftarrow} + (1 - \alpha)FE \qquad (12)$$

where $(1 - \alpha)$ is the anodic transfer coefficient. Both $\Delta G^{\ddagger}_{\rightarrow}$ and $\Delta G^{\ddagger}_{\leftarrow}$ are standard chemical free energies of activation at zero electrical potential difference and depend on the chemical nature of the electrode and of the reaction.

In terms of the transition state theory (25), the rate of the $H_3O^+_{aq}$ discharge process (1) can be expressed as

$$\text{Rate}^{\rightarrow} = \left(\frac{kT}{h}\right)(1 - \theta_H)C^*_{H_3O_{aq}} \exp\left(-\frac{\Delta G^{\ddagger}_{\rightarrow} - \alpha FE}{RT}\right) \qquad (13)$$

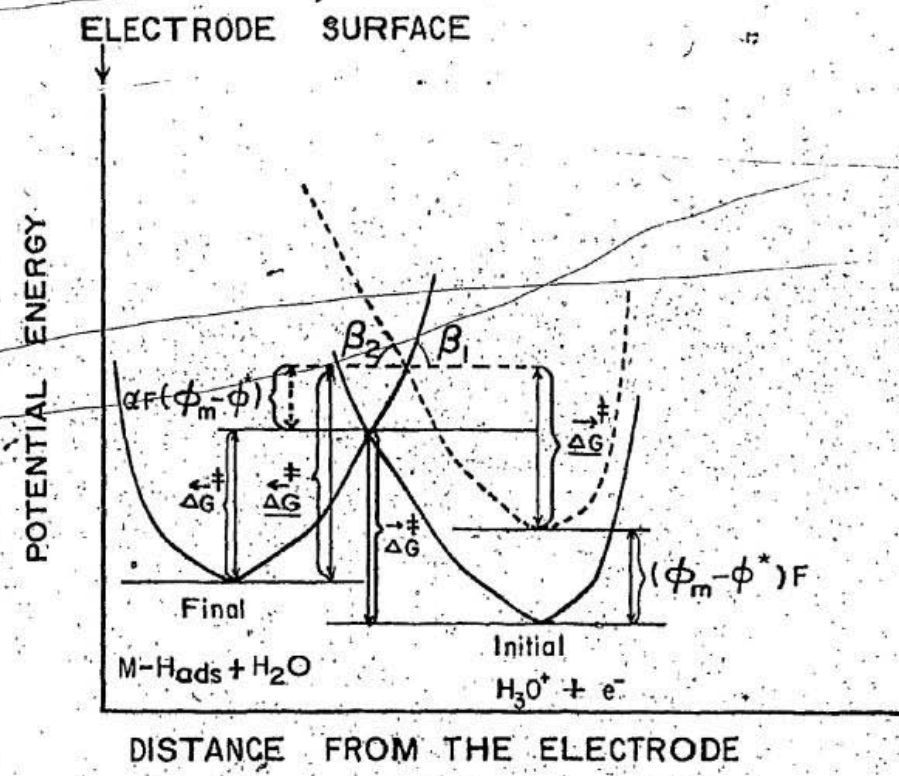

Fig. 2. Potential energy diagram for electrode reaction $H_3O^+_{aq.} + e^- + M = H_2O + M\text{-}H_{ads}$. The solid curves at the left and the right represent the potential energy profiles of final and initial states, respectively, in the absence of an electrical potential difference. The dashed curve at the right hand represents the potential energy profile for initial state on applying the electrical potential $\phi_m - \phi^*$.

where k is Boltzmann's constant and h is Planck's constant. Using equation (13), the cathodic current density will be represented by

$$\vec{i} = -F\left(\frac{kT}{h}\right)(1 - \theta_H)C^*_{H_3O} \exp\left(-\frac{\Delta\vec{G}^{\ddagger} - \alpha FE}{RT}\right) \qquad (14)$$

The corresponding anodic current density, for the ionisation of H_{ads}, will be

$$\overleftarrow{i} = F\left(\frac{kT}{h}\right)\theta_H \exp\left(-\frac{\Delta\overleftarrow{G}^{\ddagger} + (1 - \alpha)FE}{RT}\right) \qquad (15)$$

At the equilibrium potential E_o these two rates (equations 14 and 15) are of equal magnitude but opposite in sign. The net current is zero but the exchange currents may be appreciable. Irrespective of sign (direction), the exchange c.d.'s are given the symbol i_o.

$$i_o = F\left(\frac{kT}{h}\right)(1 - \theta_H)C^*_{H_3O} \exp\left(-\frac{\Delta\vec{G}^{\ddagger} - \alpha FE_o}{RT}\right) =$$

$$F\left(\frac{kT}{h}\right)\theta_H \exp\left[-\frac{\Delta\overleftarrow{G}^{\ddagger} - (1 - \alpha)FE_o}{RT}\right] \qquad (16)$$

and evidently

$$\exp\left(-\frac{FE_o}{RT}\right) = \frac{(1 - \theta_H)C^*_{H_3O}}{\theta_H} \exp\left(-\frac{\Delta\vec{G}^{\ddagger} - \Delta\overleftarrow{G}^{\ddagger}}{RT}\right) \qquad (17)$$

If the electrode is polarised to another potential E, in which $E = \eta + E_o$, then the cathodic current density becomes

$$\vec{i} = -F\left(\frac{kT}{h}\right)(1 - \theta_H)C^*_{H_3O} \exp\left[-\frac{\Delta\vec{G}^{\ddagger} - \alpha F(E_o + \eta)}{RT}\right] \qquad (18)$$

Substituting the left hand side of equation (17) into equation (18), this will be converted to

$$\vec{i} = [-F(\frac{kT}{h})(1 - \theta_H)C^*_{H_3O} \exp(-\frac{\Delta\vec{G}^{\ddagger}}{RT})] \times$$

$$[\frac{(1 - \theta_H)C^*_{H_3O}}{\theta_H}]^{\alpha} \exp[\frac{\alpha(\Delta\vec{G}^{\ddagger} - \Delta\overleftarrow{G}^{\ddagger})}{RT}] \times [\exp(\frac{\alpha F\eta}{RT})] =$$

$$\{-F(\frac{kT}{h})[(1 - \theta_H)C^*_{H_3O}]^{1 + \alpha} \times (\theta_H)^{-\alpha}$$

$$\exp[-\frac{(1 - \alpha)\Delta\vec{G}^{\ddagger} + \alpha\,\Delta\overleftarrow{G}^{\ddagger}}{RT}]\} \exp(\frac{\alpha F\eta}{RT}) \qquad (19)$$

The term within { } is another expression for the exchange current density and therefore the cathodic current density is expressible as

$$\vec{i} = i_o \exp(\frac{\alpha F\eta}{RT}) \qquad (20)$$

The equivalent expression for the anodic current density is

$$\overleftarrow{i} = i_o \exp[-\frac{(1 - \alpha)F\eta}{RT}] \qquad (21)$$

Equations (20) and (21) are basic relations in electrode kinetics and much of the work in studying electrode processes is directed towards evaluation of i_o and α.

The net electrode current i is the difference between the two individual currents, i.e. $i = \vec{i} - \overleftarrow{i}$. Thus, the net current density is given by

$$i = i_o\{\exp(\frac{\alpha F\eta}{RT}) - \exp[-\frac{(1 - \alpha)F\eta}{RT}]\} \qquad (22)$$

though not accurate, may be used for the determination of i_o for many high overvoltage metals, for which experimental measurements are impossible close to E_o.

IV. Double-Layer Effects on Charge-Transfer

Since changes in overvoltage will give rise to changes in ϕ^*, therefore, the rate of the electrochemical reaction will be affected only by part of the applied overvoltage

$$\eta_{effective} = \eta_{applied} - \phi^* \tag{25}$$

Therefore, the effective potential difference which enters into the activation energy would be that between the electrode surface and the pre-electrode state. Depending on the magnitude of ϕ^*, the current-overvoltage relationship, i.e. (22), may be seriously distorted by the effect of ϕ^*. The effect of ϕ^* was previously ignored in the consideration of kinetic effect of the interfacial potential difference.

Equation (22) can be rewritten with the ϕ^* term taken into account as

$$i = i_o^t \{\exp [\frac{(\alpha - 1)\phi^* F}{RT}] [\exp (- \frac{\alpha F \eta}{RT})$$

$$- \exp [\frac{(1 - \alpha) F \eta}{RT}]\} \tag{26}$$

where the true exchange current density i_o^t is equal to the equal and opposite current densities at the equilibrium potential E_o for $\phi^* = 0$, that is, in the absence of the double layer effect. Comparing equations

At small overvoltages, i.e. $|\eta| \leq 10$ mV, the exponential term of equation (22) can be expanded to a single term and therefore

$$i = i_o \frac{F\eta}{RT} \qquad (23)$$

Under these conditions the current density is directly proportional to both the exchange current density and the overvoltage. This is observed in practice and the measurement of the small currents resulting from such "micropolarisations" can be used to determine i_o.

At large, e.g. cathodic overvoltage, i.e. $|\eta| \geq 100$ mV, one of the component currents (anodic current) becomes negligibly small. Then the net current can be equated to the cathodic current density. Therefore, at high cathodic polarisation,

$$-i = \vec{i} = i_o \exp\left(\frac{\alpha F\eta}{RT}\right) \qquad (20)$$

and it follows that

$$\ln(-i) = \ln i_o + \left(\frac{\alpha F\eta}{RT}\right) \qquad \text{or}$$

$$-\eta = \frac{2.303\ RT}{\alpha F} \log_{10} i_o - \frac{2.303\ RT}{\alpha F} \log_{10} (-i) \qquad (24)$$

Equation (24) can be written in the form of the Tafel equation, i.e. $-\eta = a - b \log_{10} (-i)$.

Plots of $-\eta$ against $\log_{10} (-i)$ under these assumed conditions should be linear. The factor b = 116 mV at 298 K (if $\alpha = 0.5$) may be compared with the experimentally observed value of b. Extrapolation of Tafel plots to $\eta = 0$ also permits determination of i_o. This method,

$$\Delta\eta = (1 - \frac{1}{\alpha})\Delta\phi^* \tag{28}$$

In the case in which there is no specific adsorption, $\Delta\phi^*$ can be calculated from diffuse double-layer theory by equating $\phi^* = \phi_2$ (i.e. the pre-electrode state at OHP). Then ϕ_2, can be calculated using Gouy-Chapman theory for a Z-Z electrolyte as

$$\phi_2 = \frac{2RT}{ZF} \sinh^{-1} (\frac{q_m}{2A}) \tag{29}$$

and

$$A = (\frac{\varepsilon RTC_{ion}}{2\pi})^{\frac{1}{2}} \tag{30}$$

where q_m is the charge on the metal per unit area, ε is the dielectric constant in the diffuse layer and C_{ion} is the concentration of cations or anions (for a solution containing Z-Z electrolyte, $C_{cation} = C_{anion}$) in the solution. Thus calculated values of $\Delta\phi^*$ can be used to test equation (28) and thereby (26) with experimental results. In practice, if corrected (-i) versus (-η) plots are independent of the supporting electrolyte, it is assumed that double layer effects are suitably accounted for and accurate kinetic parameters may be obtained using equation (26).

The equation (26) can be written for the cathodic h.e.r. in the form

$$-i \frac{\exp (\frac{F\phi_2}{RT})}{1 - \exp (\frac{F\eta}{RT})} = i_o^t \exp [\frac{(\phi_2 - \eta)\alpha F}{RT}] \tag{31}$$

Here, it was again assumed that $\phi^* = \phi_2$. A plot of the logarithm of the left-hand side of equation (31) against $(\phi_2 - \eta)$ is linear

(22) and (26), the apparent, measured, exchange currenty density i_o may be defined by

$$i_o = i_o^t \exp\left[\frac{(\alpha - 1)F\phi^*}{RT}\right] \qquad (27)$$

Since ϕ^* varies with the electrode potential and the concentration of ions in the solution, it is obvious from (26) that the kinetic parameters obtained from polarisation curves using (22) alone will be erroneous to varying extents. Therefore, in calculating accurate electrode kinetic data one must take into account ϕ^* effects.

In electrode kinetic studies the ionic strength is often held constant by the use of an excess of inert electrolyte. One of the important functions of this supporting electrolyte is to suppress the ϕ^* potential and to reduce its variation with the electrode potential as far as possible.

In experiments in which the behaviour of metals in pure acid solutions is studied, it is not possible to add supporting electrolytes. In other cases in which such an electrolyte is added, the results often depend strongly on the ionic components of the supporting electrolytes. In order to rationalize these effects and to obtain accurate kinetic information from raw data, the terms containing ϕ^* must be understood.

In the absence of specific adsorption of supporting electrolyte, the change of overvoltage $\Delta\eta$ resulting from a variation $\Delta\phi^*$ at constant current is

B. Adsorption of Hydrogen by Metals

It is generally accepted that the adsorbed hydrogen produced during the discharge of $H_3O^+_{aq}$ ions or the ionisation of H_2 molecules by metals with E* (M-H) $\geq$ 213 kJ mol^{-1} (27) during the h.e.r. is chemisorbed on the metal electrodes. The study of hydrogen adsorption is helpful in the elucidation of the mechanism of the h.e.r. During the h.e.r., adsorbed H atoms are produced and consumed. The surface concentration of adsorbed hydrogen is thought to be potential dependent. Information concerning the adsorption of hydrogen atoms on the surface of an electrode can be obtained from suitable kinetic studies involving measurements of the electrode capacitance or surface coverage of the electrode by adsorbed hydrogen.

I. The Adsorption Pseudocapacitance

Early investigations of the h.e.r. revealed (28,29) the presence of H_{ads} atoms, but the existence of an adsorption pseudocapacitance, C_{ps}, due to adsorbed hydrogen atoms was first predicted and demonstrated by Eucken and Weblus (30). The term pseudocapacitance was introduced by Grahame (31) to distinguish the capacitance arising in a reaction such as (1) or (3) which is associated with charge transfer across the interface from the strictly non-faradaic capacitance associated with the dependence of ionic and electronic charge in the double layer on potential. The prefix "pseudo" is used because C_{ps} refers to a leaky capacitor, that cannot exist unless the interphase leaks,

---

*Binding energies of adsorbed hydrogen atoms on metals.

and has the slope $\frac{\alpha F}{RT}$. The true transfer coefficient α is thus obtained.

The theory of double layer effects can be extended to systems in which specific adsorption of supporting electrolyte occurs. Treatment for specific adsorption is more uncertain than in the absence of specific adsorption because details of the double layer structure, as Delahay (26) noted, are not fully understood. At least two effects may be considered: (a) partial coverage of the electrode by specifically adsorbed ions which causes a reduction in the current, at constant overvoltage, because of the decreased area available for current flow namely, the uncovered part of the electrode and (b) variation of the potential ϕ^* or ϕ_2 (it is assumed that the pre-electrode state may still be identified with the OHP) caused by specific adsorption. Anion specific adsorption causes ϕ_2 to be less positive and increases the rate of reduction of $H_3O^+_{aq}$ ions at a given cathodic overvoltage. On the other hand, cation specific adsorption has the opposite effect on ϕ_2 and on the rate of reduction of $H_3O^+_{aq}$ ions.

The Frumkin correction (the effect of ϕ^* or ϕ_2 on the kinetic parameters) is often neglected in kinetic studies of the behaviour of metals in pure acid solutions. This may be justified when high electrolyte concentrations are used so that the variation of ϕ^* with ϕ_m is negligible.

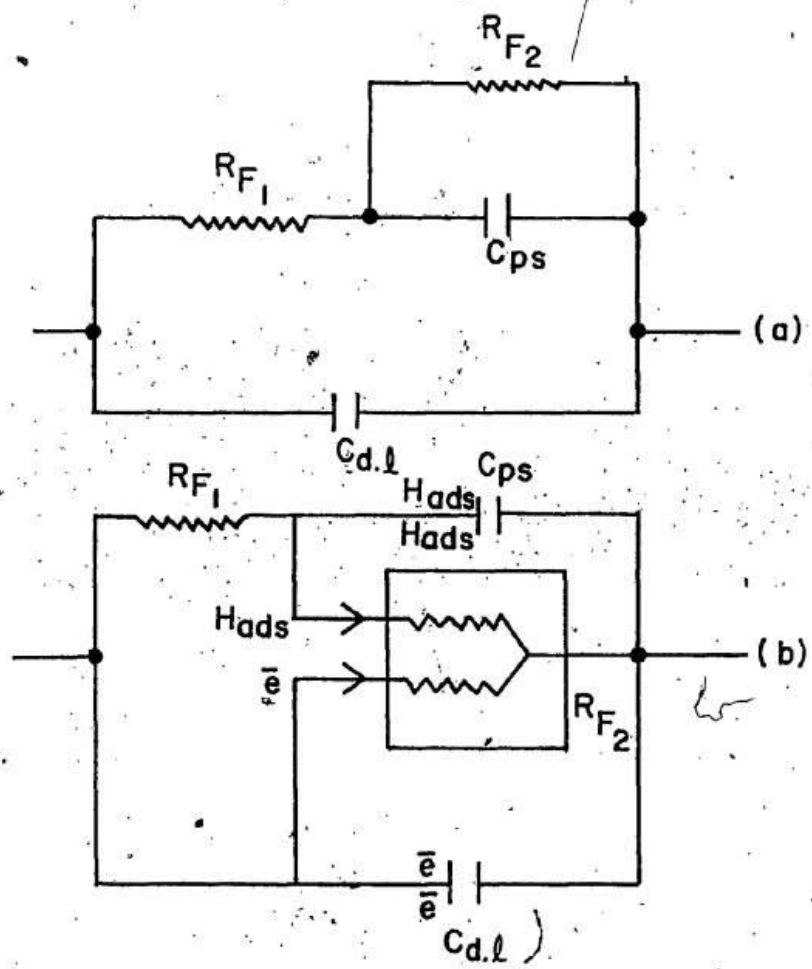

Fig. 3. Equivalent circuit for system exhibiting an adsorption pseudocapacitance.

(a) Volmer discharge with Tafel desorption step.

(b) Volmer discharge with Heyrovsky desorption step.

R-Reaction resistance: R_{F_1} for charging step and R_{F_2} for desorption step, respectively.

that is, unless charge is transferred across it (32).

Since, however, electron transfer is an essential requirement for the formation of adsorbed hydrogen atoms, the presence of these adsorbed intermediates on the surface is equivalent to the storage of electricity in the interface as in a condenser and the corresponding capacitance, C_{ps} behaves like an ordinary capacitance except that it may vary to a much greater extent (relative to the double layer capacitance) with potential and frequency.

The electrochemical behaviour of the electrode-electrolyte interface can be represented by the electrical behaviour of equivalent circuit elements (32,32a,32b). So long as an ideal polarised electrode* is considered and no faradaic charge-transfer is involved, the capacitance representation of the double layer is adequate. When a charge-transfer process can occur at a rate dependent on the electrode potential, representation as a pure capacitance is inadequate. In this case the adsorption pseudocapacitance plays an important role in the total measured electrode capacitance. The adsorption pseudocapacitance must be charged through the non-ohmic resistance, R_{F_1}, corresponding (at a given potential) to the reciprocal of the rate of the $H_3O^+_{aq}$ ion discharge step producing H_{ads}. The series combination of C_{ps} and R_{F_1} must be in parallel with $C_{d.l.}$ since it provides a leakage path across the double layer (32,32a,32b). Then,

---

*The characteristic of an ideal polarised electrode is that there is no exchange of electric charge between the two phases.

unsatisfactory manual procedures and the rise-time dependence of the capacitance makes it rather difficult to interpret the results for C_{ps} values obtained by these methods. Direct differentiation of the open-circuit decay curve is free from some of these disadvantages.

The direct differential galvanostatic method was developed by Angerstein-Kozlowska and Conway (38) and later Conway, Gileadi and Angerstein-Kozlowska (39) pointed out that any method based on the rate of decay of potential on open-circuit following steady-state polarisation will represent a true equilibrium pseudocapacitance, i.e. the value corresponding to an infinitely low frequency using the a.c. bridge method, and is therefore to be preferred. The direct differential galvanostatic method (rapid-open circuit decay) is most suitable for studies of the potential dependence of adsorption pseudocapacitances. This method is based on the assumption that the Faradaic process taking place during steady-state polarisation, continues on open-circuit by a self-discharge* process which momentarily, at the beginning of the open-circuit transient, has the same rate as that corresponding to the initial steady-state polarisation current density at the instant of current interruption.

---

*For instance, in the h.e.r. involving steps (1) and (3), the open-circuit discharge of the adsorption pseudocapacitance occurs by continuing desorption of H_{ads} by step (3) with reverse of step (1) providing the electrons for step (3).

if hydrogen recombination is the desorption step in the h.e.r., C_{ps} is also short-circuited by a second non-ohmic resistive component, R_{F_2}, which is the reciprocal of the rate of recombination. The representation is hence as shown in Figure 3a. The whole of the combination of R_{F_1}, C_{ps} and R_{F_2} is in parallel across $C_{d:l.}$ in the case of a non-ideally polarisable electrode.

When desorption is by an electrochemical step, i.e. atom + ion desorption (3), a special representation is required as shown in Figure 3b, where the non-ohmic resistance, R_{F_2}, corresponding to the reciprocal rate of the Heyrovsky atom + ion desorption step is drawn with two parallel input channels, one for electrons and $H_3O^+_{aq}$ ions and the other for the H_{ads} atoms removed as equivalent charge from C_{ps}.

II. Determination of Adsorption Pseudocapacitance Involving Open-Circuit Decay

Methods for determination of the capacitance-potential relationship have been based on (a) geometrical differentiation of d.c. galvanostatic charging curves, e.g. the double-charging method of Devanathan, Bockris and Mehl (33), or of open-circuit decay curves by Conway and Gileadi (34,35,36), (b) direct a.c. bridge capacitance studies (30,37) or (c) direct differentiation of charging or decay curves (38). The interpretation of results for C_{ps} values from the a.c. capacitance studies is complicated by the large frequency dependence of the capacitance which was still observed down to very low frequencies. The methods involving geometric differentiation rely on rather

whereby the oxidation of the adsorbed hydrogen atoms is completed before readsorption becomes appreciable. Breiter, Knorr and Volkl (42) used this method for the noble metals Pt, Pd, Ir, Rh and Au under cathodic polarisation. The method can only be successfully applied if there is a considerable potential difference between the potential corresponding to the completion of adsorbed hydrogen oxidation and that corresponding to the commencement of the next anodic process (e.g. oxide formation, evolution of oxygen, etc.), a condition found only with the noble metals. By the use of the rapid galvanostatic method, the succeeding anodic processes overlap with adsorbed hydrogen oxidation at the silver electrode in alkaline solution. Therefore, Devanathan et al (33) developed a double charging method to overcome this difficulty. Application of cyclic voltammetry (43) is another direct method used widely for evaluation of θ_H on the noble metals and their alloys.

Each value of hydrogen coverage corresponds to a charge q_H required to reach that coverage from zero coverage, i.e.

$$q_H = k'\theta_H \qquad (33)$$

where k' is the charge needed to form a complete monolayer of adsorbed hydrogen atoms. Its numerical value is of the order of 200 $\mu C\ cm^{-2}$ for a hydrogen atom occupying a single site on the surface of a metal. The variation of θ_H, and hence of q_H, with overvoltage gives rise to a pseudocapacitance

The electrode capacitance, C_{expt}, can be calculated from the initial rate of decay $(\frac{d\eta}{dt})_{t=0}$ using the following equation

$$C_{expt} = \frac{-i}{(\frac{d\eta}{dt})_{t=0}} \qquad (32)$$

where -i is the steady-state cathodic current density at the time of current interruption, t=0 (t is the time elapsed after the current interruption) and $C_{expt} = C_{d.l.} + C_{ps}$ (because C_{ps} is in parallel with $C_{d.l.}$, see Figure 3). If $C_{ps} << C_{d.l.}$ at very small values of cathodic charge passed, -Q, then it can be assumed that $C_{expt} = C_{d.l.}$ at this value of -Q and the increase of C_{expt} with -Q can be used to evaluate C_{ps}, i.e. $C_{ps} = (C_{expt} - C_{d.l.})$; otherwise we must be content with ΔC_{ps}, that is the increase of pseudocapacitance with -Q. By polarising the electrode at various current densities -i and recording $-\eta$ at the instant of interruption of current, followed by open-circuit decay, C_{ps} or rather ΔC_{ps} can be obtained as a function of overvoltage.

III. Evaluation of Hydrogen Coverage

The hydrogen coverage θ_H can be directly obtained by measuring precisely the charge required for deposition or removal of hydrogen atoms on the surface of the metal over a certain potential range. The rapid galvanostatic charging method was originated by Bowden and Rideal (40) and used by Pearson and Butler (41) and others (42). Difficulties associated with the readsorption of hydrogen from dissolved hydrogen molecules in solution, or from bubbles on the electrode, are minimized by using high anodic current densities,

$$C_{ps} = \frac{dq_H}{d\eta} = k' \frac{d\theta_H}{d\eta} \qquad (34)$$

Thus, knowledge of C_{ps} may be used to evaluate θ_H values by integration of $\frac{1}{k'} \int C_{ps}\, d\eta$. In this method, only the change of coverage corresponding to a given change in potential can be obtained, unless the integration constant, i.e. the absolute value of the coverage at some reference potential, is known from an independent measurement.

C. Permeation of Hydrogen Atoms Through Metals

Permeation studies of hydrogen through metals are usually carried out in one of two ways: either by exposure of one side of a metal foil to gaseous molecular H_2 (or to H atoms) usually at high temperature and pressure and extracting it from the opposite side under vacuum, or by the cathodic evolution of hydrogen on the opposite surface of the metal. In contrast to gas phase studies, Devanathan and Stachurski (44), Züchner and Boes (45) Muju and Smith (46) and, more recently Kedzierzawski, Benczek and Sadkowski (47), have devised convenient and sensitive electrochemical and radiochemical methods for permeation studies.

In the electrochemical studies, the electrode was made in the form of a suitable membrane of thickness L and functioned as a bipolar electrode separating two regions of solution as shown in Figure 4. Hydrogen is electrolytically generated on one side of this membrane (called the cathodic side). Much of the discharging hydrogen escapes as gas into the atmosphere. A fraction of it

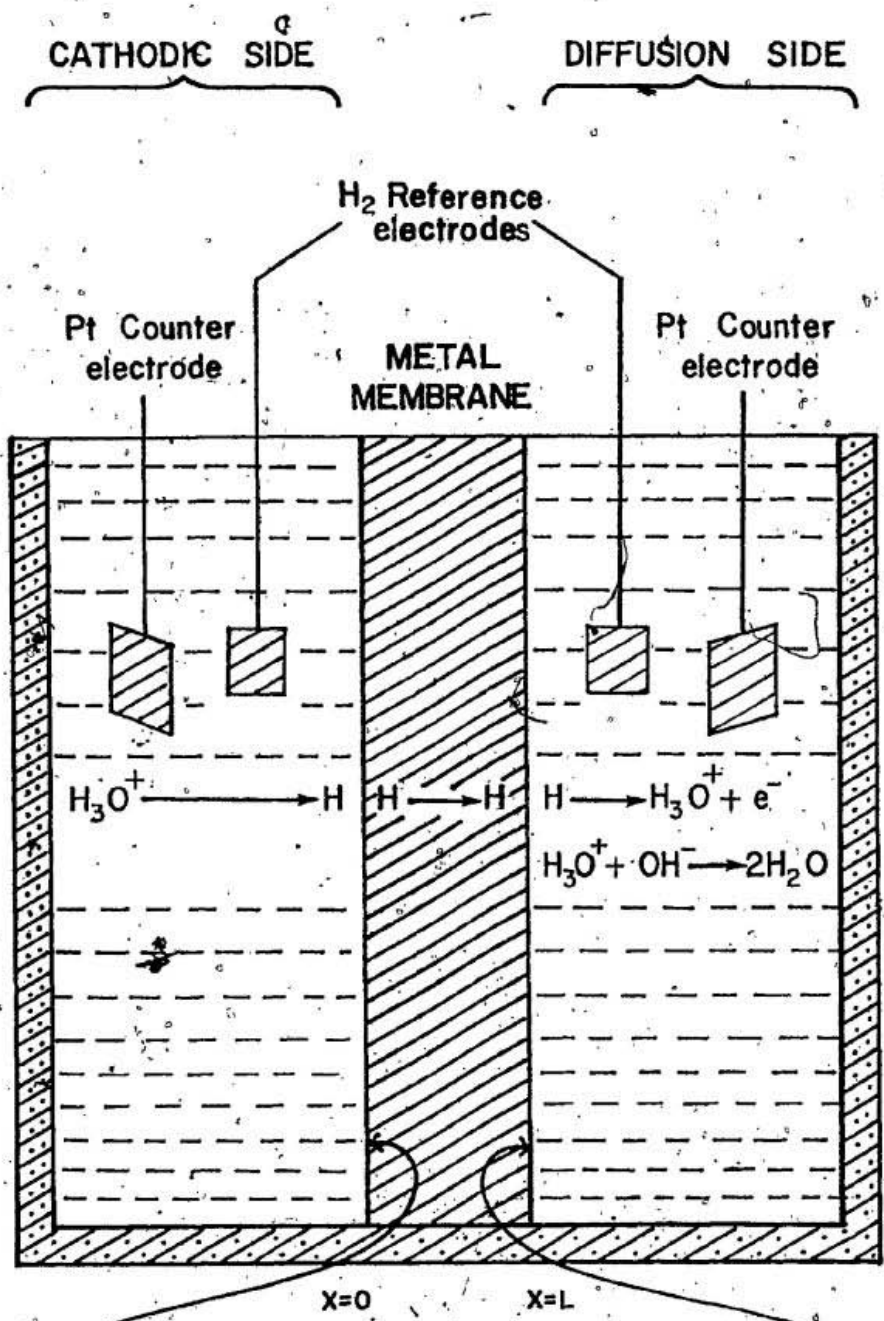

Fig. 4. SIMPLEST SCHEME OF APPARATUS FOR STUDYING DIFFUSION.

$$J_i = -D \frac{\partial C_i}{\partial x} \text{ mol cm}^{-2}\text{s}^{-1} \qquad (35)$$

Then, using Fick's first law, the steady-state permeation current, J_∞, may be written as

$$J_\infty = FD_H \frac{(C_o - C_L)}{L} = FD \frac{C_o}{L} \text{ if } C_L = 0 \qquad (36)$$

where D_H = the diffusion coefficient of hydrogen atoms, L = thickness of the metal membrane, C_o = the concentration of hydrogen in the metal just under the cathodic surface and C_L = concentration of hydrogen on diffusion side which is normally maintained at zero.

If the steady-state does not exist, i.e. the concentration of hydrogen at some point in the membrane is changing with time, then Fick's second law will be applicable.

$$\frac{\partial C_{(x,t)}}{\partial t} = D \frac{\partial^2 C_{(x,t)}}{\partial x^2} \quad ; \quad 0<x<L \qquad (37)$$

By application of the operation of Laplace transformation to equation (37) with the initial and boundary conditions

$$C_{(x,t)} = C_o; \quad x = 0; \quad t = 0$$

$$C_{(x,t)} = 0; \quad x = L; \quad t \gtrless 0$$

$$C_{(x,t)} = 0; \quad 0<x<L; \quad t < 0$$

McBreen, Nanis and Beck (48) solved the diffusion equation (37) to get an expression for the hydrogen concentration, $C_{(x,t)}$, at a point x and at a time t after switching on the cathodic polarisation.

from the adsorbed state enters the lattice and becomes dissolved as hydrogen atoms. Some of the dissolved hydrogen atoms diffuse to the opposite side of the membrane (called the anodic side). The diffusion experiment is simplest if the coverage of the membrane with adsorbed atomic hydrogen on one side (cathodic side) is maintained at a certain fixed level, while on the opposite side (diffusion side) it should always be zero. These conditions are essentially satisfied by cathodic polarisation on the cathodic side of the electrode and anodic polarisation (with a high positive potential versus a hydrogen reference electrode) on diffusion side so that all hydrogen atoms arriving at this surface are instantly oxidized and turned into an equivalent current. From measurements of permeation currents, it is possible to determine the diffusion coefficients and solubilities of hydrogen in metals. Determinations of permeation rates and of diffusion coefficients have been made by electrochemical and radiochemical methods at room temperature and in some cases at temperatures up to 353 K, at various cathodic currents or potentials, for various metals such as Pd, Pt, Ni, Pb, Fe, and for steel, Fe-Cr, Fe-Ni and Pd-Ag alloys, among others.

Let the concentration of hydrogen at $x = 0$ (see Figure 4) be assumed to be at C_o throughout, while at $x = L$ it is assumed to be zero. The rate of diffusive transport of hydrogen in the metal will depend on the gradient of hydrogen concentration in the metal as described by Fick's first law of diffusion. Fick's first law describes the steady-state diffusion of a species down a concentration gradient, $\frac{\partial C_i}{\partial x}$, at a distance x, i.e.

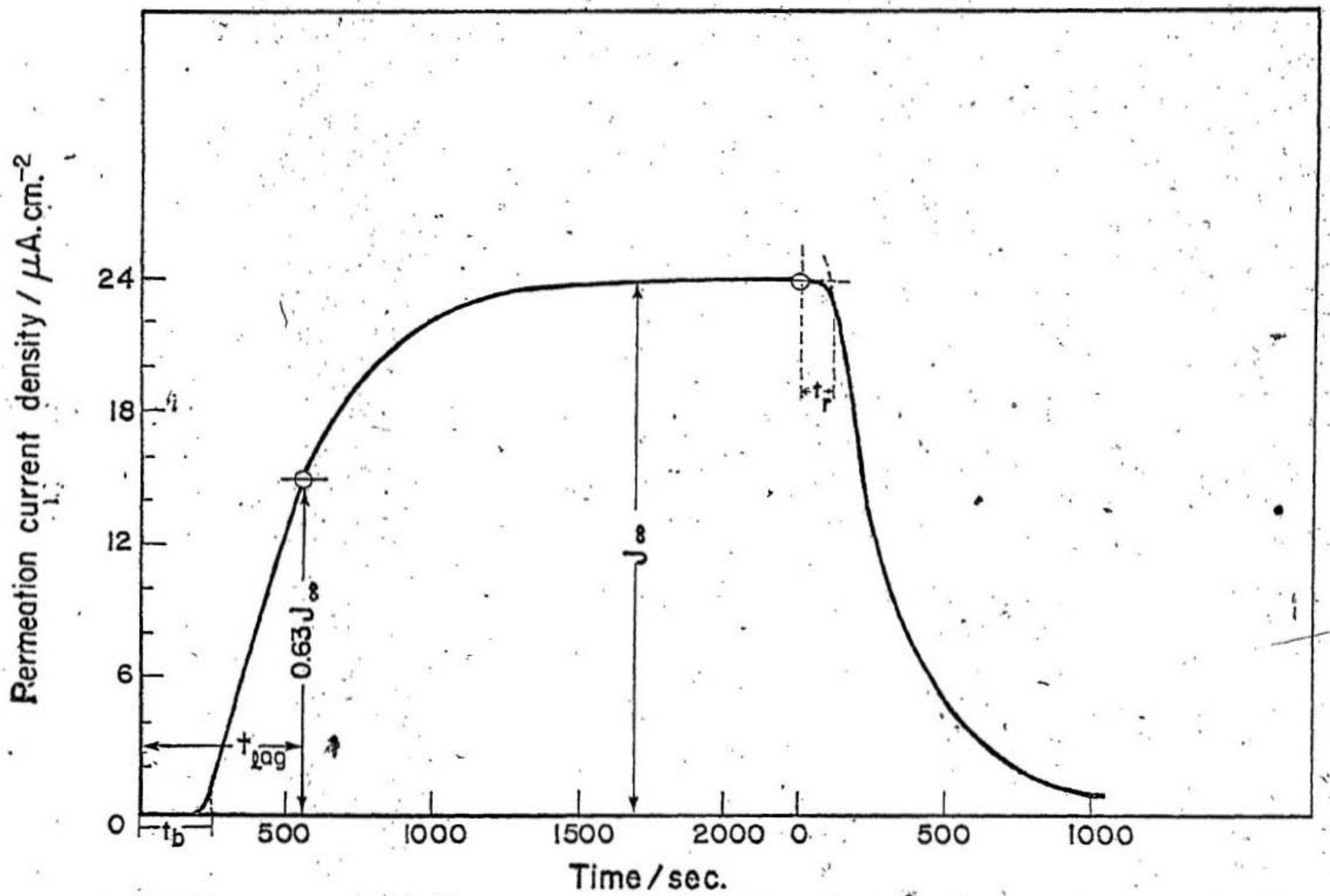

Fig. 5 Hydrogen permeation transient (Devamathan & Stachurski, 44)

$$\frac{C_{(x,t)}}{C_o} = \sum_{n=0}^{\infty} (-1)^n \operatorname{erfc} \frac{x + 2nL}{2\sqrt{D_H t}} -$$

$$\sum_{n=0}^{\infty} (-1)^n \operatorname{erfc} \frac{2L(n + 1)-x}{2\sqrt{D_H t}} \qquad (38)$$

The measured permeation current at time t, at x = L is

$$J_t = -D_H \left(\frac{\partial C_t}{\partial x}\right)_{x=L} \qquad (39)$$

I. Methods of Measuring Diffusion Coefficient of Hydrogen in Metals

(a) Time-Lag Method: By integrating the rising part of the permeation current versus time curve, the quantity of hydrogen which has permeated through a metal membrane can be obtained at various times. An extrapolation to zero concentration of the plot of this quantity versus time gives the time lag, t_{lag}. The time lag is related to the diffusion coefficient by

$$t_{lag} = \frac{L^2}{6D} \qquad (40)$$

Devanathan et al (44) have shown that t_{lag} may be equated to the time at which the rate of permeation is 0.63 times the steady-state value J_∞ (Fig. 5). Figure 5 shows a typical permeation transient.

(b) Rise-Time Method: According to Devanathan et al (44), the equation of the rising transient is given by

$$\ln\left(\frac{J_t - J_\infty}{J_\infty}\right) = \ln(1 - e^{-3t/t_o} + e^{-8t/t_o})$$

$$+ \ln 2 - t/t_o \qquad (41)$$

For some membranes like high strength steel it takes more than 24 hours to reach a steady-state. Equation (43) can be written for two short times t_1 and t_2

$$\frac{J_{t_1}}{J_{t_2}} = \left(\frac{t_2}{t_1}\right)^{1/2} \exp \frac{-L^2}{4D} \left(\frac{1}{t_1} - \frac{1}{t_2}\right) \qquad (45)$$

Thus, it is not necessary to wait until a steady-state is reached in order to evaluate the diffusion coefficient.

(c) Breakthrough time: The breakthrough time, t_b, as represented in Figure 5 can be written as the difference between the time lag, t_{lag}, and the rise-time constant, t_o. Then from equations (40) and (42) one can write

$$t_b = t_{lag} - t_o = \frac{L^2}{D}\left(\frac{1}{6} - \frac{1}{\pi^2}\right) = \frac{L^2}{15.3D} \qquad (46)$$

(d) Decay time constant: When the concentration of hydrogen in the metal membrane is some function of x, the general solution of Fick's laws is different from when an initially uniform concentration exists in the membrane. The decrease in permeation current for the decay transient (see Fig. 5), from the time of interruption of the cathodic current (i.e. t = 0) is given by Devanathan et al (44) in the form of

$$J_{x=0,t} = J_{x=0,t=0} \exp(-t/t_o) \qquad (47)$$

where $J_{t=0}$ is the permeation current at the time t = 0 and $t_o = \frac{L^2}{\pi^2 D}$. Hence, a plot of $\ln\left(\frac{J_t}{J_{t=0}}\right)$ versus time must be a straight line with slope $\frac{\pi^2 D}{L^2}$. Devanathan et al corrected the decay time constant

where the rise time constant t_o is related to the diffusion coefficient by

$$t_o = \frac{L^2}{\pi^2 D} \tag{42}$$

The first term of the right hand side of equation (41) approaches zero when t increases. Hence, a plot of $\ln(\frac{J_t - J_\infty}{J_\infty})$ versus t must be a straight line with an intercept of ln 2 and a gradient of $\frac{1}{t_o}$. Thus, from the gradient D can be calculated using equation (42). Cadersky, Muju and Smith (49) used this type of calculation to evaluate D for hydrogen in Pb.

McBreen et al (48) developed a sensitive electrochemical method for the precise measurement of diffusion coefficients. They used equations (35) and (38) and found an expression between the permeation current at time t, i.e. J_t, and the permeation current at the steady-state, i.e. J_∞.

$$\frac{J_t}{J_\infty} = \frac{2}{\pi^{1/2}} \frac{1}{\tau^{1/2}} \exp^{-1/4\tau} \tag{43}$$

where $\tau = \frac{Dt}{L^2}$ is a dimensionless parameter. This equation is valid up to $J_t = 0.965\ J_\infty$. It is possible to calculate D by finding the time to attain any fraction of the steady-state permeation rate. For the particular case (most commonly used) of $\frac{J_t}{J_\infty} = 0.5$, the parameter τ has a value of 0.138 and the corresponding time $t_{0.5}$, denoted as the half-rise time, is given by

$$t_{0.5} = \frac{0.138L^2}{D} \tag{44}$$

giving the value of $\lim|I_a|$. Then using equation (48) the value of Z and hence the diffusion coefficient can be obtained.

II. Diffusivity and Solubility of Hydrogen in Metals

The diffusion coefficient of hydrogen in metals may be considered independent of cathodic potential (50), cathodic current (51,52,53,54), composition of the solution {in particular the presence of traces of added surface poisons (53)} except where these cause changes in bulk properties, but may be dependent on bulk properties and usually varies with bulk hydrogen concentration, as found by Cadersky et al (49) for Pb and by Nanis and Namboodhiri (55) for Fe (D_H in Pb and Fe increases with the cathodic current). The bulk H concentration depends on the solubility of hydrogen atoms in metals. This may vary with the cathodic c.d. and/or the potential (49,55). The solubility of hydrogen apparently decreases with increase in the activation energy of absorption and increases as the number of d-vacancies increases in transition metals (56). The diffusion coefficient increases with a rise in temperature. Züchner and Boes (45) showed that the diffusion coefficient slightly increased for Pd-Ag alloys up to 20% of silver content. At higher silver contents, D_H decreased sharply and the activation energy increased slightly, the values obtained for D_H ranging from 10^{-6} cm^2s^{-1} in pure Pd to 10^{-10} cm^2s^{-1} in Pd-Ag alloys of 60% silver content. In influencing the diffusion of hydrogen in the Pd-Ag alloys, two opposing effects seem to be important. The first promotes the diffusion, the second, dominating at higher silver contents, retards it. According to them, the promotion

for the relaxation time t_r* (see Fig. 5) to obtain the transients on a time scale which refers to the concentration in the membrane rising at $t = 0$ to C_o at $x = 0$.

(e) Alternating Current Method: In 1976, Kedzierzawski et al (47) developed a new alternating current method for investigation of the diffusion of hydrogen in metals. In this method, the cathodic side of the metal is polarised by means of an alternating cathodic current, the hydrogen concentration on this side changing sinusoidally so that an alternating anodic current of hydrogen oxidation leaving the anodic side is recorded. They found a relation between the ratio of the amplitude of the alternating current of hydrogen oxidation on the diffusion side, $|I_a|$, to the limiting value of this amplitude for frequency, f, going to zero, and $Z = L\sqrt{\frac{\omega}{2D}}$ where $\omega = 2\pi f$ is the angular frequency, i.e.

$$\frac{|I_a|}{\lim_{f \to 0} |I_a|} = \frac{\sqrt{2}\, Z}{\sqrt{\sinh^2 Z + \sin^2 Z}} \qquad (48)$$

The amplitude of the alternating current of hydrogen oxidation, $|I_a|$, is measured directly, whereas the limit of this amplitude can be determined by measuring the alternating permeation current at various frequencies and extrapolating $|I_a|$ to zero frequency, the intercept

---

*This relaxation may be regarded as being due to the finite rate constant for the transfer of hydrogen atoms from the surface into the metal phase.

The nature of chemical bonding in metallic hydrides is still poorly understood. There are three different models, each with some supporting evidence, to explain the bonding of hydrogen in metals. However, none of the three models is completely satisfactory. The first model assumes that the hydride is an alloy (in the usual metallic sense) of hydrogen and the metal. The electrons from hydrogen occupy the d-bands of the transition metal and hydrogen, therefore, exists essentially as protons in the metal lattice. The high electronic conductivities and other metallic properties and magnetic behaviour of the metallic hydrides may be taken as evidence for this model.

The second model assumes a predominantly covalent bond between the metal and hydrogen. Some observations of internuclear distances and structural consideration in hydrides support this concept of bonding in some metallic hydrides.

The third model is essentially the converse of the first. According to this model the hydrogen exists as anions formed by removal of an electron from the metal to give a partially ionic bond. Evidence for this model are observed metal-hydrogen distances, which are in agreement with known ionic radii.

of diffusion might be attributed to the dilation of the lattice by which the activation energy is lowered. The experiments of Buchold and Sicking (57) on the diffusion of tritium in Pd-B alloys in which a decrease in activation energy and increased diffusion coefficient of tritium for small additions of B in Pd were observed confirmed Züchner and Boes' views. With addition of more silver to the palladium lattice the blocking of diffusion jump paths gains importance. Therefore, the activation energy rises and the diffusion coefficient drops.

By simultaneous measurements of hydrogen-deuterium separation factors on both the cathode and diffusion sides of 25% Ag-Pd alloy, Smith and Hammerli (58) showed a higher diffusivity for deuterium than for hydrogen. From this observation they concluded that this phenomenon is associated with a higher energy of activation for the lighter isotope.

Hydrogen absorption by metals during the h.e.r. can be regarded as a side effect of the overall hydrogen evolution process in which protons in acid media are discharged and liberated as molecular hydrogen gas. Since hydrogen evolution can be affected by the condition of the bulk metal phase via the interface, a correlation between θ_H and C_o might exist. Many workers (59,60) assumed the relationship $\theta_H \propto C_o$ at low coverage. However, Breger and Gileadi (50) showed by simultaneous measurements of C_o and θ_H on Pd that at low $\theta_H \leq 0.15$, $C_o \propto \exp(\theta_H)$; while at $\theta_H \simeq 0.5$, $C_o \propto \theta_H$. An exponential relation between C_o and θ_H was also suggested by Rao (61) for Pb in acid solution.

Chapter 1

INTRODUCTION

Volatile, condensable, but otherwise unidentified lead hydride products from the action of atomic hydrogen on lead in the acid treatment of a sheet of magnesium coated with radioactive thorium B ($^{212}_{82}Pb$) were first reported by Paneth and Norring (62) in 1920. Schultze and Müller (63) in similar experiments found that the trapped hydride could not be re-evaporated. This could be attributed to the formation of PbH_4 and its subsequent decomposition on warming, in view of the instability of PbH_4 at ambient temperatures. However, the possibility that the hydride which was formed was in fact a hydride radical rather than PbH_4 cannot be precluded. More recently the existence of traces of volatile lead hydride PbH_4 has been demonstrated by Saalfeld and Svec (64) using a mass-spectrometer in the dissolution of Mg-Pb alloys in acid solution. Owing to the instability of PbH_4, thermodynamic data pertaining to it are quite difficult to determine. The melting and boiling points of PbH_4 are unknown. But the energy of formation of PbH_4 was reported to be 250 kJ mol^{-1} at 298 K (64). In earlier work on the reduction of alkali-metal plumbates, $MPb(OH)_3$, with aluminum foil in aqueous solution, a grey solid dilead dihydride Pb_2H_2, which decomposed in vacuum to Pb and H_2, was said to have been formed (65).

The interaction of atomic hydrogen with evaporated and sintered films of lead has been investigated by Wells, M.W. Roberts and Young (66,67) in the gas phase. At 273 K, lead films very rapidly absorbed large quantities of atomic hydrogen, the volume absorbed

PART 1

CATHODIC DISINTEGRATION OF LEAD

being directly proportional to the mass of the film. The hydrogen was distributed through the lattice and not confined to a region close to the surface. Since the amount of hydrogen absorbed was a function of the mass of lead and not its surface area, Roberts et al concluded that the absorption indicated hydride formation rather than adsorption on the surface. The slope of the linear relationship between hydrogen uptake and the mass of the lead phase (up to 30 mg) observed by Roberts and Young (67) suggested a finite stoichiometric ratio between lead and hydrogen, i.e. $PbH_{0.2}$ at 273 K and $PbH_{0.22}$ at 195 K. On heating, the hydride gave off molecular hydrogen in steps, i.e. slow desorption of a small fraction (8%) of the hydrogen as molecules occurred at 273 K and a greater fraction (25%) at 413 K and so on, indicating either discrete absorption centres of different energies or possibly rate-limiting diffusion or recombination of hydrogen atoms. The events of hydrogen absorption and desorption can be described by the following reaction sequence:

$$Pb \xrightarrow[\text{vaporisation}]{10^{-6}\ \text{torr}} \text{Pb coating of glass walls} \xrightarrow[+H]{273\ K} PbH_{0.2} \xrightarrow[\text{25\% H loss}]{413\ K} PbH_{0.14} \xrightarrow[\text{50\% H loss}]{463\ K} PbH_{0.1}$$

Roberts et al (67) concluded from their data that the activation energy of desorption (67-84 kJ mol^{-1}) corresponds to that for hydrogen motion (or diffusion) in the metal. They also suggested that at low hydrogen concentrations ($PbH_{0.1}$) the activation energy might approach the Pb-H bond energy (less than 218 kJ mol^{-1}).

Moreover, by an electron paramagnetic resonance study with X-irradiated $Pb(C_2H_3O_2)_2 \cdot 3H_2O$ using crystals and powders at 77 K, H.C. Roberts and Eachus (68) have detected the species PbH^{2+}.

Salzberg et al (69,70,71), following earlier work by Haber, Bredig and Sack (72,73), reported that lead cathodes disintegrate in alkaline solutions of varying pH and salt concentrations and also at very high c.d's in aqueous sulphuric acid. This disintegration seemed to involve transient formation of PbH_2, suggested as a volatile species.

Angerstein (74), however, failed to detect disintegration of lead cathodes in pure acid solutions. Therefore, she proposed the formation of alkali metal or alkaline - earth metal alloy as the cause of the cathodic disintegration of lead. According to her observations, above a certain cathodic c.d., the reduction of alkali and alkaline - earth cations takes place on the lead cathode. The deposited metals combine with lead on the surface of the cathode to form an alloy. The disintegration of the lead cathode was associated with a decompositon of the alloy by water. The phenomenon can be described by the following reactions:

$$xPb + M^{n+}(aq) + ne^- = MPb_x \quad \text{"alloy formation"}$$

$$MPb_x + nH_2O = M^{n+}(aq) + \underset{\text{particles}}{xPb} + \frac{n}{2} H_2(g) + nOH^-(aq)$$

"alloy decomposition"

this hydride was volatile and unstable, breaking down to lead particles and H_2 molecules immediately after escaping from the cathode. There is still no direct proof of the formation of volatile lead dihydride, due to its apparent instability at room temperature.

The hypothesis of Haber, Bredig and Sack (72,73) and Angerstein (74) of alkali metal-lead alloy formation was recently supported by Russian workers. Kabanov et al (76,77) deduced that insertion of alkali cations into lead and formation of alkali metal-lead alloy occurred during cathodic polarisation of lead in alkaline solution by observing that the overvoltage shifted in the negative direction with time of polarisation for relatively small negative potentials. At high negative potentials but less negative than -2.2 V versus standard hydrogen electrode (78), the rate of penetration of alkali metal into lead seemed to be sharply increased, while at potentials more negative than -2.2 V the lead cathode disintegrated. In order to explain the rapid insertion of alkali metal into lead at high negative potentials, Chernomorskii et al (78) proposed that as the negative potential increased the decrease in activation energy of the process became sufficient for an increase in the rate of introduction of alkali metal into the lattice of the lead cathode. An investigation was also carried out by Chernomorskii and Kabanov (79) using chronopotentiometry which enabled a calculation of the amount of alkali metal introduced into the lead lattice from the time required for the potential to fall from a constant value when a constant anodic current was imposed after the initial cathodic polarisation . They found a direct relationship between the polarisation potential and logarithm

This explanation agrees with the conclusions on the cause of disintegration, drawn earlier by Haber, Bredig and Sack (72,73) on the basis of a comparison of the cathodic disintegration of lead and the spontaneous decomposition of alkali metal-lead alloy (containing 4.8 - 8% alkali metal) with water.

Salzberg et al (69,70,71) had a different opinion of the cause of disintegration using several lines of evidence:

(1) Disintegration occurred in acid solutions only at very high cathodic c.d's, i.e. at $i < -100$ mA cm^{-2}.

(2) Increasing the alkali metal ion concentration in, for example, aqueous NaOH solution, caused the threshold c.d. (minimum c.d. required to observe visible disintegration) to rise.

(3) The rate of disintegration at constant c.d. decreased with increasing alkali metal cation concentration at constant pH.

(4) In dilute alkaline solutions disintegration rates were essentially the same at the same c.d. for all alkali metal salt solutions, although some sort of arrangement based on the electromotive series might have been expected.

(5) The observed threshold c.d. had little or no dependence on the nature of the alkali metal cation.

In light of the above evidence, Salzberg et al (69,70,71), supported by observations of van Muylder and Pourbaix (75), supposed that the interaction of lead with cathodically generated hydrogen atoms and with water to produce lead dihydride PbH_2 was the principal mechanism of cathodic disintegration of lead. It was further supposed that

Previous workers measured lead disintegration rates by weighing the electrodes before and after a known cathodic treatment. In order to avoid discontinuities inherent in such an approach and to improve the sensitivity of detection of dissolution, in the present work the solution was sampled at intervals and analysed either by differential pulse anodic stripping voltammetry or by differential pulse polarography. In this way, disintegration rates could be followed over shorter or longer periods, up to several days, the lead cathode being maintained throughout at a given constant current. For a particular solution and experimental conditions, there was only a short delay before the lead particles formed during disintegration dissolved in the electrolyte. Therefore, the concentration of Pb^{2+} ions, correcting for the decreasing volume during an experiment, gave a reliable measure of the total amount of lead disintegration in a known time interval. Special attention was paid to stringent deoxygenation of the system and cleaning of the lead electrode and special care was taken to prevent admission of air to the cell during sampling, because of the possibility that tarnishing of the lead cathode, as reported by Kabanov and Jofa (81) and by Smith (9) and later by Rao (61), might affect the results.

of the amount of, e.g. sodium, introduced into the lead cathode for the concentration range of 1-5 mol ℓ^{-1} NaOH. But there were deviations from this relation for high and low concentrations, i.e. >5 and < 1 mol ℓ^{-1} NaOH, respectively. The deviation for high alkali metal ion concentration was explained as a disintegration of the lead cathode accompanied by a change in the structure of the surface layer of the electrode and the formation of spongy lead, leading to additional accumulation of the alkali metal. The deviation for low alkali metal ion concentrations suggested that a longer cathodic polarisation was required for disintegration to begin at a particular potential, because of slower accumulation of alkali metal in the lead cathode. They concluded that the cathodic disintegration of lead in alkaline solution involves chemical decomposition of an alkali metal-lead alloy with a large amount of alkali metal, e.g. K_2Pb, by water.

Tomashova et al (80) studied the incorporation of alkali metal into the lead lattice using dimethylformamide as solvent. They found that the amount of alkali metal in the lead electrode was three orders of magnitude greater than in the case of an aqueous solution under the same conditions. It was assumed that this is due to the chemical instability of the lead-alkali metal alloy in an aqueous solution and the absence of chemical decomposition of the lead-alkali metal alloy in water-free dimethylformamide.

In order to establish whether cathodic disintegration of lead requires the presence of alkali metal or alkaline-earth metal cations, the present study was undertaken using pure aqueous acid solutions.

passed as small droplets down a column of dilute nitric acid containing $Hg_2(NO_3)_2$ and CCl_4, then distilled three times using an all-Pyrex glass still.

Lead nitrate: Fisher Scientific Co. $Pb(NO_3)_2$ (Fe, 0.005%; Cu, 0.001%; insoluble matter, 0.003%) was used for preparation of standard solutions needed in calibrating the analytical methods.

Lead: Lead rods of 3 mm diameter were used as supplied by Johnson-Matthey and Co. of 99.9995% Pb.

Platinum: Johnson-Matthey and Co. Pt(apparatus grade, i.e. grade 4) was used for counter electrodes, for the cylindrical counter electrodes for electropolishing and for pinch-seals and other electrical connections. All Pt foils and cylindrical electrodes were cleaned with boiling HNO_3, and washed with triple distilled water. Then, they were platinized (82) in lead-free 2% chloroplatinic acid solution (solution of commercial platinic chloride in 2 mol ℓ^{-1} hydrochloric acid) for 2-3 minutes at 100-200 $mA \cdot cm^{-2}$.

The grey platinized electrodes were washed with distilled water, concentrated HNO_3 and triple distilled water before use.

Glassware: Pyrex was used throughout this work. All glassware was cleaned with hot nitric acid and copiously washed with distilled water and finally with triple distilled water. After final cleaning, most of the apparatus was dried in a stainless steel oven reserved for clean glassware and then assembled.

Tubing: Heat-shrinkable Teflon tubing was used to tightly cover a part of the lead electrode (see Fig. 6). Tygon tubing was used for the nitrogen gas line in the electrochemical analysis of lead.

Chapter 2

EXPERIMENTAL METHODS AND PROCEDURE

In this Chapter, the experimental methods and procedure used in the study of cathodic disintegration of lead electrodes in aqueous perchloric acid, sulphuric acid and sodium hydroxide solutions are described.

I Materials

Perchloric acid: B.D.H. Aristar 72 ± 1% $HClO_4$ (Na, 0.2 ppm; Fe, 0.1 ppm; Pb, 0.005 ppm; Cu, 0.005 ppm; Ni, 0.002 ppm; Li, 0.01 ppm; K, 0.05 ppm; Na, 0.2 ppm; SiO_3^{2-}, PO_4^{2-}, ClO_3^-, and NO_3^-, 1 ppm each; SO_4^{2-}, 2.5 ppm was used for preparation of the experimental solutions. G.F. Smith and Co. 60% $HClO_4$ was used for chemical polishing and electropolishing of the lead electrodes.

Sulphuric acid: B.D.H. Aristar 98% H_2SO_4 (Cl^-, 0.2 ppm; non-volatile matter, 10 ppm; NO_3^-, 0.1 ppm; Pb, 0.005 ppm; Fe, 0.05 ppm; Cu, 0.01 ppm; Ni, 0.005 ppm; Co, 0.005 ppm; As, 0.005 ppm) was used for preparation of experimental solutions.

Sodium hydroxide: Baker Analysed Reagent 98.2% NaOH(Na_2CO_3, 4 ppm; Cl^-, 0.005 ppm; PO_4^{3-}, 0.002 ppm; Fe, 0.005 ppm; Ni, 0.005 ppm; heavy metals, as Ag, 0.005 ppm) was diluted to 1 mol ℓ^{-1} as an experimental solution.

Water: Single distilled water was further distilled twice from alkaline $KMnO_4$ solution using an all-Pyrex glass still.

Mercury: Fisher Scientific Co. Hg (foreign metals, 0.0005%) was oxidized in dilute nitric acid with air bubbled through it, then

II Preparation of Lead Electrodes

The necessity of an uncontaminated and oxide-free electrode surface can be achieved by only a few methods of surface preparation. In the case of electrodes prepared outside the experimental cell, besides meeting the above requirements, it would be desirable to be able to transfer the electrodes rapidly to the cell in order to minimize tarnishing.

(a) Electropolishing and Comments Concerning its Mechanism

Beginning about 1935, serious consideration was given to an electrolytic method of polishing. Chemical polishing and electrolytic (anodic) polishing are among the most efficient methods of surface cleaning.

In anodic polishing the specimen is made the anode in an electrochemical cell, and under certain fairly critical conditions the burrs and rough spots are stripped from the surface. The production of a specularly reflecting surface by the method of electropolishing of an initially rough metal involves (i) smoothing by elimination of large scale irregularities and (ii) brightening of the surface by removal of irregularities of the order of a hundredth of a micrometre thick. During electropolishing, oxygen is evolving on the anode, the more rapidly the higher the current density used.

Muller (85) had observed the passivity of nickel and iron, in sulphuric acid solutions during electropolishing. In the passive state, metal dissolution ceases but oxygen is still evolved. He first attributed passivity to an interior change in the metal. But later, after Evans (86) had isolated a thin compact oxide film from

Gases: Matheson ultra-high purity hydrogen (H_2, 99.999%; O_2 < 2 ppm; N_2 < 2 ppm) deoxygenated further by an Engelhard Deoxo Cartridge and passed through prereduced BTS catalyst (83,84) from Badische Anilin-und Soda-Fabrik (containing 30% copper in a very finely dispersed form, stabilized on a carrier, activated by various reagents, and capable of removing O_2 to less than 0.1 ppm) placed in a glass tube and maintained at 410 K in an electrically heated furnace. After deoxygenation of H_2 gas it was divided into separate lines, where necessary, by grease-free high-vacuum taps (made by Ace Glass Inc. model 8194) followed in all cases by a liquid N_2-cooled trap (93 K) and one presaturator, filled with triple distilled water.

Canadian Liquid Air L-grade nitrogen (N_2, 99.99%; O_2, 20 ppm maximum; moisture < 10 ppm; Ar, 80 ppm) was used for deoxygenation of solutions in electrochemical analyses for lead.

(b) Method and Solutions Used in the Present Work

Aqueous perchloric acid was chosen as a polishing agent because, in spite of the discussion in (a) above, it was also important to minimize the possible sources of contamination of the cell solution with foreign cations and surface-active organic substances, thus avoiding the possible explosion hazard of perchloric acid and organic mixtures (often used for electropolishing) and also because lead perchlorate is highly soluble and high purity perchloric acid readily available.

Before electropolishing, lead rods were chemically polished for 2 minutes in 60% $HClO_4$ in contact with a ca. 20 cm^2 Pt gauze, washed with triple distilled water and then steamed (using steam from triple distilled water) until grease-free (for $\geq$ 1 hour). The oxide film that developed during this treatment had no effect on subsequent behaviour.

In preliminary experiments lead electrodes were electropolished at 1 A cm^{-2} in 60% $HClO_4$ for 2.5 minutes in a separate cell (Fig. 6). Later, the time of electropolishing was increased to 5 minutes. The polishing cell (Fig. 6) consisted of a ca. 35 cm^2 area cylindrical Pt cathode surrounding the central Pb anode. The lead rod of 3 mm diameter made contact with a fine platinum wire inserted into a freshly-cut slot, closed-up tight and protected from the solution by heat-shrinkable Teflon tubing {to avoid a possible bimetallic (Pb/Pt joint) contact with the solution}, fitting tightly over the lead and the glass tubing enclosing the wire (see Figs. 6 and 7). The lead electrode was suspended from a movable Pyrex plunger.

anodically passivated metal, he assumed that it is caused by formation of a compact oxide film. Hoar and Mowat (87) postulated formation of a solid oxide film (NiO) on nickel during the electropolishing of nickel in sulphuric acid. They suggested many electropolished metals behave, from the corrosion or tarnishing point of view, as if a very thin compact oxide film is left after polishing. In some cases, for instance, aluminum, a relatively thick compact film has been demonstrated by microscopic observations (88). Hoar and Farthing (89) obtained direct evidence of the presence of a compact solid film during electropolishing of copper and α-brass anodes in an orthophosphoric acid/water bath. Calculation shows that the thickness of the film formed before dissolution can only be of the order of a few unit cells. The thickness of the compact film after electropolishing differs for different metals which have different electrical conductivities and ease of dissolution of the oxides. Several workers (89,90,91,92,93) were able to obtain evidence for the presence of oxide films on many metals (Al, Au, Fe, Ni, Zn, Pb, Sn, W, Cu, Mo, Cd, Ag, Ti, U and In) when these metals were polished anodically.

The evidence for the presence of an oxide film on the surface of lead after electropolishing in perchloric acid solution is not very strong, but even if an oxide were present, its thickness, is unlikely to be great. The result of Nikiforova and Jofa (94) that passivation of lead in concentrated perchloric acid does not occur at current densities of <0.1 A cm^{-2} confirms that it is difficult for oxides to form in this system.

After electropolishing, the mirror-bright electrode was throughly washed for a few seconds with one litre of N_2 saturated triple distilled water and transfered wet directly to the three litre reservoir cell (Fig. 7) containing the electrolyte to be studied, already deaerated by bubbling hydrogen gas for about 16 h before the test electrode was introduced. The electrode became automatically cathodic on meeting the solution.

To find the geometrical area of the lead rod after electropolishing, a blank electropolishing experiment was carried out. The lead electrode was removed from the electropolishing cell, washed with distilled water, wiped and then its diameter and height were determined with calipers and the area calculated. The power supply for electropolishing was a custom galvanostat, based on a Hewlett Packard 6824A amplifier, its maximum current and voltage capabilities being ±1A and ±50 V, respectively.

1. LEAD ANODE.
2. PLATINUM CATHODE.
3. PLUNGER TUBE.
4. HEAT SHRINKABLE TEFLON.
5. OUTFLOW TAP.
6. FINE PLATINUM WIRE FOR ELECTRICAL CONTACT.

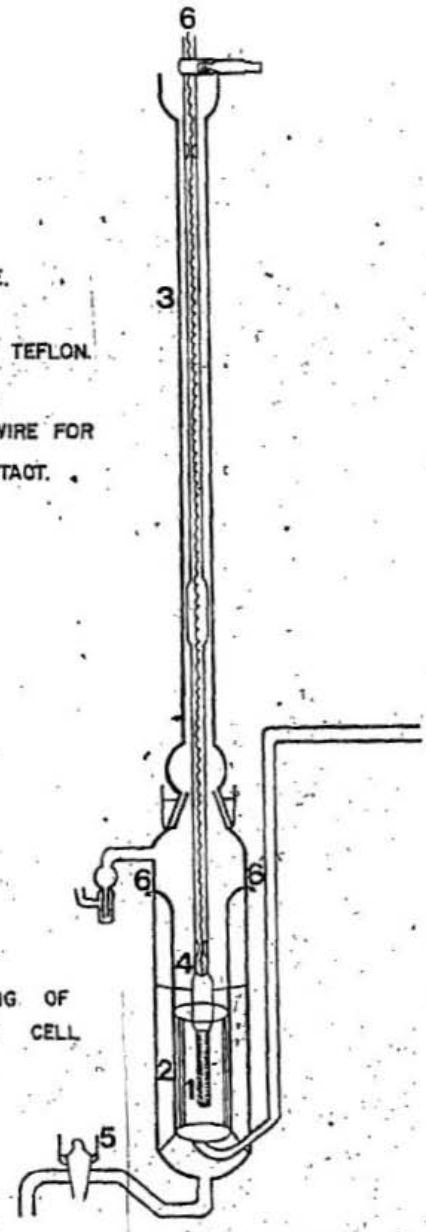

FIG. 6. SECTIONAL DRAWING OF ELECTROPOLISHING CELL

III Procedure

A sectional drawing of the main reservoir cell is illustrated in Fig. 7. It consisted of a 3 ℓ Pyrex flask with two vertical arms for lightly platinized platinum counter electrodes (2 of 25 to 30 cm^2 area each) which acted essentially as H_2 oxidation anodes. The central part of the flask contained the lead cathode described in the previous section. The cell was equipped with a graduated burette for delivery of a known volume of sample using a water-sealed solution control tap. The cathode, anodes and burette sections of the cell were supplied with ultra-high purity hydrogen. This hydrogen was supplied through copper and Pyrex tubing and was further deoxygenated and purifed by use of B.A.S.F. BTS Catalyst at 413 K, a cold trap at 93 K and pre-saturator with triple distilled water. Leakage of air through the cathode plunger and control tap was minimized by maintaining a positive pressure of hydrogen in the cell and in the burette. The gas lines to the cell, were of all glass construction, without joints or greased taps. All cup-cones and sockets were water sealed.

The electrolytes were prepared by dilution of high purity acid with triple distilled water. In some experiments a sample was taken from the freshly prepared acid solution for determination of alkali metal cations using atomic absorption spectroscopy. At the beginning of an experiment a sample of solution for a blank determination of lead was obtained before introduction of the electropolished electrode into the electrolyte, the burette portion (see Fig. 7) of the cell

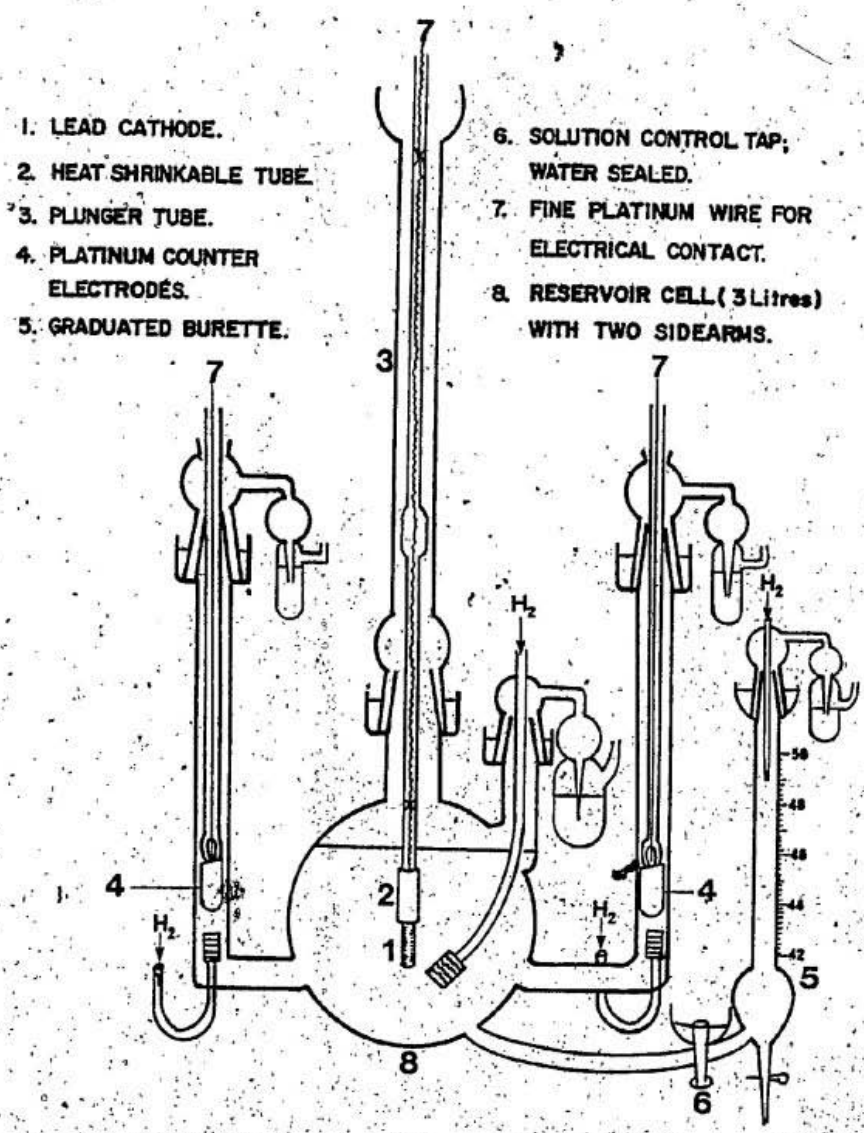

FIG. 7. SECTIONAL DRAWING OF MAIN RESERVOIR CELL

being left empty of solution, i.e. displaced by H_2 gas. As soon as possible after the introduction of the lead electrode a fixed cathodic current was applied to the lead cathode and a sample of electrolyte was taken to enable an estimate to be made of the quantity of Pb^{2+} ions carried over from the electropolishing cell. Further samples of solution were taken at suitable intervals, in each case the electrolyte being allowed to fill the burette before being displaced by H_2 gas back into the reservoir, this process being repeated once to aid homogeneity of samples for analysis. Samples were expelled from the burette into clean dry 50 ml conical flasks, using H_2 pressure with tap 6 (Fig. 7) closed. In earlier experiments each sample was 44.7 ± 0.1 ml and in later ones 43.2 ± 0.1 ml in volume.

IV Electrical Measurements

A Keithley 225 current source (with an accuracy of ±0.5% of reading, ±0.05% of full range) supplied up to 100 mA. Higher currents (up to 1 A) were obtainable using a custom galvanostat, based on a Hewlett Packard 6824A amplifier. A Keithley 160 digital multimeter (with an accuracy of ±0.2% of reading, ±1 digit on the 100 nA to 10 mA ranges, ±0.3% of reading, ±1 digit on the 0.1 and 1 A ranges) was used to measure currents.

This permits mixtures to be analysed much more easily than with solid electrodes.

The only important limitation of the application of a mercury electrode is the electrolytic dissolution of mercury itself, which prevents more positive potentials than about +0.4 V versus a saturated KCl calomel reference electrode to be reached.

Among the anodic stripping methods, a relatively new technique known as differential pulse anodic stripping voltammetry (DPASV) using a HMDE, has characteristics well worth considering for ultratrace level determination of heavy metals. The HMDE probably is one of the most widely used electrodes (98,99). Several features of the HMDE made it a desirable electrode for DPASV. Reproducible electrode areas can be obtained and the electrode is easily renewed.

In DPASV, at the negative potential first applied to the mercury electrode, metal ions will be reduced as rapidly as they reach the electrode surface and then the potential is scanned in the positive direction to strip the deposited metal anodically from the electrode.

Differential pulse polarography is another electrochemical method in which the current flowing between a counter electrode and a dropping mercury electrode (DME) at a particular potential, is related to the concentration of one of the species present in the solution through which the current is flowing. Differential Pulse Polarography is a less sensitive technique than DPASV for trace level determination of heavy metals due to lack of preconcentration and stripping steps. In this technique only a reduction of metal ions on the working mercury electrode is involved, in contrast to DPASV.

V Lead Analysis

Detection of heavy metals in an aqueous environment has long been of interest to the analytical chemist. Anodic stripping voltammetry and polarography are powerful methods for analysis of elements in aqueous solution. Anodic stripping voltammetry is used to determine metal ions that may be reduced to the metallic state during the preliminary electrolysis, and is based on the anodic currents obtained when the metals are re-oxidised. It can be more easily operated using stationary electrodes such as a hanging mercury drop electrode (HMDE), a mercury pool, or solid electrodes of various materials, e.g. glassy carbon. Determination of metals by anodic stripping from solid electrodes has generally given low results (95,96). The causes of these errors have been investigated, and ways of correction have been devised (97).

Mercury electrodes, however, have advantages over solid ones for determination of metals by anodic stripping voltammetry. The high hydrogen overvoltage on mercury is one of the chief factors responsible for the wide applicability of analysis with mercury electrodes, because it greatly extends the negative potential range over which the electrode can function without interference from evolution of hydrogen. The reduction of many chemical species can be studied at mercury electrodes, but not at electrodes made of most other materials. The other important advantage is that, if a mixed amalgam is sufficiently dilute, its different constituents can be re-oxidised independently, a separate peak being obtained for each.

Fig. 8 STRIPPING ANALYSIS CELL

1. Polarographic Cell Containing Test Solution.
2. Bridge Containing Test Solution.
3. Saturated KCl Calomel Electrode.
4. Hanging Mercury Drop Electrode.
5. Platinum Wire.
6. Magnet In Glass.
7. Wire For Electrical Contact.

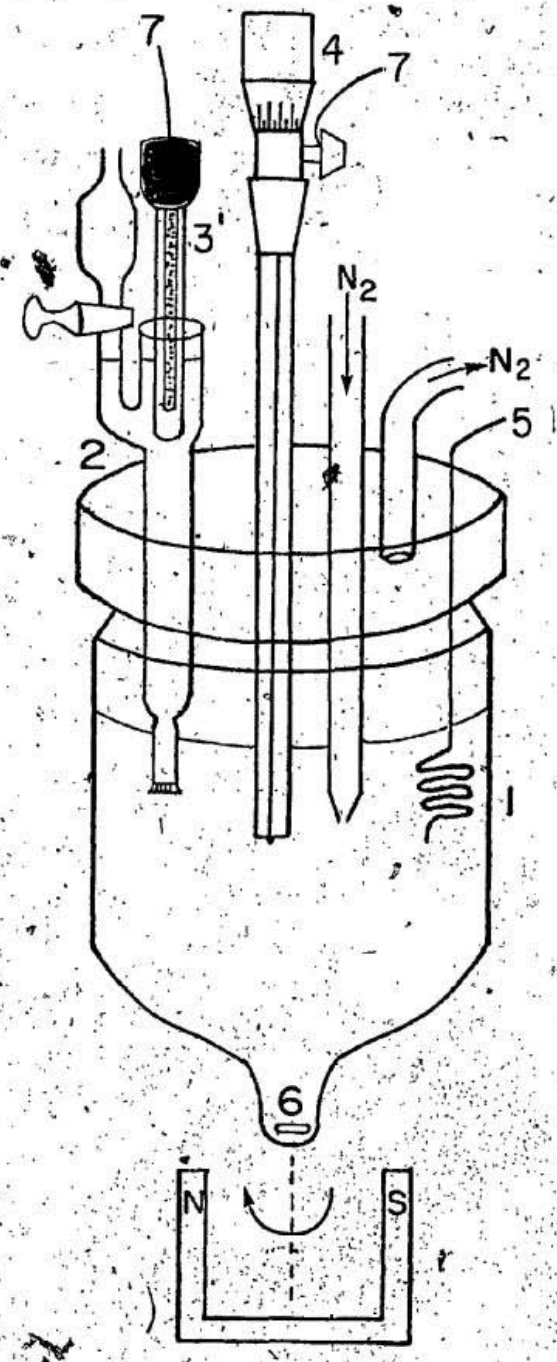

(a) Preparation of Calibration Curves for Pb^{2+}

(i) Differential Pulse Anodic Stripping Voltammetry (DPASV)

A Princeton Applied Research (PAR*) Model 174 polarographic analyzer and its accessories were used. Standard solutions of Pb^{2+} were prepared by weighing lead nitrate, $Pb(NO_3)_2$, using an analytical balance. Various concentrations of Pb^{2+} were made up using Grade A pipettes and Grade A volumetric flasks in 0.01 mol ℓ^{-1} $HClO_4$ (Aristar 72 ± 1% $HClO_4$ + triple distilled water) as supporting electrolyte. Supporting electrolyte increases the conductivity of the solution and ensures that the electroactive species moves by diffusion and not by electrical migration in the electric field across the cell. The choice of perchloric acid as a supporting electrolyte was because it is a strong acid and does not react either with Pb^{2+} ions in the solution or with the metallic mercury and because high purity $HClO_4$ is available. A sample of standard solution (about 25 ml) was placed in the Model 9300 pholarographic cell (see Fig. 8) fitted with a four holed cap and deaerated for 15 minutes with L grade nitrogen. The sample should be deoxygenated, because an aqueous solution when exposed to air may contain a concentration of dissolved gaseous oxygen as high as 0.25 mmol ℓ^{-1}. Oxygen often interferes with the determination of cations, especially in dilute solutions, because the reduction waves of oxygen occur at approximately -0.05 V and -0.8 V versus SCE**.

---

*PAR is a trademark of Princeton Applied Research Corporation.

**SCE is the abbreviation for saturated KCl calomel reference electrode.

Output offset	off
Display direction	"-"
Low pass filter	off
Pushbutton	initial
Recorder	x-axis 100 mV $inch^{-1}$ y-axis 1V $inch^{-1}$

The solution was gently stirred with a glass-enclosed magnetic stirrer. The stirring rate was slow enough so that no turbulence was visible in the solution and the mercury drop was stationary. The selector switch was turned to "External cell" and timed for 60 seconds. Then the stirrer was switched off and after 15 seconds further (the period necessary for the solution to become tranquil) the pen was lowered onto the chart recorder and the potential scanned in the positive direction. The deposition time was kept as short as practicable in order that diffusion of lead in the mercury was kept to a minimum and complicating reactions in the amalgam minimized. The oxidation current of lead from the mercury drop was recorded, the characteristic peak of the anodic stripping current of lead being obtained at -0.45 V versus SCE. The mercury drop was renewed for each run. The stirring rate, mercury drop size etc., were maintained the same for all runs. After each analysis, the vessel was washed carefully with distilled water, rinsed with triple distilled water and finally rinsed with the solution to be analysed.

At first, it was thought that DPASV using a HMDE would be suitable for all analyses. The calibration curve in (Fig. 9) showed, however,

Furthermore, the product of oxygen reduction in unbuffered solutions may change the pH of the solution in the vicinity of the electrode. This change in pH can interfere with the desired reaction by causing precipitation or complex formation of the electroactive species at the electrode surface. Nitrogen was passed over the solution during the actual electrochemical experiment to prevent the re-adsorption of oxygen.

After deaeration was complete, the Model 9302 hanging mercury drop electrode using triple distilled mercury was inserted into the cell and a mercury drop of suitable size obtained. Rotation of the micrometer drive by six divisions produced a drop (ca. 3.2 mm^2 area) which has been found to be suitable.

A Model 9311 saturated KCl calomel reference electrode, isolated from the test solution through a salt bridge tube filled with the solution to be analysed (to minimize contamination from mercurous ions and impurities in calomel) was inserted into the cell. A Model 9312 platinum spiral serving as a counter electrode was placed directly in the test solution. Connection to the PAR 174 were made through the accessory cable connector with alligator clips and the instrument was set in the following way:

Scan rate	2 mV s^{-1}
Scan direction	"+"
Range	1.5 V
Initial potential	"-0.5 V vs SCE"
Modulation amplitude	25 mV
Current range	various

that a non-linear response existed at high concentrations of Pb^{2+} ions. Therefore, with the conditions applied above, DPASV was not accurate over the whole range of concentrations of interest. DPASV is quite a good technique with its high sensitivity for determination of low concentrations of lead in the solution. The results of the analysis of standard lead solutions in the range of 1 to 140 ppb Pb^{2+} (average of two different runs in each case) are given in Table 1a and illustrated in Figure 10 showing that this method can be applied for determination of lead concentrations at low levels in the solutions. The least squares value of the slope of Figure 10 is 0.016324 ± 0.000544, the corresponding intercept is -0.0011166 ± 0.026129 with a correlation coefficient of 0.997. The value of the slope and intercept were used to calculate the concentration of lead in the unknown samples.

(ii) Differential Pulse Polarography

Because of the unsuitability of DPASV for analysis of high concentrations of Pb^{2+} ions, differential pulse polarography with a dropping mercury electrode appeared to be a reasonable answer to this problem. The apparatus used in this method was similar to that used in DPASV but, instead of the hanging mercury drop electrode in DPASV, a dropping mercury electrode was used.

The dropping mercury electrode consisted of a glass capillary attached to a reservoir of triple distilled-mercury. Drops of mercury fell from the orifice of this capillary at a constant rate. A drop timer mounted on a ring stand was connected for a typical analysis, the toggle switch on the drop timer being positioned for three-

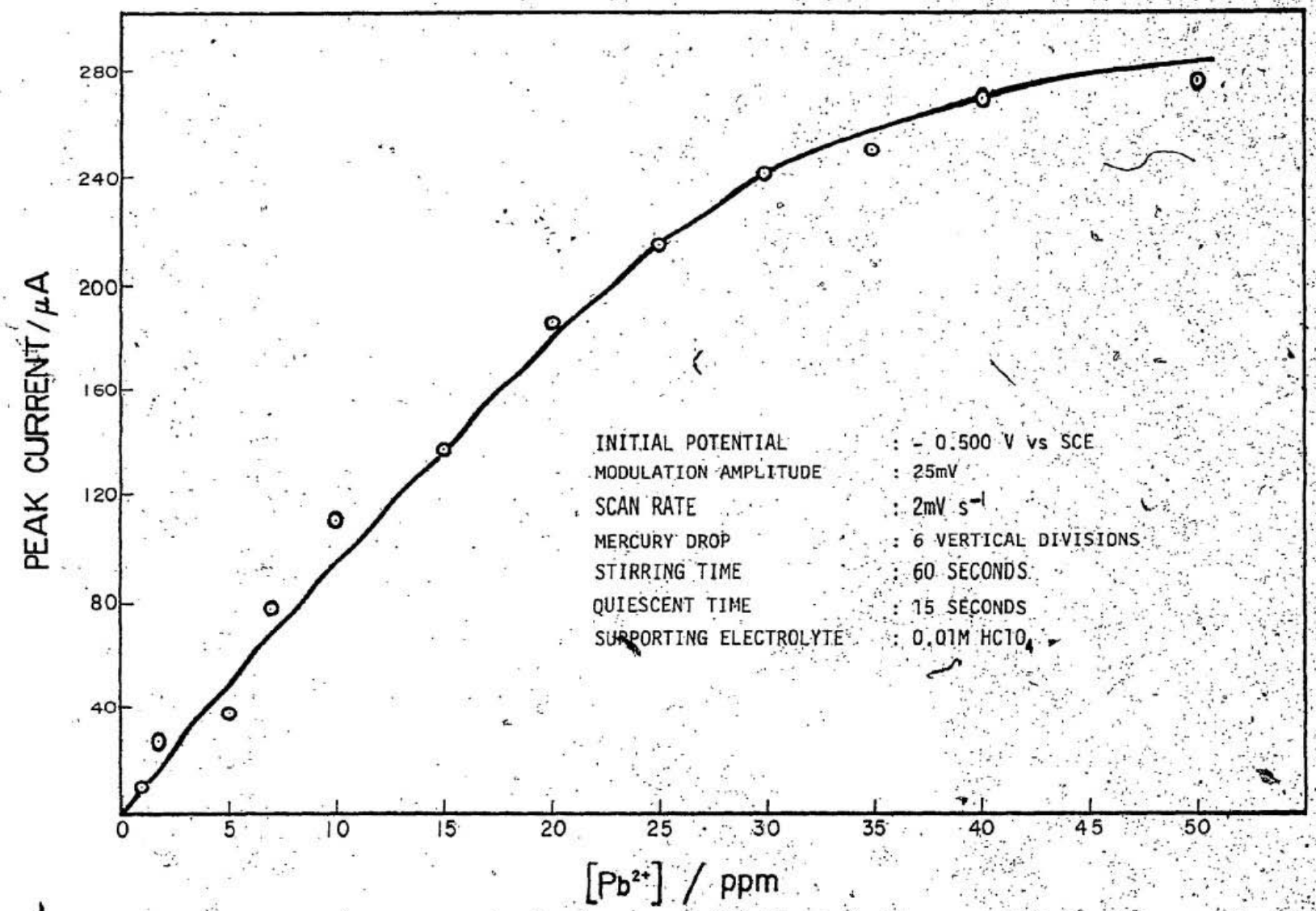

FIG. 9. ANALYSIS OF STANDARD Pb^{2+} SOLUTION USING DIFFERENTIAL PULSE ANODIC STRIPPING (CONCENTRATION RANGE : 1.0 TO 50 ppm)

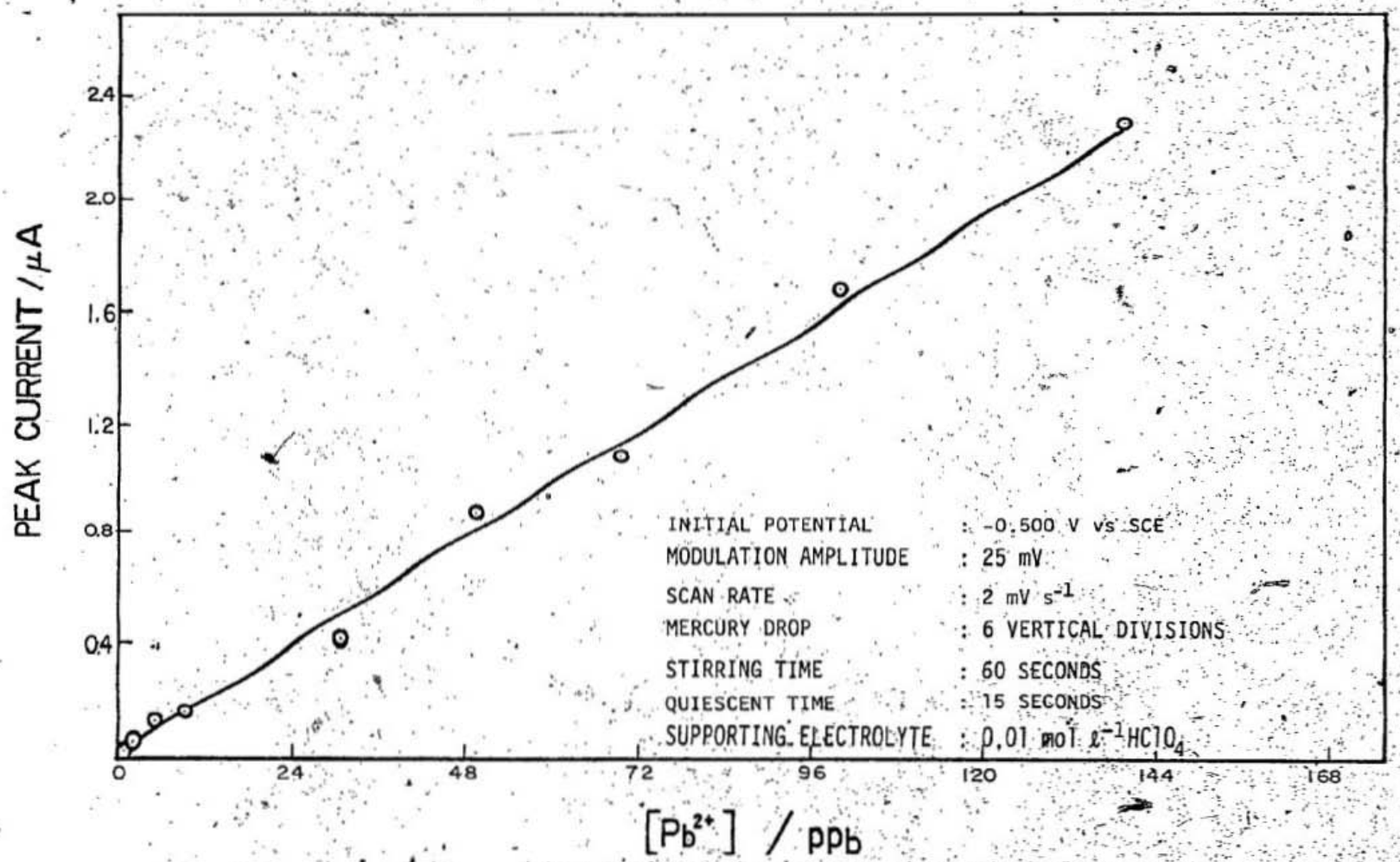

Fig. 10. CALIBRATION CURVE FOR Pb^{2+} ANALYSIS BY DIFFERENTIAL PULSE ANODIC STRIPPING (CONCENTRATION RANGE : 1.0 TO 140 PPb).

TABLE 1

(a) CALIBRATION DATA FOR DPASV ANALYSIS OF Pb^{2+} IN 0.01 mol ℓ^{-1} $HClO_4$ FROM 1 ppb to 140 ppb

Concentration/ppb	1	2	5	10	30	50	50	70	100	140
Peak current/μA	0.027	0.046	0.112	0.150	0.415	0.87	0.83	1.07	1.68	2.28

(b) CALIBRATION DATA FOR DIFFERENTIAL PULSE POLAROGRAPHY ANALYSIS OF Pb^{2+} IN 0.01 mol ℓ^{-1} $HClO_4$ FROM 0.1 ppm to 60 ppm

Concentration/ppm	0.1	0.1	0.2	0.5	0.5	0.7	0.7	1	1	2	2	5	5
Peak current/μA	0.022	0.023	0.042	0.103	0.110	0.144	0.148	0.21	0.21	0.393	0.398	0.99	0.99

Concentration/ppm	7	10	15	20	25	30	35	50	60
Peak current/μA	1.4	2.0	3.0	4.0	5.0	6.0	7.05	10.1	12.4

electrode operation. Preparation of standard solutions, deoxygenation of solution, washing of cell and electrodes, etc. were similar to those described under DPASV in previous section. After connection of the PAR 174 through the standard drop time connector, the electrode connections were made. The following instrumental settings were used.

Scan rate	2 mV s^{-1}
Scan direction	"-"
Range	1.5 V
Initial potential	"-0.25 V vs SCE"
Modulation amplitude	25 mV
Operation mode	differential pulse
Current range	various
Output offset	off
Display direction	"+"
Selector	off
Low pass filter	off
Drop time	2s
Pushbutton	initial
Recorder	x-axis 100 mV $inch^{-1}$ y-axis 1V $inch^{-1}$

After setting the instrument, the selector switch was turned to "External cell" and about 30 drops were allowed to fall in order to bring the memory circuit to full charge. Then the recorder pen was lowered and the keyboard button (scan) was pressed.

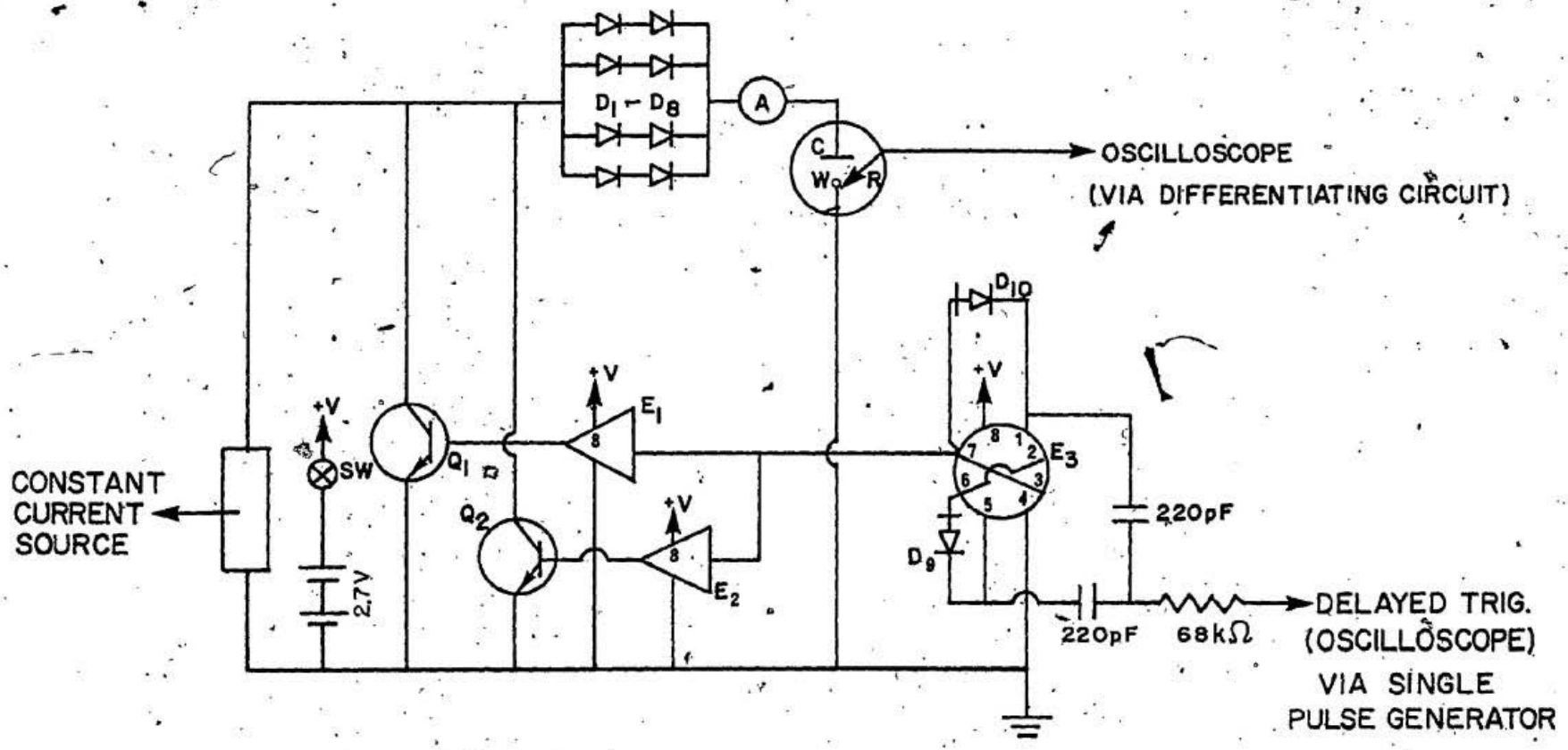

Fig. 37. Schematic of transistor switch: W=cathode, C=counter electrode, R=reference electrode, $D_1 \cdots D_{10}$-diodes, E_1, E_2, E_3-micrologic elements, Q_1 and Q_2-transistors, SW-power switch, A-current meter.

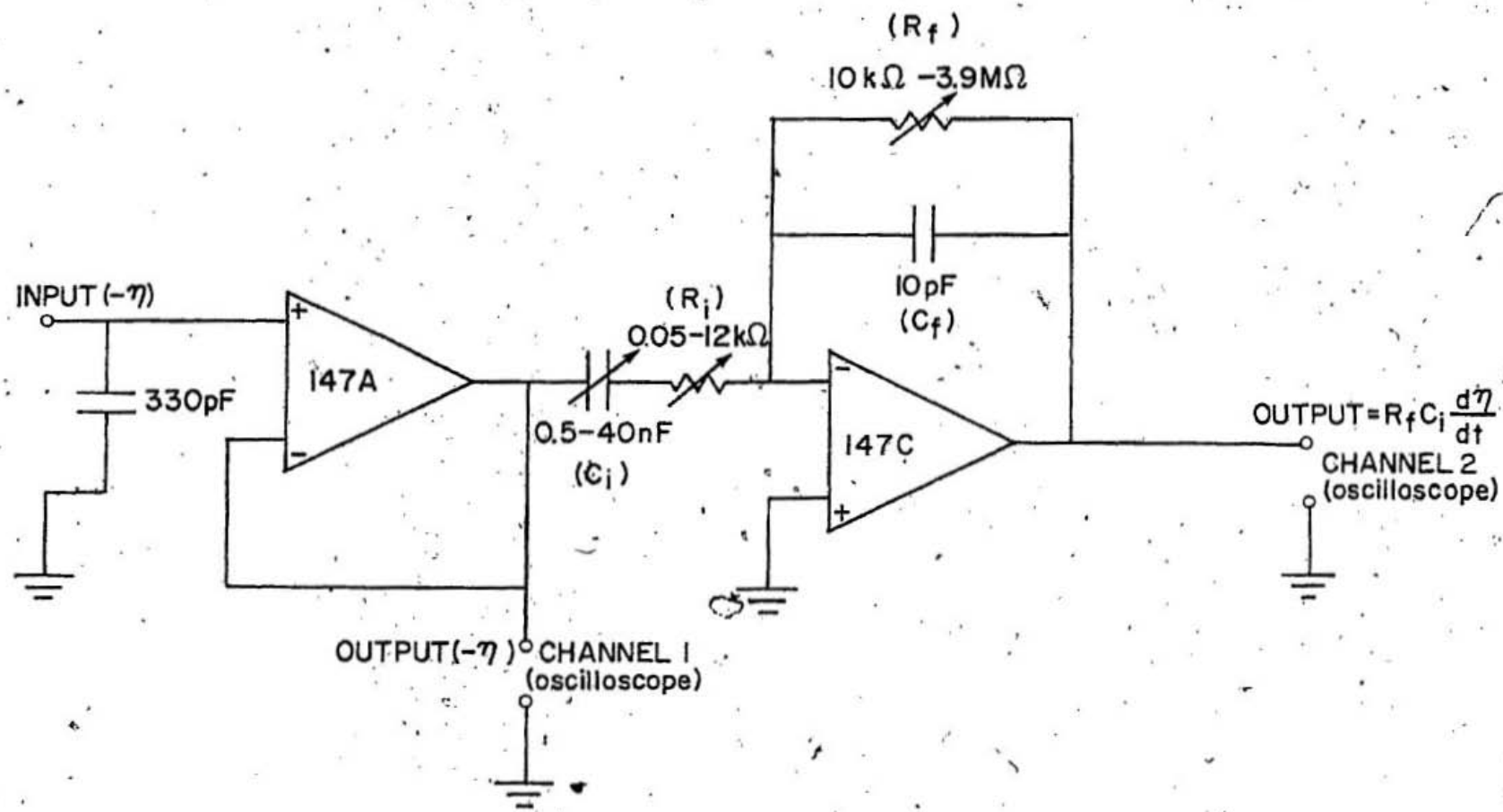

Fig. 38. DIFFERENTIATING CIRCUIT.

forward-biased. Micrologic elements E_1 and E_2 (type MC 900G) serve as buffer elements and ensure that enough current is supplied to Q_1 and Q_2. The micrologic elements are powered by two mercury batteries in series, i.e. by 2.7 V. The 68 kΩ resistance serves to isolate the bistable circuit from the pulse generator (General Radio 1340 Pulse Generator which was also fed to the 5B42 delaying time base in a Tektronix 5441 oscilloscope). The +V signal was connected to pin 8 of E_1, E_2 and E_3 (Fig. 37). The bistable was triggered by the delay trigger (from the pulse generator) that supplied a sharp positive-going spike of about 10 V at the end of the delay period to interrupt the current to the cell. The next pulse turned the transistors off and the current to the cell was restored.

The differentiating circuit (see Fig. 38) consisted of an operational amplifier (Analog Devices 147A) used in a non-inverting circuit to provide both high input impedence ($10^{12}\Omega$) and fast response (10 MHz) at the input stage of the oscilloscope. To improve the stability of the non-inverting amplifier and to eliminate the high frequency noise, a capacitance of 330 pF was inserted between the + terminal of the 147A amplifier and ground. The differentiating unit of the circuit consisted of an operational amplifier (Analog Devices 147C), having similar characteristics to the 147A, but superior in certain respects, e.g. input offset voltage of ±2 μV K^{-1} of 147C compared with ±15 μV K^{-1} of 147A, in an inverting circuit. A known variable input capacitor C_i (0.5 -

40 nF) was in series with an ohmic feed-back link, R_f (10 kΩ - 3.9 MΩ), which was itself between the input and output of the amplifier 147C. A small noise-suppression capacitor C_f (10 pF) in parallel with the feed-back resistor R_f increased the stability of the circuit and improved the transient response. The variable resistor* R_i (0.05 kΩ-12 kΩ) in series with C_i at the input stage of the 147C amplifier was used to isolate the capacitive load at high frequency and to improve the stability of the circuit.

The input signal ($-\eta$) through the 147A (output = $-\eta$) was fed to channel 1 of a Tektronix 5A48 dual trace plug-in amplifier in a Tektronix 5441 oscilloscope, and its derivative obtained from the differentiating unit, output = $R_f C_i (d\eta/dt)$, fed simultaneously to channel 2 of the plug-in. Both signals were photographed simultaneously with Polaroid type 667 film in a Tektronix oscilloscope camera C-12. The magnitude of $R_f C_i$ was kept as small as possible to achieve the best performance of the differentiator. The accuracy of the method was examined using an Exact type 301 function generator to produce a variable linear saw-tooth input signal, the slope of which, $\frac{dV}{dt}$, could be measured from oscillographic photographs. The differential signal was switched in during the course of a signal saw-tooth transient and the magnitude of the differential coefficient was proportional to the height of the discontinuity exhibited by the

---

*Generally, R_i = 1 kΩ or 4.9 kΩ (i.e. $R_f \gg R_i$) to minimize the effect of this resistor on the output voltage.

channel 2 trace from the base line. The differential sweep rates, $\frac{dV}{dt}$, were calculated using the height of the discontinuity, i.e. output signal, exhibited by the channel 2 trace and then using the relation, channel 2 signal $= R_f C_i (\frac{dV}{dt})$. Such calibration data are shown in Table 16 for a range of voltage sweep rates from 6.4 to 5.0 x 10^4 V s^{-1}. It is evident from Table 16 that agreement within 1-2% was obtained between the known voltage sweep rate, $\frac{dV}{dt}$, and the calculated value, $\frac{dV}{dt}$, for all the sweep rates examined. The linear relation between the calibration $\frac{dV}{dt}$ obtained from the slope of saw-tooth signal and $\frac{dV}{dt}$ calculated from C_i and R_f from differentiated voltage signal is shown in Figure 39. The least squares value of the slope of Figure 39 is 1.0079 ± 0.0025, the corresponding intercept is -0.024 ± 0.008, i.e. zero, within experimental error.

A typical record of overvoltage decay (channel 1 upper curve) and of its differentiated signal (channel 2 lower curve) are shown in Figure 40 (under real experimental conditions). From the height of the discontinuity exhibited by the channel 2 trace, i.e. output signal and knowing the values of R_f and C_i by using the equation, output signal $= R_f C_i (\frac{d\eta}{dt})$, the initial slope, $(\frac{d\eta}{dt})_{t=0}$, (i.e. the slope immediately after the interruption of polarising current) of the overvoltage decay curve was obtained. Knowing $(\frac{d\eta}{dt})_{t=0}$, the electrode capacitance, $C_{expt.}$, was calculated using equation (32), i.e. $C_{expt} = \frac{-i}{(\frac{d\eta}{dt})_{t=0}}$ where -i is the cathodic current density at the time of current interruption, t = 0 (t is the time elapsed after the current interruption).

TABLE 16 CALIBRATION DATA FOR THE DIFFERENTIAL GALVANOSTATIC METHOD

Time base/ ms div.$^{-1}$	Saw-tooth signal		Differential curve				
	Vertical sensitivity/ V div.$^{-1}$	$\frac{dV}{dt}$/V s^{-1}	R_f/kΩ	C_i/nF	Vertical sensitivity/ V div.$^{-1}$	Output signal/mV $= R_f C_i (\frac{dV}{dt})$	$\frac{dV}{dt}$/V s^{-1} from R_f and C_i values
1×10^2	1	6.4	2.24×10^3	10.20	0.05	150	6.5
5×10^1	1	1.4×10^1	9.99×10^2	1.11	0.05	150	1.5×10^1
5×10^1	1	1.2×10^1	2.24×10^3	10.2	0.05	275	1.2×10^1
2×10^1	1	3.7×10^1	3.60×10^3	39.1	1	5800	4.1×10^1
2×10^1	1	2.9×10^1	9.99×10^3	20.2	0.1	600	3.0×10^1
1×10^1	1	6.7×10^1	9.99×10^1	2.1	0.005	14	6.7×10^1
5	1	1.3×10^2	9.99	39.1	0.02	52	1.3×10^2
1	1	6.0×10^2	4.99×10^1	10.2	0.05	300	5.9×10^2
1×10^{-1}	1	5.8×10^3	3.0×10^1	1.11	0.05	190	5.7×10^3
5×10^{-2}	1	8.3×10^3	9.99	1.11	0.02	91	8.2×10^3
2×10^{-2}	1	1.3×10^4	9.99	1.11	0.05	140	1.3×10^4
2×10^{-2}	1	3.0×10^4	9.99	0.856	0.05	250	2.9×10^4
1×10^{-2}	1	5.0×10^4	9.99	0.663	0.05	310	4.7×10^4

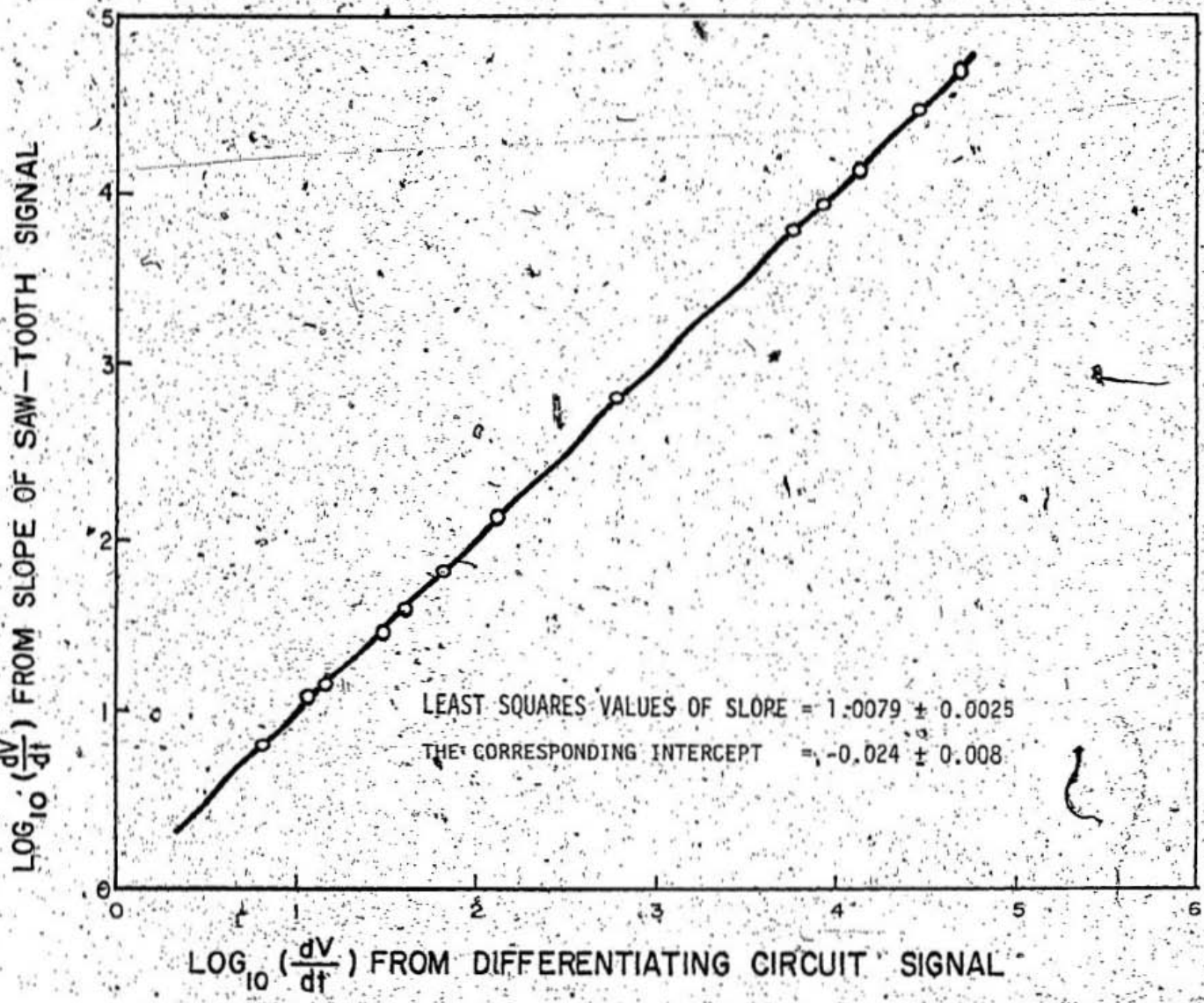

Fig. 39. LINEAR RELATION BETWEEN $\frac{dV}{dt}$ OF CALIBRATION (SAW-TOOTH SIGNAL) AND $\frac{dV}{dt}$ CALCULATED FROM R_f AND C_i FROM THE DIFFERENTIATED VOLTAGE SIGNAL (LOG SCALES)

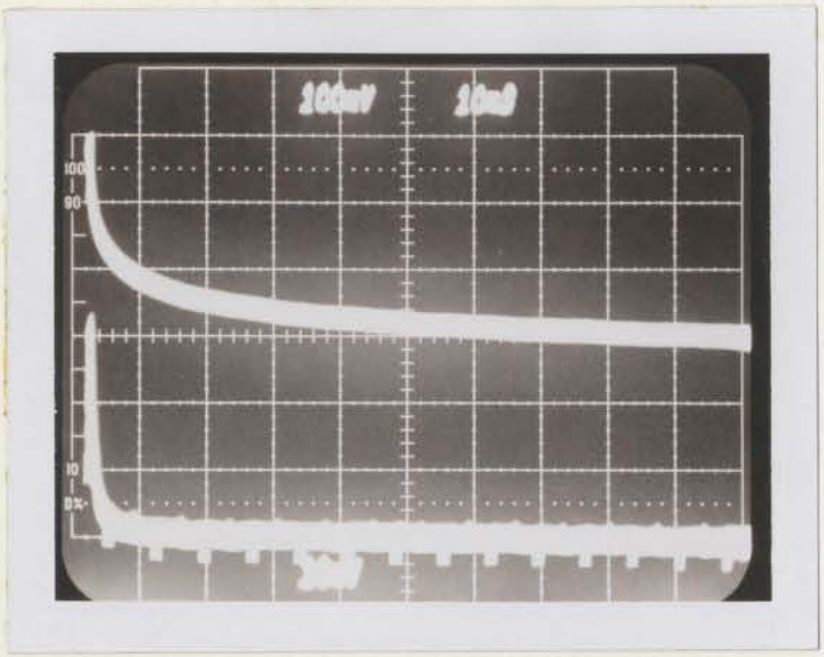

Fig. 40. OVERVOLTAGE DECAY SIGNAL (UPPER CURVE, CHANNEL 1) AND ITS DIFFERENTIATED SIGNAL (LOWER CURVE, CHANNEL 2). NUMBERS ON THE GRID ARE VOLTAGE ON ORDINATE(100 AND 10 mV div.$^{-1}$ FOR CHANNEL 1 AND 2, RESPECTIVELY) AND TIME BASE ON ABSCISSA : 10 ms div.$^{-1}$

In capacitance measurements, the silver electrodes of 0.125 mm thickness, were cathodised galvanostatically (initially at 30 μA to 1 mA). Capacitance measurements were begun after passage of cathodic current for about 1 to 2 h. Then, the overvoltage decay and its derivative were photographed, as described earlier. Also, $-\eta$ corresponding to the cathodic current density, $-i$, at the time of the current interruption, $t = 0$, was recorded. Thus, the calculated $C_{expt.}$ using measured $\left(\frac{d\eta}{dt}\right)_{t=0}$ and $-i$ with equation (32) correspond to $-\eta$ recorded at $t = 0$. Later, the steady-state current density was increased to other values in a step-wise manner and kept constant at the new current density for a pre-determined time (which ranged from 3 to 8 minutes). At the end of the pre-determined time, open-circuit decays were followed from each polarisation current. The overvoltages at the instant of current interruption, at each current, were also recorded. Thereby, $C_{expt.}$ was calculated at different $-\eta$. This sequence of measurements was repeated up to 5 consecutive days.

In order to diminish probable errors from the instrumentation, the capacitance measurements were usually carried out with R_f, C_i and the voltage and time-base settings of the oscilloscope kept constant from the first up to last capacitance measurement at a particular current density in a given experiment.

Because of the low hydrogen overvoltages ($-\eta < 140$ mV) on silver at cathodic c.d.'s of $-i < 0.69$ mA cm^{-2}, the measurements of the signal fed to channel 2 of the oscilloscope (using high values of R_f and C_i) were of low accuracy. Therefore, in this work the capacitances determined at such low cathodic currents are not reported.

Chapter 3

RESULTS

In this chapter, the results obtained from the study of hydrogen adsorption and absorption by silver in acid media are given.

The main cell (see Fig. 34) was designed originally for long term hydrogen overvoltage measurements on silver and to study hydrogen diffusion through silver. It was later used for measuring capacitance at silver cathodes.

Experiments A1 to A7 were to investigate the permeation of cathodically generated hydrogen through silver foils as well as to measure hydrogen overvoltages, while in experiments A8 to A10 only the variation of overvoltage with time at constant cathodic current density was recorded. Experiment A1 was carried out with unpurified 1 mol ℓ^{-1} $HClO_4$ and a non-electropolished silver electrode. Experiments A2 and A3 were also carried out with unpurified 1 mol ℓ^{-1} $HClO_4$ but with the silver electrodes electropolished <u>in situ</u>. Experiments A4 to A10 were carried out using pre-electrolysed 1 mol ℓ^{-1} $HClO_4$ and electropolished silver electrodes. Electrode A4 was electropolished <u>in situ</u> but A5 to A10 were electropolished in the separate cell of Figure 35. Charcoal-cleaned pre-electrolysed acid was used only in experiment A10.

In an attempt to discover whether the capacitance of silver electrodes increases with total cathodic charge as Rao (61) found with lead electrodes, some other experiments (B1 to B5) involved

measurements of hydrogen overvoltage as well as electrode capacitance at a silver cathode in acid solutions. Experiment B1 was carried out using unpurified 1 mol ℓ^{-1} $HClO_4$ mainly to check the capacitance circuitry. Experiments B2 and B3 were carried out with charcoal-cleaned pre-electrolysed 1 mol ℓ^{-1} $HClO_4$ (pre-electrolysed at i = -20 to -30 mA cm^{-2} for 4 days). The capacitance measurements of experiment B4 and B5 were made with charcoal-cleaned 0.1 mol ℓ^{-1} $HClO_4$ pre-electrolysed for 4 days in experiment B4 and for 10 days in B5. The preparation of electrodes was similar to that described for experiments A5 to A10.

The results of this chapter will be considered under three headings:

I. Electrolytic Hydrogen Diffusion Through Silver.

II. Hydrogen Overvoltage Measurements at a Silver Cathode.

III. Capacitance Measurements at a Silver Cathode.

I. Electrolytic Hydrogen Diffusion Through Silver

The limited results of the diffusion study are presented here. Let us first consider the difficulties which have been overcome in the permeation study. The permeation study was begun following the same procedure as used by Cadersky et al (49) for studying electrolytic hydrogen diffusion through lead, i.e. 1 mol ℓ^{-1} $HClO_4$ and 0.2 mol ℓ^{-1} KOH were the electrolytes used for cathodic and diffusion sides of the silver foil, respectively, and the diffusion side of the silver foil was potentiostated at +200 mV versus a hydrogen reference electrode. By applying +200 mV potential on the diffusion side, the Keithley 150B Microvolt-Ammeter indicated a cathodic current instead of an anodic current. Therefore, on increasing the anodic potential from 200 to 650 mV, the current on the diffusion side changed its sign from negative to positive. At +650 mV, some sort of transient signal was recorded. In order to determine whether these transients actually corresponded to the permeation of hydrogen or to some anodic reaction of silver and production of electrons, chronopotentiometry was carried out on the diffusion side of silver in 0.2 mol ℓ^{-1} KOH at a constant -10 μA cathodic current. The result of this investigation is shown in Figure 41. It is apparent from Figure 41 that at a positive potential of +650 mV an oxide film was formed on silver in 0.2 mol ℓ^{-1} KOH. The formation of oxide film on silver at relatively high positive potentials in solutions of high pH was confirmed by the potential-pH diagram of Pourbaix (150). Therefore, 0.2 mol ℓ^{-1} KOH was not suitable for the purpose of the permeation study for silver electrodes. The next step was to find out which electrolyte was most suitable for

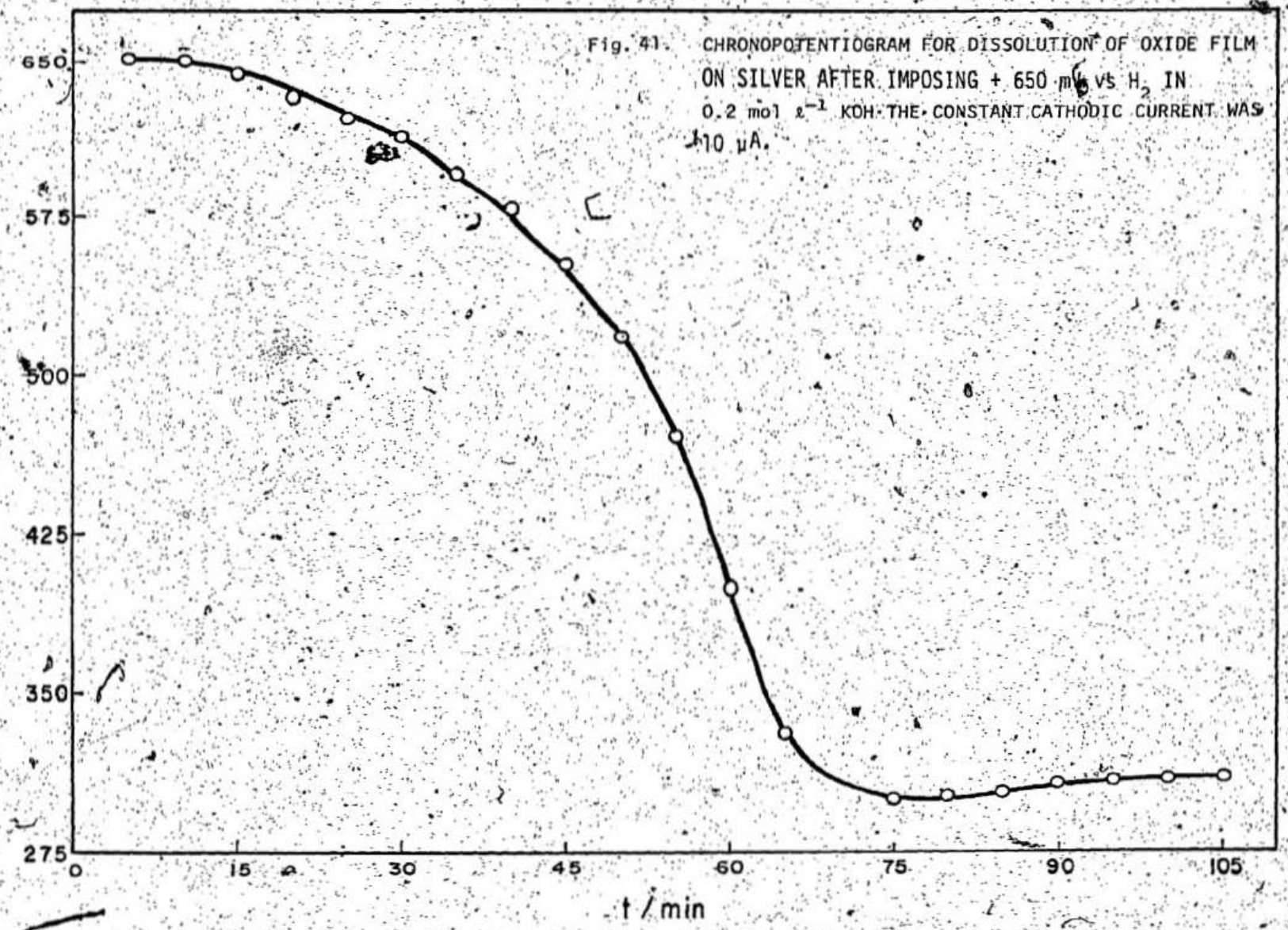

Fig. 41. CHRONOPOTENTIOGRAM FOR DISSOLUTION OF OXIDE FILM ON SILVER AFTER IMPOSING + 650 mV vs H_2 IN 0.2 mol ℓ^{-1} KOH. THE CONSTANT CATHODIC CURRENT WAS 10 μA.

the diffusion side of the silver foils. Solutions of KOH and NaOH with concentrations of less than 0.2 mol ℓ^{-1} were examined in various trial experiments. Anodic polarisation (applying anodic current and measurements of potential) and subsequent chronopotentiometry showed that even at low anodic currents of the order of a few microamperes, the formation of an oxide film occurred on silver using these electrolytes. Some other trial experiments were carried out using $NaClO_4$ plus $HClO_4$ at various pH's and finally it was concluded that an electrolyte of 0.2 mol ℓ^{-1} $NaClO_4$ plus $HClO_4$ to bring it to pH = 4 was suitable for the diffusion side of the silver electrode. Using this electrolyte, it was possible to apply a positive potential of up to 780 mV versus H_2 electrode on silver without danger of formation of any oxide film or anodic dissolution of silver. The results of this trial were theoretically confirmed by considering a potential-pH diagram of Pourbaix (150).

Several experiments (A1 to A7) were carried out to look for permeation of hydrogen through silver using a solution of 0.2 mol ℓ^{-1} $NaClO_4$ plus $HClO_4$ to pH = 4 for the diffusion side of the cell (see Fig. 34) and maintaining a positive potential of 700 mV. After establishing a steady-state anodic current on the chart paper of the recorder, the cathodic current was changed in a step-wise manner, e.g. from 0.1 to 10 μA, 10 to 100 μA, 100 μA to 1 mA, 1 to 10 mA and 10 to 45 mA. This procedure was also carried out in the reverse order of cathodic currents. Only in experiment A5, did the transients have the theoretically expected shape (see Fig. 5) and these were accepted for determination of the diffusion current.

For calculation of the diffusion coefficient, D_H, of hydrogen atoms through silver, the rising transient equation (41), i.e. $[\ln(\frac{J_t - J_\infty}{J_\infty}) = \ln(1 - e^{-3t/t_o} + e^{-8t/t_o} - \cdots) + \ln 2 - t/t_o]$ was used. J_t and J_∞ are the diffusion current at time t and at the steady-state, respectively, t_o has a value of $\frac{L^2}{\pi^2 D_H}$ where L is the thickness of the membrane. A plot of $-\log_{10} (\frac{J_\infty - J_t}{J_\infty})$ against time is shown in Figure 42. From the gradients, i.e. $\frac{1}{2.303\ t_o}$, D_H values of 2.3×10^{-6}, 4.2×10^{-6} and 4.6×10^{-6} $cm^2\ s^{-1}$ were obtained for cathodic currents of 100 μA, 1 mA and 10 mA, respectively. For calculation of the concentration of hydrogen just inside the silver foil, C_o, Fick's first law, i.e. equation (36) $J_\infty = \frac{FD(C_o - C_L)}{L} = \frac{FDC_o}{L}$ if $C_L = 0$ at the diffusion side) was applied under steady-state diffusion conditions and C_o values of 5×10^{-8} to 8×10^{-8} g atom H cm^{-3} of silver were obtained.

The calculated diffusion coefficient was higher than had been expected, suggesting that the diffusion of hydrogen through silver is faster than diffusion of hydrogen through lead [D_H in Pb $\simeq 1.2 \times 10^{-7}$ $cm^2\ s^{-1}$ (49)]. Theoretically, it is expected that diffusivity of hydrogen through silver should be less than through lead, because lead is a softer metal than silver.

Eichenauer et al (112) measured the diffusivity of hydrogen in silver in gas phase studies. From the relationship between diffusivity and $\frac{1}{T}$, Einziger (151) deduced an expression over the temperature range 661 K to 873 K for the diffusion coefficient

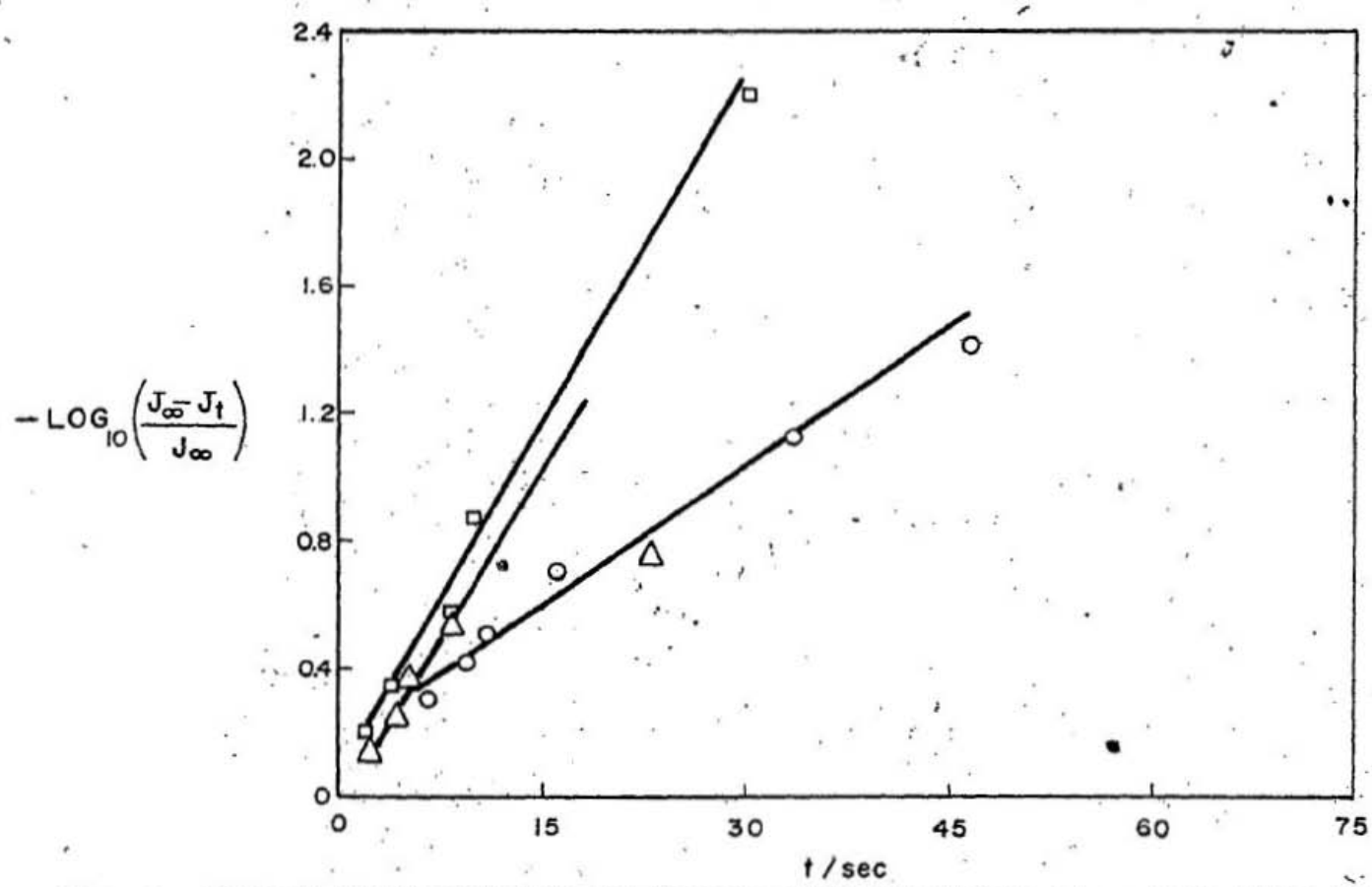

Fig. 42. PLOTS OF RISING TRANSIENTS FOR HYDROGEN PERMEATION THROUGH 0.1 mm THICK SILVER FOIL CATHODISED IN 1 mol ℓ^{-1} $HClO_4$ SUCCESSIVELY AT 100μA, ○; 1mA, △; 10mA, □; J_t AND J_∞ ARE ANODIC CURRENT DENSITIES(μA cm^{-2}) ABOVE BACKGROUND, AT TIME t AFTER APPLICATION OF CATHODIC CURRENT AND AT STEADY STATE, RESPECTIVELY.

$$D_H = 2.82 \times 10^{-3} \exp\left(\frac{-7500}{RT}\right) \qquad (3.1)$$

Thomas (113) used a mass spectrometer and measured the solubility of hydrogen in silver over the temperature range 873 K to 1073 K. From the relationship between the solubility and $\frac{1}{T}$, Einziger (151) obtained an expression similar to that of the diffusion equation for the solubility of hydrogen in this temperature range

$$C_o = 4.569 \exp\left(-\frac{15725}{RT}\right) \qquad (3.2)$$

If we assume that these two equations (3.1) and (3.2) are valid for room temperature, the diffusivity and solubility of hydrogen in silver at 298 K would be 9×10^{-9} cm^2 s^{-1} and 1.9×10^{-15} g atom H cm^{-3} of silver, respectively. The predicted diffusion coefficient and solubility are lower than the experimental values. Because of this discrepancy and also since duplication of the experimental results was not successful, it is difficult for us to accept that the values of D_H and C_o obtained by us are correct.

The predicted D_H and C_o using theoretical expressions suggest that since diffusion of hydrogen in silver is very slow and the solubility of hydrogen atoms in silver is very low at room temperature, it might be desirable to use a more sensitive technique for evaluation of D_H such as the alternating current method proposed recently by Kedzierzawski et al (47) and pre-electrolysed solution for the diffusion side of the silver foil. A better designed apparatus might also be helpful.

II. Hydrogen Overvoltage Measurements

The results of this section will be considered under three different headings: (a) hydrogen overvoltage, $-\eta$, as a function of cathodic charge passed, $-Q$, (b) overshoot hysteresis and (c) Tafel plots.

(a) Overvoltage as a Function of Total Cathodic Charge

In experiment A1, $-\eta$ increased with time of cathodisation. As indicated in Table 17, $-\eta$ increased with $-Q$, e.g. after about one hour of cathodisation at 116 μA cm^{-2}, $-\eta$ had increased from 76 mV to 156 mV at $-Q$ = 544 coulombs. An increase of $-\eta$ with $-Q$ was also observed at higher c.d.'s on this electrode, e.g. at -11.56 mA cm^{-2}, $-\eta$ had increased from its initial value of 387 mV to 407 mV at the same value of $-Q$.

In experiments A2 and A3, $-\eta$ decreased rather than increased with $-Q$. Table 17, which gives some examples of current densities and overvoltages at various cathodic charges for experiments A1 to A6, indicates that with electrode A2 at -11.56 mA cm^{-2}, $-\eta$ decreased from its initial value of 323 mV to 232 mV while $-Q$ increased to 127 coulombs. This phenomenon of decreasing $-\eta$ with $-Q$ was observed at every c.d. studied in experiments A2 and A3. This decrease of $-\eta$ with $-Q$ is attributed to the progressive removal from the solution of Ag^+ ions, presumably left after in situ electropolishing and washing of electrodes A2 and A3.

Experiments A4, A5 and A6 differed from experiments A1 to A3 in that pre-electrolysed solution was used. As indicated in Table 17, at all current densities studied in experiment A4, the overvoltage

TABLE 17. HYDROGEN OVERVOLTAGES FOR SILVER (THICKNESS = 0.1 mm, PURITY 99.97%) IN 1 mol ℓ^{-1} $HClO_4$ IN EXPERIMENTS A1 TO A6.

Experiment number	Current density to which quoted η's correspond/ mA cm^{-2}.	Initial $-\eta$/mV	Final $-\eta$/mV.	Final $-Q$/Coulombs	Condition of electrodes and solutions
A1	0.116	76	156	544	Electrode was not electropolished and solution was not pre-electrolysed.
	11.56	387	407	545	
A2	0.01	64	12	124	Electropolished in situ (500 mA for 27 ± 3 seconds in 1 mol ℓ^{-1} $HClO_4$) and not pre-electrolysed 1 mol ℓ^{-1} $HClO_4$ was used
	11.56	323	232	127	
A3	0.116	136	25	52	Electropolished in situ (500 mA for 27 ± 3 seconds in 1 mol ℓ^{-1} $HClO_4$) and not pre-electrolysed 1 mol ℓ^{-1} $HClO_4$ was used.
	1.16	235	127	50	
A4	1.16	209	236	94	Electropolished in situ (500 mA for 27 ± 3 seconds in 1 mol ℓ^{-1} $HClO_4$) and 1 mol ℓ^{-1} $HClO_4$, pre-electrolysed at 12-30 mA cm^{-2} for 4 days.
	5.78	275	301	96	
	23.1	329	354	105	

TABLE 17 (cont'd)

Experiment number	Current density to which quoted η's correspond/ mA cm^{-2}	Initial $-\eta$/mV	Final $-\eta$/mV	Final $-Q$/Coulombs	Condition of electrodes and solutions
A5	1.16	194	226	272	Electropolished (1A for 15 ± 3 seconds in 1 mol ℓ^{-1} $HClO_4$) and 1 mol ℓ^{-1} $HClO_4$, pre-electrolysed at 12-30 mA cm^{-2} for 4 days.
	11.56	276	306	274	
A6	0.116	148	194	965	Electropolished (1A for 15 ± 3 seconds in 1 mol ℓ^{-1} $HClO_4$) and 1 mol ℓ^{-1} $HClO_4$, pre-electrolysed at 20 mA cm^{-2} for 3 days.
	1.16	244	289	965	
	11.56	335	375	697	

rose by 26 ± 1 mV with the cathodic passage of some 100 coulombs. A systematic increase of $-\eta$ with $-Q$ was also observed in experiments A5 and A6 which differed from A4 in that a separate cell was used for electropolishing. Table 17 shows that passage of 273 coulombs at $i = -1.16$ mA cm^{-2} in experiment A5 led to an increase of $-\eta$ of 31 ± 1 mV, while in A6 passage of 965 coulombs caused $-\eta$ to increase by 45 ± 1 mV. The initial overvoltage measurements in unpurified solution were higher than in purified solutions, e.g. in experiments A1 and A5 at $i = -11.56$ mA cm^{-2}, the overvoltages were 387 mV and 276 mV, respectively. This discrepancy was also after the passage of some cathodic charge (see Table 17).

In an attempt to clarify the relationship between overvoltage and the quantity of charge passed cathodically, it was decided to run three separate experiments (A8 to A10), in which the cathodic current was kept constant at 1.16 mA cm^{-2}. Table 18 indicates the overvoltages observed initially, i.e. after ca. 30 minutes and after various amounts of charging. It is apparent from Table 18 that the initial overvoltage for electrode A8, i.e. 233 mV is greater than that for electrodes A9 and A10, i.e. 206 ± 1 mV. It may be due to the fact that experiment A8 was studied in 1 mol ℓ^{-1} $HClO_4$ that had been pre-electrolysed for 3 days at c.d.'s of 10-20 mA cm^{-2}, while the solution for A9 and A10 had been pre-electrolysed for longer periods (4 days) at c.d.'s of 10-20 and 10-30 mA cm^{-2}, respectively (the comparison of overvoltage in A1 and A5 can also confirm this statement). Table 18 indicates that the initial overvoltage for

TABLE 18 HYDROGEN OVERVOLTAGES FOR SILVER ELECTRODES A8 AND A9 (THICKNESS = 0.1 mm, PURITY 99.97%) AND FOR SILVER ELECTRODE A10 (THICKNESS = 0.125 mm, PURITY 99.99^{+}%) IN 1 mol ℓ^{-1} $HClO_4$ AT CONSTANT CATHODIC CURRENT DENSITY OF 1.16 mA cm^{-2}.

Experiment number	Initial $-\eta$/mV after ca. 30 min. of cathodisation	$-\eta$/mV at $-Q$ = 37 C	Final		Condition of electrodes and solutions
			$-\eta$/mV.	$-Q$/C	
A8	233	248	260	335	Electropolished (1A for 15 ± 3 seconds in 1 mol ℓ^{-1} $HClO_4$) and 1 mol ℓ^{-1} $HClO_4$, pre-electrolysed at 10-20 mA cm^{-2} for 3 days.
A9	207	220	240	276	Electropolished (1A for 15 ± 3 seconds in 1 mol ℓ^{-1} $HClO_4$) and 1 mol ℓ^{-1} $HClO_4$ pre-electrolysed at 10-20 mA cm^{-2} for 4 days.
A10	208	231	255	277	Electropolished (1A for 15 ± 3 seconds in 1 mol ℓ^{-1} $HClO_4$) and 1 mol ℓ^{-1} $HClO_4$, pre-electrolysed at 10-30 mA cm^{-2} for 4 days. Adsorption cleaning with activated charcoal.

electrodes A9 and A10 (the only expt. in which activated charcoal was also used) are identical within experimental error but after passage of some 37 coulombs at constant -1.16 mA cm^{-2}, the overvoltages had increased by different amounts (13 mV and 23 mV, respectively, for electrodes A9 and A10). A larger difference is observed for the final overvoltages of these two electrodes after the same amount of charging (276 ± 1 coulombs). The larger increase of overvoltage for the same amount of charging could be because of the use either of higher purity silver or of activated charcoal, or both in experiment A10.

Variation of $-\eta$ with $\log_{10}(-Q)$ for electrodes A8, A9 and A10 is shown in Figure 43, which indicates that the overvoltage at -1.16 mA cm^{-2} initially fell, as had been observed by Gossner et al (117), and then rose continuously with $-Q$ finally reaching a plateau. The same trend was also observed by Antoniou and Wetmore (116). The initial fall could be associated with the removal of oxygen from the solution. It is obvious from Figure 43 that a similar but not identical increase of $-\eta$ with $-Q$ occurred in each experiment and the slopes of $-\eta$ versus $\log_{10}(-Q)$ range from 4-10 mV, obtained for small amounts of charge, and from 17 to 49 mV for larger amounts of charge. Moreover, the slopes in Figure 43 for the same range of $-Q$ for different experiments are almost the same. This suggests that the phenomenon which causes the increase of $-\eta$ with $-Q$ occurred on all three electrodes. The changes in slope indicate that the charging up

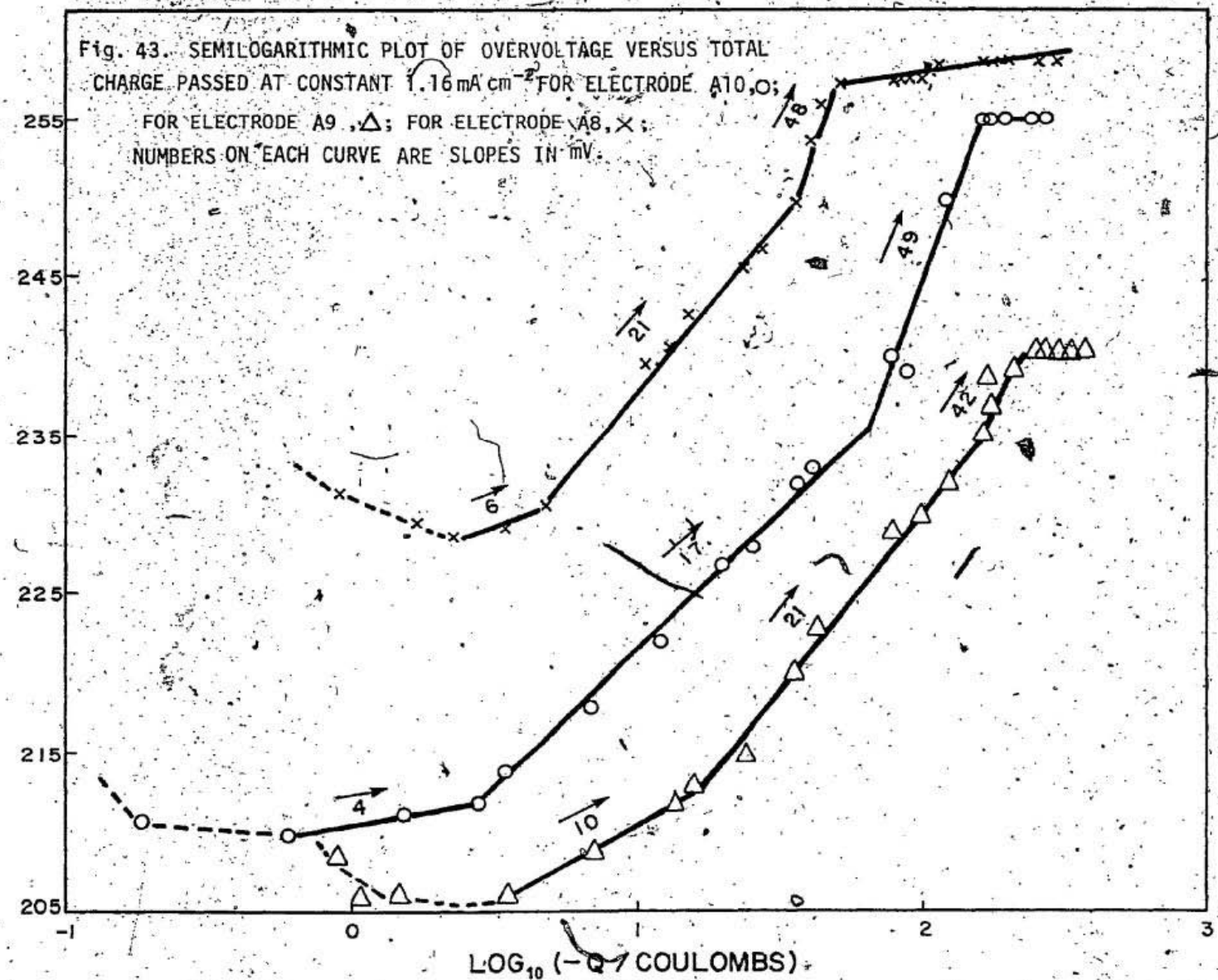

Fig. 43. SEMILOGARITHMIC PLOT OF OVERVOLTAGE VERSUS TOTAL CHARGE PASSED AT CONSTANT 1.16 mA cm^{-2} FOR ELECTRODE A10, ○; FOR ELECTRODE A9, △; FOR ELECTRODE A8, ×; NUMBERS ON EACH CURVE ARE SLOPES IN mV.

of the double layer is not the only process occurring during this increase of overvoltage.

In general, the trend of overvoltage increasing during long periods of cathodic polarisation was common for all silver electrodes. The increase of overvoltage with -Q may perhaps be attributed to the adsorption or absorption of hydrogen atoms on or in silver electrodes during cathodic h.e.r. in much the same way as Ives and Smith (9,107) suggested for the decrease of overvoltage at lead.

(b) Overshoot Hysteresis

Ives and Smith (9,107) observed overshoot hysteresis at lead cathodes defined as follows: for each step-change of the current from a steady-state the immediate potential jump was followed by an exponential change of potential in the reverse direction. Overshoot hysteresis was also seen in the present work. Current changes were made from steady-state overvoltages. Typical examples for increasing and decreasing c.d.'s for electrodes A7, A9 and A10 are shown in Figures 44 to 46. Figure 44 shows that the extent of overshoot decreases as -Q increases, i.e. for electrode A7 when the cathodic current was decreased from 11.6 to 1.16 mA cm^{-2} and was kept at 1.16 mA cm^{-2} to reach a steady-state, the extent of overshoot was 21 and 14 mV respectively, for the passage of 61 and 655 coulombs. The curves in Figures 44 to 46 suggest that there may be an exponential relation between overvoltage and time. Figure 47 confirms that such relations ($-\eta$ linear with $\log_{10} t$) exist for the data of Figures 45 and 46.

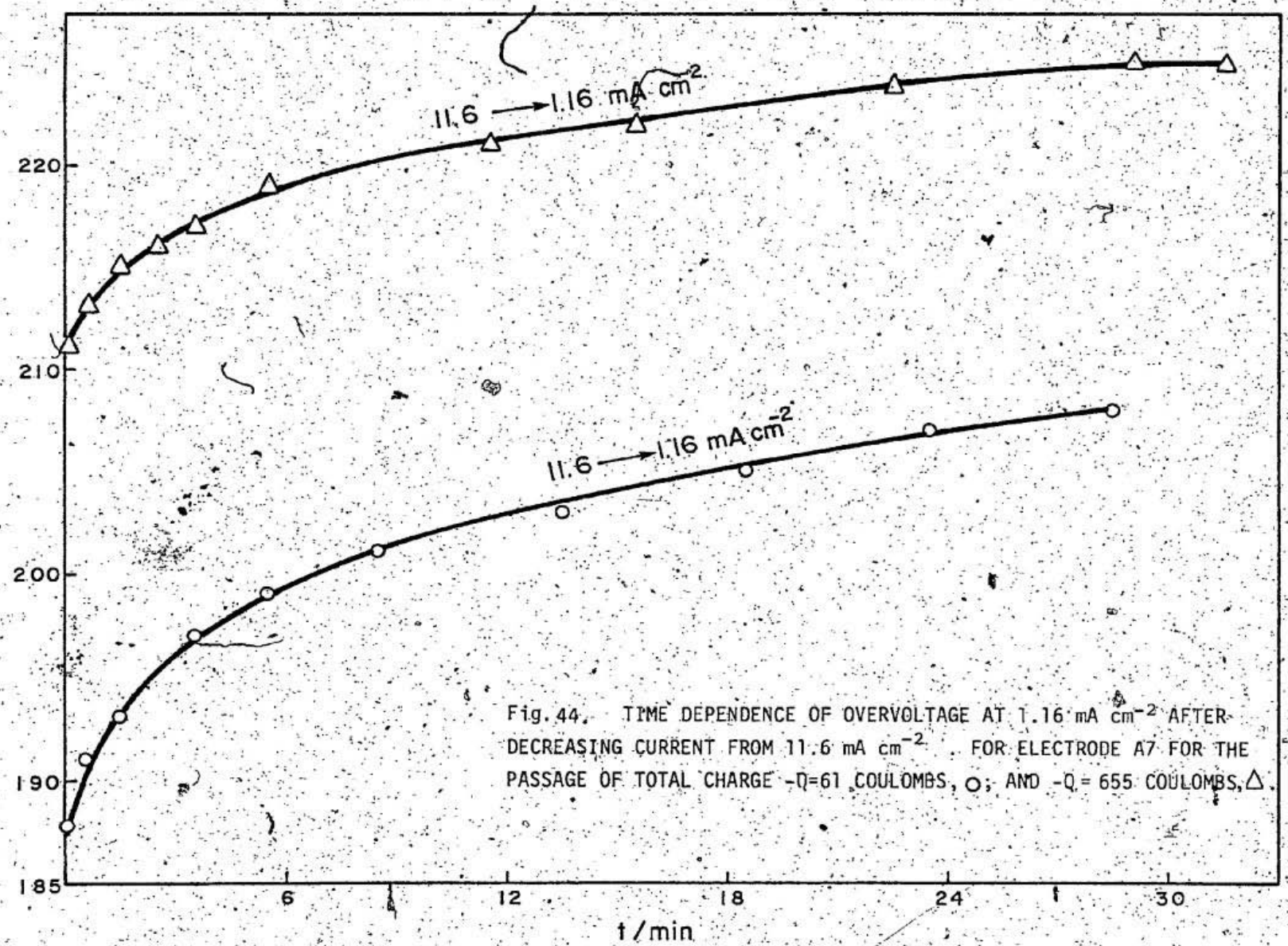

Fig. 44. TIME DEPENDENCE OF OVERVOLTAGE AT 1.16 mA cm^{-2} AFTER DECREASING CURRENT FROM 11.6 mA cm^{-2} . FOR ELECTRODE A7 FOR THE PASSAGE OF TOTAL CHARGE $-Q$=61 COULOMBS, ○; AND $-Q$ = 655 COULOMBS, △.

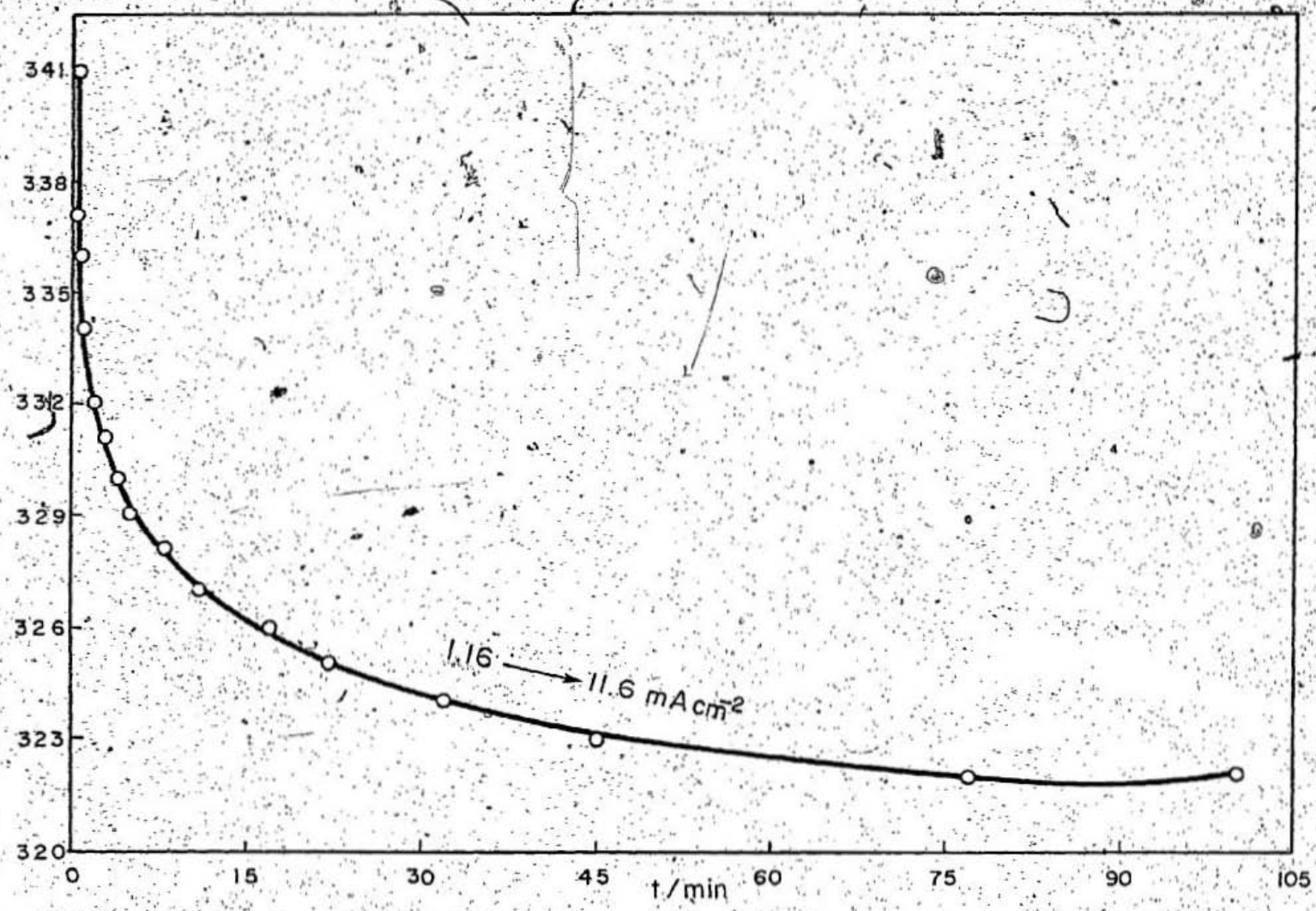

Fig. 45. TIME DEPENDENCE OF OVERVOLTAGE AT 11.6 mA cm^{-2} AFTER INCREASING CURRENT FROM 1.16 mA cm^{-2} FOR ELECTRODE A9 FOR THE PASSAGE OF TOTAL CHARGE -Q = 276 COULOMBS.

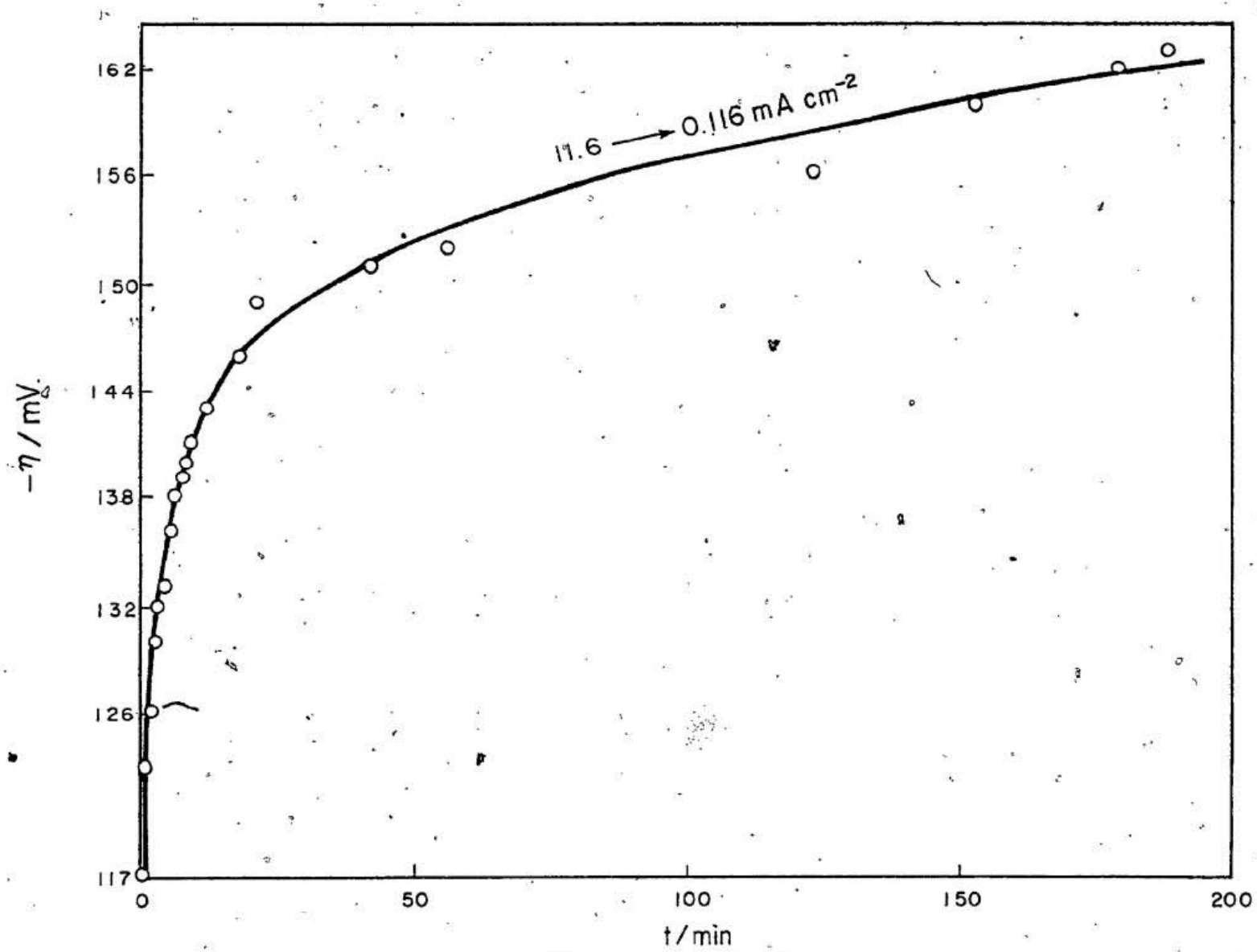

Fig. 46. TIME DEPENDENCE OF OVERVOLTAGE AT 0.116 mA cm^{-2}. AFTER DECREASING CURRENT FROM 11.6 $mAcm^{-2}$ FOR ELECTRODE A10 FOR THE PASSAGE OF TOTAL CHARGE -Q = 531 COULOMBS

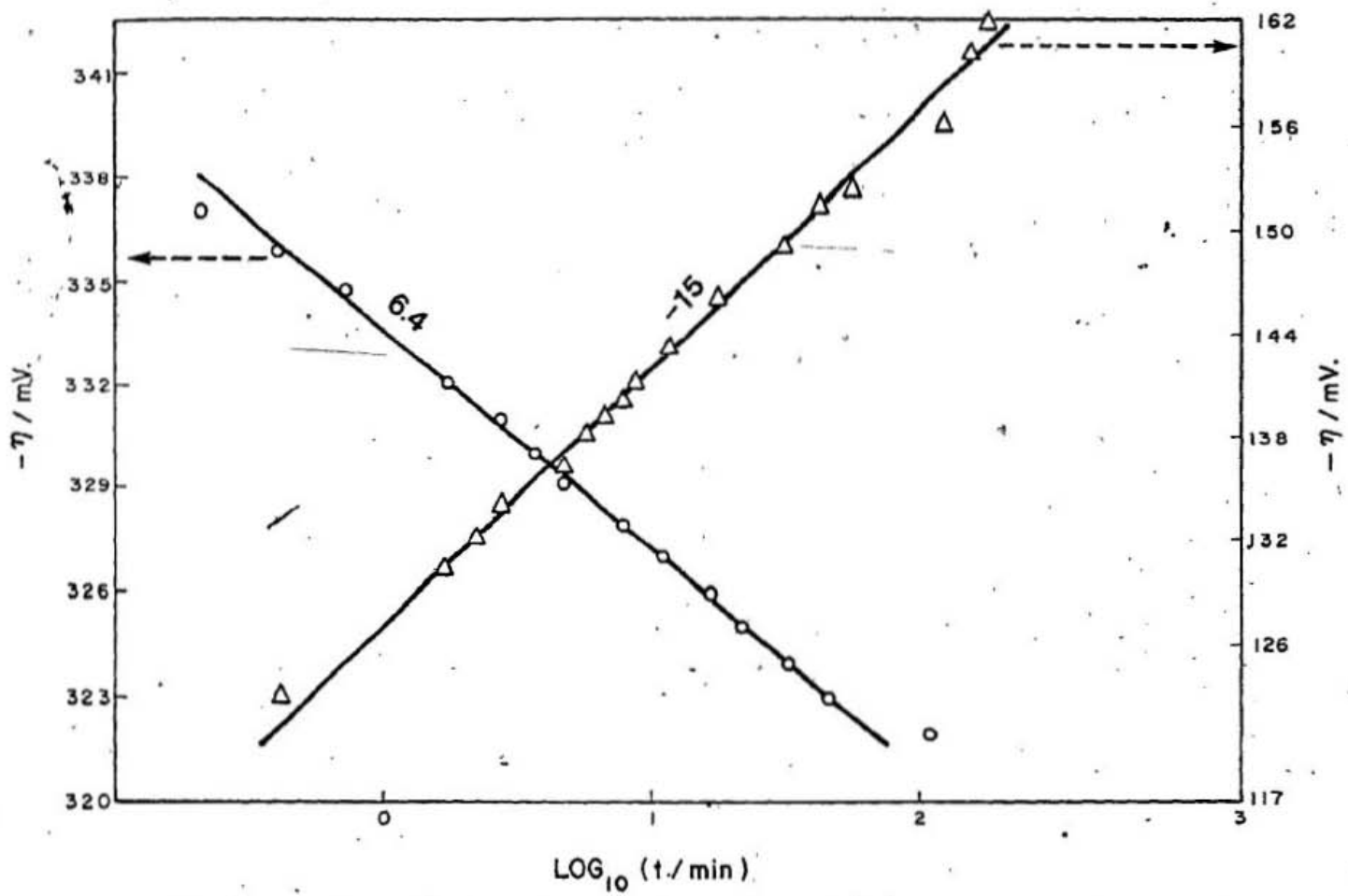

Fig. 47. DATA FROM Fig. 46. , Δ ; AND FROM FIG. 45. , o ; PLOTTED SEMI-LOGARIMICALLY: OVERVOLTAGE VERSUS LOG_{10} t AT 0.116 m A cm^{-2} FOR ELECTRODE A10 WHEN CURRENT DECREASED FROM 11.6 mA cm^{-2}, Δ (FOR THE PASSAGE OF TOTAL CHARGE -Q = 531 COULOMBS) AND AT 11.6 mA cm^{-2} FOR ELECTRODE A9 WHEN CURRENT INCREASED FROM 1.16 mA cm^{-2}, o(FOR THE PASSAGE OF TOTAL CHARGE -Q = 276 COULOMBS). NUMBER ON EACH CURVEIS SLOPE IN mV $DECADE^{-1}$.

The overvoltage generally increased with -Q for silver electrodes as discussed before. The overshoot hysteresis behaviour is, consequently, opposite to what might have been expected from the general increase of $-\eta$ with cathodisation, but is very similar to the behaviour observed with lead where, however, the overvoltage decreases with cathodic charging. This question will be considered further later.

(c) Tafel Plots

Tafel plots were observed by the rapid-run method, the current being kept constant for pre-determined periods (1 - 5 minutes) uniform within each run, between changes of c.d.

Figure 48, a typical Tafel plot for "dirty" experiment A1, illustrates an increase of Tafel slope from 62 to 107 mV for low c.d.'s and decrease of Tafel slope from 183 to 154 mV for high c.d.'s. The high Tafel slopes are consistent with the use of unpurified $HClO_4$ and a non-electropolished silver electrode.

Tafel plots for electrode A2, shown in Figure 49, had 3 regions with three different slopes. At cathodic c.d.'s higher than ca. 5 mA cm^{-2}, i.e. the higher portion of Tafel plots, the b values decreased from 149 to 141 mV after passage of 90 coulombs of additional charge but the slope of the middle portion did not change very much. The multi-linearity of the Tafel plots of experiments A2 (see Fig. 49) and A3 (not shown here) is attributed to the present of Ag^+ ions in the electrolyte, presumably left after in situ electropolishing and washing of the electrodes A2 and A3.

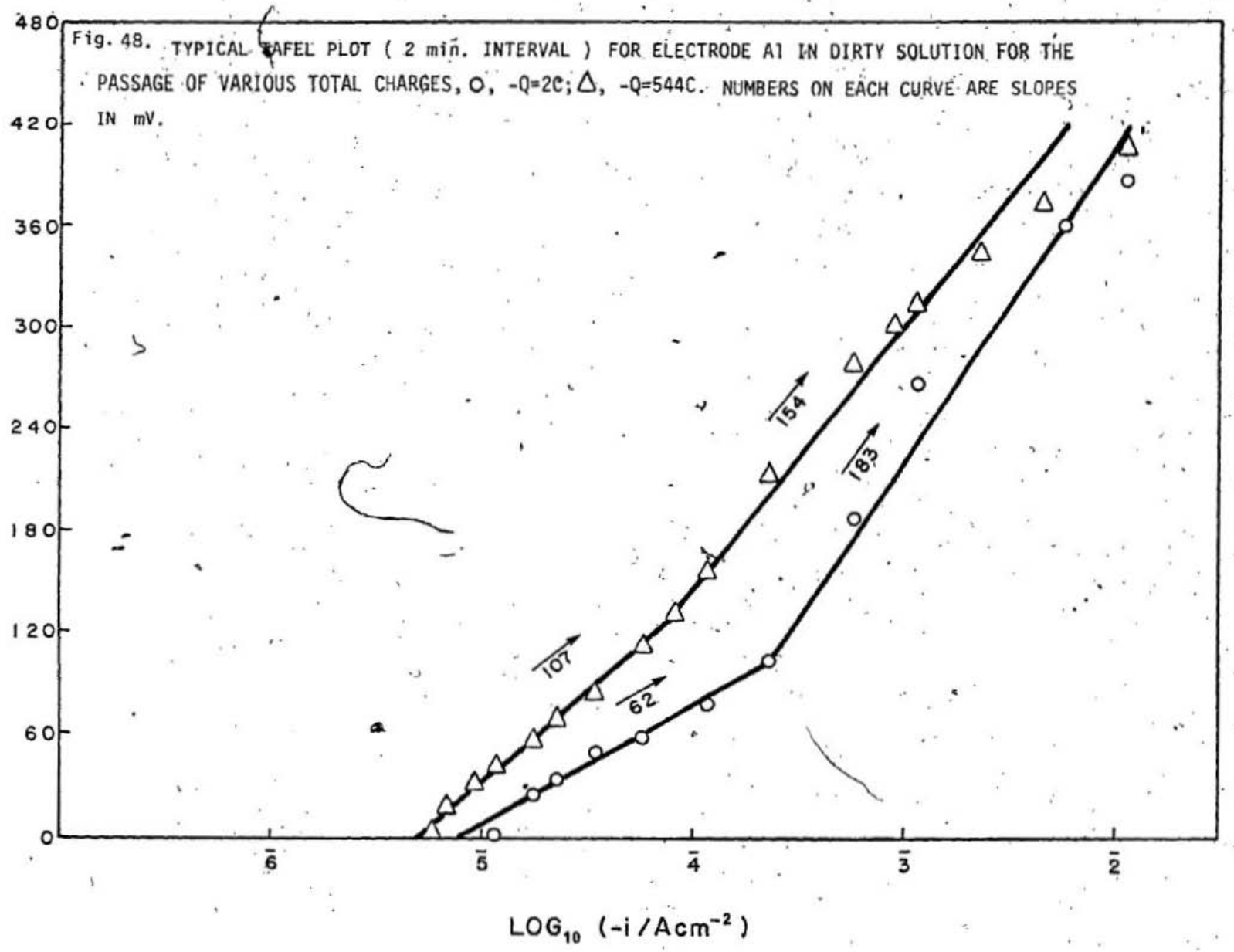

Fig. 48. TYPICAL TAFEL PLOT (2 min. INTERVAL) FOR ELECTRODE Al IN DIRTY SOLUTION FOR THE PASSAGE OF VARIOUS TOTAL CHARGES, O, -Q=2C; Δ, -Q=544C. NUMBERS ON EACH CURVE ARE SLOPES IN mV.

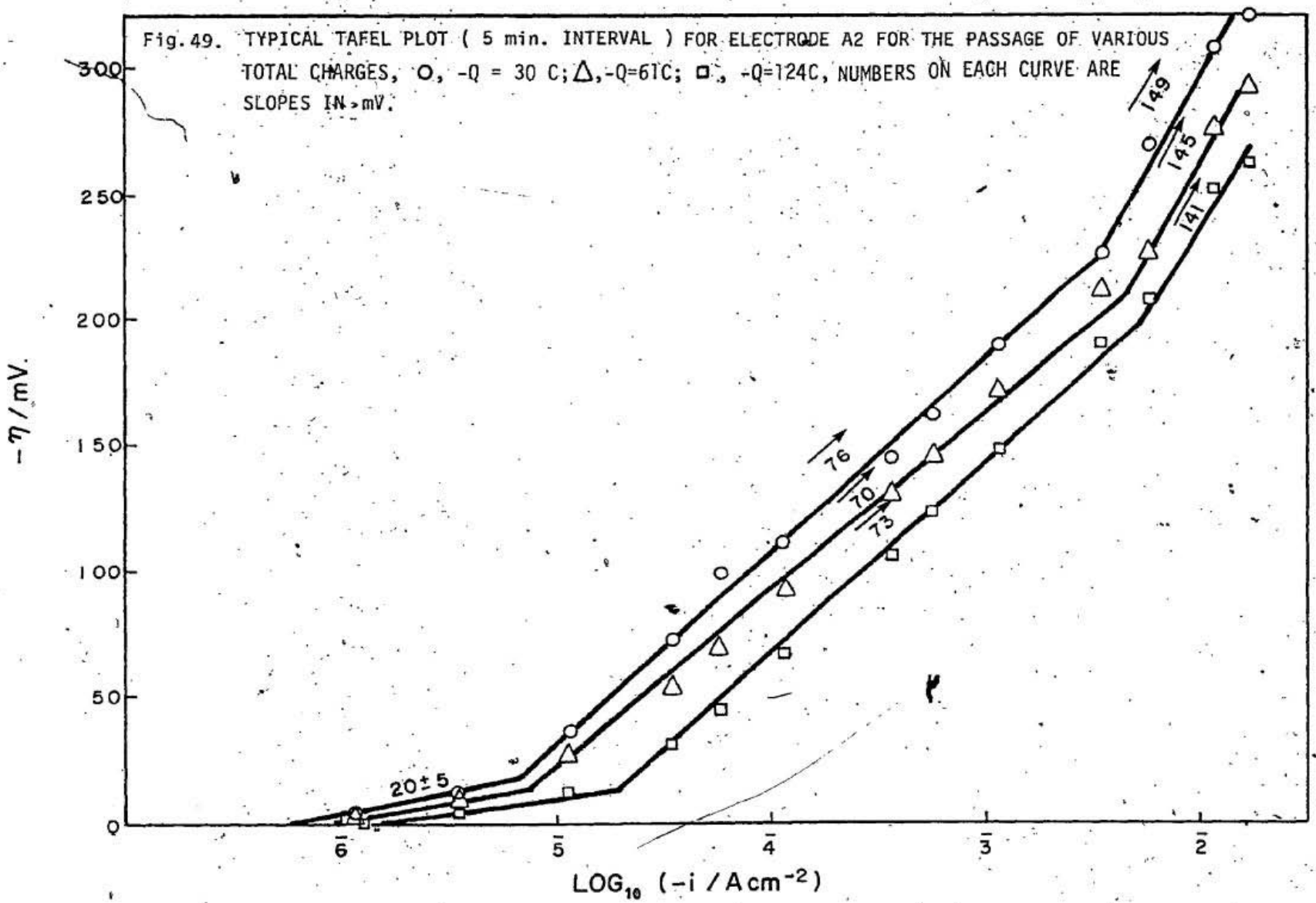

Fig. 49. TYPICAL TAFEL PLOT (5 min. INTERVAL) FOR ELECTRODE A2 FOR THE PASSAGE OF VARIOUS TOTAL CHARGES, O, -Q = 30 C; Δ, -Q=61C; □, -Q=124C, NUMBERS ON EACH CURVE ARE SLOPES IN mV.

Experiments A5 and A6 were carried out using electropolished silver electrodes and pre-electrolysed 1 mol ℓ^{-1} $HClO_4$. Tafel slopes of 60 ± 1 mV for low c.d.'s and 95 ± 8 mV for high c.d.'s were observed. Figure 50 shows that overvoltages for the descending branch were greater than those for the ascending branch for electrode A5 with a hysteresis of 10 to 25 mV. Overvoltage measurements over a limited range of c.d. at the beginning of experiment A6 gave linear Tafel plots which exhibited two sections with different slopes for low and high c.d.'s (see Figure 51) after passage of ca. 7 coulombs charge. Tafel slopes for high cathodic c.d.'s [illegible]eased on prolonged cathodisation, e.g. from ca. 90 to 10[illegible] after passage of an additional 960 coulombs in experiment A6. The existence of two Tafel slopes for clean silver electrodes in pre-electrolysed acid solution was also observed by some previous workers (116,121,122, 123,124).

According to Vetter (2), when the overvoltages are small, i.e. $|\eta| < RT/F$ or 29.6 mV at 298 K, the Tafel equation is no longer valid, since in this region (lower portion of our Tafel plots) the reverse reaction becomes more and more important and finally causes the net c.d. to approach zero as $-\eta$ goes to zero. The overvoltage is now proportional to c.d. and this relation at low c.d.'s gives a better measurement of the exchange c.d., i_o, than from Tafel plot extrapolation. Using the current-overvoltage relation for low overvoltage, i.e. equation (23): $i = i_o \frac{F\eta}{RT}$, the exchange current densities were calculated for electrodes A1, A5 and A6 at different -Q values.

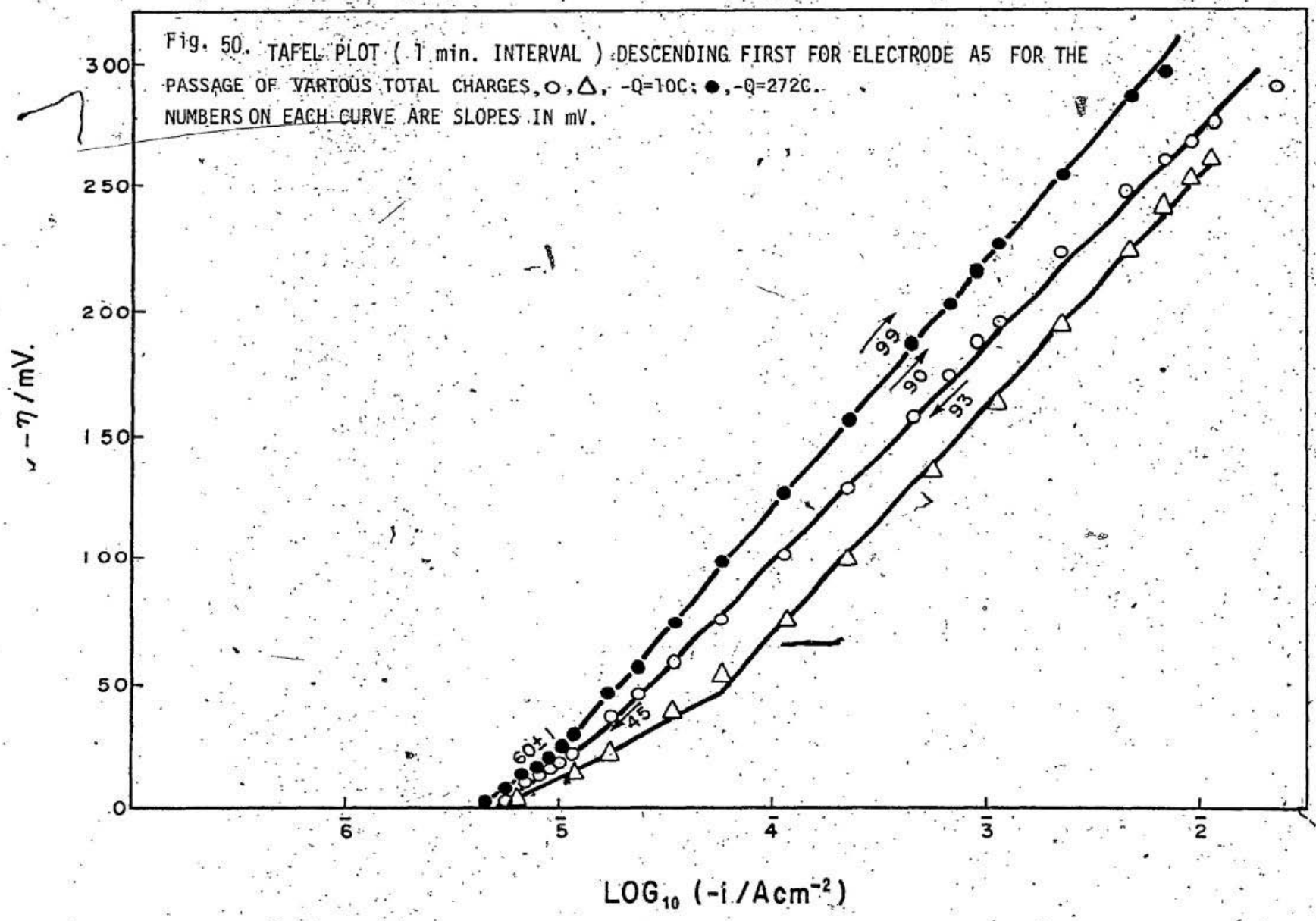

Fig. 50. TAFEL PLOT (1 min. INTERVAL) DESCENDING FIRST FOR ELECTRODE A5 FOR THE PASSAGE OF VARIOUS TOTAL CHARGES, ○, △, -Q=10C; ●, -Q=272C. NUMBERS ON EACH CURVE ARE SLOPES IN mV.

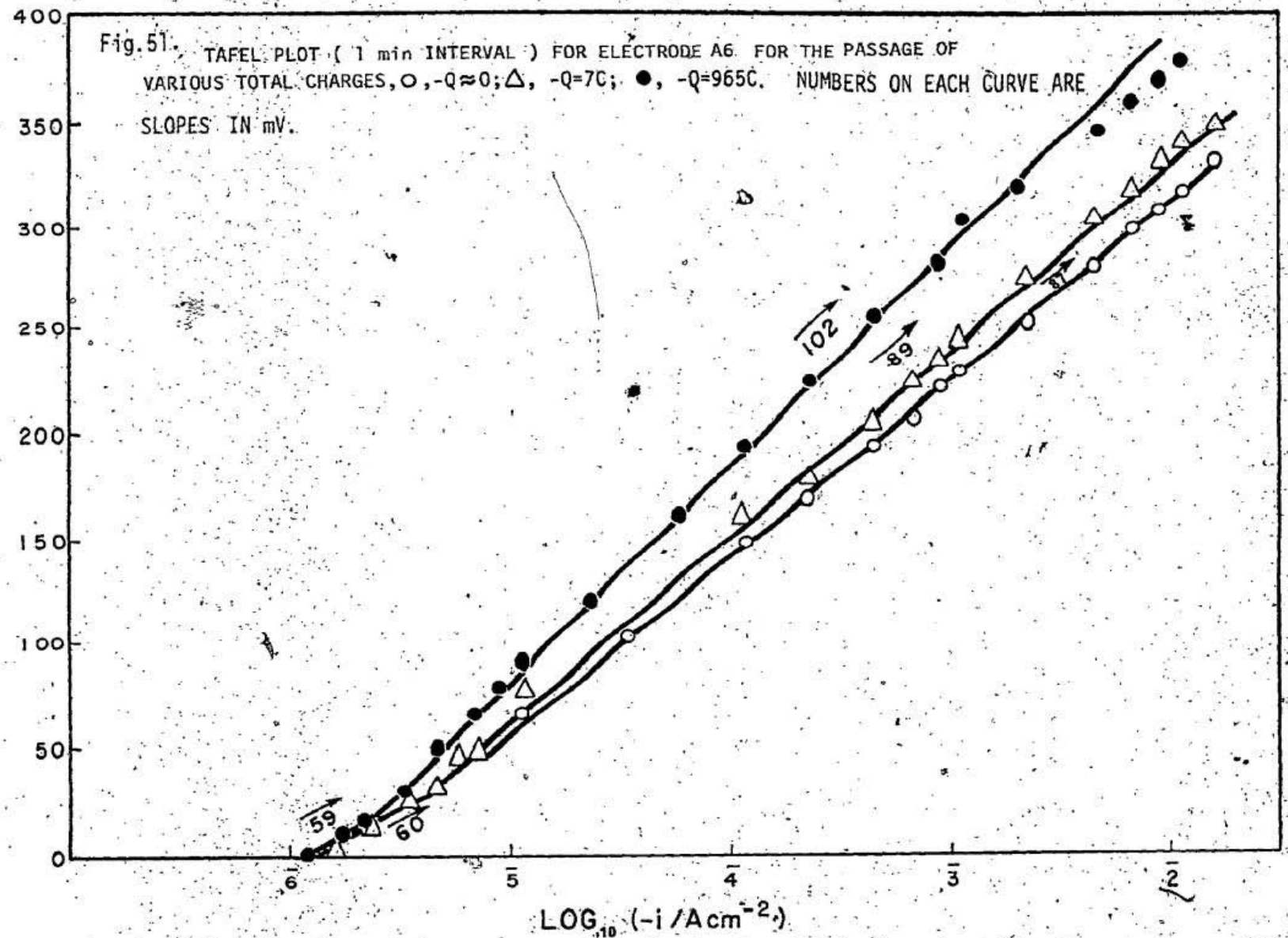

Fig.51. TAFEL PLOT (1 min INTERVAL) FOR ELECTRODE A6 FOR THE PASSAGE OF VARIOUS TOTAL CHARGES, ○, -Q≈0; △, -Q=7C; ●, -Q=965C. NUMBERS ON EACH CURVE ARE SLOPES IN mV.

The results are tabulated in Table 19. For experiments A5 and A6 after passage of quite large cathodic charges the exchange c.d.'s were unchanged (within experimental error) being, respectively, $5 \pm 1 \times 10^{-6}$ A cm^{-2} in A5 and $1.9 \pm 0.5 \times 10^{-6}$ A cm^{-2} in A6, while i_o for A1 decreased from 6.6×10^{-6} to 3.1×10^{-6} A cm^{-2}. The exchange current densities were also calculated using the Tafel slopes of Figures 50, 51 and using Tafel equations at different values of -Q. Using this method, the value of i_o was $3 \pm 2 \times 10^{-6}$ A cm^{-2}. Calculated values of i_o are in fair agreement with the values obtained by some previous investigators (116,120,121,123,127,129). The results of exchange current density measurements and b values suggest that the catalytic activity of silver electrodes at the equilibrium potential does not change during the h.e.r.

TABLE 19 VARIATION OF EXCHANGE CURRENT DENSITIES WITH TOTAL CATHODIC CHARGE PASSED, FROM LINEAR -i vs -η PLOTS AT SMALL -η.

Experiment number	-Q/C	$i_o \times 10^6$/A cm^{-2}	Notes
A1	2	6.6	Dirty electrode in
	544	3.1	dirty solution.
A5	10	4.5	Electropolished
	272	5.5	electrodes in
A6	7	1.8	pre-electrolysed
	965	1.9	solution.

III. Capacitance Measurements at Silver Cathodes

(a) Preliminary Experiment

The results of capacitance measurements made with the silver electrode in experiment B1 were not like those of later experiments. In this experiment the silver electrode was cathodised at $i = -1.16$ mA cm^{-2} for about 2 hours and then capacitance measurements were begun in a step-wise manner. Whenever the capacitance measurements were not carried out, a current density of -1.16 mA cm^{-2} was held on the silver electrode. Results for experiment B1 are tabulated in Table 20 and illustrated in Figure 52, from which it can be seen that $-\eta$ increased with $-Q$ at a particular c.d., e.g. at $i = -1.16$ mA cm^{-2}, $-\eta$ increased from 179 mV after passage of 8 coulombs cm^{-2} to 222 mV after passage of 295 coulombs cm^{-2} (see Table 20). But the observed capacitance, $C_{expt.}$, decreased both with time of cathodisation at 1.16 mA cm^{-2} and with $-Q$ at a particular overvoltage, e.g. for $-\eta = 250$ mV, $C_{expt.}$ decreased from 68 μF cm^{-2} at $-Q = 8$ coulombs cm^{-2} to 53 μF cm^{-2} at $-Q = 295$ coulombs cm^{-2} (see Figure 52).

(b) Experiments with Charcoal-cleaned Pre-electrolysed Solutions

Tables 21 to 24 detail the measured electrode capacitances and overvoltages for experiments B2 to B5 at various c.d.'s after different periods of constant current cathodisation. These data show that the increase of $C_{expt.}$ was generally accompanied by an increase of $-\eta$, e.g. in B3 at $i = -1.16$ mA cm^{-2}, $C_{expt.}$ increased from 54.3 to 68.4 μF cm^{-2}, while $-\eta$ increased from 250 to 277 mV during passage of an additional 190 coulombs cm^{-2} at -0.231 mA cm^{-2} (see Table 22) and in

TABLE 20 EXPERIMENTAL CAPACITANCES OF A SILVER ELECTRODE B1 IN UN-PURIFIED 1 mol ℓ^{-1} $HClO_4$ DURING PASSAGE OF -295 C cm^{-2} AT i = -1.16 mA cm^{-2} AND AT THE HIGHER CURRENT DENSITIES OF THE CAPACITANCE MEASUREMENTS.

Total cathodic charge passed $-Q/C\ cm^{-2}$	Cathodic current density/mA cm^{-2}													
	1.16		2.31		4.63		9.25		13.87		17.34		22.99	
	$-\eta$/mV	$C_{expt.}$/μF cm^{-2}	$-\eta$/mV	$C_{expt.}$/μF cm^{-2}	$-\eta$/mV	$C_{expt.}$/μF cm^{-2}	$-\eta$/mV	$C_{expt.}$/μF cm^{-2}	$-\eta$/mV	$C_{expt.}$/μF cm^{-2}	$-\eta$/mV	$C_{expt.}$/μF cm^{-2}	$-\eta$/mV	$C_{expt.}$/μF cm^{-2}
.8	179	65.4	219	68.9	255	67.0	291	73	312	75	322	79.5	334	84.4
94	204	59.1	246	59.3	282	68	312	78.8	327	78.2	335	86.0	345	85.9
204	214	52.3	253	58.7	290	59.3	319	74.1	333	82.8	340	87.2	350	98.2
295	222	49.5	261	55.5	296	64.4	324	68.9	338	77.2	345	82.2	353	92.5

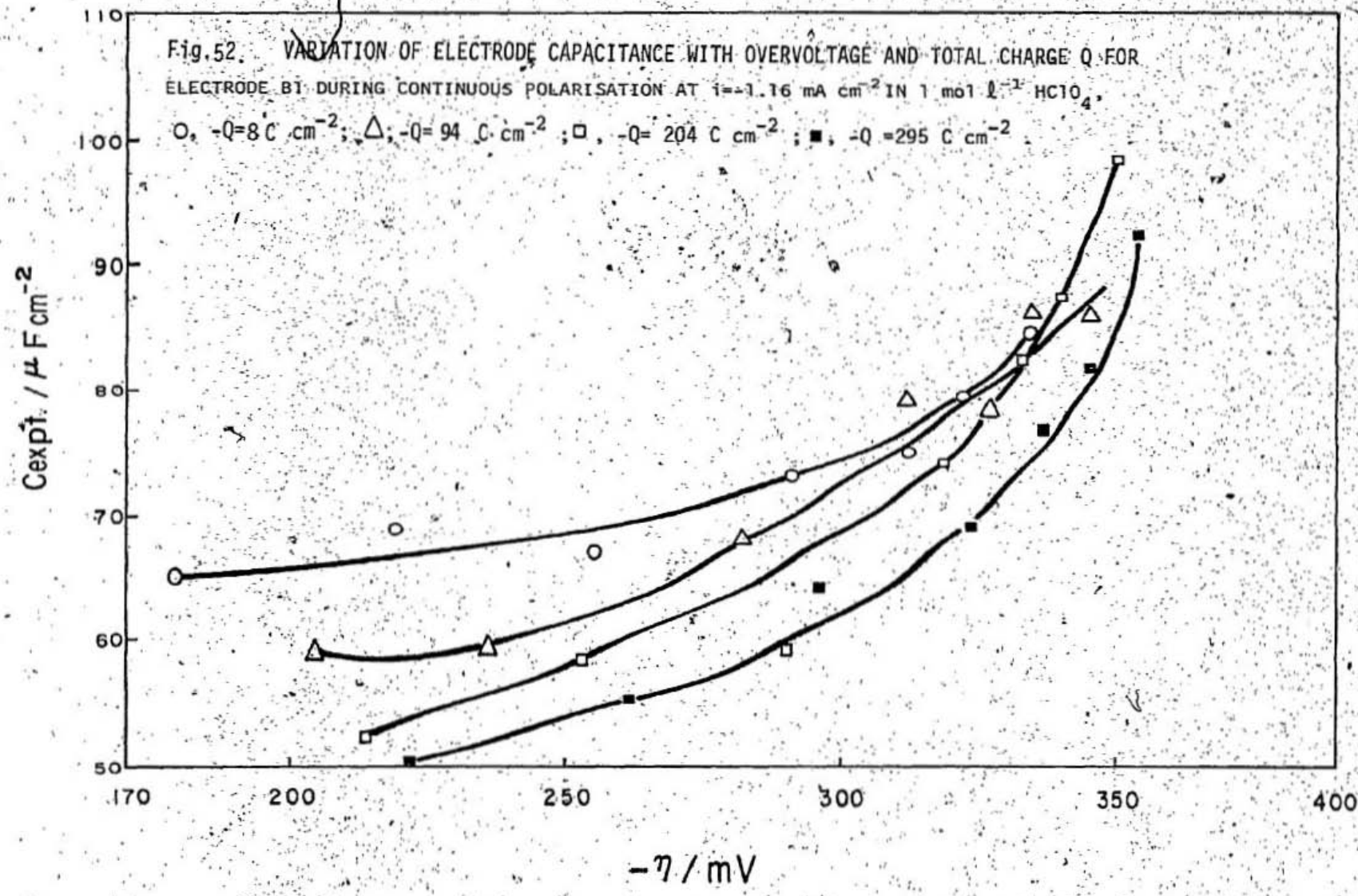

Fig.52. VARIATION OF ELECTRODE CAPACITANCE WITH OVERVOLTAGE AND TOTAL CHARGE Q FOR ELECTRODE B1 DURING CONTINUOUS POLARISATION AT $i = -1.16$ mA cm^{-2} IN 1 mol ℓ^{-1} $HClO_4$.

○, $-Q = 8$ C cm^{-2}; △, $-Q = 94$ C cm^{-2}; □, $-Q = 204$ C cm^{-2}; ■, $-Q = 295$ C cm^{-2}.

B5 at $i = -34.68$ mA cm^{-2}, $C_{expt.}$ rose from 108.3 to 219.8 μF cm^{-2} while $-\eta$ increased from 356 to 368 mV as $-Q$ (passed at $i = -0.116$ mA cm^{-2}) increased from 1 to 171 C cm^{-2} (see Table 24).

Figures 53 to 56 show the essential features of experiments B2 to B5, i.e. the relationship between $C_{expt.}$ and $-\eta$ at particular values of $-Q$. In all cases, the electrode capacitance increased monotonically with $-Q$, in some cases by large amounts, e.g. in 0.1 mol ℓ^{-1} $HClO_4$ (see Figures 55 and 56) the increase of $C_{expt.}$ at high c.d.'s was greater than in more concentrated acid.

It is evident from Tables 21 to 24 that the variation of overvoltage is small whereas that of the capacitance is large at high c.d.'s. The trend is reversed at the lower c.d.s at which the capacitance was measureable. In most cases a large change of overvoltage and capacitance was observed between the first two consecutive capacitance measurements after which the increase both of $-\eta$ and of $C_{expt.}$ was much slower, e.g. in experiment B5 at $i = -13.87$ mA cm^{-2} (Table 24), $C_{expt.}$ rose from 70.6 to 142.8 μF cm^{-2} corresponding to an increase of $-\eta$ from 337 to 345 mV as $-Q$ increased from 6 to 46 C cm^{-2}, while after passage of an additional 83 C cm^{-2} the capacitance increased only from 142.8 to 144.7 μF cm^{-2} while $-\eta$ increased from 345 to 355 mV. In all cases, the increase of $C_{expt.}$, in experiments B4 and B5 with 0.1 mol ℓ^{-1} $HClO_4$ at a particular c.d. and charge, was <u>larger</u> than in experiments B2 and B3 using the more concentrated 1 mol ℓ^{-1} $HClO_4$.

Taking values of $C_{expt.}$ at various values of $-Q$ on a given electrode at constant $-\eta$, it was possible to demonstrate that $C_{expt.}$

TABLE 21 EXPERIMENTAL CAPACITANCES OF A SILVER ELECTRODE B2 IN 1 mol ℓ^{-1} $HClO_4$ DURING PASSAGE OF -262 C cm^{-2} AT i = -0.116 mA cm^{-2} AND AT THE HIGHER CURRENT DENSITIES OF THE CAPACITANCE MEASUREMENTS.

Total cathodic charge passed $-Q/C\ cm^{-2}$	Cathodic current density $-i/mA\ cm^{-2}$											
	1.16		6.94		13.87		18.50		25.43		34.68	
	$-\eta$/ mV	$C_{expt.}$/ $\mu F\ cm^{-2}$	$-\eta$/ mV	$C_{expt.}$/ $\mu F\ cm^{-2}$	$-\eta$/ mV	$C_{expt.}$/ $\mu F\ cm^{-2}$	$-\eta$/ mV	$C_{expt.}$/ $\mu F\ cm^{-2}$	$-\eta$/ mV	$C_{expt.}$/ $\mu F\ cm^{-2}$	$-\eta$/ mV	$C_{expt.}$/ $\mu E\ cm^{-2}$
0.36	250	63.7	317	67.1	341	71.5	351	77.4	360	87.2	369	95.4
26	277	57.7	330	69.6	348	76.2	355	77.4	363	87.2	371	99.4
51	275	59.6	330	70.5	348	77.2	355	82.3	363	88.7	373	100.7
83	281	61.6	334	71.5	350	78.2	357	84.1	366	91.7	375	109.9
201	277	63.7	332	73.4	351	79.3	360	84.1	368	95.0	376	113.3
229	281	66.0	337	76.6	354	82.7	360	92.1	368	98.5	376	108.2
262	278	68	336	78.6	354	85.1	360	96.7	370	100.4	379	120.9

TABLE 22 EXPERIMENTAL CAPACITANCES OF A SILVER ELECTRODE B3 IN 1 mol ℓ^{-1} $HClO_4$ DURING PASSAGE OF -192 C cm^{-2} AT i = -0.231 mA cm^{-2} AND AT THE HIGHER CURRENT DENSITIES OF THE CAPACITANCE MEASUREMENTS.

Total cathodic charge passed $-Q/C\ cm^{-2}$	Cathodic current density $-i/mA\ cm^{-2}$											
	1.16		5.78		11.56		18.50		27.75		34.68	
	$-\eta$/ mV	$C_{expt.}$/ $\mu F\ cm^{-2}$	$-\eta$/ mV	$C_{expt.}$/ $\mu F\ cm^{-2}$	$-\eta$/ mV	$C_{expt.}$/ $\mu F\ cm^{-2}$	$-\eta$/ mV	$C_{expt.}$/ $\mu F\ cm^{-2}$	$-\eta$/ mV	$C_{expt.}$/ $\mu F\ cm^{-2}$	$-\eta$/ mV	$C_{expt.}$/ $\mu F\ cm^{-2}$
2	250	54.3	320	70.5	347	76.6	358	80.6	367	85.4	376	95.4
46	279	59.6	324	75.1	339	81.8	351	90.0	361	101.8	367	111.6
97	279	66.0	328	77.7	350	86.1	360	96.7	370	107.5	380	117.0
143	279	68.4	329	79	347	81.8	360	96.7	378	109.5	385	117.0
192	277	68.4	329	80.3	346	86.5	362	104.6	376	111.6	386	117.0

TABLE 23 EXPERIMENTAL CAPACITANCES OF A SILVER ELECTRODE B4 IN 0.1 mol ℓ^{-1} $HClO_4$ DURING PASSAGE OF -293 C cm^{-2} AT i = -1.16 mA cm^{-2} AND AT THE HIGHER CURRENT DENSITIES OF THE CAPACITANCE MEASUREMENTS.

Total cathodic charge passed	Cathodic current density -i/mA cm^{-2}											
	1.16		5.78		11.56		17.34		23.12		34.68	
-Q/C cm^{-2}	-η/ mV	$C_{expt.}$/ μF cm^{-2}	-η/ mV	$C_{expt.}$/ μF cm^{-2}	-η/ mV	$C_{expt.}$/ μF cm^{-2}	-η/ mV	$C_{expt.}$/ μF cm^{-2}	-η/ mV	$C_{expt.}$/ μF cm^{-2}	-η/ mv	$C_{expt.}$/ μF cm^{-2}
19	233	37	292	53.3	321	53.9	337	78.7	350	86.4	366	102
183	274	54.3	330	88.1	346	123.8	355	143.2	358	160.8	368	201
293	264	57.7	327	92.0	344	130.9	352	146	362	166.3	372	209.5

Current density was increased from -0.116 to -1.16 mA cm^{-2} after passage of 1 C cm^{-2} cathodic charge.

TABLE 24. EXPERIMENTAL CAPACITANCES OF A SILVER ELECTRODE B5 IN 0.1 mol ℓ^{-1} $HClO_4$ DURING PASSAGE OF -171 C cm^{-2} AT i = -0.116 mA cm^{-2} AND AT THE HIGHER CURRENT DENSITIES OF THE CAPACITANCE MEASUREMENTS.

Total cathodic charge passed	Cathodic current density $-i$/mA cm^{-2}															
	0.694		1.16		4.62		9.25		13.87		20.81		27.75		34.68	
$-Q$/C cm^{-2}	$-\eta$/mV	$C_{expt.}$/μF cm^{-2}	$-\eta$/mV	$C_{expt.}$/μF cm^{-2}	$-\eta$/mV	$C_{expt.}$/μF cm^{-2}	$-\eta$/mV	$C_{expt.}$/μF cm^{-2}	$-\eta$/mV	$C_{expt.}$/μF cm^{-2}	$-\eta$/mV	$C_{expt.}$/μF cm^{-2}	$-\eta$/mV	$C_{expt.}$/μF cm^{-2}	$-\eta$/mV	$C_{expt.}$/μF cm^{-2}
1	230	40.9	260	51.3	308	50.3	328	63	337	70.6	347	86.1	350	92.1	356	108.3
41	287	44.2	299	56.0	330	89.7	341	109.4	345	142.8	350	150.3	357	161.2	360	186.0
84	290	50.2	302	57.7	333	91.9	345	111.1	350	137.5	355	159.0	359	170.7	367	196.0
124	290	52.6	304	59.6	335	94.3	347	111.1	354	141.0	358	162.1	364	187.2	367	213.3
171	289	55.2	304	61.6	334	95.5	348	118.3	355	144.7	357	172.3	364	187.2	368	219.8

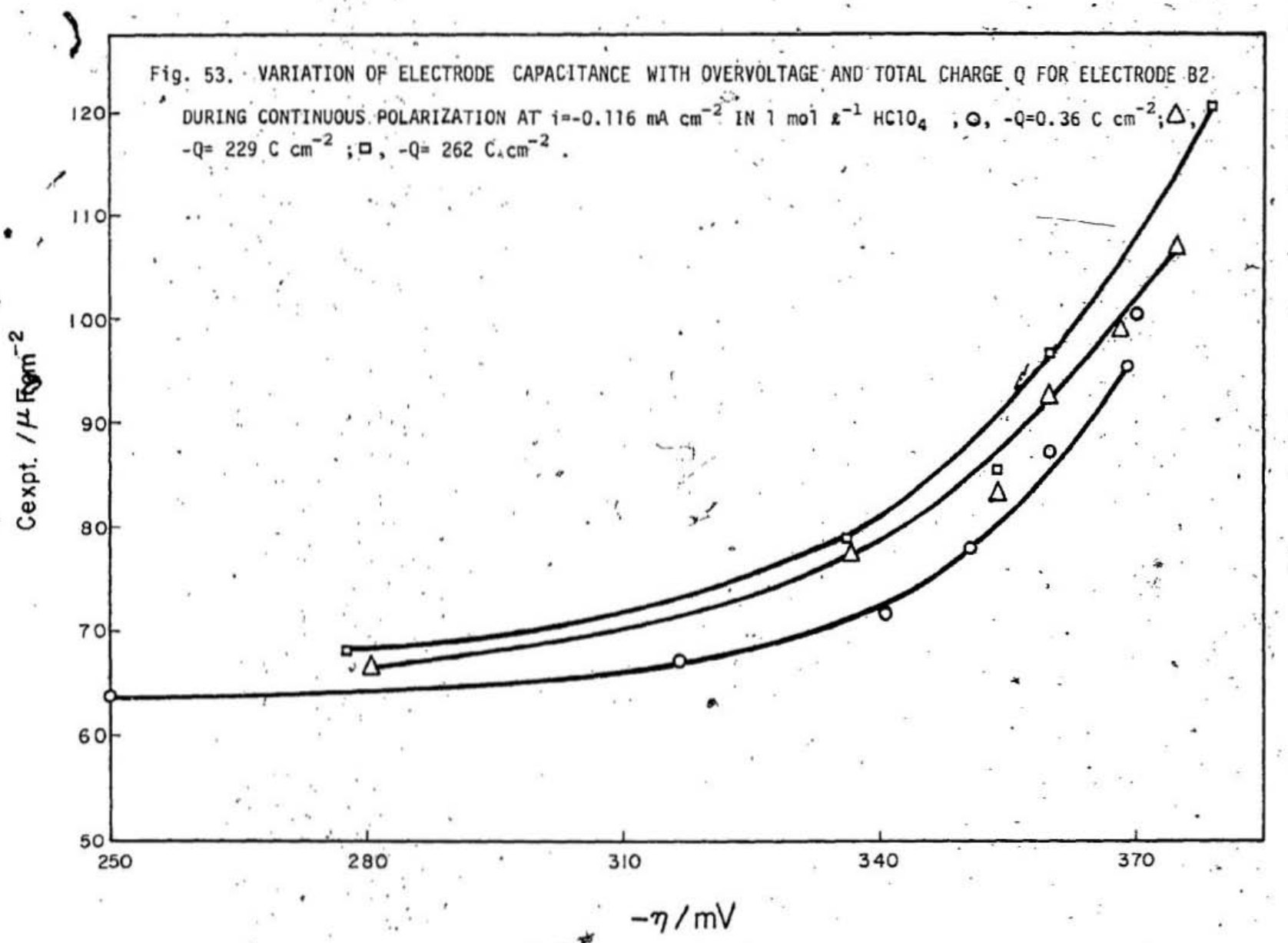

Fig. 53. VARIATION OF ELECTRODE CAPACITANCE WITH OVERVOLTAGE AND TOTAL CHARGE Q FOR ELECTRODE B2 DURING CONTINUOUS POLARIZATION AT $i=-0.116$ mA cm^{-2} IN 1 mol ℓ^{-1} $HClO_4$, ○, $-Q=0.36$ C cm^{-2}; △, $-Q=229$ C cm^{-2} ; □, $-Q=262$ C cm^{-2} .

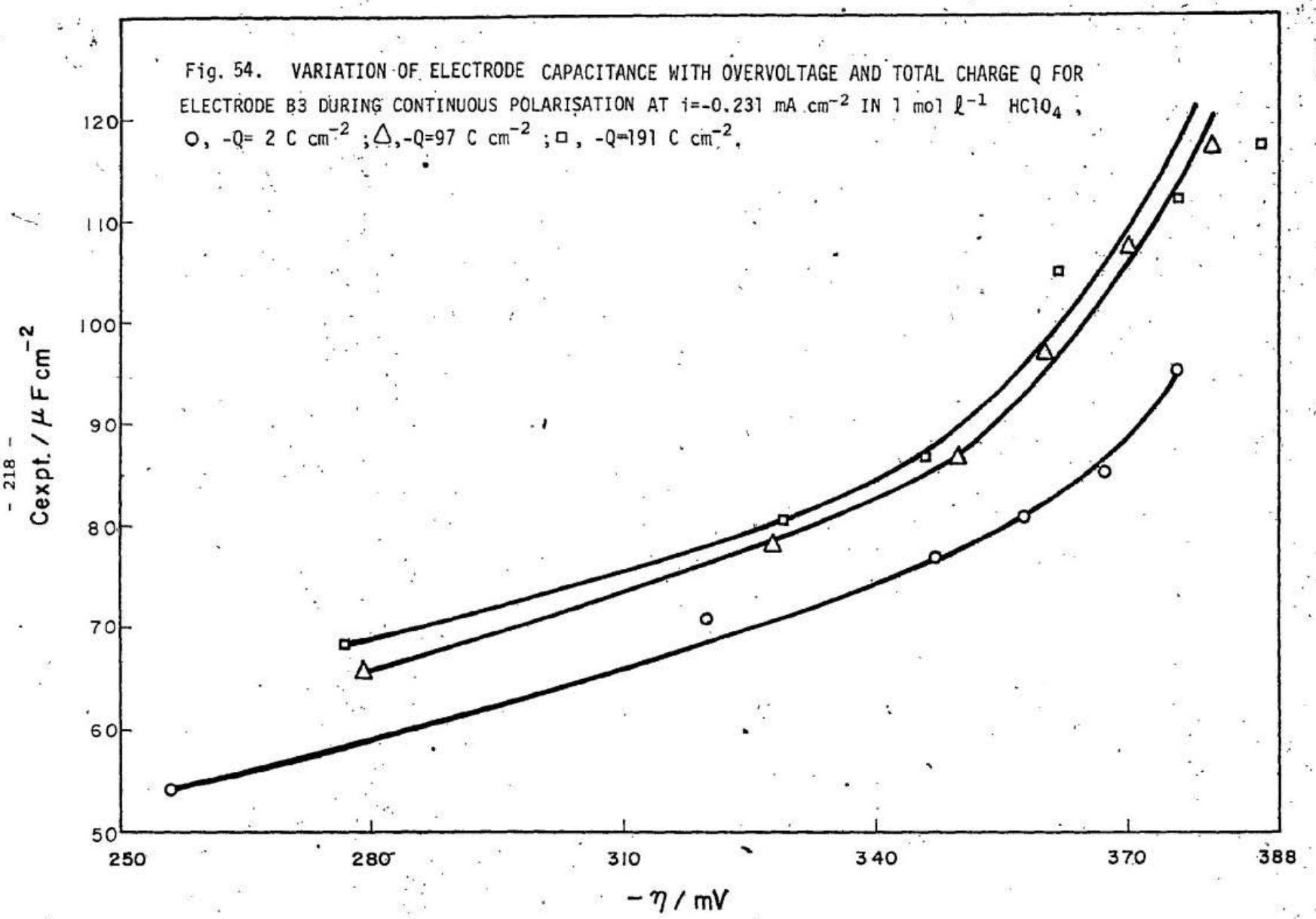

Fig. 54. VARIATION OF ELECTRODE CAPACITANCE WITH OVERVOLTAGE AND TOTAL CHARGE Q FOR ELECTRODE B3 DURING CONTINUOUS POLARISATION AT $i=-0.231$ mA cm^{-2} IN 1 mol ℓ^{-1} $HClO_4$, ○, $-Q=2$ C cm^{-2}; △, $-Q=97$ C cm^{-2}; □, $-Q=191$ C cm^{-2}.

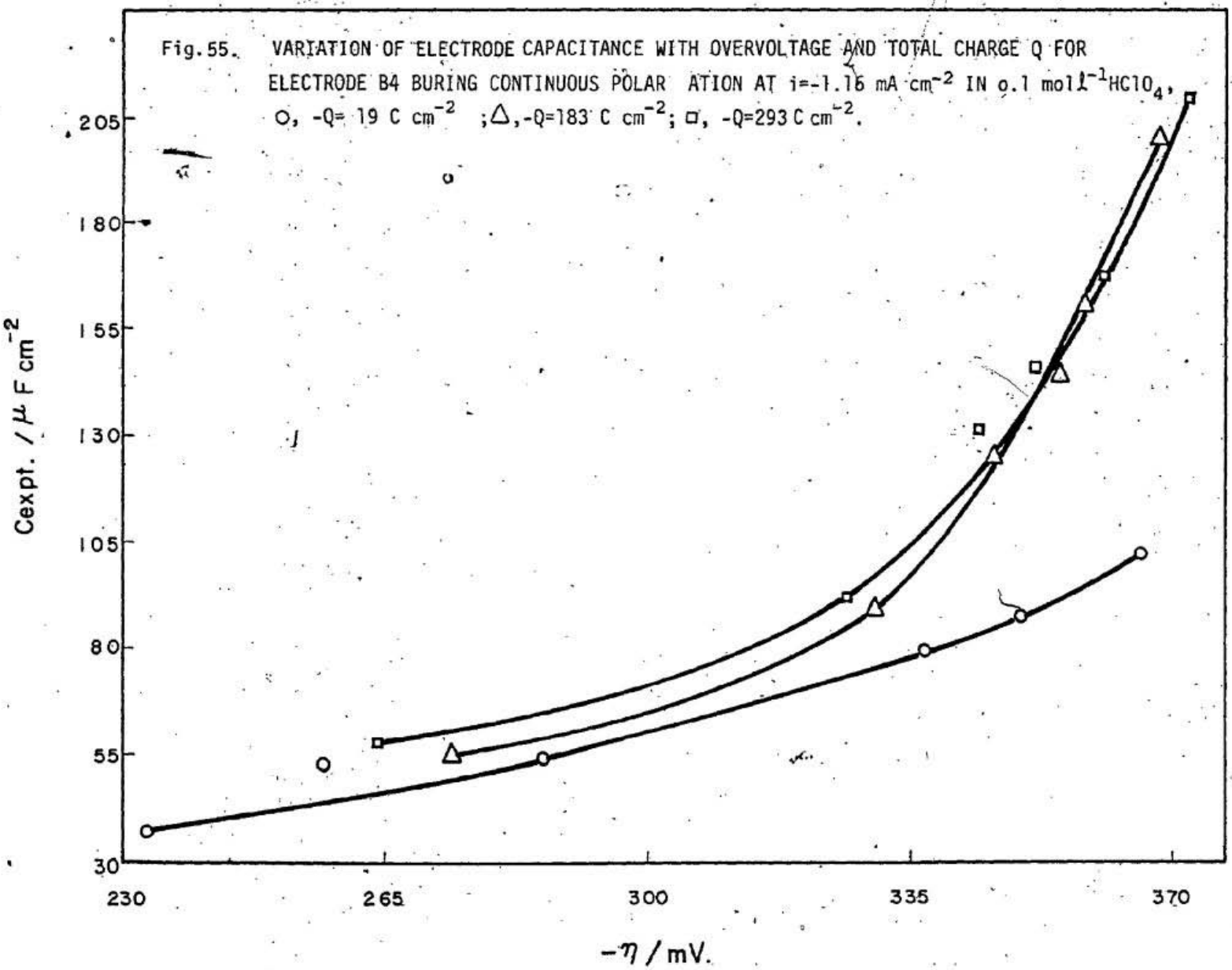

Fig. 55. VARIATION OF ELECTRODE CAPACITANCE WITH OVERVOLTAGE AND TOTAL CHARGE Q FOR ELECTRODE B4 BURING CONTINUOUS POLAR ATION AT i=-1.16 mA cm^{-2} IN o.1 mol l^{-1} $HClO_4$, ○, -Q= 19 C cm^{-2} ;△,-Q=183 C cm^{-2}; □, -Q=293 C cm^{-2}.

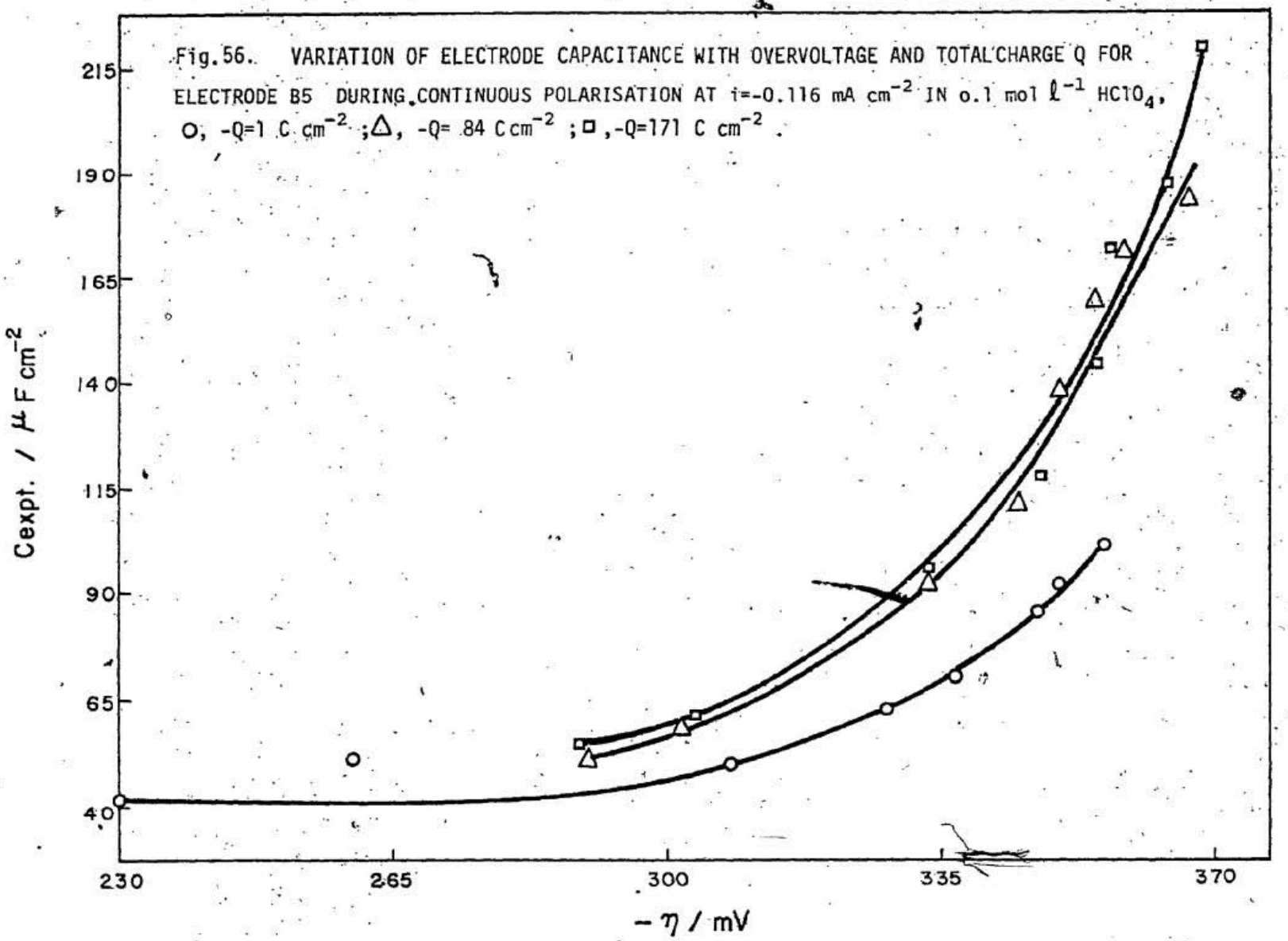

Fig.56. VARIATION OF ELECTRODE CAPACITANCE WITH OVERVOLTAGE AND TOTAL CHARGE Q FOR ELECTRODE B5 DURING CONTINUOUS POLARISATION AT $i=-0.116$ mA cm^{-2} IN 0.1 mol ℓ^{-1} $HClO_4$, ○, $-Q=1$ C cm^{-2} ; △, $-Q=84$ C cm^{-2} ; □, $-Q=171$ C cm^{-2} .

increases with $\log_{10}$ (-Q) at least for not too large values of -Q. A number of plots of $C_{expt.}$ versus $\log_{10}$ (-Q) at three different overvoltages are given in Figures 57 to 59. It is apparent from these figures that at a particular overvoltage on a given electrode, $C_{expt.}$ does indeed increase with $\log_{10}$ (-Q) up to ca. 60 C cm^{-2}. These increases are probably indicative of a pseudocapacitance caused by hydrogen adsorbed on the silver electrodes. At higher charges (> 60 C cm^{-2}) this increase is followed by a plateau region of essentially constant $C_{expt.}$. A similar trend was also observed in the relationship between $-\eta$ and $\log_{10}$ (-Q) as presented in Figure 43.

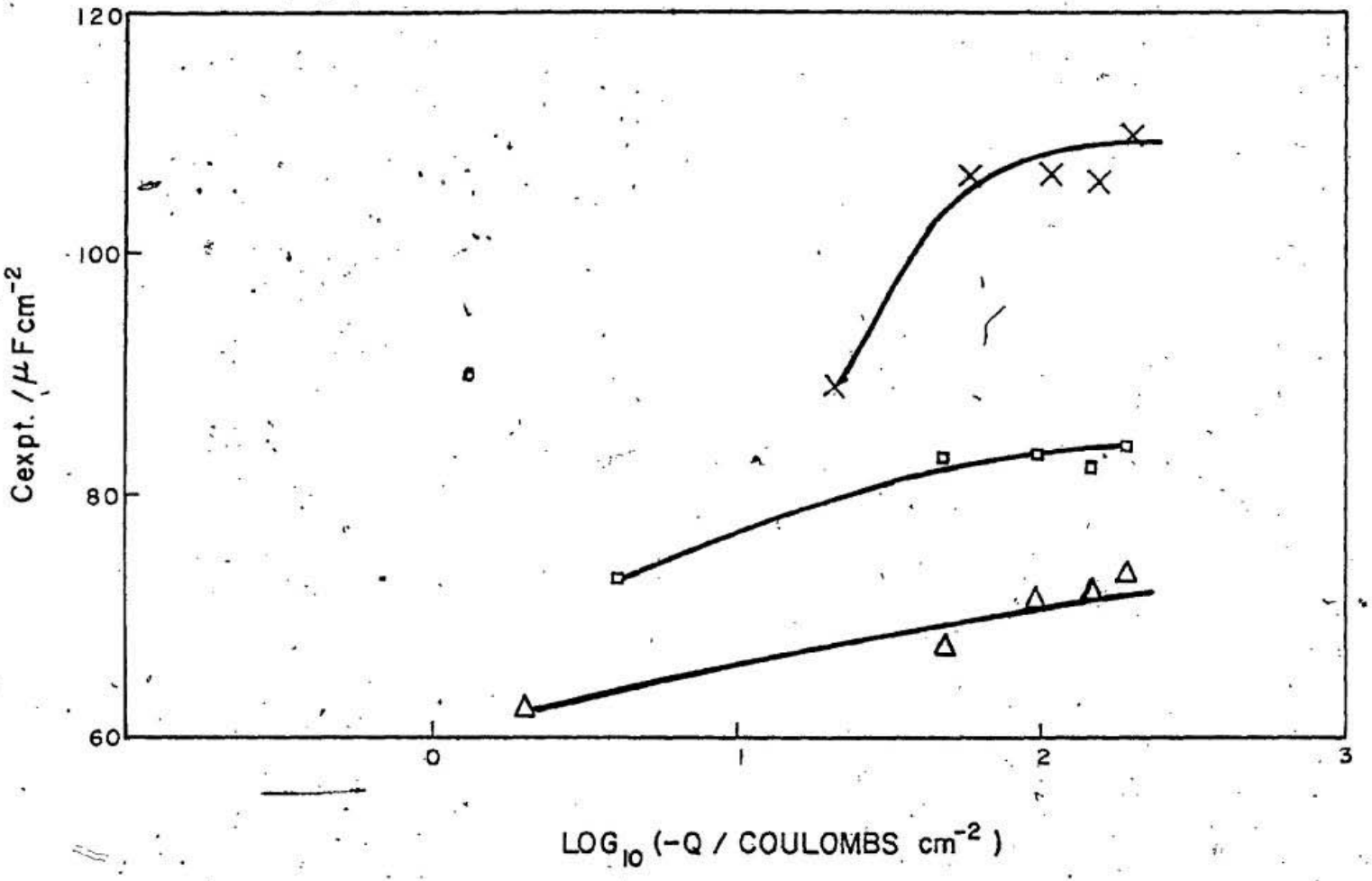

Fig. 57. RELATIONSHIPS BETWEEN ELECTRODE CAPACITANCES AT CONSTANT -η' s (Δ , 300 mV. ; □, 340 mV.; ×, 370 mV.) AND LOG_{10} (-Q) FOR ELECTRODE B3 .

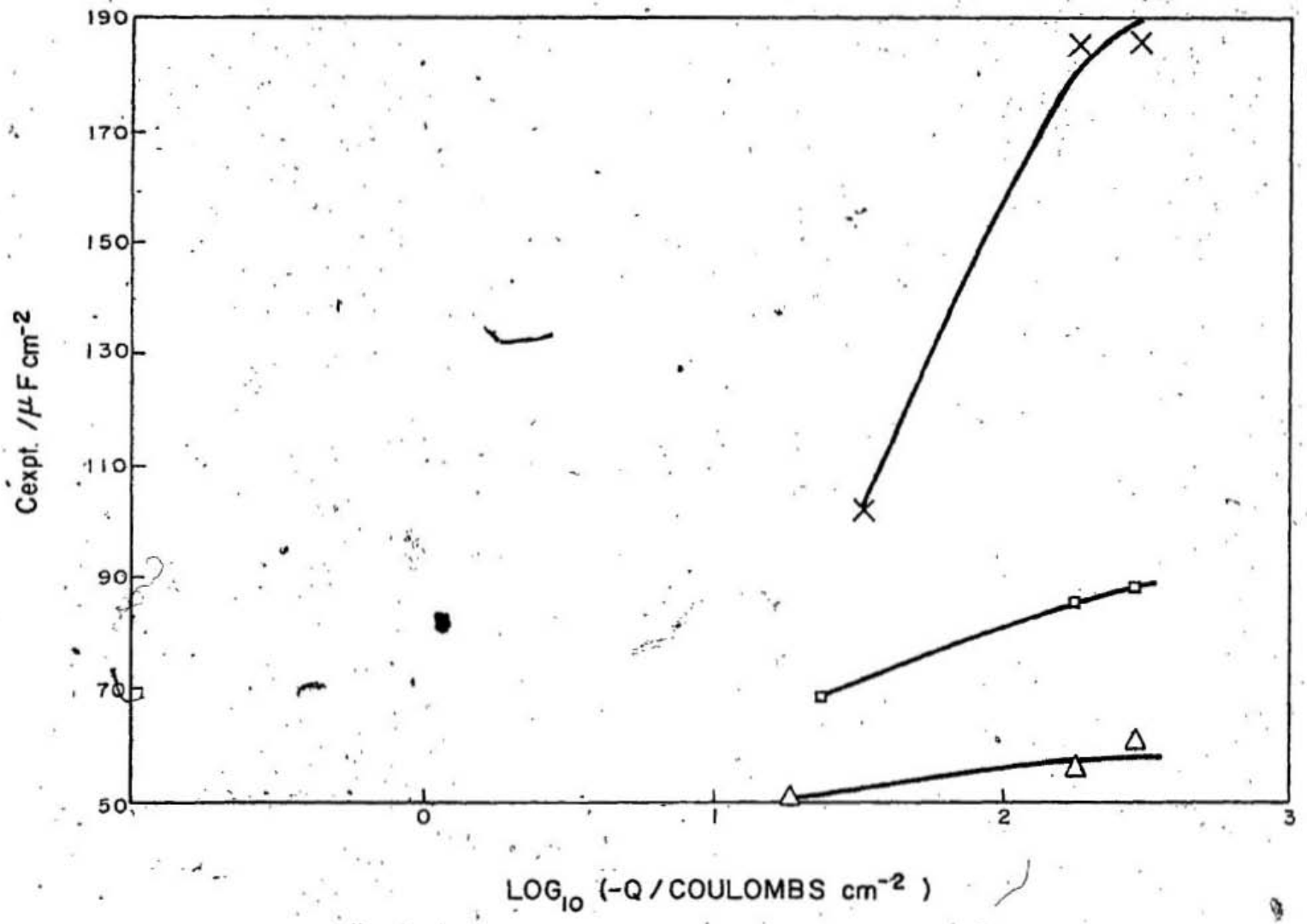

Fig. 58. RELATIONSHIPS BETWEEN ELECTRODE CAPACITANCES AT CONSTANT -η's (△ , 280 mV.; □ , 325 mV.; X, 366 mV.) AND LOG_{10} (-Q) FOR ELECTRODE B4

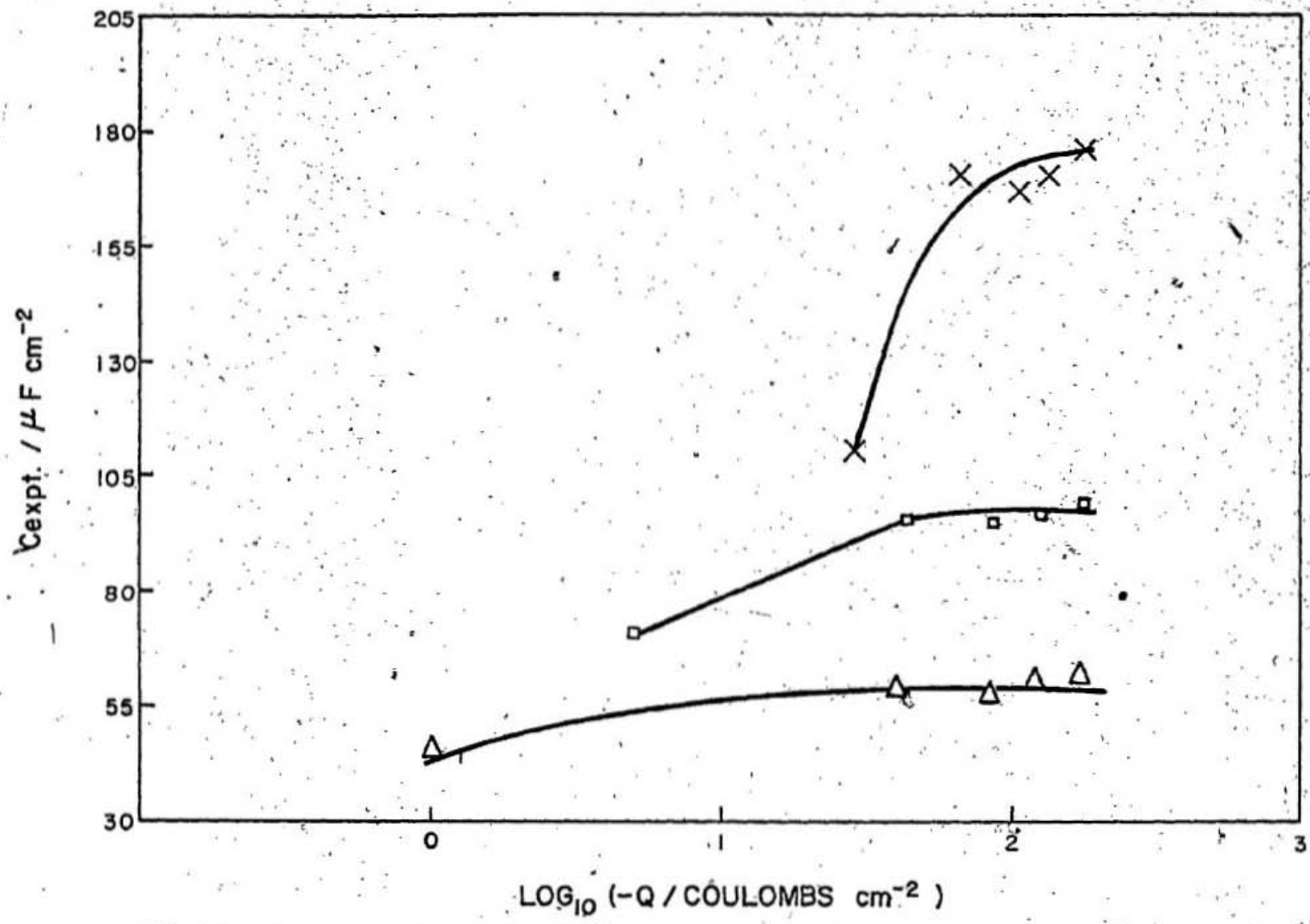

Fig. 59. RELATIONSHIPS BETWEEN ELECTRODE CAPACITANCES AT CONSTANT - η's (△ , 300mV. ; □, 335 mV. ; ×, 360 mV.) and $LOG_{10}(-Q)$ FOR ELECTRODE B5

IV. Calculation of Hydrogen Coverage

This increase of electrode capacitance, $C_{expt.}$, with $-Q$ is presumed to have been caused by a continuous increase in surface coverage with adsorbed hydrogen, θ_H. By observing the increase of $C_{expt.}$ at a given overvoltage, from the initial low value of $-Q$ to the value at various higher values of $-Q$ (increase of cathodic charge $-\Delta Q$) and deducting the former $C_{expt.}$ from the latter, the increase in pseudocapacitance, ΔC_{ps}, has been estimated. The increase in pseudocapacitance has been calculated in this way as a function of overvoltage at higher values of $-Q$ (towards the end of capacitance measurements in a given experiment) and the results presented in Tables 25 to 28. These results have been used to estimate hydrogen coverages or rather, the increase in hydrogen coverage, $\Delta\theta_H$, from the lowest overvoltage at which measurements were made. Data of Tables 25 to 28 are plotted in Figure 60 which shows that $-\eta$ increases linearly with $\log_{10}(\Delta\theta_H)$ for four experiments (B2 to B5).

The coincidence of the straight line relationship in Figure 60 for the same acid concentration is moderately good. An intermediate step is the calculation of the charge equivalent to the adsorbed hydrogen, or rather, its increase Δq_H, relative to the value of q_H at the lowest $-\eta$ of the measurements. The equations defining Δq_H and $\Delta\theta_H$ are:

$$\Delta q_H = k'\Delta\theta_H \longrightarrow k' = \frac{nF}{N} \qquad (3.3)$$

$$\Delta q_H = -\int_{(-\eta)_{min}}^{-\eta} \Delta C_{ps}\, d\eta \qquad (3.4)$$

TABLE 25. CALCULATION OF INCREASE OF HYDROGEN COVERAGE FOR SILVER ELECTRODE B2 CATHODISED IN 1 mol ℓ^{-1} $HClO_4$ AT A CURRENT DENSITY 0.116 mA cm^{-2} AFTER THE PASSAGE OF ADDITIONAL CATHODIC CHARGE $-\Delta Q = 261.64$ C cm^{-2}. TOTAL CATHODIC CHARGE $-Q = 262$ C cm^{-2}.

$-\eta$/mV	ΔC_{ps}/μF cm^{-2}	Δq_H/μC cm^{-2}	$\Delta\theta_H$
278	5	-	-
336	8	0.40	0.0025
354	10	0.56	0.0034
360	11	0.62	0.0038
370	11.5	0.73	0.0045
379	12.5	0.84	0.0052

TABLE 26. CALCULATION OF INCREASE OF HYDROGEN COVERAGE FOR SILVER ELECTRODE B3 CATHODISED IN 1 mol ℓ^{-1} $HClO_4$ AT A CURRENT DENSITY 0.231 mA cm^{-2} AFTER THE PASSAGE OF ADDITIONAL CATHODIC CHARGE $-\Delta Q$ = 190 C cm^{-2}. TOTAL CATHODIC CHARGE $-Q$ = 192 C cm^{-2}.

$-\eta$/mV	ΔC_{ps}/μF cm^{-2}	Δq_H/μC cm^{-2}	$\Delta\theta_H$
277	9.5	-	-
329	10	0.51	0.0031
346	11.5	0.69	0.0042
362	18	0.93	0.0057
376	22.5	1.21	0.0074
386	26*	1.45	0.0089

*Obtained by the extrapolation.

TABLE 27. CALCULATION OF INCREASE OF HYDROGEN COVERAGE FOR SILVER ELECTRODE B4 CATHODISED IN 0.1 mol ℓ^{-1} $HClO_4$ AT CURRENT DENSITIES 0.116 and 1.16 mA cm^{-2} AFTER THE PASSAGE OF ADDITIONAL CATHODIC CHARGE $-\Delta Q$ = 274 C cm^{-2}. TOTAL CATHODIC CHARGE ΣQ = 293 C cm^{-2}.

$-\eta$/mV	ΔC_{ps}/μF cm^{-2}	Δq_H/μC cm^{-2}	$\Delta\theta_H$
264	10	-	-
327	20	0.95	0.0058
344	41.3	1.45	0.0089
352	52.5	1.84	0.011
362	66.3	2.44	0.015
372	92.5	3.23	0.02

TABLE 28. CALCULATION OF INCREASE OF HYDROGEN COVERAGE FOR SILVER ELECTRODE B5 CATHODISED IN 0.1 mol ℓ^{-1} $HClO_4$ AT A CURRENT DENSITY 0.116 mA cm^{-2} AFTER THE PASSAGE OF ADDITIONAL CATHODIC CHARGE $-\Delta Q$ = 171.6 C cm^{-2}. TOTAL CATHODIC CHARGE $-Q$ = 172 C cm^{-2}.

$-\eta$/mV	ΔC_{ps}/μF cm^{-2}	Δq_H/μC cm^{-2}	$\Delta\theta_H$
289	11.2	-	-
304	15.1	0.20	0.0012
334	26.3	0.82	0.0050
348	38.8	1.27	0.0078
355	50.0	1.58	0.0097
357	62.5	1.70	0.01
364	75	2.18	0.013
368	91.3	2.51	0.015

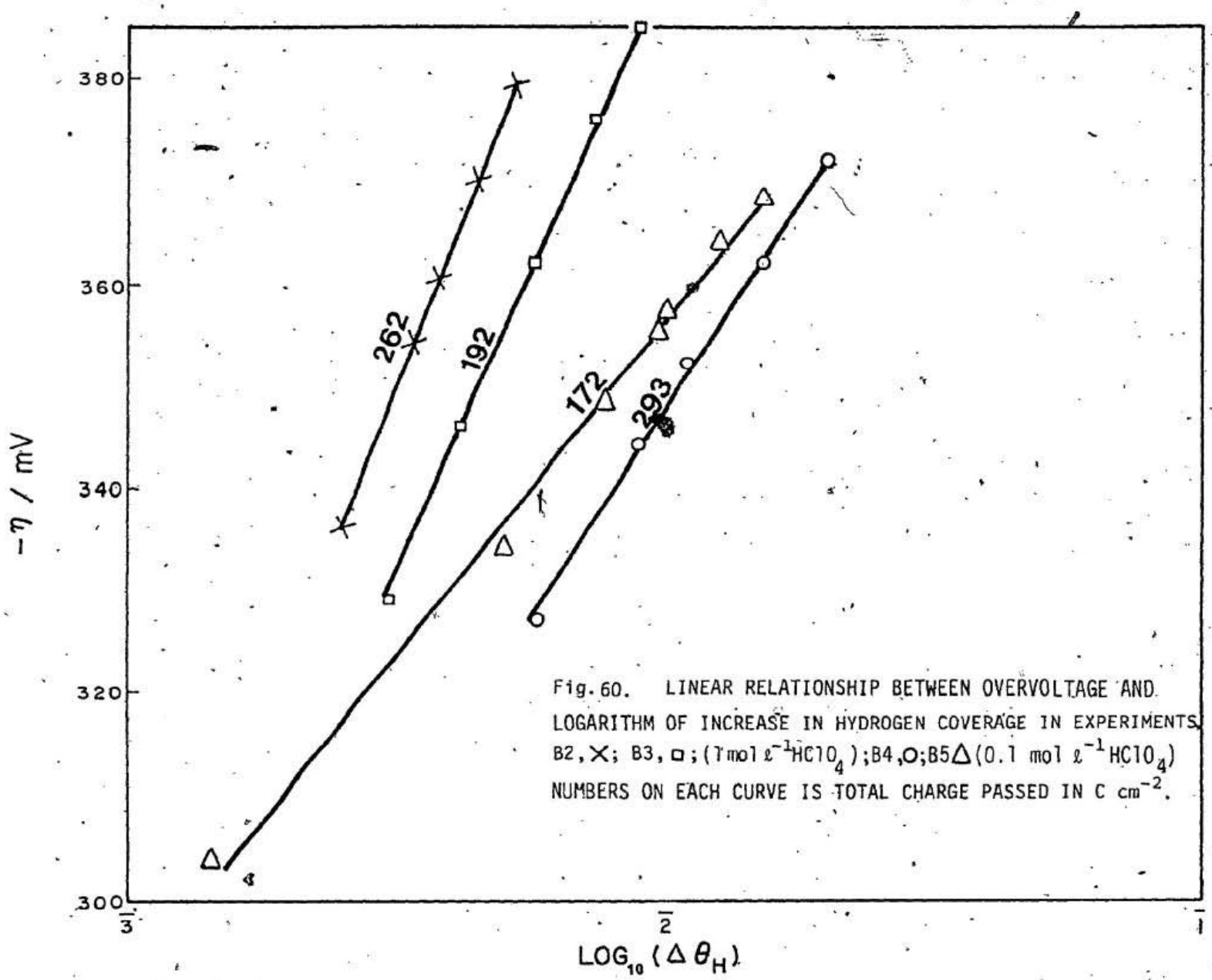

Fig. 60. LINEAR RELATIONSHIP BETWEEN OVERVOLTAGE AND LOGARITHM OF INCREASE IN HYDROGEN COVERAGE IN EXPERIMENTS B2, ×; B3, □; (1 mol ℓ^{-1} $HClO_4$); B4, ○; B5 △ (0.1 mol ℓ^{-1} $HClO_4$) NUMBERS ON EACH CURVE IS TOTAL CHARGE PASSED IN C cm^{-2}.

$$\Delta\theta_H = \int_{\theta_{min}}^{\theta} = \frac{1}{k'} \int_{(-\eta)_{min}}^{-\eta} \Delta C_{ps}\, d\eta$$

$$= \frac{N}{nF} \int_{(-\eta)_{min}}^{-\eta} \Delta C_{ps}\, d\eta \qquad (3.5)$$

Where k' is the value of q_H at $\theta_H = 1$, or the total charge required to form a monolayer of adsorbed hydrogen atoms, N is Avogadro's number, n is the number of adsorption sites cm^{-2} and F is the Faraday. A similar method was used by Rao (61) to calculate $\Delta\theta_H$ for lead cathodised in $HClO_4$.

Although polycrystalline silver samples were used, in order to estimate k' the reasonable assumption was made that the low index planes (100 to 110) of silver are, on the average, equally exposed at the surface. This assumption was also made by Spenadel and Boudart (152) for platinum and by Anderson and Baker (153) for tungsten for determination of the surface areas of platinum and tungsten, respectively. The site densities (number of silver atoms per cm^2) of (100) and (110) faces of face-centred cubic silver crystals are 1.20×10^{15} and 8.47×10^{14}, respectively, giving an average of 1.02×10^{15} sites cm^{-2}. From the average number of sites cm^{-2} with the assumption of one hydrogen atom per silver atom, k' = 163 $\mu C\ cm^{-2}$ was calculated.

Increases of hydrogen coverage up to 2% in 0.1 mol ℓ^{-1} $HClO_4$ are indicated by these calculations. The values of 2% and 0.89% were calculated for silver electrodes in experiment B4 (see Table 27)

and B3, respectively, (see Table 26) after passage of some 293 and 192 C cm^2. Interpretations arise in these calculations and in others, suggesting that ΔC_{ps} or $\Delta\theta_H$ increased with increase of hydrogen overvoltage (see Fig. 60) on silver. Calculation of the increase in fractional surface coverage with adsorbed hydrogen atoms of silver, $\Delta\theta_H$, suggests that the values in 0.1 mol ℓ^{-1} $HClO_4$ are higher than in 1 mol ℓ^{-1} $HClO_4$. This estimate of $\Delta\theta_H$ for silver may be low because the integration was carried out over the very narrow range of $-\eta$ which has been studied on the silver electrode and in particular because of the lack of $C_{expt.}$ data extending to $-\eta \simeq 0$.

The above conclusions concerning estimated hydrogen coverages depend on an assumption that impurities present in solution are not being deposited on the silver cathode to such an extent as to give rise to the phenomena observed. This assumption might be tested by such improvements in technique as would give rise to more rapid changes in overvoltages and capacitances than have been reported here.

Chapter 4

DISCUSSION

The most important phenomena observed in this part of the work are the simultaneous rise of overvoltage and increase in capacitance with the logarithm of the total charge passed up to about 60 C cm^{-2}. The possibility that these phenomena are due to oxygen evolution at the anode, impurities, Pt dissolution from the anode and plating out on the cathode, changes in the condition of the electrode, e.g. area increase or decrease, or anion adsorption can be discounted for the following reasons:

(i) The presence of O_2 in the electrolyte would cause a complete reversal of the increase of $-\eta$ with $-Q$. This has in fact been observed in the initial overvoltage measurements in experiments A8 to A10. The decrease of overvoltage for about 30 minutes from the beginning of the experiment could be attributed to the removal of O_2 from the electrolyte (see Figure 43).

Hickling and Salt (115), and Bockris and Azzam (120,154) claimed earlier that stringent deoxygenation is unnecessary at $-i > 1$ mA cm^{-2}. This argument contradicts some well known facts. It is well known that chemisorption of O_2 by most metals is extremely rapid and, in many cases, irreversible. Thus, despite very favourable chemisorption equilibria for hydrogen on metals, such as tungsten, pre-adsorption of O_2 inhibits the chemisorption of H_2 (155,156).

It has been found that O_2 (in the gas phase) is chemisorbed on silver in both the atomic and molecular forms (157). The predominance of

one or other form depends on the coverage of the surface by O_2 and the time of contact of O_2 with the metallic surface. Zhutaeva and Shumilova (158) pointed out that adsorption of O_2 on silver in acid solutions takes place in close to reversible conditions. They also observed the existence of atomic and molecular chemisorbed oxygen on silver using electrochemical methods. It was further concluded that it is very difficult to free the surface of silver completely of chemisorbed oxygen in the presence of oxygen. When oxygen is present in the electrolyte, it will be cathodically reduced to the intermediate product, H_2O_2. In this case, the overall electrode reaction must take into account the formation of H_2O_2, i.e. $O_2 + 2H_3O^+_{aq} + 2e^- = H_2O_2 + 2H_2O$.

In the present investigation hydrogen- saturated acid solutions were used so that even if oxygen were evolved at the anode it would not be likely to interfere, because oxygen evolved in the anode compartment should have been removed by the stream of purified hydrogen passing through that compartment. The large anode used in this work minimized the anodic processes (such as O_2 evolution and Pt dissolution) by increasing the surface available for the anodic oxidation of H_2, i.e. decreasing the current density at the counter electrode.

(ii) Hydrogen overvoltage measurements on silver in solutions containing Ag^+ ions are associated with a decrease of $-\eta$ (see Table 17) and bilinear Tafel lines (see Fig. 49). Evidently, this kind of behaviour is associated with a significant concentration of Ag^+ in solution. The gradual decrease of $[Ag^+]$ explains the decrease of $-\eta$ during cathodisation in such experiments.

The high values of $-\eta$ and subsequently the existence of high b values in A1, could be because a dirty electrode was used in a dirty solution. The high Tafel slopes may be explained as being due to the presence of oxide film on the silver. The steeper portion of the Tafel curve (see Fig. 48) decreased in slope from 183 to 150 mV after passage of some cathodic charge. This change of the slope may be associated with reduction of part of the oxide film initially present on the silver surface or adsorption of surface active impurities (if they are present in the electrolyte) on the silver cathode. Oxides of metals are said to be reduced by atomic hydrogen (159) but this process appears to proceed slowly under electrolysis conditions.

The increase of $-\eta$ and $C_{expt.}$ with $-Q$ is unlikely to be due to the presence of impurities such as surface-active compounds and foreign metal cations because this increase was observed both in pre-electrolysed solutions and those also purified by passage over activated charcoal. The residual concentration of foreign metal ions, after extensive pre-electrolysis at a silver electrode in the pre-electrolysing cell, is likely to be very small. Surface-active impurities are unlikely to persist in solution after using activated-charcoal (experiments A10 and B2 to B5).

The above arguments strongly suggest that both the increase in $-\eta$ and rise in electrode capacitance with $-Q$ are not associated with the presence of impurities in solution.

(iii) A decrease or increase in surface area of silver electrode with cathodisation was also considered as a possible explanation for the increase of $-\eta$ and rise in $C_{expt.}$ with $-Q$. A decrease in surface area would cause an increase in c.d., increasing $-\eta$ and decreasing the electrode capacitance. An increase in surface area causes changes in the reverse direction. However, in the present work it was observed that both $-\eta$ and $C_{expt.}$ increased with $-Q$ in charcoal-cleaned pre-electrolysed solutions, so this hypothesis will not explain the observations.

(iv) The present phenomena are not caused by anion adsorption because the measurements were carried out in aqueous $HClO_4$ and, according to Noninski et al (143), there is insignificant specific adsorption of ClO_4^- on a polycrystalline silver electrode.

Thus, with the above arguments it is obvious that the silver + hydrogen + hydronium ion system is not well suited to critical examination of the h.e.r. unless a high degree of purity and deoxygenation is maintained. Such conditions have been approached in our satisfactory experiments, which involved electropolished silver in $HClO_4$, pre-electrolysis of the solution for sufficient time and the use of activated-charcoal. In these satisfactory experiments the overvoltage increased with periods of cathodisation and also capacitances have been found to increase with the cathodic charge when compared at constant $-\eta$ (see Figs. 57 to 59).

It was concluded from the results of increase of $-\eta$ with $-Q$ that the hydrogen surface coverage of a silver electrode might increase

in the course of cathodisation. The growth of hydrogen coverage (see Tables 25 to 28) which appears to us to be the only reasonable explanation of the pseudocapacitance data obtained in the present work, provides evidence for our hypothesis. The fact is that both $-\eta$ and $C_{expt.}$ increase linearly with $\log_{10}(-Q)$ and finally reached a plateau. The measured capacitances increased with time of cathodisation by quite large amounts and it is difficult to conceive of any other explanation (refer to the alternative possibilities discussed above) consistent with all of the facts than that of a growing hydrogen adsorption pseudocapacitance.

The hydrogen surface coverages deduced ranged up to about 2% of a monolayer, i.e. $\Delta\theta_H = 0.02$ for 0.1 mol ℓ^{-1} $HClO_4$, produced after passage of an additional 274 C cm^{-2}. The coverage was smaller, $\Delta\theta_H = 0.009$, in the case of the more concentrated 1 mol ℓ^{-1} $HClO_4$ after passage of an additional amount of charge of 190 C cm^{-2}. The degree of hydrogen coverage observed by others for silver in alkaline solutions (33,136) is much higher than the values deduced by us for acid solutions. These higher values of θ_H, i.e. 10% of a monolayer in 0.1 mol ℓ^{-1} NaOH (33) and 25% of a monolayer in 0.5 mol ℓ^{-1} KOH (136) support the view that θ_H increases with increasing pH as we found for the acid solutions used in our investigations.

Bockris and Conway (121) attributed the existence of two Tafel slopes at the silver cathode in acid solutions, to a phenomenon related to the specific adsorption of $H_3O^+_{aq}$ on the electrode and suggested that the mechanism is probably slow discharge followed by

Tafel combination. Bockris, Ammar and Huq (122) pointed out that the low current slope, $\frac{2.3\ RT}{F}$, can not be explained in terms of a simple interpretation of mechanisms already proposed, except by unrealistic values of α. In order to account for the slope, they proposed that the Tafel slopes of $\frac{2.3\ RT}{F}$ are consistent with the migration of H atoms over the surface as a rate determining process. They concluded that electrochemical desorption is the slow step throughout. The slow discharge process may be rate limiting at high currents as proposed by Fleischmann et al (160), Antoniou et al (116), Conway (123) and Bystrov et al (124). Antoniou et al proposed that the lower slope, $\frac{2.3\ RT}{F}$, at a silver cathode could be attributed to slow surface migration or another process which is first order with respect to H atoms or H_2. According to Conway (123) for the lower Tafel slope region, the Volmer reaction may more certainly be the r.d.s presumably at lower adsorbed hydrogen coverages than at high c.d.'s. But for the higher Tafel slope, $4.6\ \frac{RT}{F}$, the Heyrovsky reaction might be the r.d.s. Bystrov et al (124) observed the part of the Tafel curve with gradient $\frac{2.3\ RT}{F}$ did not change its position with change of pH for HCl solutions. They proposed that adsorption of hydrogen practically does not occur in this potential region. The most probable mechanism was suggested to be the slow discharge with subsequent rapid electrochemical desorption for higher c.d.'s.

The present work confirms the existence of two Tafel slopes, from which it should be noted that the h.e.r. at silver cathodes may have two different mechanisms for the two portions of differing gradients.

It should be noted that the two Tafel slopes are observed even in highly purified solution and do not, therefore, arise from the adsorption of some impurities. The low hydrogen coverage at silver cathodes in acid solutions gives us a basis for concluding that the slow discharge is the r.d.s. for the portion with b value of about $\frac{4.6\ RT}{F}$ (calculated $\alpha \simeq 0.5$). Decreasing the acid concentration increased the hydrogen coverage in the present work. A possible reason for the difference in hydrogen coverage using 0.1 and 1 mol ℓ^{-1} $HClO_4$ might be due to an increase in the rate of the Heyrovsky reaction in more concentrated acid solution because the $[H_3O^+]$ plays an important role in the electrochemical desorption step. Therefore, the mechanism of the h.e.r. at silver cathodes might be slow discharge followed by rapid electrochemical desorption:

$$H_3O^+(aq) + Ag + e^- \overset{slow}{=} Ag\text{-}H_{ads} + H_2O \qquad (4.1)$$

$$H_3O^+(aq) + H_{ads}\text{-}Ag + e^- \overset{fast}{=} Ag + H_2(g) + H_2O \qquad (4.2)$$

At low c.d.'s where the Tafel slope is given by $\frac{2.3\ RT}{F}$, taking into account that adsorption of hydrogen practically does not occur (124), and the lack of data for θ_H at cathodic c.d.'s smaller than 600 μA cm^{-2}, it is difficult to deduce what mechanism actually governs the reaction in this Tafel region.

Since the rate of step (4.2) depends on collision between hydronium ions and $Ag\text{-}H_{ads}$, it is obvious that an increase in the rate of reaction (4.2) seems likely to occur if θ_H increases from a low value to some larger value. It follows that hydronium ion

discharge (4.1) must itself increase in rate since no other adsorbed hydrogen production processes are involved in 0.1 and 1 mol ℓ^{-1} $HClO_4$ at the c.d.'s applied here (the initial limiting current density for the discharge of $H_3O^+_{aq}$ is discussed in Chapter 4 of Part 1). These processes, however, continue when a steady-state is reached, i.e. at a steady-state, the rate of production and consumption of adsorbed hydrogen being linked by an equilibrium, i.e. $k_V (1 - \theta_H) = k_H \theta_H$ where k_V and k_H are the rate constants for the Volmer (4.1) and Heyrovsky (4.2) reactions, respectively. When the steady-state is reached after about 60 C cm^{-2} of cathodisation, there are no further changes of overvoltage and $C_{expt.}$ with $-Q$ as has been found in the present work (see Figures. 43,57,58,59).

Let us now consider overshoot hysteresis. One important difference exists between the increase of $-\eta$ with $-Q$ and the overshoot phenomenon. The overall increase of $-\eta$ appear to be irreversible; it occurs once only with each electrode. The extent of overshoot hysteresis decreased as $-Q$ increased. The overshoot hysteresis is opposite to what might have been expected from the general increase of $-\eta$ with cathodisation. In experiment A10, for instance, decreasing the current density from 11.6 to 0.116 mA cm^{-2}, $-\eta$ increased by about 45 mV. One may claim that the overshoot hysteresis, e.g. for decreasing c.d., might be due to (i) the desorption of surface-active impurities; or to (ii) desorption of adsorbed or absorbed hydrogen from the surface or bulk of the silver cathode, respectively. It is not likely to be due to (i) because (a) intensive pre-electrolysis

was carried out and the behaviour was found to be the same even with charcoal-cleaned pre-electrolysed solution; (b) the values of slopes observed in the low c.d's range were in good agreement with other workers (116,121,122) who used pre-electrolysed solutions. The overshoot hysteresis at silver electrodes could be largely a surface phenomenon while a long term increase of $-\eta$ might be a bulk one.

The variation of $-\eta$ with time of electrolysis during the h.e.r. has been observed for many metals: Pb (9,61,107), Pt (51,122), Fe (147), Pd (161), Ta, Tl and Mo (154) and Ag (116). Both increase in $-\eta$ on Pd, Pt, Fe, Ta, Tl and Mo and decrease in $-\eta$ with time on Pb have been interpreted in terms of adsorption of hydrogen on the surface of Ta, Tl and Mo and a change in the properties of the Pb, Pt, Fe and Pd due to hydrogen absorption.

During cathodisation, hydrogen atoms are produced in large numbers at the electrode-electrolyte interface. Thus, for an electrode of 0.865 cm^2, surface area, as in the present case, 141 μC generates a monolayer of hydrogen atoms (with the assumption of one hydrogen atom per silver atom), i.e. 14.1 μA generates a monolayer in 10 seconds. The rate of penetration of hydrogen atoms into the bulk of silver will depend on the diffusion constant and the concentration gradient of hydrogen atoms. It may, therefore, be anticipated that penetration will increase with the imposed c.d. up to some limit at which the surface concentration attains a maximum value.

When a steady-state current has passed for some time it effects little change in the bulk or surface hydrogen atom concentration because

at the steady-state c.d., a constant flow of atoms occurs from the surface to the bulk, i.e. at the steady-state permeation current the H concentration gradient in the bulk metal is constant. Changing the constant cathodic c.d. alters the steady-state situation more or less rapidly, and time is required for the establishment of a new steady-state. Increasing the cathodic c.d. leads initially to much faster diffusion from the surface to the bulk, but later the diffusion rate falls as the concentration gradient near the surface gets less steep than initially, though steeper than at the lower current. Decreasing the current results in a considerable slowing down of the diffusion rate so that the hydrogen coverage initially remains close to that at the higher current.

In permeation studies, we have shown that the diffusion of electrolytic hydrogen through silver foil of 0.1 mm thickness possibly occurs with a diffusivity of about 2.5 to 4.5 x 10^{-6} $cm^2 s^{-1}$. The steady-state permeation current and the diffusion coefficient of hydrogen atoms in silver (with the assumption that the values of D_H obtained are correct) were used to calculate the H concentrations just beneath the cathode surface, C_o, for different c.d.'s with the results of 5 x 10^{-8} to 8 x 10^{-8} g atom H cm^{-3} of silver. The values of 2.1 x 10^{-5}, 2.87 x 10^{-5} and 3.74 x 10^{-5} cm^2 s^{-1} for D_H in silver at temperatures of 773, 823 and 873 K, respectively, obtained by Eichenauer et al (112), cannot be compared directly with the D_H values obtained by us using the electrochemical method at room temperature. But extrapolation of their results gives $D_H \simeq 9 \times 10^{-9}$

$cm^2\ s^{-1}$ at 298 K which is about 500-fold lower than the values obtained by us.

Using a more modern method of gas analysis, i.e. using a mass spectrometer, Thomas (113) obtained more reliable data for the solubility of H in silver, e.g. 4.7×10^{-8} and 4.8×10^{-7} g atom H cm^{-3} of silver for temperatures 873 K and 1173 K, respectively. The solubility values obtained by Thomas are considerably less than (ca. 10-fold for the same temperature) the values deduced by other workers (110, 111,112) who used volume measurements which were unreliable, because silver also dissolves oxygen atoms (162). Extrapolation of Thomas's results gives $C_o \simeq 1.9 \times 10^{-15}$ g atom H cm^{-3} of silver at 298 K. Thomas's results for the bulk H concentration in silver show that the C_o is negligible in silver and probably with the electrochemical methods used by us could not be measured.

Recently Diederichs (163) extended the time-lag method to hydrogen diffusion in pure silver, applying ultrahigh vacuum evaporation techniques. He used thin silver films of some 1000Å thickness, evaporated onto palladium foils which acted only as a support for mechanically stable diffusion foils necessary for time-lag experiments. The preliminary D_H was $7 \pm 3 \times 10^{-13}$ $cm^2\ s^{-1}$ for silver at 303 K.

SUMMARIZING CONCLUSIONS

Differential pulse anodic stripping voltammetry and differential pulse polarography have been used to determine the Pb^{2+} concentrations generated by lead disintegration, which has been measured under appropriate experimental conditions in perchloric and sulphuric acid solutions. Initial rates were determined from linear $[Pb^{2+}]$ versus time plots. Disintegration rates increased linearly with cathodic current density, above threshold current densities, which have been found to be much lower than Gastwirt and Salzberg (70) measured for aqueous H_2SO_4. Increasing the hydronium ion concentration, at a particular c.d., caused the disintegration rate to drop drastically for concentrations greater than 0.01 mol ℓ^{-1}. Threshold c.d.'s increased with $[H_3O^+]$. Discontinuous disintegration was detected at a cathodic current density of ca. 10 mA cm^{-2} depending on acid concentration. At $i = -1$ mA cm^{-2} no disintegration whatsoever was detected during five days of cathodisation.

Hydride formation as a cause of cathodic disintegration has been discussed in the light of evidence from gas phase hydrogen interactions with lead. Support has not been obtained for a definite PbH_2 composition as an intermediate. Water molecules appear to play an important role in cathodic disintegration in the absence of alkali metal cations, which accelerate disintegration when they are present. Hydronium ions clearly inhibit cathodic disintegration, most probably because of the alternative desorption path they provide for adsorbed hydrogen atoms. Diffusion of hydrogen atoms into the lead lattice

and their subsequent combination to H_2 are proposed as important steps in the process of discontinuous disintegration, which is reported here for the first time. Measurements of electrode potential under disintegration conditions are recommended for further investigation of these phenomena.

The surface hydrogen coverage, Θ_H, of a silver cathode in acid solution is not immeasureably small. Electrode capacitances of silver cathodes have been observed to grow during cathodisation, simultaneously with an increase in the hydrogen overvoltage. Both changes occur in highly purified systems, well supplied with hydrogen and are attributed to adsorption and/or absorption of hydrogen by silver. The increase in hydrogen coverage during cathodisation with charge passed, $\Delta\Theta_H$, increase with hydrogen overvoltage and suggest at $-\eta$ of about 370 mV a Θ_H of at least 2% of a monolayer in 0.1 mol ℓ^{-1} $HClO_4$ and smaller values in 1 mol ℓ^{-1} solution. Evidence of other work suggests the hydrogen coverage of silver increases with pH.

The increase of overvoltage at constant c.d. as a function of cathodic charging, if it is related to hydrogen atoms on the surface or in the bulk of the silver, suggests a decreased availability of electrons for charge transfer as hydrogen builds up. The behaviour of silver is, in this respect, opposite to that found by Rao and Smith (9,61,61a,107) with lead. Overshoot hysteresis on silver cathodes is in the same direction as found on lead, suggesting a common origin, e.g. a slow surface or a bulk phenomenon. The long term increase of overvoltage with $-Q$ shows evidence of a saturation effect, which is

also shown by the capacitance data. This could indicate that a surface phenomenon is responsible or it could be consistent with the very low bulk solubility of H in silver extrapolated from Thomas's high temperature data (113).

Further work to determine the diffusivity and solubility of electrolytically generated hydrogen in silver must utilise a more sensitive technique and probably superior experimental conditions compared with the present work.

REFERENCES

1. J. Tafel, Z. Phys. Chem., 1905, 50, 641.

2. K.J. Vetter, "Electrochemical Kinetics", Academic Press, New York, 1967.

3. J. O'M. Bockris and E.C. Potter, J. Electrochem. Soc., 1952, 99, 169.

4. R. Parsons, J. Chim. Phys., 1952, 49, C82.

5. S. Schuldiner and J.P. Hoare, J. Phys. Chem., 1957, 61, 705.

6. D.J.G. Ives, Can. J. Chem., 1959, 37, 213.

6a. C.A. Knorr, Z. Elektrochem., 1955, 59, 647.

7. F.A. Lewis, "Recent Progress in Surface Science", eds. J.F. Danielli, A.C. Riddiford and M.D. Rosenberg, Academic Press, New York, Vol. 3, 1970, 71.

8. C.V. King, J. Electrochem. Soc., 1955, 59, 193.

9. F.R. Smith, Ph.D. Thesis, London, 1964.

10. H.L.F. van Helmholtz, Ann. Physik, 1853, 89, 211; 1879, 7, 337.

11. G. Gouy, J. Phys. Radium, 1910, 9, 457.

12. D.L. Chapman, Phil. Mag., 1913, 25, 475.

13. O. Stern, Z. Elektrochem., 1924, 30, 508.

14. D.C. Grahame, J. Chem. Phys., 1950, 18, 903.

15. L. Levine, G.M. Bell and D. Calvert, Can. J. Chem., 1962, 40, 518.

16. J. O'M. Bockris, M.A.V. Devanathan and K. Muller, Proc. Roy. Soc. (London), 1963, A274, 55.

17. J.A.V. Butler, Trans. Faraday Soc., 1923, 19, 729; 1932, 28, 379.

18. R.W. Gurney, Proc. Roy. Soc. (London), 1931, A134, 137.

19. A.N. Frumkin, Z. Phys. Chem., 1932, A160, 116; 1933, A164, 121.

20. M. Volmer and T. Erdey-Gruz, Z. Phys. Chem., 1930, A150, 203.

21. J. Horiuti and M. Polanyi, Acta Physicochim. U.R.S.S., 1935, 2, 505.

22. D.B. Matthews, Austral. J. Chem., 1959, 22, 1349.

23. J. O'M. Bockris and D.B. Matthews, Proc. Roy. Soc. (London), 1966, A292, 479.

24. A.N. Frumkin, "Adv. Electrochem. and Electrochem. Eng.", ed. P. Delahay, Interscience-Wiley, New York, Vol. 1, 1961, 65.

25. H. Eyring, S. Glasstone and K.J. Laidler, J. Chem. Phys., 1939, 7, 1053.

26. P. Delahay, "Double Layer and Electrode Kinetics", Interscience-Wiley, New York, 1965, 197.

27. F.R. Smith, Private communication.

28. G. Armstrong and J.A.V. Butler, Trans. Faraday Soc., 1933, 29, 1261.

29. A.N. Frumkin, V.S. Bagotsky, Z.A. Jofa and B.N. Kabanov, "Kinetics of Electrode Processes", Moscow Univ. Press, Moscow, 1952.

30. A. Eucken and B. Weblus, Z. Elektrochem., 1951, 55, 114.

31. D.C. Grahame, J. Electrochem. Soc., 1952, 99, 370C.

32. E. Gileadi and B.E. Conway, "Modern Aspects of Electrochemistry", eds. J. O'M. Bockris and B.E. Conway, Butterworths, London, Vol. 3, 1964, 347.

32a. B.E. Conway, "Theory and Principles of Electrode Processes", Ronald Press, New York, 1965.

32b. E. Gileadi, E. Kirowa-Eisner and J. Penciner, "Interfacial Electrochemistry An Experimental Approach", Addison-Wesley, London, 1975.

33. M.A.V. Devanathan, J. O'M. Bockris and W. Mehl, J. Electroanal. Chem., 1959/60, 1, 143.

34. B.E. Conway and E. Gileadi, Can. J. Chem., 1964, 42, 90.

35. E. Gileadi and B.E. Conway, J. Chem. Phys., 1963, 39, 3420.

36. B.E. Conway, E. Gileadi and M. Dzieciuch, Electrochim. Acta, 1963, 8, 143.

37. M. Breiter, "Trans. Symp. on Electrode Processes" (1959), ed. E. Yeager, The Electrochemical Society, John Wiley and Sons, New York; 1961, 307.

38. H. Angerstein-Kozlowska and B.E. Conway, J. Electroanal. Chem., 1964, 7, 109.

39. B.E. Conway, E. Gileadi and H. Angerstein-Kozlowska, J. Electrochem. Soc., 1965, 112, 341.

40. P.P. Bowden and E.K. Rideal, Proc. Roy. Soc. (London), 1928, A120, 59, 80.

41. J. Pearson and J.A.V. Butler, Trans. Faraday Soc., 1938, 34, 1163.

42. M. Breiter, C.A. Knorr and V. Völkl, Z. Elektrochem., 1955, 59, 881.

43. R. Woods, "Electroanalytical Chemistry", ed. A.J. Bard, Marcel Dekker Inc., New York, Vol. 9, 1976, 1.

44. M.A.V. Devanathan and Z. Stachurski, Proc. Roy. Soc. (London), 1962, A270, 90.

45. H. Züchner and N. Boes, Ber. Bunsenges Phys. Chem., 1972, 76, 783.

46. B.L. Muju and F.R. Smith, Can. J. Chem., 1971, 49, 2406.

47. P. Kedzierzawski, K.M. Benczek and A. Sadkowski, Bull. Acad. Pol. Sci., 1976, 24, 595.

48. J. McBreen, L. Nanis and W. Beck, J. Electrochem. Soc., 1966, 113, 1218.

49. I. Cadersky, B.L. Muju and F.R. Smith, Can. J. Chem., 1970, 48 1789.

50. V. Breger and E. Gileadi, Electrochim. Acta, 1971, 16, 177.

51. E. Gileadi, M.A. Fullenwider and J. O'M. Bockris, J. Electrochem. Soc., 1966, 113, 926.

52. N. Pangarov and I. Christova, Bulg. Acad. Sci., 1969, II, 813.

53. T.P. Radhakrishnan and L.L. Shrier, Electrochim. Acta, 1966, 11, 1007.

54. I.I. Phillips, P. Poole and L.L. Shreir, Corros. Sci., 1972, 12, 855.

55. L. Nanis and T.K.G. Namboodhiri, J. Electrochem. Soc., 1972, 119, 691.

56. J. O'M. Bockris, M.A. Genshaw and M.A. Fullenwider, Electrochim. Acta, 1970, 15, 47.

57. H. Buchold and G. Sicking, Ber., 1972, 2, 391.

58. F.R. Smith and M. Hammerli, Z. Phys. Chem. (N.F.), 1971, 74, 75.

59. C.D. Kim and B.E. Wilde, J. Electrochem. Soc., 1971, 118, 202.

60. J. O'M. Bockris, J. McBreen and L. Nanis, J. Electrochem. Soc., 1965, 112, 1025.

61. G.M. Rao, Ph.D. Thesis, Memorial University, 1973.

61a. G.M. Rao and F.R. Smith, J. Chem. Soc.: Chem. Comm., 1972, 266.

62. F. Paneth and O. Norring, Ber., 1920, 53B, 1693.

63. G. Schultze and E. Müller, Z. Phys. Chem., 1930, 6B, 267.

64. F.E. Saalfeld and H.J. Svec, Inorg. Chem., 1963, 2, 46.

65. E.J. Weeks, J. Chem. Soc., 1925, 127, 2845.

66. B.R. Wells and M.W. Roberts, Proc. Chem. Soc., 1964, 173.

67. M.W. Roberts and N.J. Young, Trans. Faraday Soc., 1970, 66, 2636.

68. H.C. Roberts and R.S. Eachus, J. Chem. Phys., 1972, 57, 3022.

69. H.W. Salzberg, J. Electrochem. Soc., 1953, 100, 146.

70. L.W. Gastwirt and H.W. Salzberg, ibid., 1957, 104, 701.

71. H.W. Salzberg, F. Mies and L.W. Gastwirt, U.S. Govt. Research Rept., 1959, Nonr 1597 (02), Nr 359-367.

72. G. Bredig and F. Haber, Ber., 1898, 31, 2741.

73. F. Haber and M. Sack, Z. Elektrochem., 1902, 8, 245.

74. H. Angerstein, Bull. Acad. Pol. Sci., 1955, 3, 447.

75. J. van Muylder and M. Pourbaix, C.I.T.C.E. Rept., 6th Meeting (1954), Butterworths, London, 1955, 342.

76. B.N. Kabanov, I.C. Kiseleva, I.I. Astakhov and N.N. Tomashova, Elektrokhim., 1965, 1, 1023.

77. B.N. Kabanov, Electrochim. Acta, 1968, 13, 19.

78. A.I. Chernomorskii, I.G. Kiseleva and B.N. Kabanov, Elektrokhim., 1970, 6, 280, 429.

79. A.I. Chernomorskii and B.N. Kabanov, ibid., 1970, 6, 1224; 1972, 8, 140.

80. N.N. Tomashova, I.G. Kiseleva and B.N. Kabanov, ibid., 1971, 7, 438; 1972, 8, 112.

81. B.N. Kabanov and Z.A. Jofa, Acta Physicochim. U.R.S.S., 1939, 10, 617.

82. G.J. Hills and D.J.G. Ives, "Reference Electrodes", eds. D.J.G. Ives and G.J. Janz, Academic Press, New York, 1961, 71.

83. M. Schutze, Angew. Chem., 1958, 70, 697.

84. D.J.C. Yates, J. Chem. Ed., 1967, 44, 699.

85. W.J. Muller, Sitz. Akad. Wiss. Wien., 1927, 136, 559.

86. U.R. Evans, Nature, 1930, 126, 130.

87. T.P. Hoar and J.A.S. Mowat, Nature, 1950, 165, 64.

88. A. Hone and E.C. Pearson, Met. Progress, 1948, 53, 363.

89. T.P. Hoar and T.W. Farthing, Nature, 1952, 169, 324.

90. M. Cole and T.P. Hoar, C.I.T.C.E. Rept., Eight Mtg. (1956), Butterworths, London, 1958, 158.

91. I.A. Menzies, G.W. Marshall and G.B. Griffin, Corros. Sci., 1969, 9, 287.

92. M. Novak, A.K.N. Reddy and H. Wroblowa, J. Electrochem. Soc., 1970, 117, 733.

93. T.P. Hoar, "Modern Aspects of Electrochemistry", ed. J. O'M. Bockris, Butterworths, London, Vol. 2, 1959, 262.

94. M.M. Nikiforova and Z.A. Jofa, Proc. Acad. Sci. U.S.S.R.: Sect. Phys. Chem., 1957, 115, 575.

95. J.E. Harrar and F.B. Stephens, J. Electroanal. Chem., 1962, 3, 112.

96. A.R. Nisbet and A.J. Bard, ibid., 1963, 6, 332.

97. J.W. Bixler and S. Bruckenstein, Anal. Chem., 1965, 37, 791.

98. R. Naumann and W. Schmidt, Z. Anal. Chem., 1971, 257, 337.

99. L. Duic, S. Szechter and S. Srinivasan, J. Electroanal. Chem., 1973, 41, 89.

100. E.P. Parry and R.A. Osteryoung, Anal. Chem., 1965, 37, 1634.

101. A.A. Rostami and F.R. Smith, in "Power Sources 7", ed. J. Thompson, Academic Press, New York, 1979.

102. L.J.J. Janssen and J.G. Hoogland, Electrochim. Acta, 1970, 15, 1013.

103. H.S. Harned and W.J. Hamer, J. Amer. Chem. Soc., 1935, 57, 27.

104. D.P. Smith, "Hydrogen in Metals", Univ. of Chicago Press, Chicago, 1948.

105. H.G. Deming and B.C. Hendricks, J. Amer. Chem. Soc., 1923, 45, 2857.

106. W.R. Opie and N.J. Grant, Trans. Met. Soc. A.I.M.E., 1951, 191, 244.

107. D.J.G. Ives and F.R. Smith, Trans. Faraday Soc., 1967, 63, 217.

107a. L.W. Barr, "Diffusion Processes", eds. J.N. Sherwood, A.V. Chadwick, W.M. Muir and F.L. Swinton, Gordon and Breach Science, London, Vol. 1, 1971, 173.

108. T. Graham, Phil. Mag., 1866, 32, 503.

109. M. Baxter, J. Amer. Chem. Soc., 1899, 22, 362.

110. E.W.R. Steacie and F.M.G. Johnson, Proc. Roy. Soc. (London), 1928, A117, 662.

111. W. Siegelin, K. H. Lieser and H. Witte, Z. Elektrochem., 1957, 61, 359.

112. W. Eichenauer, Künzig and A. Publer, Z. Metallk., 1958, 49, 220.

113. C.L. Thomas, Trans. Met. Soc. A.I.M.E., 1967, 239, 485.

114. M. Knobel, P. Caplan and E. Eisemann, Trans. Electrochem. Soc., 1923, 43, 55.

115. A. Hickling and F.W. Salt, Trans. Faraday Soc., 1940, 36, 1224; 1941, 37, 451.

116. A.A. Antoniou and F.E.W. Wetmore, Can. J. Chem., 1959, 37, 222.

117. K. Gossner and F. Mansfeld, Z. Phys. Chem. (N.F.), 1968, 58, 19.

118. A.B. Kilimnik and A.L. Rotinian, Elektrokhim., 1970, 6, 330.

119. A.M. Azzam, J. O'M. Bockris, B.E. Conway and H. Rosenberg, Trans. Faraday Soc., 1950, 46, 918.

120. J. O'M. Bockris and A.M. Azzam, ibid., 1952, 48, 145.

121. J. O'M. Bockris and B.E. Conway, ibid., 1952, 48, 724.

122. J. O'M. Bockris, I.A. Ammar and A.K.M.S. Huq, J. Phys. Chem., 1957, 61, 879.

123. B.E. Conway, Proc. Roy. Soc. (London), 1960, A256, 128.

124. V.I. Bystrov and L.I. Krishtalik, Elektrokhim., 1967, 3, 1345, 1499; 1968, 4, 233.

125. A. Wetterholm, Trans. Faraday Soc., 1949, 45, 462.

126. P.J. Hillson, ibid., 1952, 48, 462.

127. H. Gerischer and W. Mehl, Z. Elektrochem., 1955, 59, 1049.

128. Ya. M. Kolotyrkin, Trans. Faraday Soc., 1959, 55, 455.

129. K. Gossner, Chr. Löffler and G.M. Schwab, Z. Phys. Chem., 1961, 28, 229.

130. L. Rüetschi, J. Electrochem. Soc., 1963, 110, 835.

131. E.G. Gagnon, ibid., 1973, 120, 1052.

132. L. Ramaley and C.G. Enke, ibid., 1965, 112, 947.

133. I.G. Dagaeva, D.I. Leikis and E.S. Sevast'yanov, Elektrokhim., 1966, 2, 820.

134. D.I. Leikis and D.P. Aleksandrova, ibid., 1967, 3, 865.

135. V.I. Bystrov and L.I. Krishtalik, ibid., 1969, 5, 392.

136. V.R. Loodmaa, V.E. Past and M.E. Khaqa, ibid., 1966, 2, 927.

137. V.E. Past, Yu. K. Tamm and L.V. Tokhver, ibid., 1969, 5, 534.

138. J. O'M. Bockris and S.D. Argade and E. Gileadi, Electrochim. Acta, 1969, 14, 1259.

139. M.A.V. Devanathan and K. Ramakrishnaiah, ibid., 1973, 18, 259.

140. T. Vitanov and A. Popov, Elektrokhim., 1974, 10, 1372.

141. T. Vitanov, A. Popov and E.S. Sevest'yanov, ibid., 1975, 11, 170; 1976, 12, 382.

142. G. Valette and A. Hamelin, J. Electroanal. Chem., 1973, 45, 301.

143. I.K. Noninski and M.E. Lazarova, Khim. Ind., 1972, 44, 74.

144. G.C. Barker, "Trans. Symp. on Electrode Processes" (1959), ed. E. Yeager, The Electrochemical Society, John Wiley and Sons, New York, 1961, 366.

145. N.A. Hampson and D. Larkin, J. Electroanal. Chem., 1968, 18, 401.

146. J.J. Bikerman, "Surface Chemistry", Academic Press, New York, 1958.

147. M. Hammerli, W.J. Olmstead, B.L. Muju and F.R. Smith, J. Electroanal. Chem., 1973, 43, 45.

148. I. Cadersky, G.M. Rao and F.R. Smith, unpublished work.

149. M. Hammerli, J.P. Mislan and W.J. Olmstead, J. Electrochem. Soc., 1970, 117, 751.

150. M. Pourbaix "Atlas of Electrochemical Equilibra in Aqueous Solutions" Pergamon Press, London, 1966, 394.

151. R.E. Einziger, Ph.D. Thesis, Rensselaer Polytechnic Institude, 1973.

152. L. Spenadel and M. Boudart, J. Phys. Chem., 1960, 64, 204.

153. J.R. Anderson and B.G. Baker, ibid., 1962, 66, 482.

154. J. O'M. Bockris, Trans. Faraday Soc., 1947, 43, 417.

155. I. Langmuir, Trans. Amer. Electrochem. Soc., 1916, 29, 260.

156. I. Langmuir, J. Chem. Soc., 1940, 577.

157. L.A. Rudnitskii and N.V. Kul'kova, Dokl. Akad. Nauk. S.S.S.R., 1965, 162, 1330.

158. G.V. Zhutaeva and N.A. Shumilova, Elektrokhim., 1968, 4, 99.

159. T. Moeller, "Inorganic Chemistry, An Advanced Textbook", John Wiley and Sons, New York, 1952.

160. M. Fleischmann, J. Sowerly and H.R. Thirsk, Trans. Faraday Soc., 1957, 53, 91.

161. A.N. Frumkin and N.A. Aladjalova, Acta Physicochim. U.R.S.S., 1944, 19, 1.

162. N.V. Kul'kova and M.I. Temkin, Dokl. Akad. Nauk. S.S.S.R., 1955, 105, 1021.

163. H. Diederichs, Münster, 1976 Dissertation.

The peak reduction current for Pb^{2+} was obtained at ca. -0.3 V versus SCE. Standard conditions were maintained for each run. The results of the analysis of (some duplicated) standard Pb^{2+} solutions (average of two different runs in each case) are given in Table 1b and the calibration curves are illustrated in Figure 11, which shows that differential pulse polarography works very well in the range 0.1 to 60 ppm Pb^{2+}. The least squares value of the slope of Figure 11 from 0.1 ppm to 10 ppm is 0.199027 ± 0.000519, the corresponding intercept is 0.003089 ± 0.001945 with a correlation coefficient of 1.00000. Using the values of slope and the corresponding intercept and knowing the peak current of each unknown lead sample, the concentration of lead disintegrated was calculated.

(b) Evaluation of Calibration Curves

A study has been made to evaluate possibly important effects of supporting electrolyte concentration on the peak current for the same Pb^{2+} concentration. The calibration curves of lead analysed by both differential pulse polarography and DPASV relied upon 0.01 mol ℓ^{-1} $HClO_4$ as a supporting electrolyte, whereas actual analyses were made in various concentrations of $HClO_4$ and H_2SO_4.

(i) Differential Pulse Polarography

Table 2 summarizes the results of lead analysis using differential pulse polarography comparing the peak currents for different supporting electrolytes concentrations with the same $[Pb^{2+}]$ with those obtained from the calibration curve, Figure 11, for which 0.01 mol ℓ^{-1} $HClO_4$ was used.

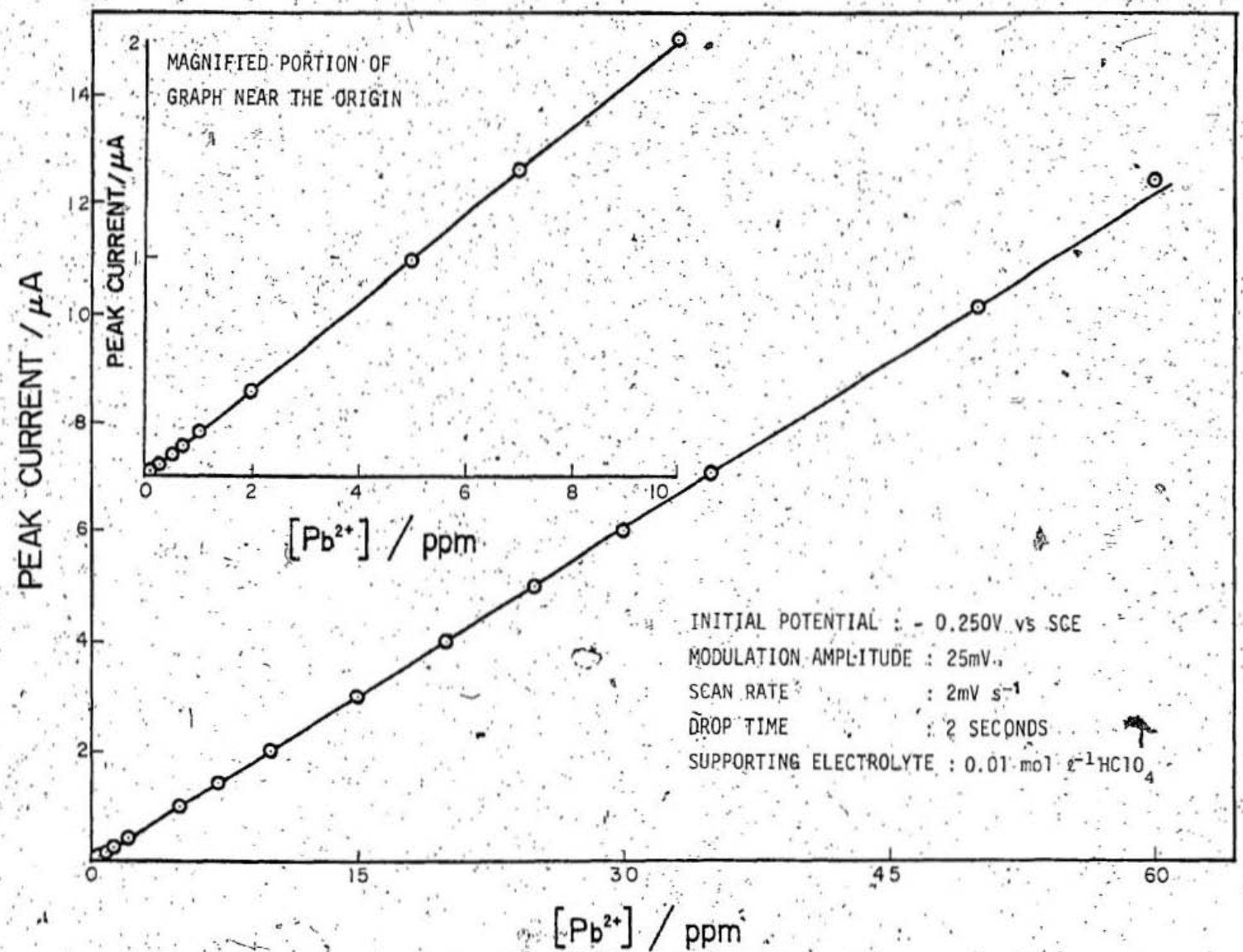

Fig.11. CALIBRATION CURVE FOR Pb^{2+} ANALYSIS BY DIFFERENTIAL PULSE POLAROGRAPHY (CONCENTRATION RANGE: 0.10 TO 60 ppm).

Parry and Osteryoung (100) showed that the supporting electrolyte (KNO_3) concentration in a three-electrode system does not affect the peak current in ordinary polarography.

According to Table 2 the peak currents for Pb^{2+} in different $HClO_4$ concentrations are close to each other for the same [Pb^{2+}], the error probably being wholly random.

For various sulphuric acid concentrations at low [Pb^{2+}], there is no significant difference between the peak currents observed and that read from the calibration curve. For 1 ppm Pb^{2+} in 0.005 to 0.1 mol ℓ^{-1} H_2SO_4 only a slight decrease in peak current is noticed (about 4%) which can probably be attributed to experimental error. At higher lead concentrations, e.g. in 0.1 mol ℓ^{-1} H_2SO_4 with 4 ppm Pb^{2+} a higher fall in peak current appeared (about 13%). About 12% of this error is due to the equilibrium which exists between Pb^{2+} and $PbSO_4$, i.e. $Pb^{2+} + SO_4^{2-} = PbSO_4$ removing Pb^{2+} as insoluble $PbSO_4$ which does not respond to the electrochemical method. This discrepancy did not affect the use of calibration curve Figure 11 for lead analysis in H_2SO_4, because at higher acid concentrations the quantity of lead disintegrated was much less than 4 ppm (in the range of ppb) and the solubility product of lead sulphate was not exceeded. In the present work, most lead analyses were carried out using differential pulse polarography.

(ii) Differential Pulse Anodic Stripping Voltammetry

Some analyses were carried out using DPASV with varying acid concentration in the supporting electrolyte. As was already mentioned

TABLE 2: ANALYSIS FOR Pb^{2+} USING DIFFERENTIAL PULSE POLAROGRAPHY WITH VARIOUS CONCENTRATIONS OF SUPPORTING ELECTROLYTE.

$[Pb^{2+}]$/ ppm	Supporting electrolyte $[H_2SO_4]$/mol ℓ^{-1}	Peak current/ μA	Supporting electrolyte $[HClO_4]$/mol ℓ^{-1}	Peak current/ μA
0.4	0.001	0.087	0.1	0.088
0.4	0.005	0.086	-	-
0.4	0.1	0.086	0.01	0.086*
0.4	0.1	0.086	-	-
1	0.001	0.2	0.003	0.203
1	0.005	0.194	0.01	0.198
1	0.01	0.192	0.01	0.20*
1	0.1	0.192	0.1	0.203
4	0.001	0.82	0.003	0.82
4	0.005	0.8	-	-
4	0.01	0.79	0.01	0.80*
4	0.1	0.70	0.1	0.82

*Obtained from Calibration Curve of Figure 11.

DPASV was used only for analysis of low lead concentrations (<140 ppb). Therefore, it is safe to say that there were no errors related to the formation of $PbSO_4$ in this case.

For 50 ppb Pb^{2+} in 0.003, 0.01 (duplicated), 0.1 and 1 mol ℓ^{-1} $HClO_4$, for example, the peak currents were 0.82 μA, 0.83 μA, 0.78 μA, and 0.75 μA, respectively, compared to the peak current of 0.81 μA and 0.87 μA obtained for 50 ppb Pb^{2+} by the use of calibration curve (Figure 10 and Table 1a, respectively). The decrease may be significant but it is probably within experimental errors for such a low Pb^{2+} concentration.

Chapter 3

RESULTS

Disintegration was studied in thirty-five different experiments, one preliminary experiment with 0.01 mol ℓ^{-1}, thirteen with 0.003 to 0.1 mol ℓ^{-1} $HClO_4$ at high current densities, five with 0.003 to 1 mol ℓ^{-1} $HClO_4$ at low current densities, and fourteen with 0.001 to 0.1 mol ℓ^{-1} H_2SO_4 at high current densities. One involved 0.01 mol ℓ^{-1} $HClO_4$ deliberately contaminated with sodium cations and one experiment utilised 1 mol ℓ^{-1} NaOH. In all these experiments the electrolyte was prepared with highly pure acid (or base) and triple distilled water, finally being deaerated in the cell (see Fig. 7). The lead electrodes were chemically polished in 60% $HClO_4$ in contact with platinum, steamed and finally electropolished in a separate cell (see Fig. 6).

Glassware was cleaned in hot nitric acid followed by distilled and triply distilled water. In one experiment sodium hydroxide was also used as a cleaning agent. Only one experiment was carried out in 1 mol ℓ^{-1} NaOH to obtain some information about the disintegration rate under our experimental conditions but in the presence of a known high concentration of Na^+ ions. This has also been a subject for investigation by previous workers (69-74).

The results of disintegration will be considered under five different headings: I perchloric acid solutions at high current densities, i.e. $-i \geq 30$ mA cm^{-2}, II perchloric acid solutions at low current densities, i.e. $-i \leq 10$ mA cm^{-2}, III sulphuric acid solutions, IV alkaline solution, and V dependence of disintegration rate on cathodic current density in acid solution.

I Perchloric Acid Solutions at High Current Densities

Experiments were begun using perchloric acid as electrolyte and DPASV to measure lead concentrations. Investigation of cathodic disintegration of lead in perchloric acid was carried out using 0.003 to 1 mol ℓ^{-1} acid at different cathodic current densities. In this section the results of disintegration at high cathodic c.d.'s, i.e. $-i \geq 30$ mA cm^{-2} are described.

The first experiment was different from the remainder, because for this experiment the lead electrode was electropolished in 60% $HClO_4$ for only 2.5 min at $i = 1$ A cm^{-2} and samples were analysed using DPASV. Therefore, the lead concentrations were determined from the non-linear calibration curve, Figure 9. The results of this preliminary experiment are tabulated in Table 3 and illustrated in Figure 12.

The product of lead disintegration in acid solution was probably lead particles detached from the electrode as a greyish-black cloud. These particles dissolved quickly in the acid solutions. The amount of lead detected in solution was taken as a measure of the total amount disintegrated up to a particular time. This assumption was reasonable at first, when the rate of disintegration was high compared with the rate of deposition of lead from solution, either on the cathode or on the anodes. Later, the amount of lead in solution decreased, as Figure 12 shows. In all disintegration experiments the quantity of lead disintegrated was plotted against time.

The amount of lead in solution, i.e. from electrode disintegration, increased linearly with time initially at a particular cathodic c.d.,

TABLE 3 DATA FOR Pb DISINTEGRATION IN 0.01 mol ℓ^{-1} $HClO_4$ AT i = -100 mA cm^{-2} (AREA = 1 cm^2) IN A PRELIMINARY EXPERIMENT.

Sample number	Time from commencement of electrolysis to beginning of sampling/min.	Peak current/μA*	$[Pb^{2+}]$/ppm	$[Pb^{2+}] \times 10^6$/ mol ℓ^{-1}	Volume of electrolyte/ litres (±0.005)	Total lead disintegrated $\times 10^6$/mol cm^{-2}
1	1.1	2.4	0.01	4.83×10^{-2}	2.955	0.014
2	3	7.7	0.51	2.46	2.911	7.16
3	6	10.2	0.74	3.57	2.866	10.2
4	8.1	13.6	1.07	5.16	2.821	14.6
5	10.2	14.0	1.10	5.31	2.776	14.7
6	12.5	14.0	1.10	5.31	2.732	14.5
7	14.8	16.8	1.37	6.61	2.687	17.8
8	24.5	18.5	1.53	7.38	2.642	19.5
9	44.3	16.0	1.29	6.23	2.598	16.2
10	63.1	14.2	1.12	5.41	2.553	13.8
11	88.2	14.0	1.10	5.31	2.508	13.3
12	152.3	12.6	0.97	4.68	2.464	11.5
13	264.7	12.6	0.97	4.68	2.419	11.3
14	460.0	9	0.86	4.15	2.374	9.85

*Analyses were carried out using differential pulse anodic stripping voltammetry.

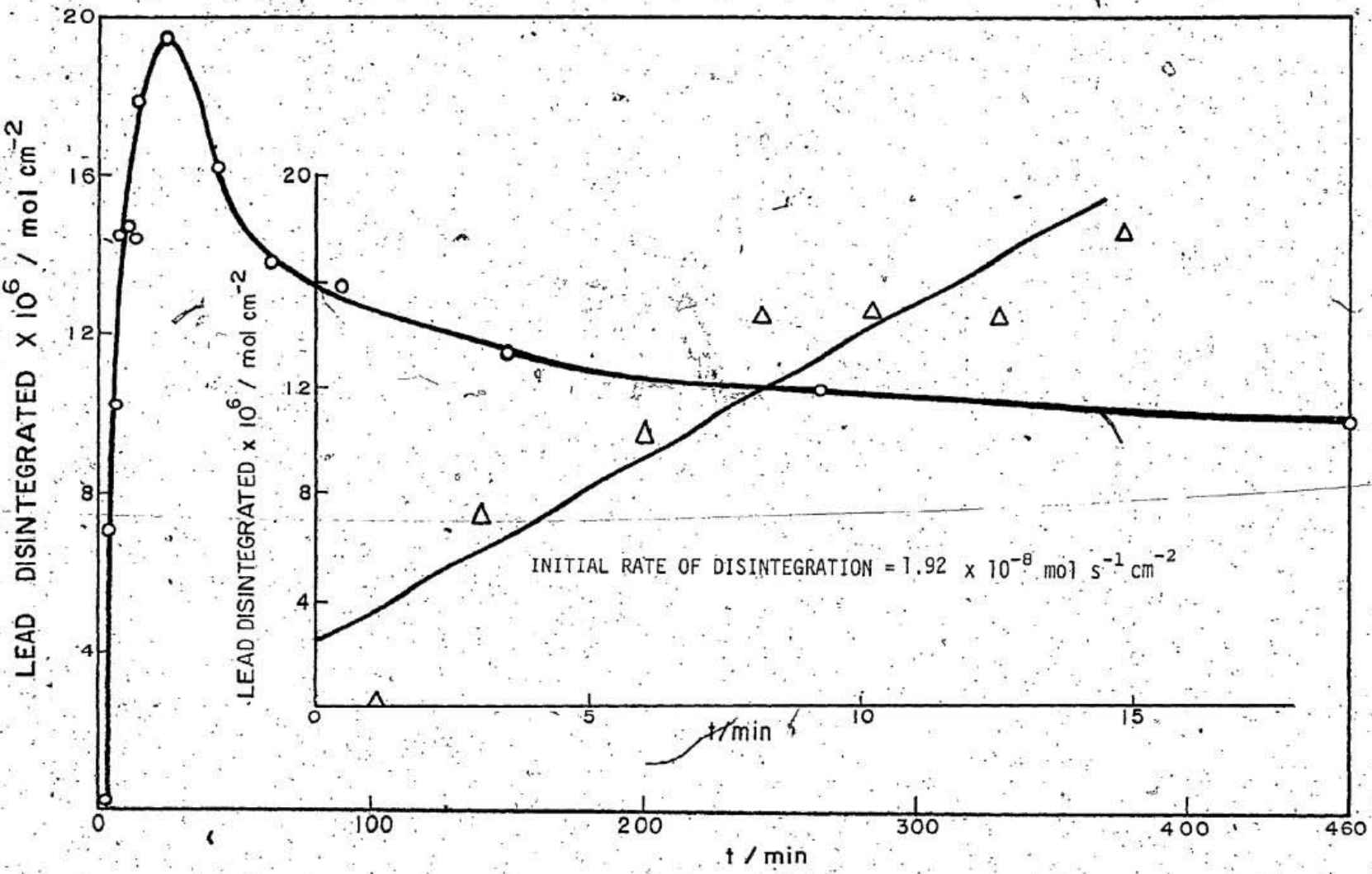

FIG. 12. MOLES OF LEAD DISINTEGRATED vs TIME IN 0.01 mol ℓ^{-1} $HClO_4$ AT -100 mA cm^{-2} (AREA = 1 cm^2) IN A PRELIMINARY EXPERIMENT

followed by a plateau region and later a region of decline in $[Pb^{2+}]$. The initial straight line passed through the origin when the rate of disintegration was high compared to the amount of Pb^{2+} ions transferred to the electrolyte with introduction of the electropolished electrode, otherwise the curve intersected the ordinate. Typical data of lead disintegration in perchloric acid are tabulated in Tables 4 and 5. Figures 13 to 18 illustrate features of lead disintegration at two different current densities each in three different concentrations of $HClO_4$.

In the lowest concentration of $HClO_4$ (0.003 mol ℓ^{-1}) disintegration of the lead cathode was visible even at such a low c.d. as 30 mA cm^{-2}. Figure 13 shows the results of this experiment (X1) which was an unusual one in two respects. Before experiment X1, an experiment was carried out with $i = -20$ mA cm^{-2} and since no visible disintegration was observed at this current density after several hours of cathodisation, the lead electrode was removed and simultaneously the current was interrupted. The remaining electrolyte and the lead electrode after electropolishing for an extra 2 min. at $i = 1$ A cm^{-2} were reused for experiment X1. All samples in experiment X1 were analysed using DPASV. Due to the relatively high $[Pb^{2+}]$ in the blank sample, i.e. 1.07×10^{-8} mol ℓ^{-1}, compared to $[Pb^{2+}]$ disintegrated in experiment X1, the quantity of lead in the blank sample was subtracted from the quantity of lead in each sample and then the result of each subtraction was divided by the area of the electropolished lead electrode (area = 0.81 cm^2). The continuous production of a greyish-black cloud of

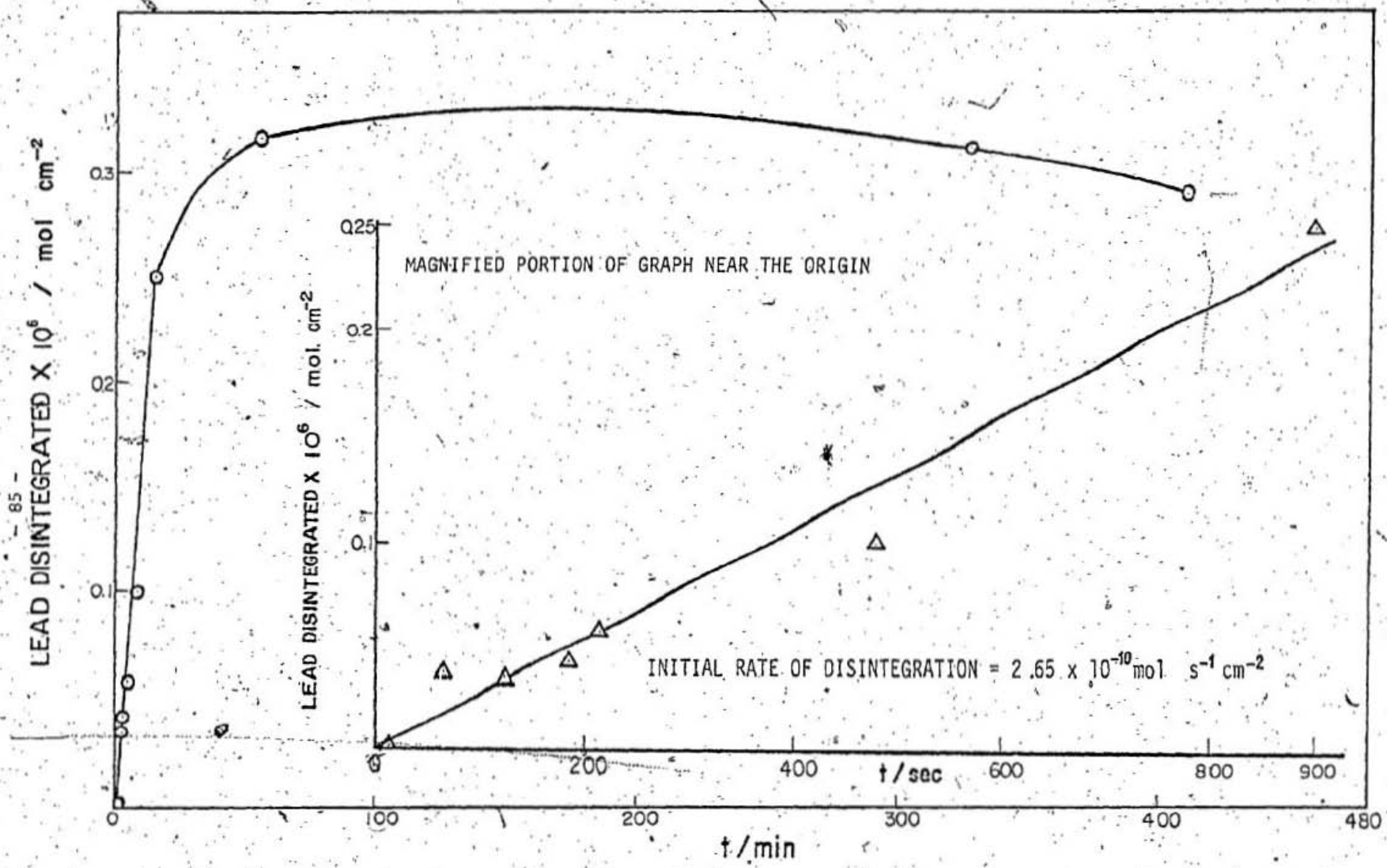

FIG. 13. MOLES OF LEAD DISINTEGRATED PER UNIT AREA vs TIME IN 0.003 mol ℓ^{-1} $HClO_4$ AT -30 mA cm^{-2} (AREA = 0.81 cm^2) IN EXPERIMENT X1

particles was visible until 70 minutes from the beginning of experiment XI. The initial rate of disintegration according to Figure 13 was 2.65×10^{-10} mol s^{-1} cm^{-2}. After prolonged cathodisation (ca. 5h) of the lead electrode the quantity of lead in solution began to fall, as expected from the reasoning given earlier on page 81.

In the remaining experiments, freshly cleaned glassware, freshly prepared electrolyte and electrodes were used. In each case the initial rate of lead disintegration was deduced from the initial slope of the lead disintegrated versus time curves. By increasing the c.d. at a constant acid concentration the disintegration rate increased substantially, e.g. in 0.003 mol ℓ^{-1} $HClO_4$ at $i = -50$ mA cm^{-2} (expt. X2) the rate of disintegration was 4.12×10^{-8} mol s^{-1} cm^{-2} (see Fig. 14) compared to 2.65×10^{-10} mol s^{-1} cm^{-2} (see Fig. 13) in the same acid concentration but at $i = -30$ mA cm^{-2}.

At higher acid concentrations, e.g. 0.01 mol ℓ^{-1} $HClO_4$, the lowest current density at which disintegration was observable, was $i = -50$ mA cm^{-2} with a disintegration rate of 2.09×10^{-8} mol ℓ^{-1} cm^{-2}. At slightly higher c.d. in the same acid concentration, e.g. at $i = -60$ mA cm^{-2} (expt. X6), the disintegration rate increased to 5.56×10^{-8} mol s^{-1} cm^{-2} (see Fig. 15). By increasing the cathodic c.d. approximately 3-fold, i.e. to $i = -200$ mA cm^{-2} in a different experiment, X9, the disintegration rate increased 10-fold, i.e. to 5.42×10^{-7} mol s^{-1} cm^{-2} as Table 4 and Figure 16 show.

With more concentrated acid, e.g. 0.1 mol ℓ^{-1} $HClO_4$, still higher c.d. was required to observe disintegration. In 0.1 mol ℓ^{-1}

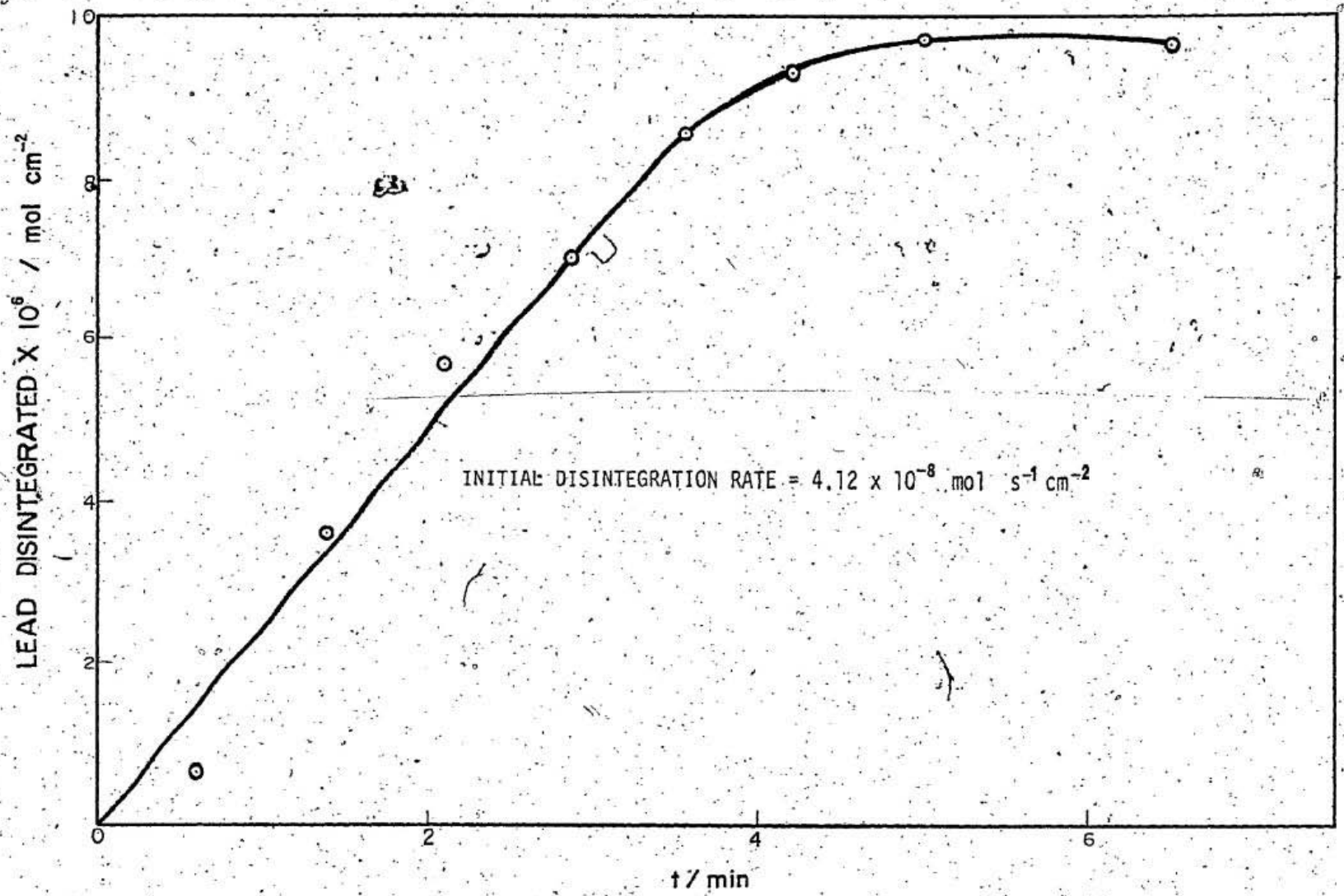

FIG. 14. MOLES OF LEAD DISINTEGRATED PER UNIT AREA vs TIME IN 0.003 mol ℓ^{-1} $HClO_4$ AT -50 mA cm^{-2} (AREA = 0.87 cm^2) IN EXPERIMENT X2

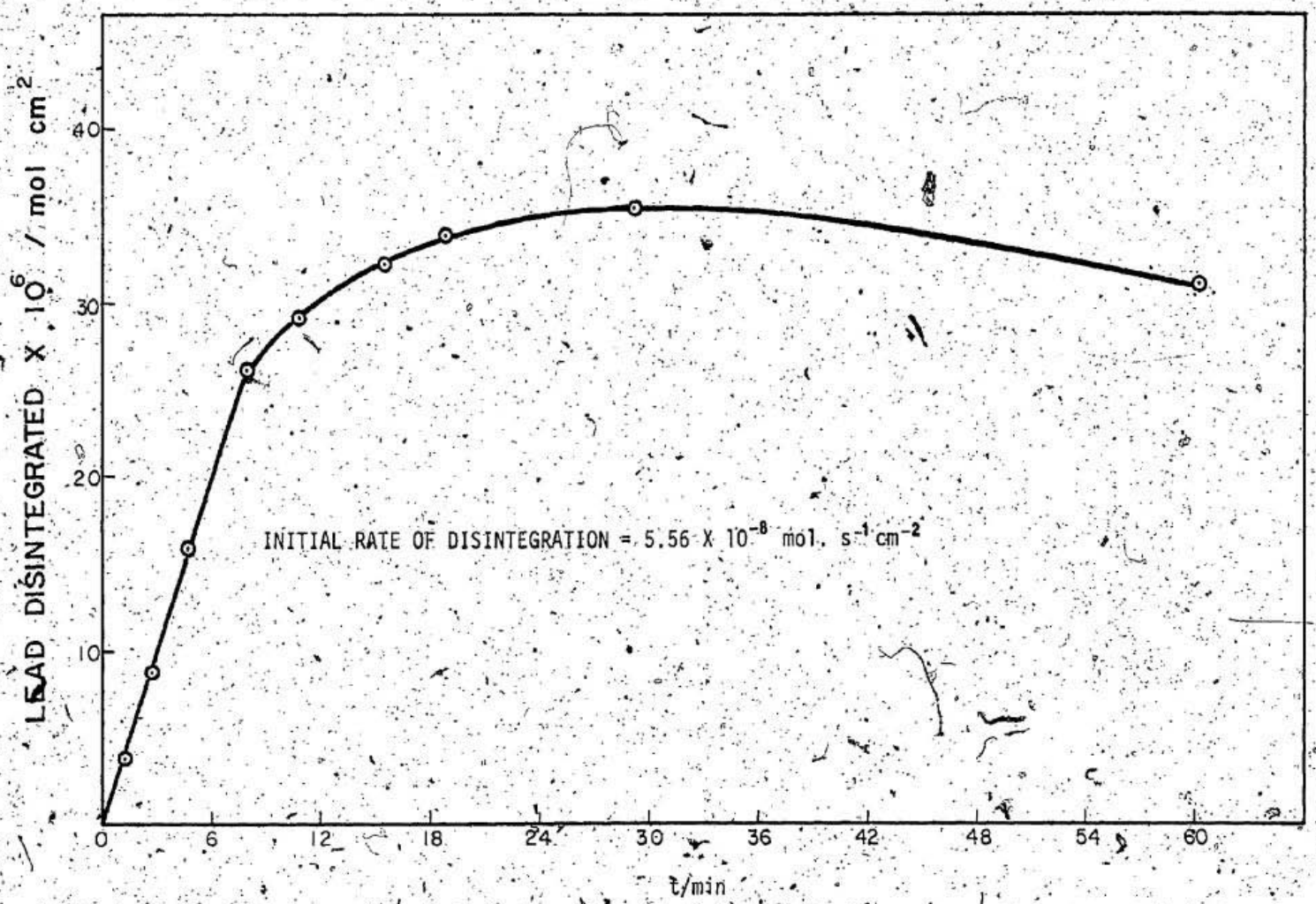

FIG. 15. MOLES OF LEAD DISINTEGRATED PER UNIT AREA vs TIME IN 0.01 mol ℓ^{-1} $HClO_4$ AT -60 mA cm^{-2} (AREA = 0.87 cm^2) IN EXPERIMENT X6.

TABLE 4 DATA FOR Pb DISINTEGRATION IN 0.01 mol ℓ^{-1} $HClO_4$ AT i = -200 mA cm^{-2} (AREA = 0.46 cm^2) IN EXPERIMENT X9.

Sample number	Time from commencement of electrolysis to beginning of sampling/min.	Peak current/μA	$[Pb^{2+}]$/ppm	$[Pb^{2+}] \times 10^5$/ mol ℓ^{-1}	Volume of electrolyte/ litres (±0.005)	Total lead disintegrated $\times 10^4$/mol cm^{-2}
Blank	-	0.035	2.20×10^{-3}	1.07×10^{-3}	2.957	*3.6×10^{-4}
1	0.20	0.450	2.76×10^{-2}	1.33×10^{-2}	2.914	8.45×10^{-3}
2	1.25	0.260	1.29	6.23×10^{-1}	2.870	3.89×10^{-1}
3	2.20	0.500	2.50	1.20	2.827	7.41×10^{-1}
4	3.20	0.715	3.58	1.73	2.784	1.05
5	4.30	0.880	4.42	2.13	2.741	1.27
6	5.30	0.970	4.86	2.34	2.698	1.38
7	6.40	1.00	5.01	2.42	2.654	1.40
8	8.20	1.02	5.11	2.47	2.611	1.40
9	12.0	0.98	4.91	2.37	2.567	1.32
10	120.0	0.900	4.52	2.18	2.525	1.20

N.B. Analyses were carried out using differential pulse polarography except blank and sample 1 which were analysed using DPASV.

*Moles of lead in 0.01 mol ℓ^{-1} $HClO_4$ (blank).

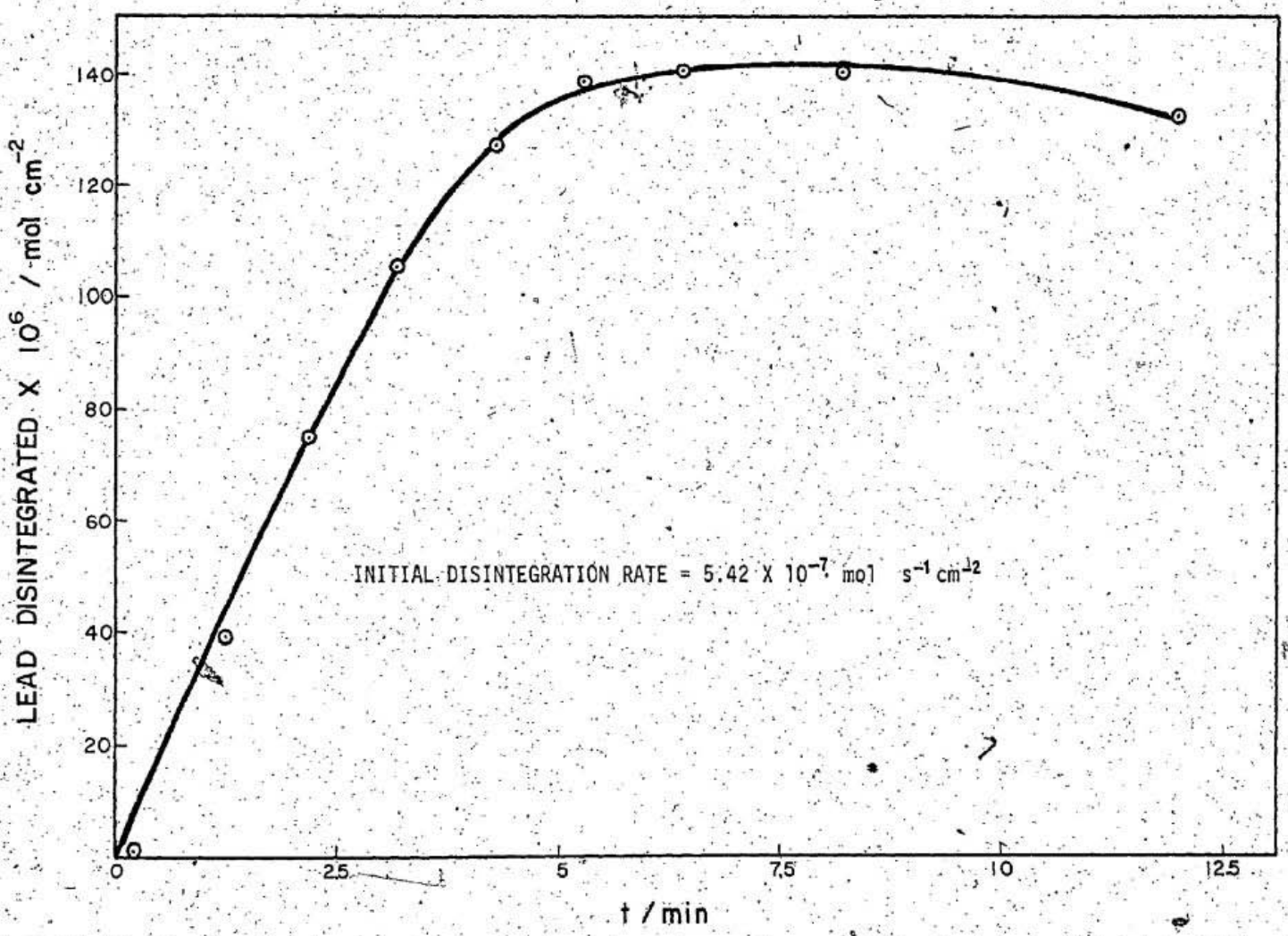

FIG. 16. MOLES OF LEAD DISINTEGRATED PER UNIT AREA vs TIME IN 0.01 mol ℓ^{-1} $HClO_4$ AT -200 mA cm^{-2} (AREA = 0.46 cm^2) IN EXPERIMENT X9

$HClO_4$ at $i = -54$ mA cm^{-2} (expt. X10) disintegration of lead was not visible, but the Pb^{2+} ion concentration increased according to DPASV measurements (see Fig. 17). In this experiment, i.e. expt. X10, the quantity of lead in the first sample at t = 1 minute was 4.72×10^{-8} mol cm^{-2} but after 400 minutes the amount of lead in solution had increased to 2.01×10^{-7} mol cm^{-2}. From the initial rise of the quantity of lead in electrolyte (Fig. 17) the disintegration rate was deduced as 2.14×10^{-11} mol s^{-1} cm^{-2}. Using the same acid concentration but in a different experiment (X11) with an approximately doubled c.d., $i = -115$ mA cm^{-2}, the disintegration rate increased 30-fold to 6.25×10^{-10} mol s^{-1} cm^{-2}. The results of experiment X11 are tabulated in Table 5 and illustrated in Figure 18. The $[Pb^{2+}]$ in blank sample in experiment X11 was slightly higher than usual, i.e. 2.4×10^{-8} mol ℓ^{-1}, (see Table 5) perhaps because of contamination of the cell.

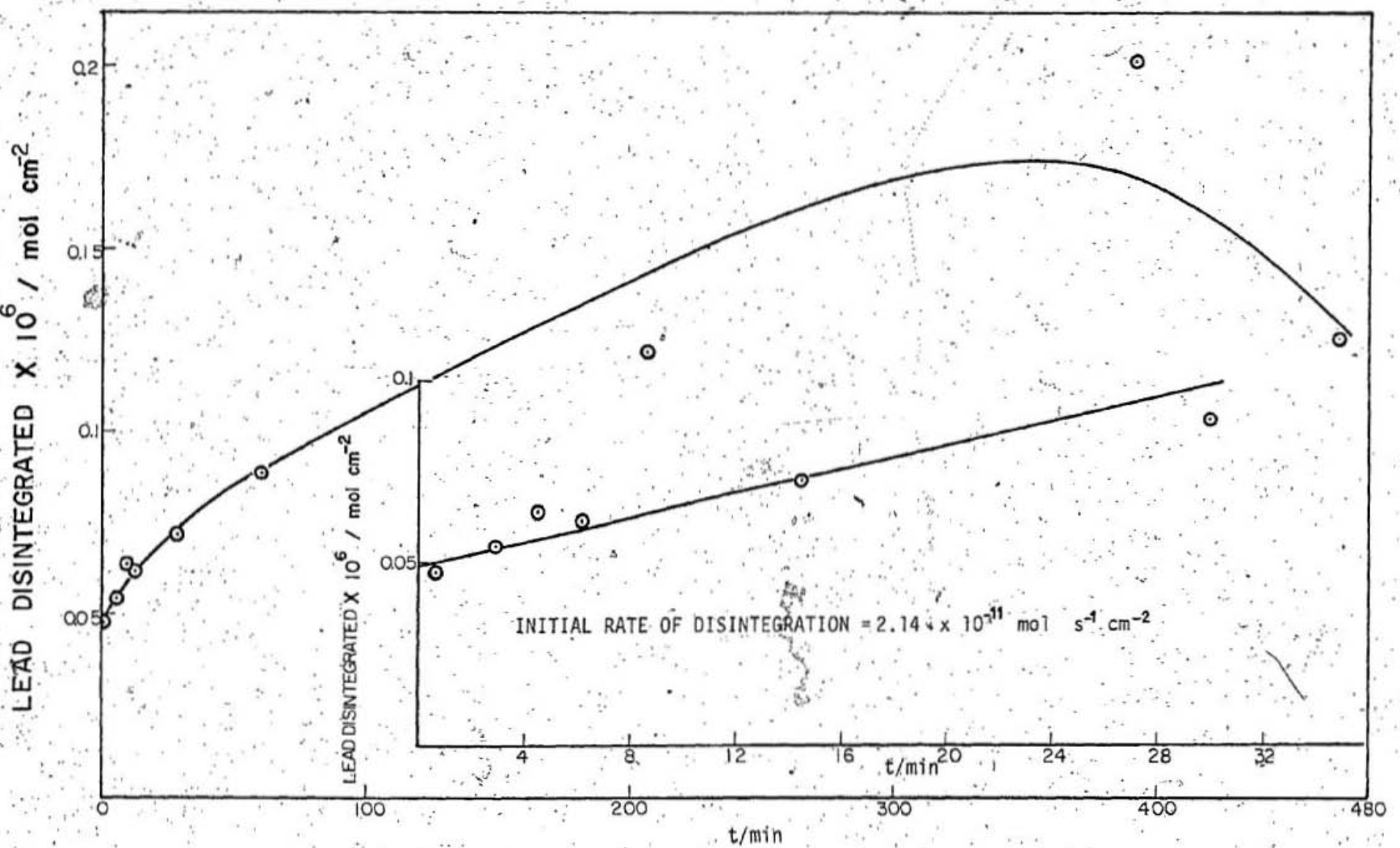

FIG. 17. MOLES OF LEAD DISINTEGRATED PER UNIT AREA vs TIME IN 0.1 mol ℓ^{-1} $HClO_4$ AT -54 mA cm^{-2} (AREA = 0.87 cm^2) IN EXPERIMENT X10

TABLE 5 DATA FOR Pb DISINTEGRATION IN 0.1 mol ℓ^{-1} $HClO_4$ AT i = -115 mA cm^{-2} (AREA = 0.87 cm^2) IN EXPERIMENT X11.

Sample number	Time from commencement of electrolysis to beginning of sampling/min.	Peak current/μA	$[Pb^{2+}]$/ppm	$[Pb^{2+}] \times 10^7$/ mol ℓ^{-1}	Volume of electrolyte/ litres (±0.005)	Total lead disintegrated $\times 10^7$/mol cm^{-2}
Blank	-	0.08	4.97	0.24	2.957	*7.09 x 10^{-1}
1	0.20	0.45	27.6	1.33	2.914	3.65
2	1.25	0.46	28.3	1.40	2.870	3.68
3	3.00	0.56	34.4	1.66	2.827	4.57
4	5.00	0.72	44.2	2.13	2.784	6.01
5	7.00	0.80	49.1	2.37	2.741	6.65
6	10.0	0.76	46.6	2.25	2.698	6.16
7	13.0	0.95	58.3	2.81	2.654	7.76
8	18.0	1.06	64.0	3.14	2.611	8.60
9	28.0	1.24	76.0	3.67	2.568	10.0
10	40.0	1.42	87.1	4.20	2.525	11.4
11	52.0	1.00	61.3	2.96	2.482	7.63
12	152	0.98	60.1	2.90	2.438	7.31
13	259	1.17	71.7	3.46	2.395	8.72
14	360	0.86	52.8	2.55	2.352	6.07
15	521	0.60	36.8	1.78	2.309	3.90

N.B. All analyses were carried out with differential pulse anodic stripping voltammetry.

The quantity of lead in the blank sample was subtracted fron the quantity of lead in each sample and then the result of each subtraction was divided by the area of the electropolished lead electrode.

*Moles of lead in blank.

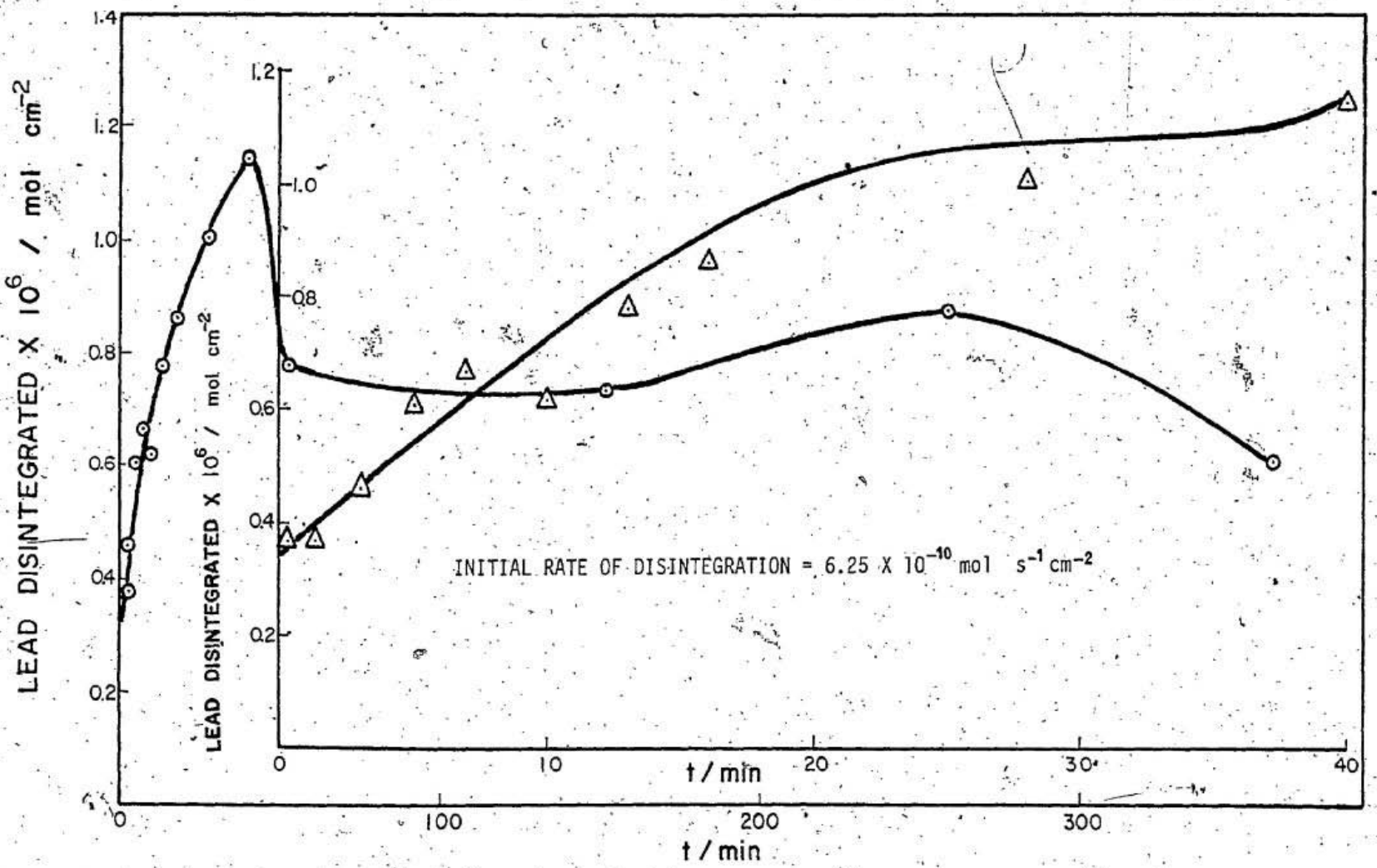

FIG. 18. MOLES OF LEAD DISINTEGRATED PER UNIT AREA vs TIME IN 0.1 mol ℓ^{-1} $HClO_4$ AT -115 mA cm^{-2} (AREA = 0.87 cm^2) IN EXPERIMENT X11

II Perchloric Acid Solutions at Low Current Densities

At low current densities, in either $HClO_4$ or H_2SO_4, no disintegration occurred, the concentration of Pb^{2+} ions decreasing exponentially with time of electrolysis. Figure 19 shows that $[Pb^{2+}]$ fell from ca. 3×10^{-8} mol ℓ^{-1}, initially to ca. 3×10^{-9} mol ℓ^{-1} in about 114 h at $i = -1$ mA cm^{-2} in 0.1 mol ℓ^{-1} $HClO_4$ (expt. X1a), stirred by H_2 bubbling.

At slightly higher cathodic current densities, ~10 mA cm^{-2}, depending on the acid concentration, discontinuous disintegration was observed as illustrated by Table 6 and Figure 20 which refer to 1 mol ℓ^{-1} $HClO_4$ in experiment X5a. In this instance, disintegration seemed to occur at a very low rate ca. 5×10^{-11} mol $cm^{-2}s^{-1}$ in the first hour or so of cathodisation, followed by an exponential fall of $[Pb^{2+}]$, from 9.2×10^{-8} to 7.9×10^{-8} mol ℓ^{-1} during the first five hours of cathodisation, later interrupted by several steep rises of $[Pb^{2+}]$, e.g. from 7.9×10^{-8} to 1.5×10^{-7} mol ℓ^{-1}. This phenomenon continued during several days of cathodisation, suggestive of bursts of lead atoms leaving the cathode. Comparable observations have been made for all $HClO_4$ concentrations studied (0.003 to 1 mol ℓ^{-1}) at around 10 mA cm^{-2}, $[Pb^{2+}]$ suddenly increasing and more slowly declining.

Fig. 19 PRE-ELECTROLYSIS OF 0.1 mol ℓ^{-1} $HClO_4$ SHOWING FALL OF $[Pb^{2+}]$ WITH TIME AT 1 mA cm^{-2} CATHODIC (AREA=0.87 cm^2) IN EXPERIMENT XIa

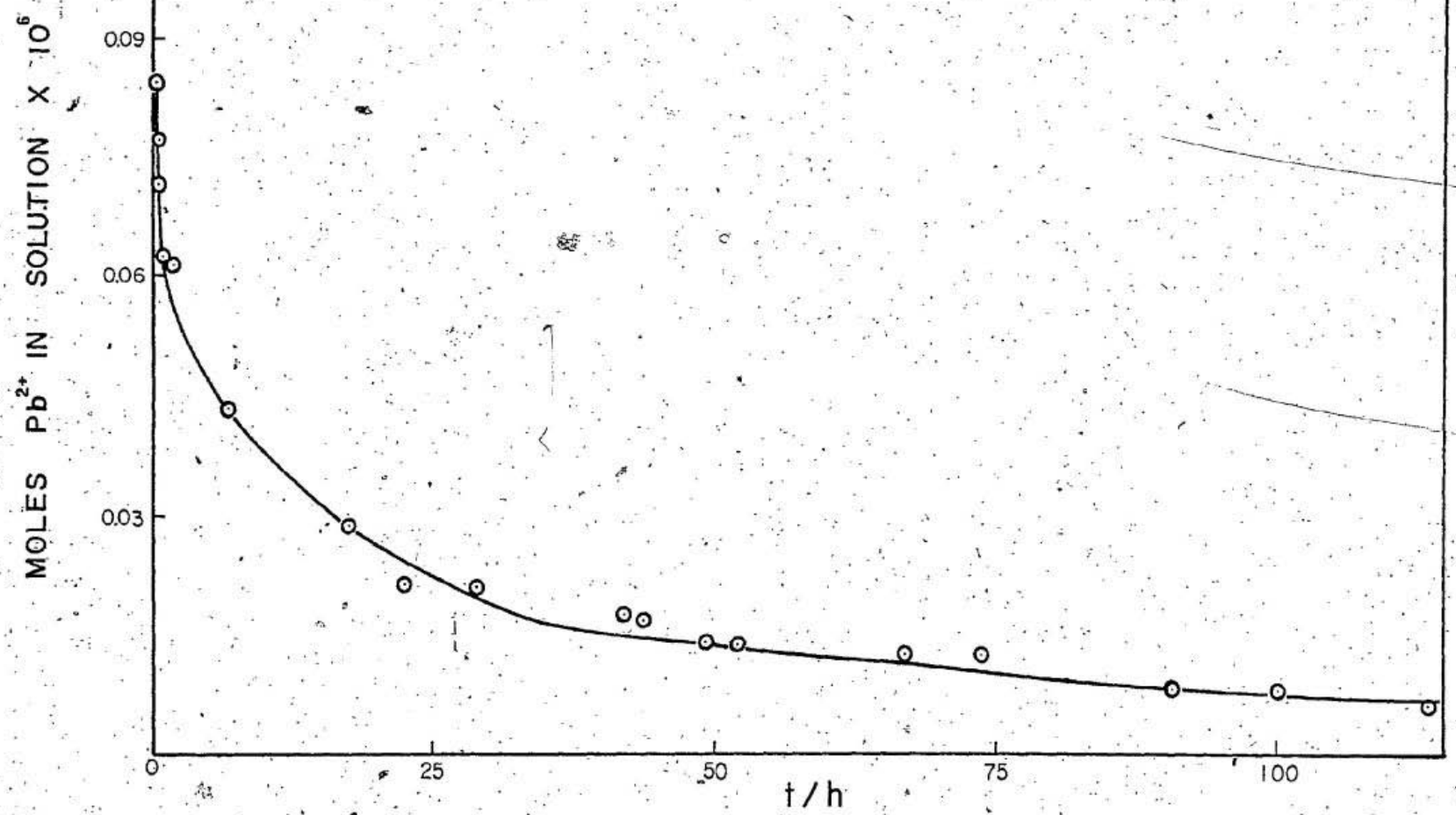

TABLE 6 DATA FOR A DISCONTINUOUS DISINTEGRATION OF Pb IN 1 mol ℓ^{-1} $HClO_4$ AT $i = -10$ mA cm^{-2} (AREA = 0.87 cm^2) IN EXPERIMENT X5a.

Sample number	Time from commencement of electrolysis to beginning of sampling/min.	Peak current/μA	$[Pb^{2+}]$/ppm	$[Pb^{2+}] \times 10^8$/ mol ℓ^{-1}	Volume of electrolyte/ litres (±0.005)	Total lead disintegrated $\times 10^8$/mol
Blank	-	0.018	1.17	5.65×10^{-1}	3.000	1.69
1	0.4	0.118	7.3	3.52	2.955	10.4
2	1.4	0.121	7.48	3.61	2.911	10.5
3	2.5	0.12	7.42	3.58	2.866	10.3
4	3.85	0.129	7.97	3.85	2.821	10.9
5	6.6	0.15	9.26	4.47	2.776	12.4
6	14.7	0.174	10.7	5.18	2.732	14.1
7	60.3	0.31	19.1	9.2	2.687	24.7
8	215.5	0.275	16.8	8.10	2.642	21.4
9	353.1	0.265	16.3	7.87	2.597	20.4
10	1152.3	0.36	22.1	10.7	2.553	27.3
11	1176.3	0.52	31.9	15.4	2.508	38.1
12	1210.9	0.505	31.0	15.0	2.463	36.9
13	1245.6	0.50	30.6	14.8	2.419	35.8
14	1356.4	0.435	26.7	12.9	2.374	30.5
15	15913	0.43	26.4	12.7	2.329	29.7

continued . . . .

TABLE 6 (continued)

Sample number	Time from commencement of electrolysis to beginning of sampling/min.	Peak current/μA	$[Pb^{2+}]$/ppm	$[Pb^{2+}] \times 10^8$/ mol ℓ^{-1}	Volume of electrolyte/ litres (±0.005)	Total lead disintegrated $\times 10^8$/mol
16	1938.2	0.56	34.4	16.6	2.285	37.9
17	1957.3	0.48	29.5	14.2	2.240	31.9
18	2798.2	0.515	31.6	15.2	2.195	33.4
19	2846.6	0.65	39.9	19.3	2.150	11.4
20	2873	0.65	39.9	19.3	2.106	40.7
21	3385.6	0.52	31.9	15.4	2.061	31.8
22	4173.0	0.56	34.3	16.6	2.016	33.4
23	4193.4	0.61	37.4	18.1	1.971	35.6
24	4226.30	0.58	35.6	17.2	1.927	33.1

N.B. All analyses were carried out using differential pulse anodic stripping voltammetry.

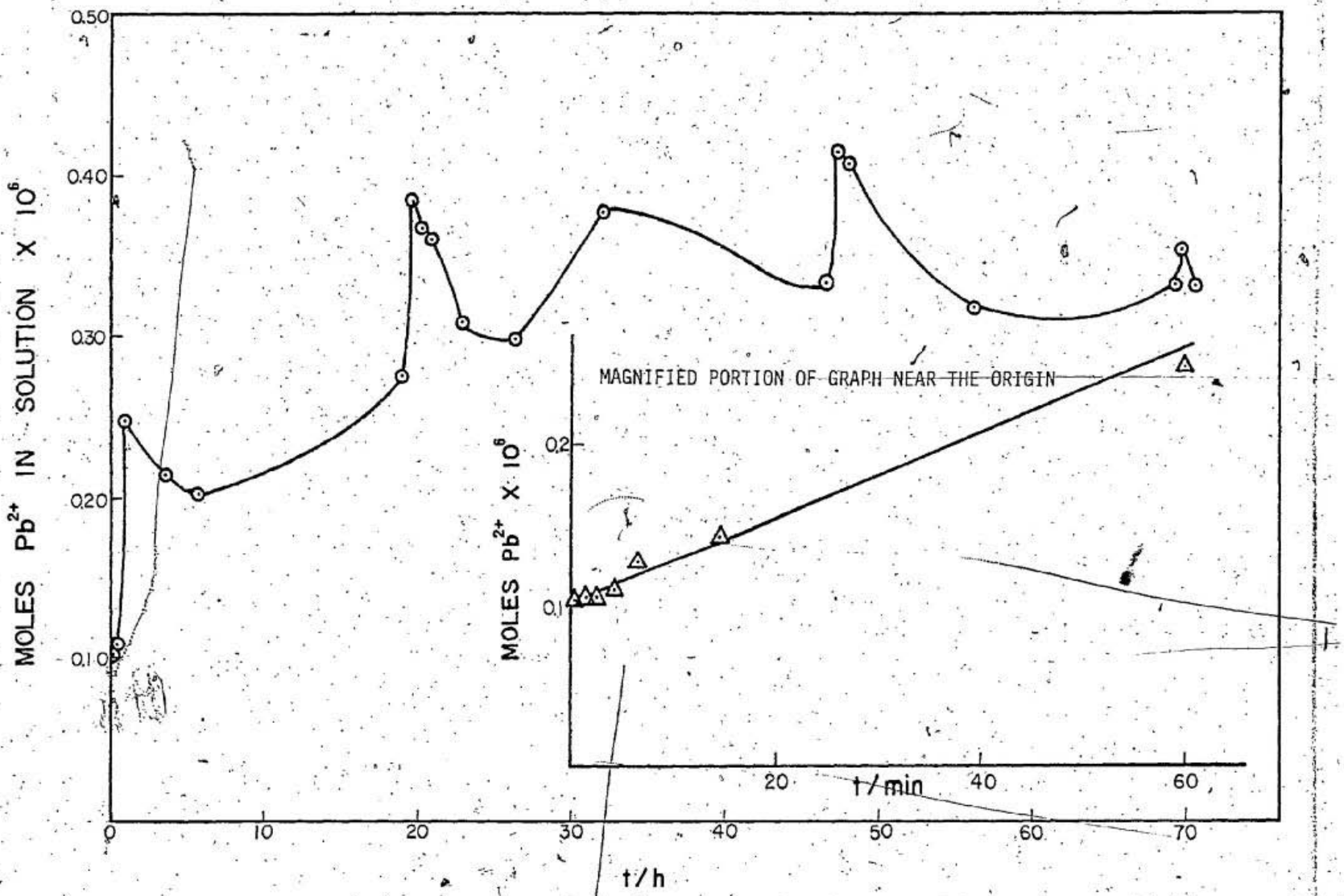

Fig. 20. MOLES Pb^{2+} IN 1 mol ℓ^{-1} $HClO_4$ vs TIME AT -10 mA cm^{-2} (AREA = 0.87 cm^2) IN EXPERIMENT X5a

III Sulphuric Acid Solutions

The results of cathodic disintegration of lead in sulphuric acid solutions were similar to those observed using perchloric acid media. Fourteen different experiments (Y1 to Y14) were carried out in which the concentration of H_2SO_4 ranged from 0.001 to 0.1 mol ℓ^{-1} H_2SO_4. Methods of carrying out experiments involving H_2SO_4 were similar to those for experiments with $HClO_4$ described in previous sections. Tables 7 and 8 give data pertaining to two experiments with 0.001 and 0.005 mol ℓ^{-1} H_2SO_4, respectively. Figures 21 to 27 show features of lead disintegration at two different current densities in each of three different concentrations of H_2SO_4 (0.001, 0.005 and 0.01 mol ℓ^{-1}) and at one c.d. in another (0.1 mol ℓ^{-1}).

In the most dilute sulphuric acid, i.e. 0.001 mol ℓ^{-1}, lead disintegration was visible at a c.d. as low as $i = -20$ mA cm^{-2}. According to Table 7 the concentration of dissolved lead continuously increased for about 12 minutes to a maximum value of 6.21×10^{-7} mol ℓ^{-1}, later falling to 4.88×10^{-7} mol ℓ^{-1} at ca. 140 minutes. From the initial rise of the amount of lead in the electrolyte versus time in Figure 21, a disintegration rate of 4.17×10^{-9} mol $s^{-1}cm^{-2}$ was deduced for experiment Y1.

Experiment Y3 was carried out at $i = -94$ mA cm^{-2} in 0.001 mol ℓ^{-1} H_2SO_4 for a direct comparison with the work of Gastwirt and Salzberg (70) at the same c.d. in the same acid concentration. The disintegration rate in our work (see Fig. 22) was 2.0×10^{-7} mol $s^{-1}cm^{-2}$ which is 25 times as large as the previous workers (70) found, i.e. 8.0×10^{-9}

TABLE 7 DATA FOR Pb DISINTEGRATION IN 0.001 mol ℓ^{-1} H_2SO_4 AT i_o = -20 mA cm^{-2} (AREA = 0.87 cm^2) IN EXPERIMENT Y1.

Sample number	Time from commencement of electrolysis to beginning of sampling/min.	Peak current/μA	$[Pb^{2+}]$/ppm	$[Pb^{2+}] \times 10^7$/ mol ℓ^{-1}	Volume of electrolyte/ litres (±0.005)	Total lead disintegrated $\times 10^6$/mol cm^{-2}
Blank	-	0.002	0.191	9.22×10^{-3}	3.000	*2.77×10^{-3}
1	0.5	0.072	4.48	2.16×10^{-1}	2.957	7.35×10^{-2}
2	1.70	0.302	18.6	8.96×10^{-1}	2.914	3.00×10^{-1}
3	2.70	0.750	46.0	8.22	2.870	7.33×10^{-1}
4	3.8	1.49	91.3	4.41	2.827	1.43
5	5.0	1.68	103	4.97	2.784	1.59
6	7.1	1.75	107.3	5.18	2.741	1.63
7	11.5	2.10	128.7	6.21	2.698	1.93
8	15.0	-	-	-	2.654	-
9	21.0	1.80	110	5.32	2.611	1.60
10	35.0	1.95	119	5.77	2.568	1.70
11	141.0	1.65	101	4.88	2.525	1.42

N.B. Analyses were carried out using differential pulse anodic stripping voltammetry.

*Moles of lead in blank solution.

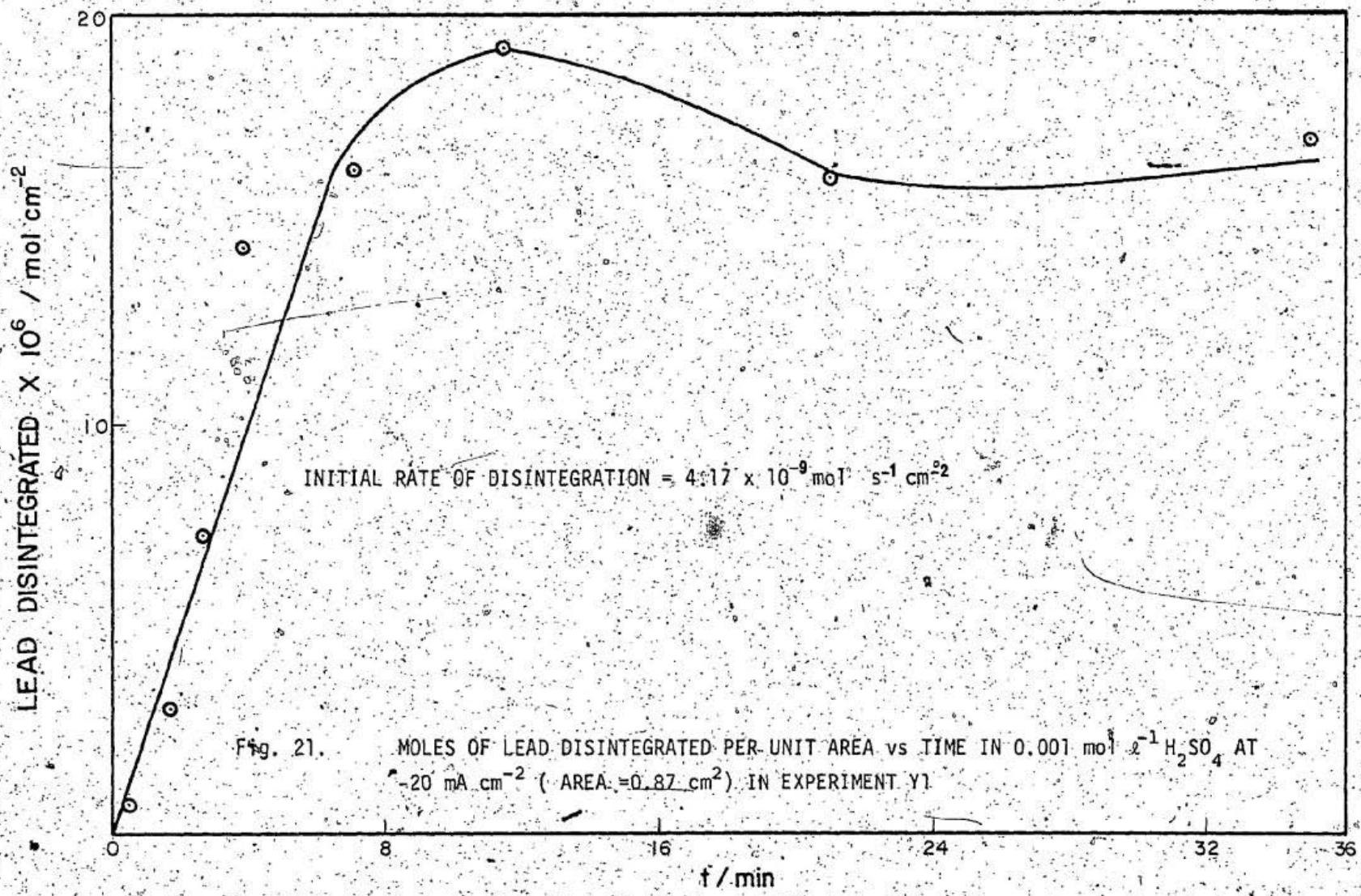

Fig. 21. MOLES OF LEAD DISINTEGRATED PER UNIT AREA vs TIME IN 0.001 mol ℓ^{-1} H_2SO_4 AT -20 mA cm^{-2} (AREA =0.87 cm^2) IN EXPERIMENT Y1

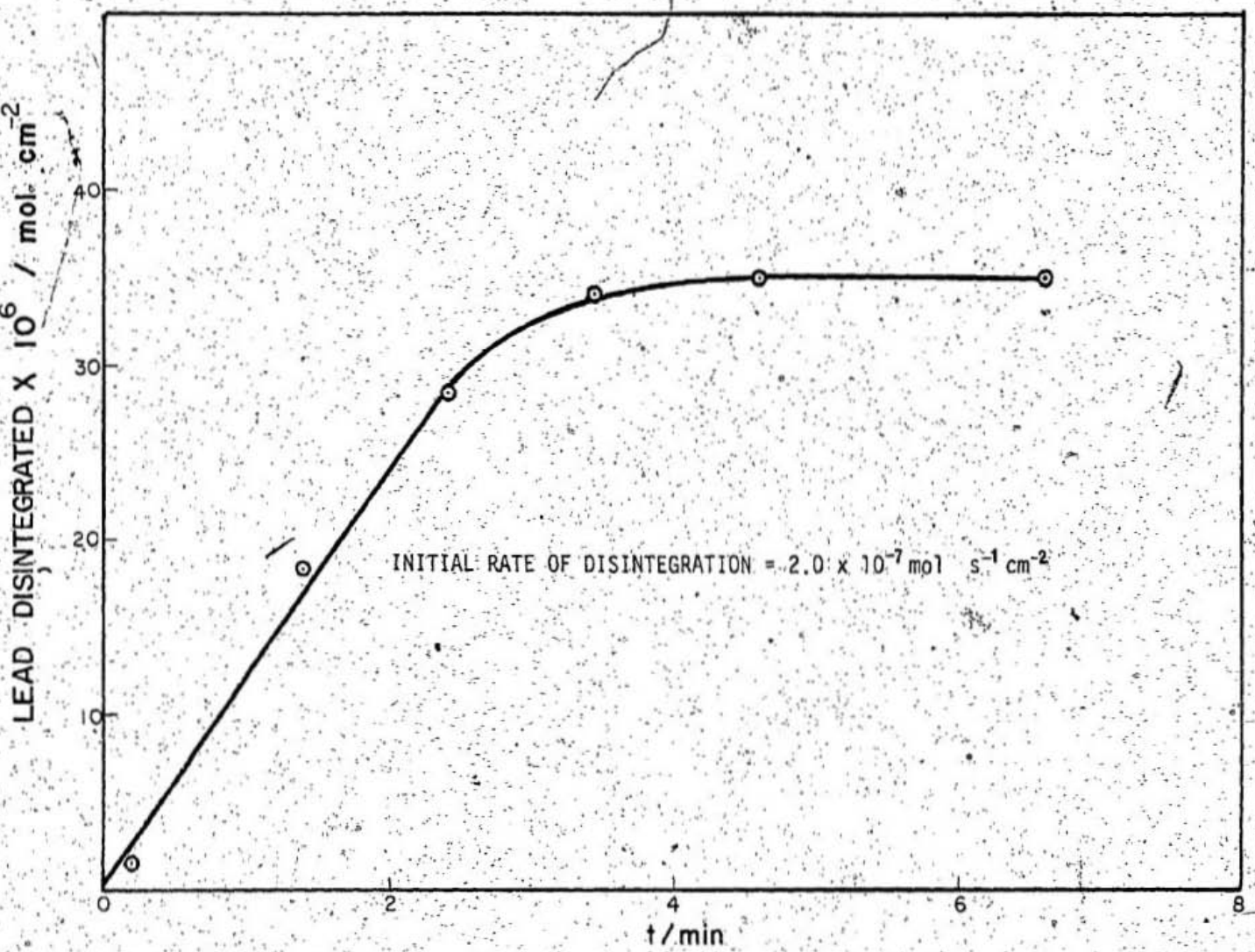

FIG. 22. MOLES OF LEAD DISINTEGRATED PER UNIT AREA vs TIME IN 0.001 mol ℓ^{-1} H_2SO_4 AT -94mA cm^{-2} (AREA = 0.46 cm^2) IN EXPERIMENT Y3

mol $s^{-1}cm^{-2}$, using the same H_2SO_4 concentration and the same c.d., but with their less well cleaned electrode and the cell open to air.

Using slightly more concentrated acid, i.e. 0.005 mol ℓ^{-1} H_2SO_4, a c.d. higher than 20 mA cm^{-2}, namely i = -30 mA cm^{-2}, was required for visible disintegration. Increasing the c.d. at constant sulphuric acid concentration, the disintegration rate, as expected from Salzberg's earlier work (69) using salt solutions and as we observed, with perchloric acid solution, increased. In experiment Y6 at i = -60 mA cm^{-2} in 0.005 mol ℓ^{-1} H_2SO_4, $[Pb^{2+}]$ continuously increased for about 18 minutes, followed by a plateau region (see Fig. 23). The results of experiment Y6 are tabulated in Table 8 and illustrated in Figure 23. A disintegration rate of 1.32×10^{-7} mol $s^{-1}cm^{-2}$ was obtained from Figure 23. In experiment Y8 at i = -115 mA cm^{-2} in 0.005 mol ℓ^{-1} H_2SO_4, the disintegration rate (3.5×10^{-7} mol $s^{-1}cm^{-2}$ from Figure 24) increased about 2.5 fold for roughly a doubling of the c.d. but $[Pb^{2+}]$ increased for <u>only</u> 11 minutes, followed by a plateau. In these circumstances the Pb^{2+} concentration built up more quickly at the higher c.d., so that Pb and PbO_2 deposition are likely to occur earlier in experiment Y8 and a plateau is then observed. It should be mentioned that Salzberg et al (69,70,71) only made observations of cathodic disintegration of lead for ca. 5 minutes, quoting an <u>average</u> value over that time period. Another complicating factor is that lead deposition on the cathode increases its area and consequently decreases the effective c.d. after a short time.

TABLE 8 DATA FOR Pb DISINTEGRATION IN 0.005 mol ℓ^{-1} H_2SO_4 AT i = -60 mA cm^{-2} (AREA = 0.87 cm^2) IN EXPERIMENT Y6.

Sample number	Time from commencement of electrolysis to beginning of sampling/min.	Peak current/μA	$[Pb^{2+}]$/ppm	$[Pb^{2+}] \times 10^5$/ mol ℓ^{-1}	Volume of electrolyte/ litres (±0.005)	Total lead disintegrated $\times 10^5$/mol cm^{-2}
Blank	-	0.016	0.001	4.83×10^{-4}	3.000	*1.45×10^{-3}
1	0.5	1.85	0.113	5.47×10^{-2}	2.957	1.85×10^{-1}
2	1.60	0.111	0.543	5.62×10^{-1}	2.914	8.76×10^{-1}
3	2.64	0.210	1.04	5.02×10^{-1}	2.870	1.66
4	3.70	0.327	1.63	7.86×10^{-1}	2.827	2.55
5	4.60	0.480	2.40	1.16	2.784	3.70
6	5.50	0.57	2.85	1.38	2.741	4.33
7	6.60	0.67	2.35	1.62	2.698	5.01
8	7.7	0.76	3.80	1.84	2.654	5.60
9	8.8	0.82	4.11	1.98	2.611	9.95
10	9.8	0.86	4.31	2.08	2.568	6.13
11	11	1.04	5.21	2.51	2.525	7.30
12	13	0.97	4.86	2.40	2.482	6.69
13	15.0	1.02	5.11	2.47	2.438	6.91
14	18.0	1.10	5.51	2.66	2.395	7.32
15	22.30	1.01	5.06	2.44	2.352	6.60

continued . . . .

TABLE 8 (continued)

Sample number	Time from commencement of electrolysis to beginning of sampling/min.	Peak current/μA	$[Pb^{2+}]$/ppm	$[Pb^{2+}] \times 10^5$/ mol ℓ^{-1}	Volume of electrolyte/ litres (±0.005)	Total lead disintegrated $\times 10^5$/mol cm^{-2}
16	26.60	1.10	5.11	2.66	2.309	7.06
17	32.0	1.2	6.01	2.90	2.266	7.56
18	37.0.	1.18	5.91	2.85	2.222	7.29

N.B. Analyses were carried out with differential pulse polarography except blank and sample 1 which were analysed using DPASV.

*Moles of lead in blank solution.

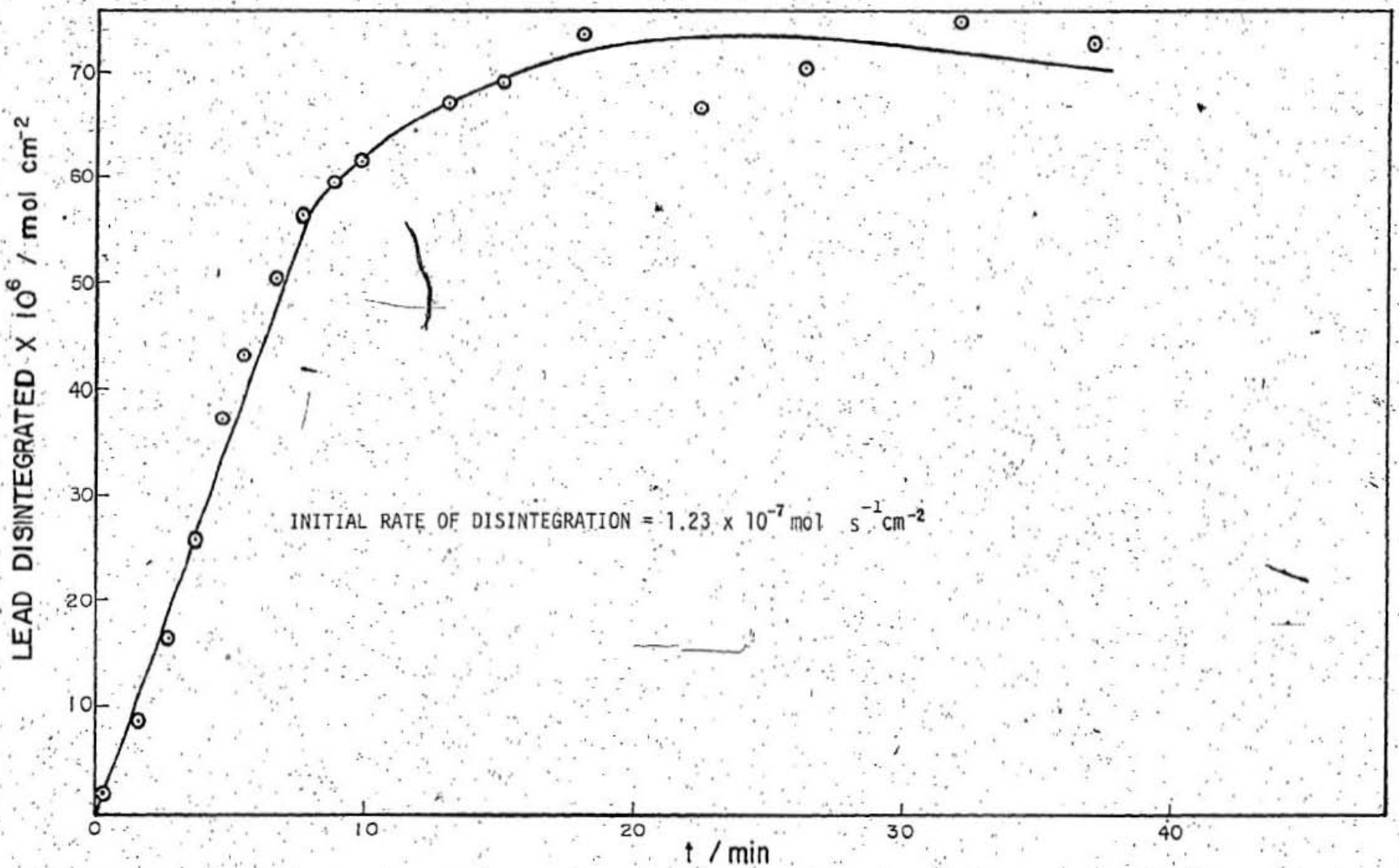

Fig. 23. MOLES OF LEAD DISINTEGRATED PER UNIT AREA vs TIME IN 0.005 mol ℓ^{-1} H_2SO_4 AT -60 mA cm^{-2} (AREA = 0.87 cm^2) IN EXPERIMENT Y6.

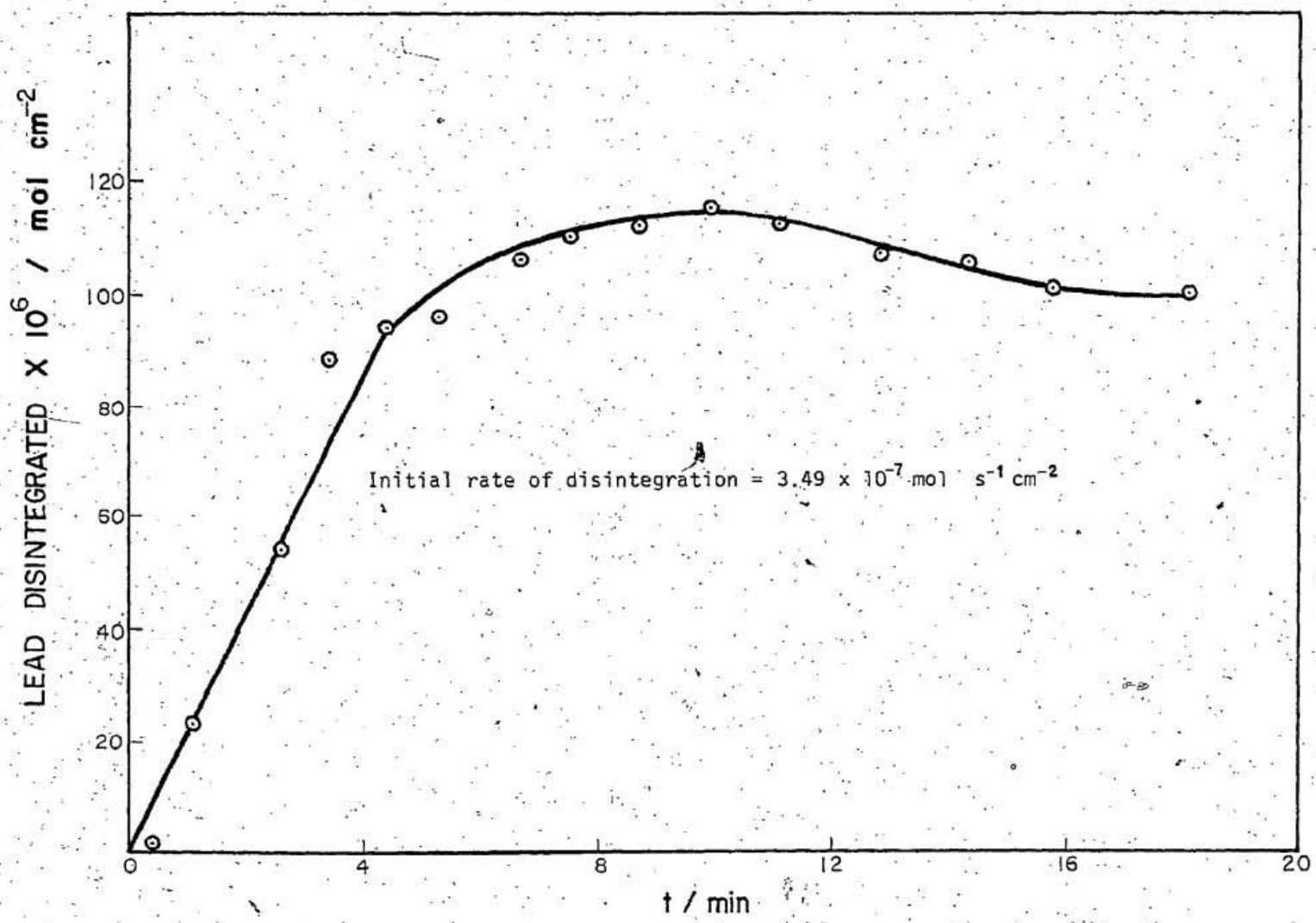

FIG. 24. MOLES OF LEAD DISINTEGRATED PER UNIT AREA vs TIME IN 0.005 mol ℓ^{-1} H_2SO_4 AT -115 mA cm^{-2} (AREA = 0.87 cm^2) IN EXPERIMENT Y8

For 0.01 mol ℓ^{-1} H_2SO_4, the minimum c.d. at which disintegration was visible was $i = -115$ mA cm^{-2} (expt. Y9) with a rate of 1.40×10^{-9} mol $s^{-1}cm^{-2}$ (see Fig. 25). In contrast, Gastwirt and Salzberg (70) observed lead disintegration only at $i = -535$ mA cm^{-2} in 0.01 mol ℓ^{-1} H_2SO_4 with the higher rate of 1.61×10^{-8} mol $s^{-1}cm^{-2}$. In another experiment (expt. Y11) using 0.01 mol ℓ^{-1} H_2SO_4 at $i = -190$ mA cm^{-2}, however, as Figure 26 indicates, the initial disintegration rate increased to 11.0×10^{-8} mol $s^{-1}cm^{-2}$, i.e. about 7 times that which Gastwirt and Salzberg (70) observed at $i = -535$ mA cm^{-2}.

Using 0.1 mol ℓ^{-1} H_2SO_4, a still higher c.d. ($-i \geq 200$ mA cm^{-2}) was required to cathodically disintegrate lead. The initial disintegration rate in 0.1 mol ℓ^{-1} H_2SO_4 at $i = -241$ mA cm^{-2} (Y12) was 3.21×10^{-10} mol $s^{-1}cm^{-2}$. Figure 27 shows that in another experiment at $i = -350$ mA cm^{-2} with the same acid concentration the initial disintegration rate increased only to 5.72×10^{-10} mol $s^{-1}cm^{-2}$ which is less than Gastwirt and Salzberg (70) observed at $i = -630$ mA cm^{-2} in 0.1 mol ℓ^{-1} H_2SO_4, i.e. 8.04×10^{-9} mol $s^{-1}cm^{-2}$. This will be commented on later.

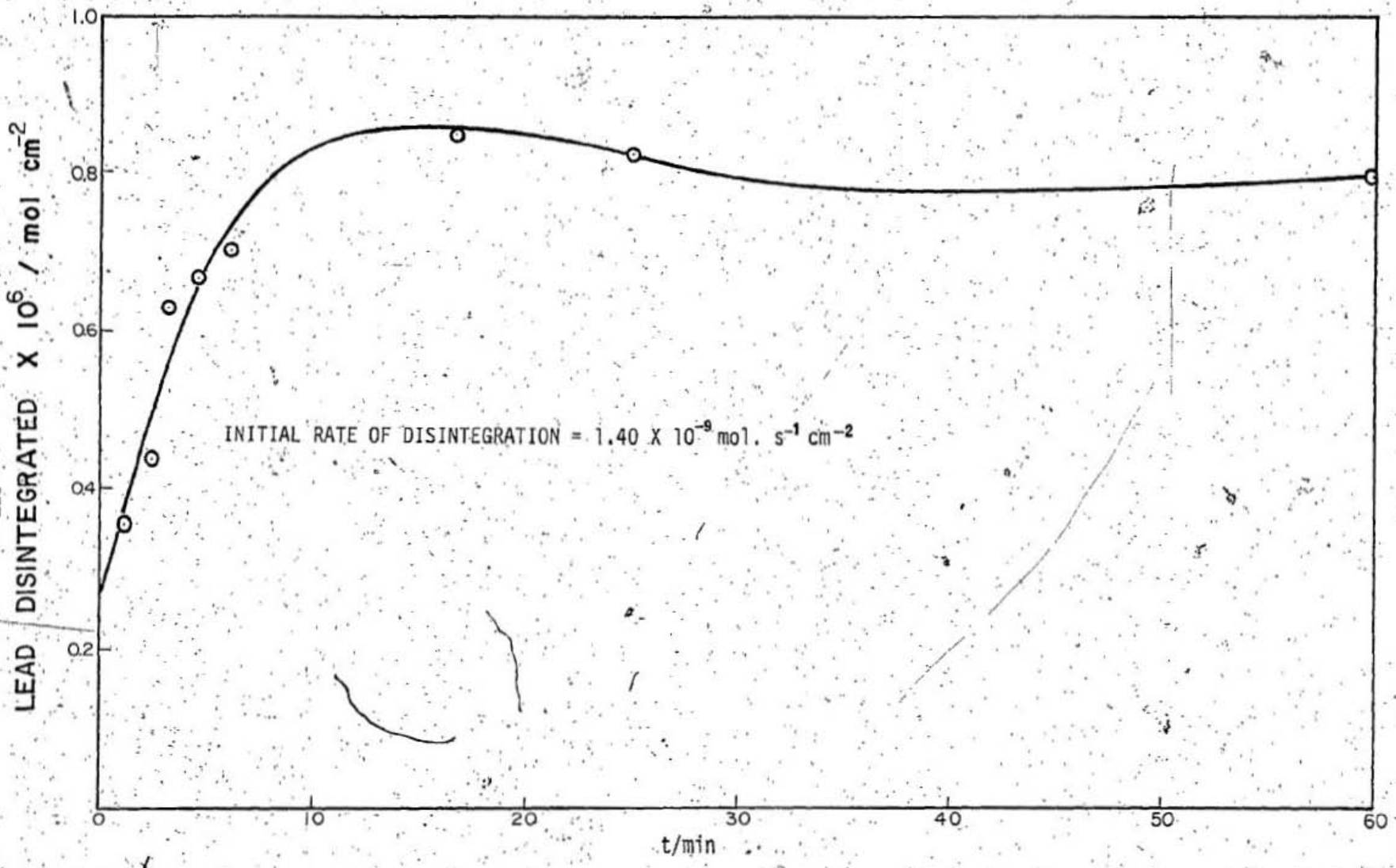

FIG. 25. MOLES OF LEAD DISINTEGRATED PER UNIT AREA vs TIME IN 0.01 mol ℓ^{-1} H_2SO_4 AT -115 mA cm^{-2} (AREA = 0.87cm^2) IN EXPERIMENT Y9

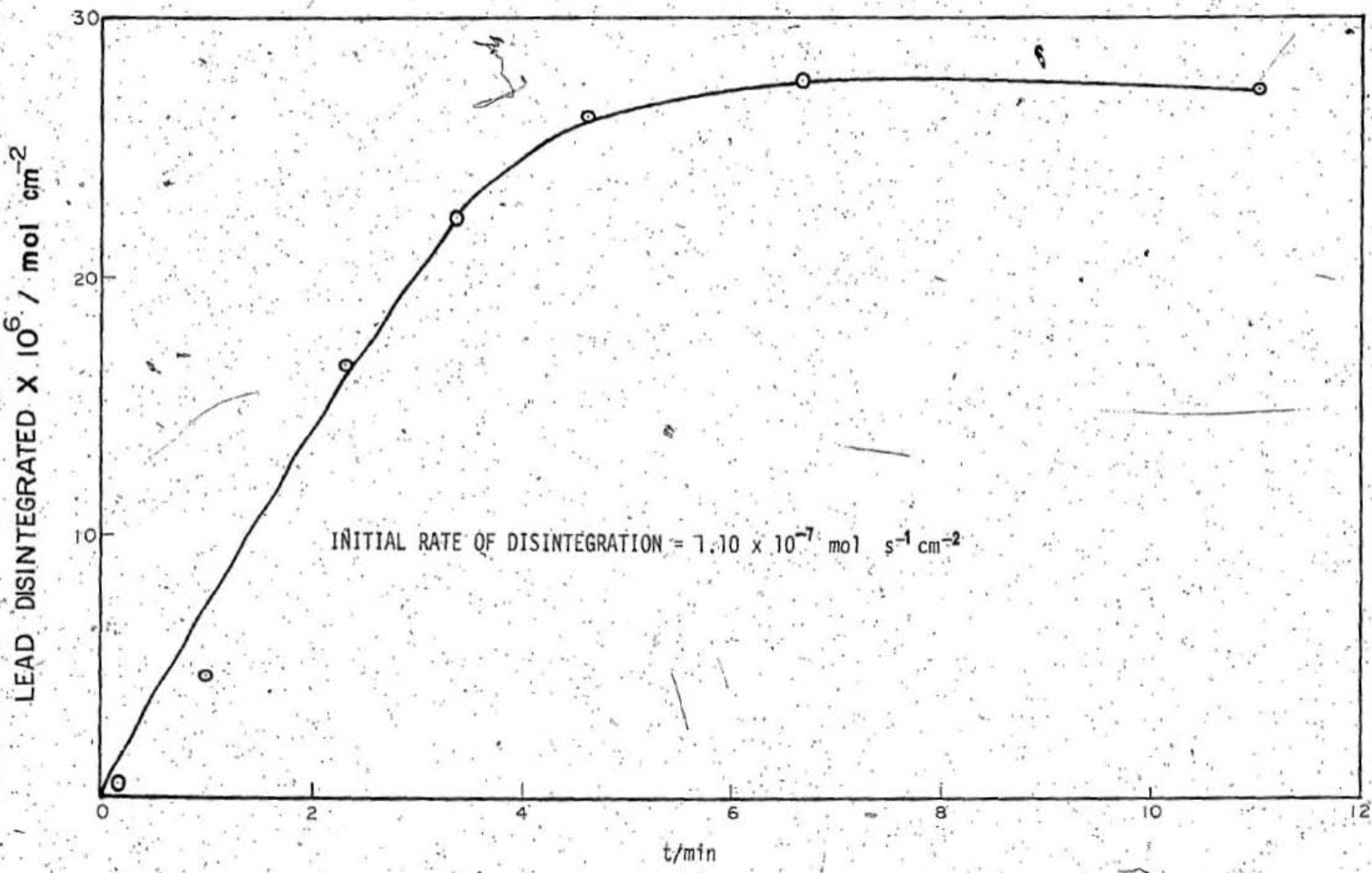

FIG. 26. MOLES OF LEAD DISINTEGRATED PER UNIT AREA vs TIME IN 0.01 mol ℓ^{-1} H_2SO_4 AT -190 mA cm^{-2} (AREA = 0.46 cm^2) IN EXPERIMENT Y11

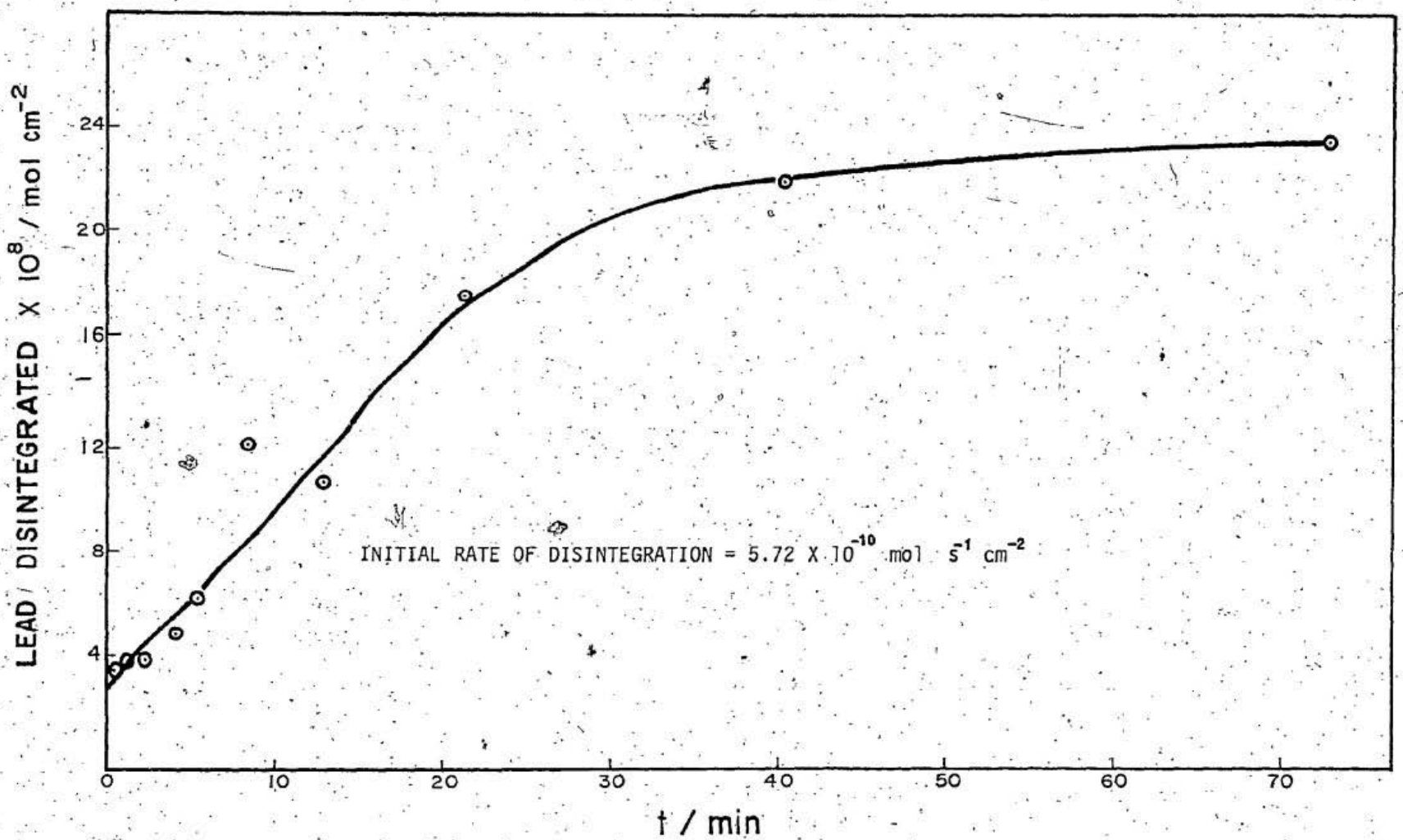

Fig. 27. MOLES OF LEAD DISINTEGRATED PER UNIT AREA vs TIME IN 0.1 mol ℓ^{-1} H_2SO_4 AT -350 mA cm^{-2}(AREA= 0.87 cm^2) IN EXPERIMENT Y13.

IV Alkaline Solution

A higher than normal disintegration rate was observed in 0.01 mol ℓ^{-1} $HClO_4$ at $i = -200$ mA cm^{-2}, after the glassware had been cleaned using sodium hydroxide, distilled water, followed by nitric acid, distilled and triple distilled water. This experiment, illustrated in Figure 28 exhibited an initial disintegration rate of 1.26×10^{-6} mol $s^{-1}cm^{-2}$, or about twice the value of 5.42×10^{-7} mol $s^{-1}cm^{-2}$ observed with the same acid concentration and the same c.d. in an experiment (see Fig. 16) in which sodium hydroxide was not used as a cleaning agent. The obvious explanation for the higher value of disintegration rate is that the sodium ions left in the system after the cleaning of the glassware caused the increase in disintegration rate.

Only one experiment was carried out in 1 mol ℓ^{-1} NaOH solution to investigate the disintegration rate under our experimental conditions but in the presence of a known large concentration of Na^+ ions. The preparation of the lead electrode and other procedures in this experiment were similar to those described in the previous sections. This experiment was carried out with 16 mA cm^{-2} cathodic c.d. According to van Muylder and Pourbaix (75) dissolved lead in alkaline solutions is in the form of biplumbite ions, $HPbO_2^-$. In order to determine the concentration of Pb^{2+} ions in solution using either differential pulse polarography or DPASV, a known volume of the sample was diluted using a known volume of 1 mol ℓ^{-1} $HClO_4$ to reduce the pH of the sample to 1-2. At this pH lead is in the form of Pb^{2+} and the

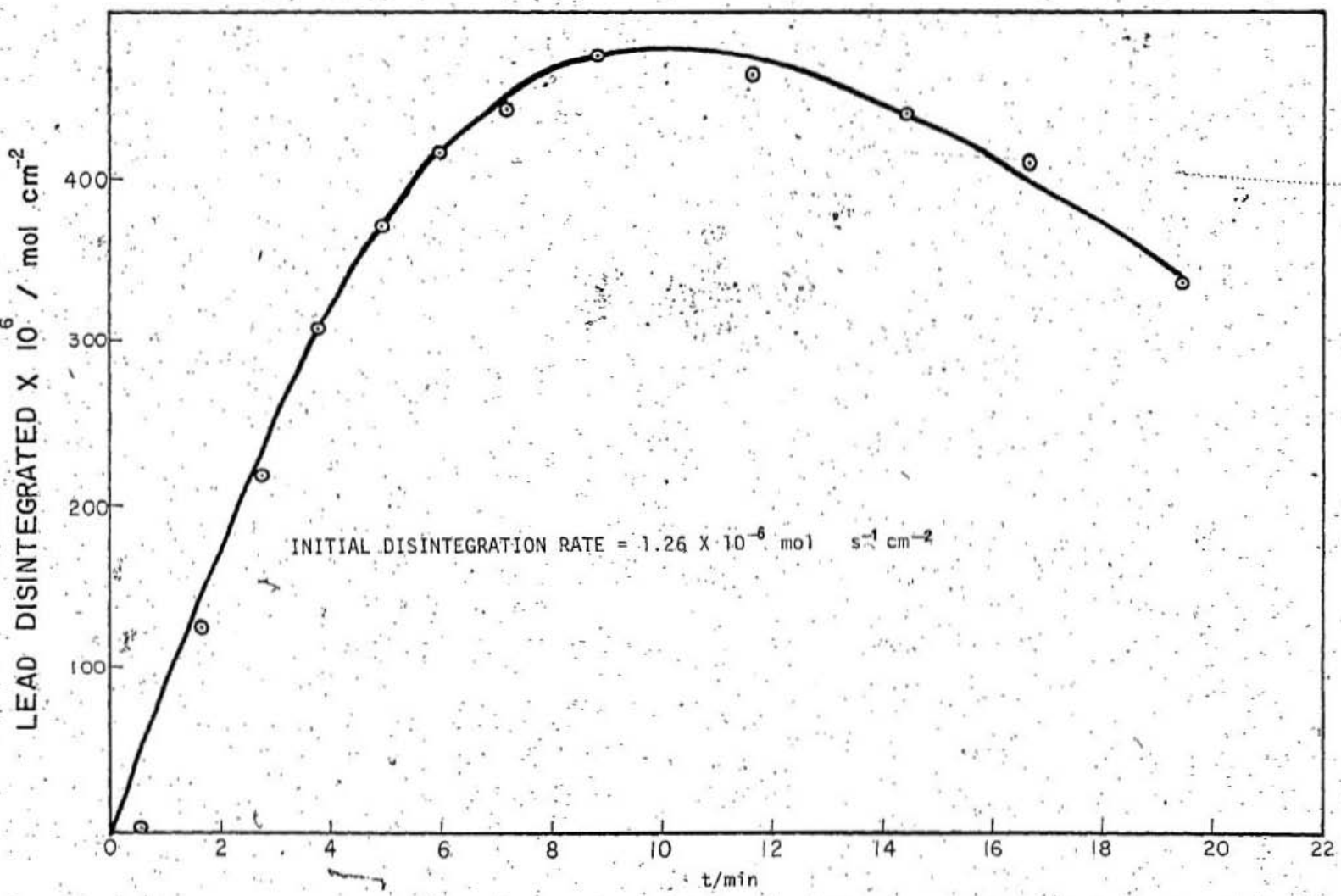

FIG. 28. MOLES OF LEAD DISINTEGRATED PER UNIT AREA vs TIME IN 0.01 $HClO_4$ AT -200 mA cm^{-2} (AREA = 0.87 cm^2). CELL HAD BEEN CLEANED WITH NaOH.

electrochemical methods are known to respond to this chemical species. The concentration of lead in 1 mol ℓ^{-1} $HClO_4$ was in the range of 1 ppb so that after dilution with $HClO_4$, the $[Pb^{2+}]$ which came from the 1 mol ℓ^{-1} $HClO_4$ had a negligible effect on the $[Pb^{2+}]$ in the sample. Data for this experiment at $i = -16$ mA cm^{-2} are tabulated in Table 9 and illustrated in Figure 29 which leads to an initial rate of disintegration of 3.84×10^{-8} mol $s^{-1}cm^{-2}$. Salzberg (69) found a disintegration rate of 2.77×10^{-8} mol $s^{-1}cm^{-2}$ in 4 mol ℓ^{-1} NaOH at $i = -40$ mA cm^{-2} and 3.40×10^{-8} mol $s^{-1}cm^{-2}$ in 0.04 mol ℓ^{-1} NaOH at $i = -25$ mA cm^{-2}. Our disintegration rate is comparable with these despite the higher c.d. applied by Salzberg (69). It should be mentioned that in Salzberg's work disintegration was observed for a maximum of five minutes but it is apparent from Figure 29 that disintegration continued at the initial rate for about the first 50 minutes in our work.

TABLE 9 DATA FOR Pb DISINTEGRATION IN 1 mol ℓ^{-1} NaOH AT $i = -16$ mA cm^{-2} (AREA = 0.87 cm^2)

Sample number	Time from commencement of electrolysis to beginning of sampling/min.	Peak current/μA	$[Pb^{2+}]$/ppm (diluted)	$[Pb^{2+}] \times 10^6$/ mol ℓ^{-1} (original)	Volume of electrolyte/ litres (±0.005)	Total lead disintegrated $\times 10^6$/mol cm^{-2}
Blank	-	0.1	0.619×10^{-2}	5.98×10^{-2}	3.000	1.79×10^{-1}
1	0.2	0.175	0.108×10^{-1}	1.30×10^{-1}	2.9468	2.37×10^{-1}
2	1.0	0.68	0.417×10^{-1}	5.03×10^{-1}	2.9136	1.48
3	1.8	1.26	0.663×10^{-1}	9.32×10^{-1}	2.9704	2.98
4	2.5	1.57	0.962×10^{-1}	1.16	2.8272	3.57
5	3.2	2.40	0.147	1.77	2.7840	5.47
6	4.1	0.057	0.271	3.27	2.7408	10.1
7	5.2	0.071	0.341	4.12	2.6976	12.6
8	6.4	0.092	0.447	5.39	2.6544	16.2
9	7.4	0.106	0.517	6.24	2.6112	18.5
10	9.8	0.128	0.628	7.57	2.5680	22.1
11	10.8	0.146	0.718	8.66	2.5248	24.9
12	12.0	0.182	0.899	10.8	2.4816	30.7
13	15.0	0.225	1.12	13.5	2.4384	37.5
14	19.0	0.29	1.44	17.4	2.3952	47.7
15	24.0	0.36	1.79	21.6	2.3520	58.3

continued . . .

TABLE 9 (continued)

Sample number	Time from commencement of electrolysis to Beginning of sampling/min.	Peak current/μA	$[Pb^{2+}]$/ppm (diluted)	$[Pb^{2+}] \times 10^6$/ mol ℓ^{-1} (original)	Volume of electrolyte/ litres (±0.005)	Total lead disintegrated* $\times 10^6$/mol cm^{-2}
16	31.0	0.43	2.15	25.9	2.3088	68.5
17	43.0	0.61	3.05	36.8	2.2656	95.6
18	60.0	0.68	3.40	41.0	2.2224	105
19	81.0	0.69	3.45	41.6	2.179	104
20	124.0	0.92	4.61	55.6	2.136	136
21	162.0	1.0	5.01	60.4	2.093	145
22	287.0	0.22	1.09	13.1	2.050	30.8

1. Before analysis, 10 mls of each original sample was diluted to 25 mls using 1 mol ℓ^{-1} $HClO_4$.

2. Analyses were carried out with differential pulse polarography except blank and samples 1 to 5 which were analysed using DPASV.

3. The $[Pb^{2+}]$ in original samples were calculated using $[Pb^{2+}]$ in diluted samples and multiplying by a factor of 2.5.

*Moles of lead in blank solution.

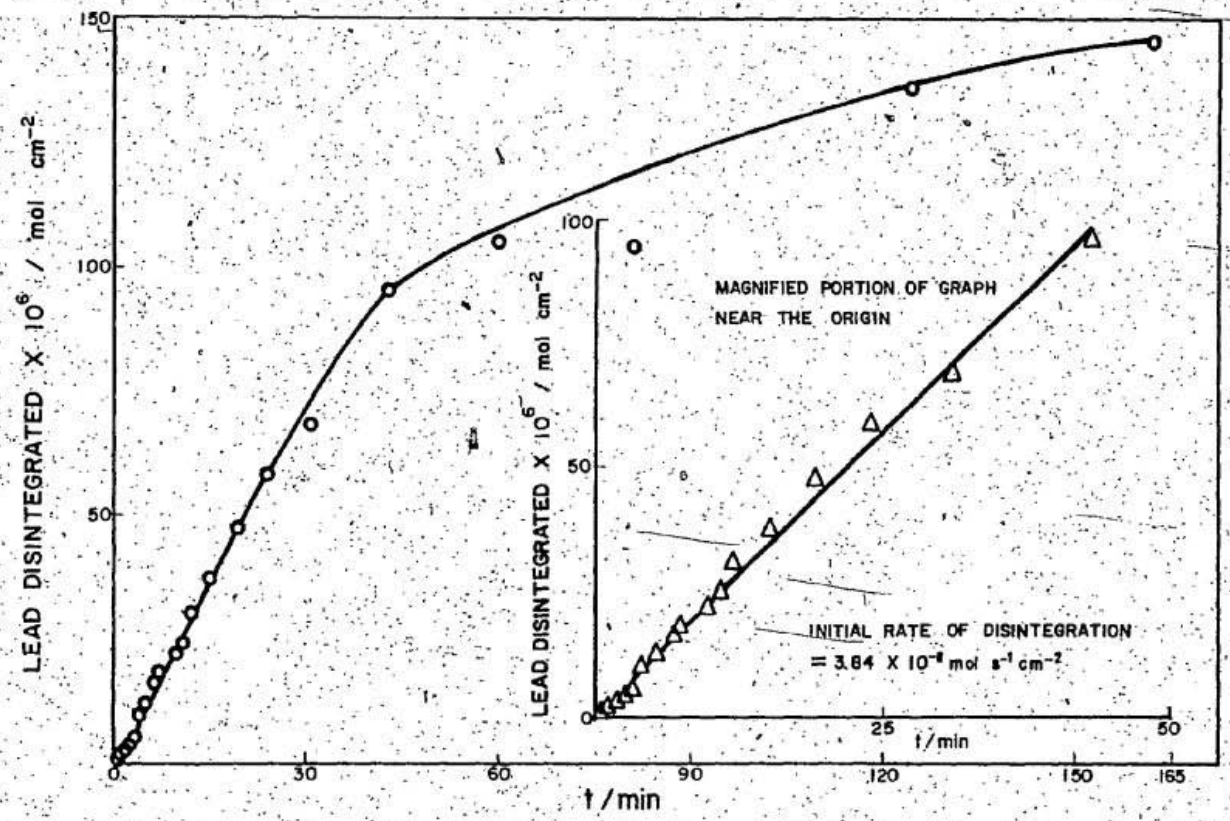

Fig. 29. MOLES OF LEAD DISINTEGRATED PER UNIT AREA vs TIME IN 1 mol l^{-1} NaOH AT $-16 mA\ cm^{-2}$ (AREA = 0.87 cm^2)

V Dependence of Lead Disintegration Rate on Cathodic Current Density in Acid Solutions

Table 10 summarizes the initial disintegration rates in our careful experiments and those of Gastwirt and Salzberg (70) in pure acid solutions.

The initial disintegration rates are plotted versus cathodic current densities in Figures 30 to 32. The curves are linear for any given acid concentration, intersecting the c.d. axis (the threshold c.d.), indicating that above some minimum c.d. there is a direct proportionality between the rate of disintegration and cathodic current density. The threshold c.d. increased by increasing the acid concentration as already noted by Salzberg et al (69,70,71) for salt solutions of various pH's. Direct comparison with Gastwirt and Salzberg's data (70) is also made in Figure 31. This plot compares our rate versus cathodic c.d. plots with one point of theirs for each of two H_2SO_4 concentrations, i.e. 0.001 mol ℓ^{-1} and 0.01 mol ℓ^{-1}. In both cases more disintegration occurred in the present work at c.d.'s lower than their -94 and -535 mA cm^{-2}, respectively, which appear to have been close to threshold values for their inferior measurement technique. The present work differs in the discovery of significantly smaller threshold cathodic current densities for acid solutions. As Figures 30 to 32 indicate, the new thresholds for 0.003, 0.01 and 0.1 mol ℓ^{-1} $HClO_4$ lie, respectively, at 30, 45 and 80 mA cm^{-2} and for 0.001, 0.005, 0.01 and 0.1 mol ℓ^{-1} H_2SO_4 lie, respectively, at 20, 30, 115 and 210 mA cm^{-2}. Gastwirt and Salzberg's thresholds

TABLE 10 INITIAL DISINTEGRATION RATES AS A FUNCTION OF ACID CONCENTRATION AND CATHODIC CURRENT DENSITY

PRESENT WORK						GASTWIRT AND SALZBERG'S WORK (70)		
$[HClO_4]$/ mol ℓ^{-1}	Cathodic current density/ mA cm^{-2}	Disintegration rate x 10^8/ mol s^{-1} cm^{-2}	$2[H_2SO_4]$/ mol ℓ^{-1}	Cathodic current density/ mA cm^{-2}	Disintegration rate x 10^8/ mol s^{-1} cm^{-2}	$2[H_2SO_4]$/ mol ℓ^{-1}	Cathodic current density/ mA cm^{-2}	Disintegration rate x 10^8/ mol s^{-1} cm^{-2}
0.003	30	0.0265	0.002	20	0.417			
0.003	50	4.12	0.002	60	13.2			
0.003	108	26.2	0.002	94	20.0	0.002	94	0.804
0.003	150	44.6	0.002	100	22.4			
0.01	50	2.09	0.01	30	0.583			
0.01	60	5.56	0.01	60	12.3			
0.01	100	16.3	0.01	80	13.7			
0.01	150	15.0	0.01	115	34.9			
0.01	200	54.2						
0.1	54	0.00214	0.02	115	0.140			
0.1	115	0.0625	0.02	168	7.68			
0.1	175	0.392	0.02	190	11.0	0.02	535	1.61
0.1	230	0.463						
			0.2	241	0.0321			
			0.2	350	0.0572			
			0.2	402	0.0890	0.2	630	0.804

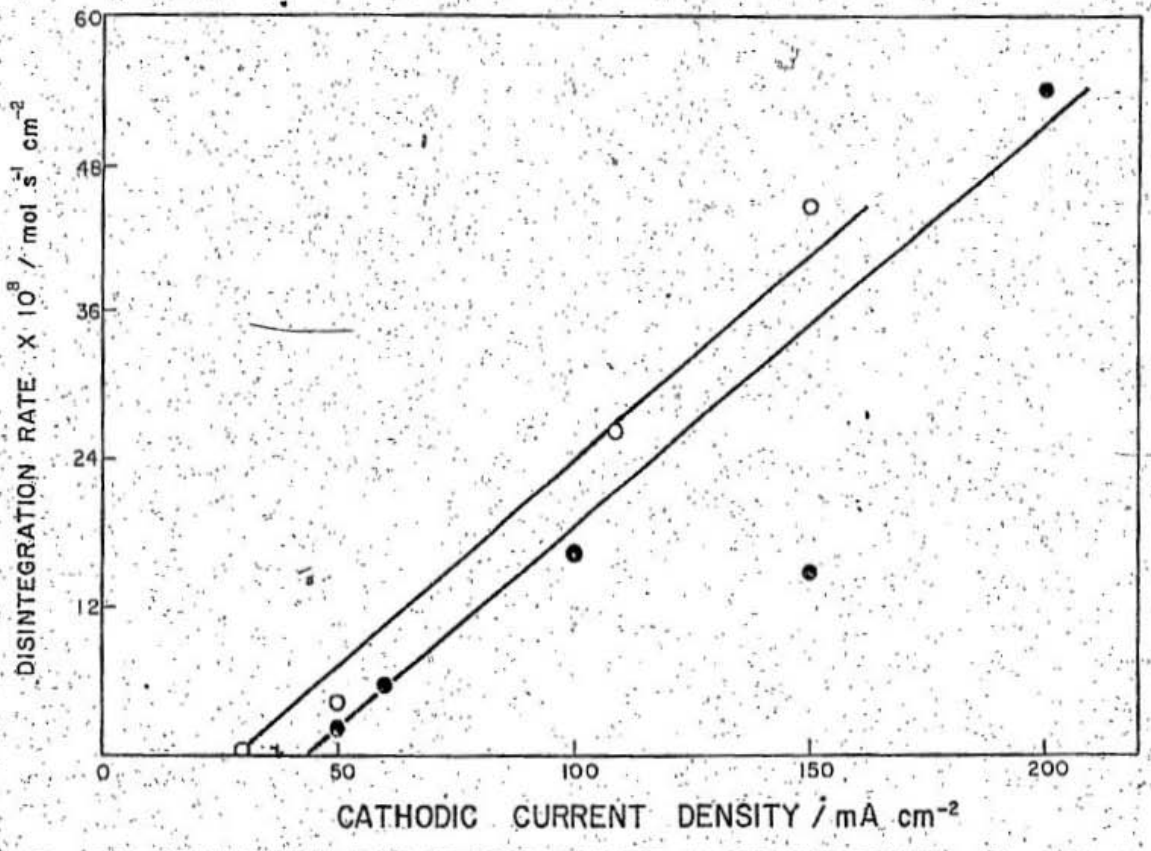

Fig. 30. DISINTEGRATION RATE OF LEAD CATHODE vs CURRENT DENSITY IN $HClO_4$: 0.003 mol ℓ^{-1}, O, AND 0.01 mol ℓ^{-1}, ●.

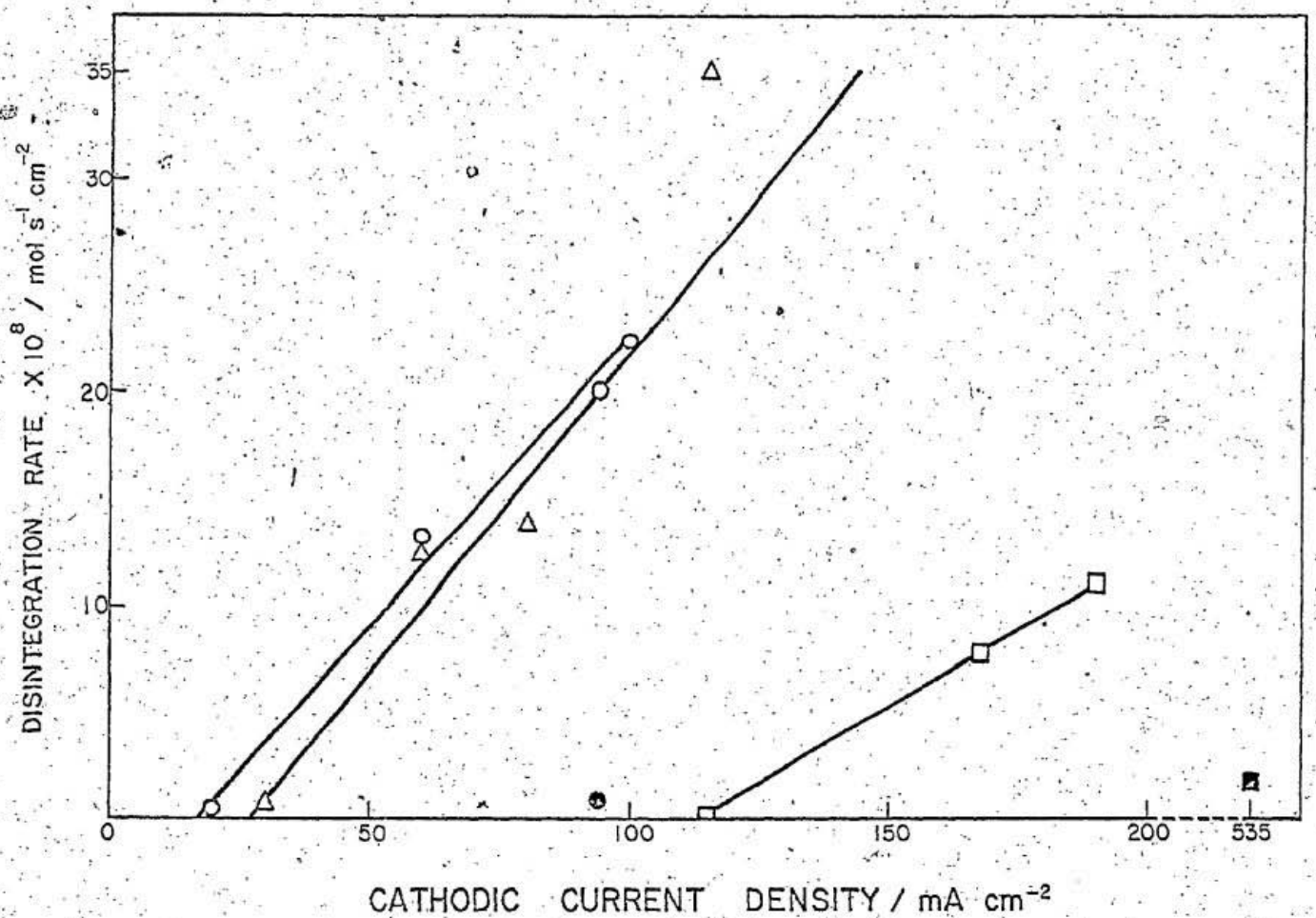

Fig. 31. DISINTEGRATION RATE OF LEAD CATHODE vs CURRENT DENSITY IN H_2SO_4 ; 0.001 mol ℓ^{-1}, ○; GASTWIRT AND SALZBERG, 0.001 mol ℓ^{-1}, ● ; 0.005 mol ℓ^{-1}, △, 0.01 mol ℓ^{-1}, □; GASTWIRT, AND SALZBERG, 0.01 mol ℓ^{-1}, ■.

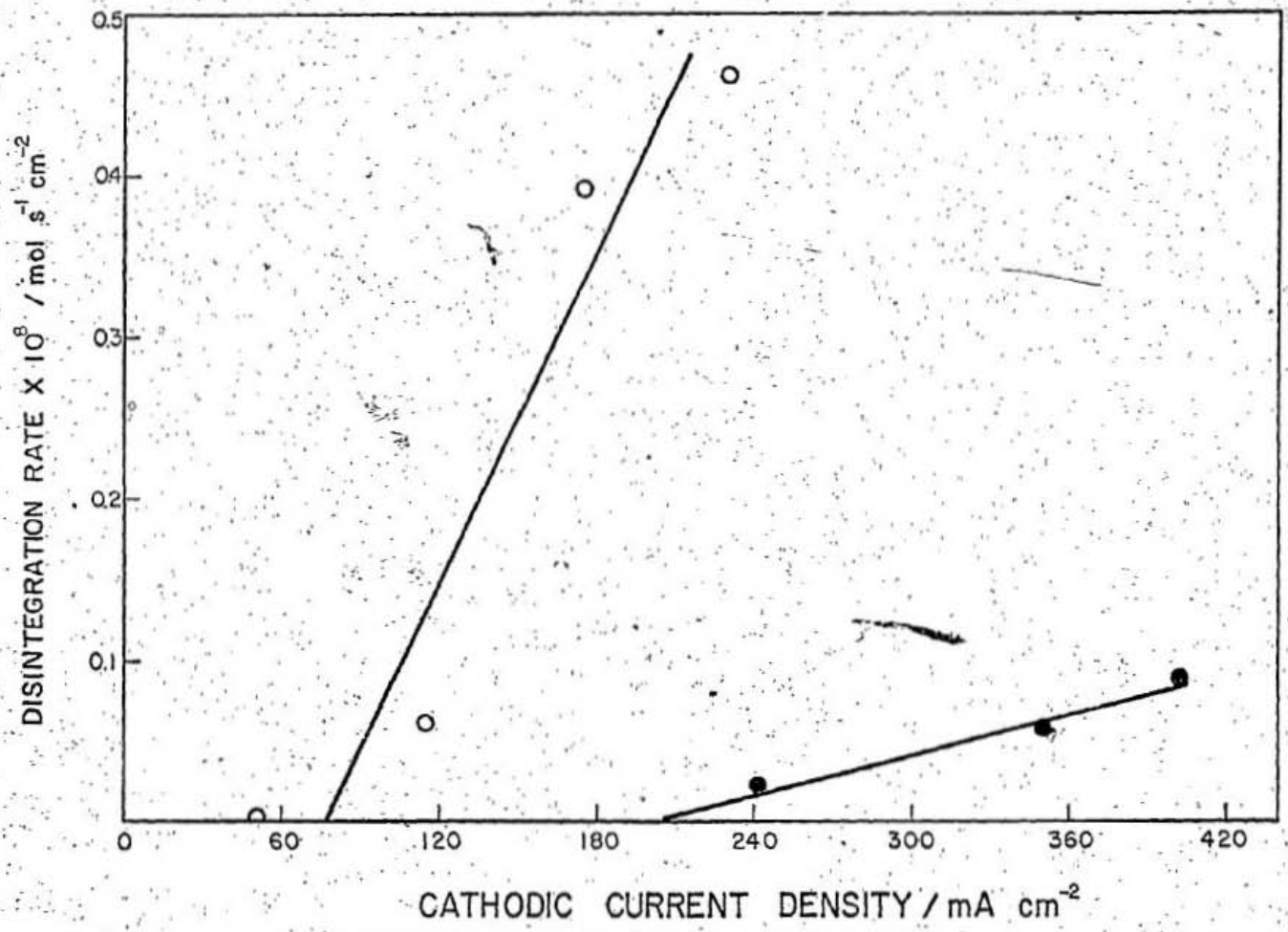

Fig. 32. DISINTEGRATION RATE OF LEAD CATHODE vs CURRENT DENSITY 0.1 mol l^{-1} $HClO_4$, O; 0.1 mol l^{-1} H_2SO_4, ●.

seemed to be at 94, 535 and 630 mA cm^{-2} for 0.001, 0.01 and 0.1 mol ℓ^{-1} H_2SO_4, respectively, as Table 10 makes clear. According to Figure 32 our threshold for 0.1 mol ℓ^{-1} H_2SO_4 is 210 mA cm^{-2} but extrapolation of the disintegration rate-current density plot to 630 mA cm^{-2} would yield a disintegration rate of 0.2×10^{-8} mol $s^{-1}cm^{-2}$ much lower than Gastwirt and Salzberg's 0.8×10^{-8} mol $s^{-1}cm^{-2}$ at this c.d. A possible reason for this difference may be the lower alkali metal ion concentration in the present work. Atomic absorption spectroscopy was used for the determination of Na^+ and K^+ ion concentrations in our acid solutions. The concentration of Na^+ ion determined at 599 nm was in the range of 10-15 ppb while the K^+ ion concentration was <10 ppb.

From the slopes of the disintegration rate-current density plots the number of moles of lead disintegrated per Faraday passed cathodically in excess of the threshold c.d. were calculated. The results of such calculations are given in Table 11. The slopes, indicating the current efficiency of $Pb \rightarrow Pb^{2+} + 2e^-$, decrease substantially as the $HClO_4$ concentration increases, i.e. as the pH decreases. The difference in behaviour at low $[H_3O^+]$ is, however, very slight. Similar data, indicating the current efficiency of cathodic disintegration, were obtained from Salzberg et at's work (69,70) in salt and alkaline solutions. They are summarized in Tables 12 and 13. Table 12 shows the tendency for the efficiency to decrease as the concentration of a given electrolyte is increased. The data of Table 13, presented by the authors (70) only in a graphical form

TABLE 11 MOLE RATIOS Pb:H AS A FUNCTION OF ACID CONCENTRATION FOR CURRENT DENSITIES ABOVE THRESHOLD.

PRESENT WORK

$[HClO_4]$/mol ℓ^{-1}	Pb:H/mol Faraday^{-1}
0.003	0.34
0.01	0.32
0.1	0.004

$2[H_2SO_4]$/mol ℓ^{-1}	Pb:H/mol Faraday^{-1}
0.002	0.29
0.01	0.30
0.02	0.14
0.20	0.0004

TABLE 12 MOLE RATIOS Pb:H AS A FUNCTION OF ELECTROLYTE AND pH FOR CURRENT DENSITIES ABOVE THRESHOLD AT 20°C FROM SALZBERG'S DATA (69).

ELECTROLYTE	pH	Pb:H/mol Faraday^{-1}
[KCl]/mol ℓ^{-1}		
1	12 - 3.7	0.49
	2.3	0.49
	1.5	0.55
	1.3	0.40
2	alkaline	0.53
4	alkaline	0.26
0.7 mol ℓ^{-1} Na_2SO_4	alkaline	0.23
1.4 mol ℓ^{-1} Na_2SO_4	alkaline	0.18
4 mol ℓ^{-1} NaOH	alkaline	0.23

TABLE 13 MOLE RATIOS Pb:H AS A FUNCTION OF SOLUTION COMPOSITION FOR CURRENT DENSITIES ABOVE THRESHOLD FROM GASTWIRT AND SALZBERG'S WORK (70).

SOLUTION COMPOSITION	APPROXIMATE pH	Pb:H/mol Faraday^{-1}
0.1 mol ℓ^{-1} Na_2SO_4 + m mol ℓ^{-1} H_2SO_4		
*m = 0	~ 7	0.53
0.01	3	0.42
0.02	2.7	0.49
0.05	2.3	0.44
0.08	2.1	0.27
0.1	2	0.24
n mol ℓ^{-1} $(NH_4)_2SO_4$ + m mol ℓ^{-1} H_2SO_4		
**n = 0.01, m = 0.001	3.3	0.56
n = 0.01, m = 0.01	2.3	0.53
n = 0.1, m = 0.01	3	0.40
n = 0.1, m = 0.1	2	0.39

*m is molar concentration of H_2SO_4.

**n is molar concentration of $(NH_4)_2SO_4$.

but evaluated by us, indicate that increasing the concentration of H_2SO_4 in aqueous Na_2SO_4 or at constant $(NH_4)_2SO_4$ concentration, i.e. decreasing the pH inhibits lead disintegration and decreases the Pb:H ratio as was also observed for pure acid solutions in the present investigation (see Table 11).

Chapter 4

DISCUSSION

As stated earlier, Salzberg et al (69,70,71) and van Muylder and Pourbaix (75), believed that cathodic disintegration of lead involves the transient formation of a volatile hydride presumed to be PbH_2, which decomposes into finely divided lead and hydrogen soon after escaping from the electrode. The main evidence of Salzberg et al (69,70,71) for this mechanism is the finding that, in certain electrolyte solutions, the disintegration rate, calculated as moles of Pb disintegrated per Faraday of electricity passed cathodically in excess of the threshold c.d. (see Tables 12 and 13) was approximately 0.5 in dilute aqueous solutions containing alkali metal cations. This relation, indicating close to 100% c.d. efficiency for disintegration above the threshold c.d. and suggesting a stiochiometry of PbH_2, held reasonably well for dilute solutions containing alkali cations, but increasing alkali cation concentration (see Table 12) or increasing acidity, e.g. in Na_2SO_4 or in $(NH_4)_2SO_4$ solutions (see Table 13) caused a shift towards a much smaller number of moles of lead disintegrated per Faraday. Salzberg et al suggested that increasing the salt or acid concentration could either lower the proportion of hydride formed because of the high interfacial concentrations of alkali cations or hydronium ions, or that the same rate of formation of hydride occurs but the high cation or hydronium concentration causes catalytic decomposition of hydride before it leaves the surface.

In our experiments with pure acid solutions (10L), essentially free of alkali metal cations (10-15 ppb Na^+ by atomic absorption)

the Pb:H ratio is approximately constant (0.32 ± 0.02 mol Faraday^{-1}) for very low concentrations (0.002 to 0.01 mol ℓ^{-1} H_3O^+ and decreases rapidly with increasing $[H_3O^+]$ to as little as 0.0004 for 0.1 mol ℓ^{-1} H_2SO_4, as Table 11 indicates. Our results do not, therefore, support the concept of a particular PbH_x composition as an intermediate.

Before giving any explanation of the experimental results in Table 11, the shape of the quantity of lead in solution versus time curves should be first discussed. Initially, the concentration of Pb^{2+} ions is negligibly small, e.g. from 1×10^{-9} to 6×10^{-9} mol ℓ^{-1} in 0.001 to 0.1 mol ℓ^{-1} H_2SO_4, respectively, from blank determinations. The lead particles generated by cathodic disintegration, dissolve rapidly in the acid solutions with the formation of divalent plumbous ions. $[Pb^{2+}]$ rises rapidly when disintegration commences and when $[Pb^{2+}]$ has increased significantly, two processes come into play tending to decrease this concentration. These are (i) cathodic reduction at the lead cathode

$$Pb^{2+}(aq) + 2e^- = Pb$$

and (ii) anodic oxidation at the platinum anodes,

$$Pb^{2+}(aq) + 2H_2O = PbO_2 + 4H^+(aq) + 2e^-$$

Evidence exists that both processes actually occur in acid solutions. Lead cathodes, in experiments exhibiting high disintegration rates, became covered with a spongy grey lead deposit and platinum anodes under the same conditions became coated by brown lead dioxide.

In the initial period of an experiment, the disintegration rate exceeds the combined rates of cathodic Pb and anodic PbO_2 deposition, because $[Pb^{2+}]$ is small. Hence, at this time the steep slopes of the quantity of lead in the electrolyte versus time give a true measure of the disintegration rate, as has been assumed here, certainly a lower limit.

Later, the rates of disintegration and deposition come closer to equality, establishing a steady state with $[Pb^{2+}] \approx$ constant, as observed in most experiments after sufficient time had elapsed. When deposition of spongy lead occurred on the cathode, the resultant increase in true surface area will cause the disintegration rate to change to correspond to the new cathodic current density so that probably both will decrease. Under such conditions $[Pb^{2+}]$ will fall, as our data indicate. Eventually, with the growth of the cathode surface area and reduction of brightness of the lead cathode accompanying lead deposition on it, continuous disintegration may cease altogether as the current density falls below the threshold.

The disintegration rate versus cathodic c.d. curves (Figs. 30, 31 and 32) show that above the threshold c.d. the disintegration rate increases linearly with c.d. in all acid solutions, with different slopes, indicating that there is a direct proportionality between disintegration rates and the cathodic c.d.'s.

Below the threshold c.d.'s, discontinuous disintegration was observed with the maximum $[Pb^{2+}]$ in the range of 4×10^{-7} mol ℓ^{-1} after a long period of cathodisation, [illegible] 70 h. (see Fig. 20). Above

the threshold c.d.'s discontinuous disintegration may also occur but the amount of lead disintegrated by this process would be negligibly small compared to the total amount of lead disintegrated, so that discontinuous disintegration has not been observed above threshold c.d.'s.

Discontinuous disintegration may involve the motion of hydrogen atoms into the lead lattice and will be discussed after consideration of the continuous disintegration, which is a better established phenomenon.

By taking account of the migration of $H_3O^+_{aq}$, the diffusion current flux in the Fick's Law expression becomes $i\ (1 - t_{H^+})$, where t_{H^+} is the transference number of hydronium ions in the diffusion boundary layer. When the concentration of $H_3O^+_{aq}$ at the pre-electrode state is equal to zero, a limiting cathodic c.d. ($i_{lim}-$) for $H_3O^+_{aq}$ transport by convective diffusion and migration should be observable, i.e. $i_{lim} = -(FD_{H^+}C_{H_3O^+})/(1 - t_{H^+})\delta$, where δ is the thickness of diffusion layer, which depends on the nature of the gas evolved, on the manner of formation of the gas bubbles, on the c.d. and on the height of the electrode (102). Under the frequently encountered conditions of external gas bubbling, $\delta \simeq 0.005$ cm; this value will be used here. It is usually assumed that t_{H^+} has the same value in the diffusion layer as in the bulk solution, which probably is reasonable in many circumstances because t_{H^+} at infinite dilution is little different from that in 0.1 mol ℓ^{-1} acid solutions.

Using the diffusion coefficient of $H_3O^+_{aq}$ ($D_{H^+} \simeq 2.5 \times 10^{-5}$ cm^2 s^{-1}) and transference number of $H_3O^+_{aq}$ ($t_{H^+} \simeq 0.825$), the initial limiting cathodic c.d.'s (assuming $\delta \simeq 0.005$ cm) for the discharge of $H_3O^+_{aq}$ in 0.003, 0.01 and 0.1 mol ℓ^{-1} $HClO_4$ are 8, 27 and 275 mA cm^{-2}, respectively, while the threshold c.d.'s observed for continuous lead disintegration (see Figs. 30 and 32) are 30, 45 and 80 mA cm^{-2}. In a similar way, the initial i_{lim} - for the discharge of $H_3O^+_{aq}$ in 0.001, 0.005, 0.01 and 0.1 mol ℓ^{-1} H_2SO_4 are 6, 27, 55 and 551 mA cm^{-2}, respectively, while the threshold c.d.'s (see Figs. 24 and 25) are 20, 30, 115 and 210 mA cm^{-2}.

Obviously, if the hydronium ions were the only source of hydrogen to form hydride, increasing the acid concentration would increase the disintegration rate. Actually, the converse occurs (see Table 11). The disintegration rate in dilute acid solutions was much greater than in concentrated ones at the same current density (see Table 11). Consequently, the discharge of water molecules which carry the largest fraction of the cathodic current passed in acid solutions of concentrations smaller than 0.1 mol ℓ^{-1} (e.g. with 0.003 mol ℓ^{-1} $HClO_4$ at 30 mA cm^{-2} about 73% of c.d is carried by H_2O), should play an important role in the production of adsorbed hydrogen atoms and in the subsequent disintegration of the lead cathode. Therefore, above the limiting c.d., depending on $[H_3O^+]$, the reduction of water molecules becomes the dominant electrode process as the source of adsorbed hydrogen:

$$Pb + H_3O^+(aq) + e^- = Pb\text{-}H_{ads} + H_2O \qquad (4.1)$$

$$Pb + H_2O + e^- = Pb\text{-}H_{ads} + OH^-(aq) \qquad (4.1a)$$

Desorption of hydrogen may occur by combination of adsorbed hydrogen atoms:

$$Pb\text{-}H_{ads} + H_{ads}\text{-}Pb = H_2(g) + 2Pb_{metal} \qquad (4.2)$$

or by electrochemical desorption steps involving either $H_3O^+_{aq}$ ions or H_2O molecules:

$$Pb\text{-}H_{ads} + H_3O^+(aq) + e^- = H_2(g) + H_2O + Pb_{metal} \qquad (4.3)$$

$$Pb\text{-}H_{ads} + H_2O + e^- = H_2(g) + OH^-(aq) + Pb_{metal} \qquad (4.3a)$$

The discharge of water molecules on hydrogen-occupied and unoccupied sites of lead may also occur to produce lead hydride:

$$Pb\text{-}H_{ads} + xH_2O + xe^- = PbH_x + xOH^-(aq) + \tfrac{1}{2}H_2(g) \qquad (4.4)$$

$$Pb + xH_2O + xe^- = PbH_x + xOH^-(aq) \qquad (4.5)$$

If a hydride is formed it must be volatile or capable of breaking away from the lead surface soon after it is formed. If the hydride formed is volatile, it must decompose rapidly to the observed lead particles, particularly in acid concentrations of less than 0.01 mol ℓ^{-1}, and hydrogen:

$$PbH_x = Pb_{particles} + \frac{x}{2}H_2(g) \qquad (4.6)$$

If it is not volatile but nevertheless leaves the lead surface it should be soluble in acid solution:

$$PbH_x + 2H_3O^+(aq) = Pb^{2+}(aq) + 2H_2O + (\frac{x+1}{2})H_2(g) \qquad (4.7)$$

More work is needed to determine the number of hydrogen atoms (x) that are involved in the formation of PbH_x. Potential measurements under disintegration conditions could be helpful.

Salzberg (69) showed that, for solutions of potassium chloride or of sodium hydroxide, the slopes of the lead disintegration rate versus c.d.'s curves were a linear function of water activity, a_{H_2O}, as the data of Table 14 indicates. We have used the expression $\ln a_{H_2O} = -\frac{m}{55.5}(\nu + \frac{\nu}{m}\int_0^{\ln} m\, d\ln\gamma)$, where m is the molality of solute, ν is the total number of ions and γ is the activity coefficient of solute (103), to calculate the water activities in the acid solutions used in this work. Such calculations are tabulated in Table 14. It is obvious from Table 14 that the linear relationship found by Salzberg for solutions of high pH does not exist in the pure acid solutions used in the present work. Table 14 indicates that as the acid concentration increases, the slopes of the lead disintegration rate versus c.d. curves decreased substantially, but there is very little change in the water activity. It is evident that there must be inhibitory effects by hydronium ions on the disintegration: because (i) an increase of the rate of the hydronium ion + atom desorption, reaction (4.3), is expected when the acid concentration is increased,

TABLE 14 WATER ACTIVITY AS A FUNCTION OF ELECTROLYTE CONCENTRATION AND SLOPE OF RATE-CURRENT DENSITY CURVE

Solution	a_{H_2O} pure H_2O = 1	Slope of rate-current density curve x 10^6/mol s^{-1} cm^{-2}-A cm^{-2}
	Salzberg's Work	
4 mol ℓ^{-1} KCl	0.870	2.17 ± 0.08
4 mol ℓ^{-1} NaOH	0.920	2.65 ± 0.56
2 mol ℓ^{-1} KCl	0.936	3.62 ± 0.40
1 mol ℓ^{-1} KCl	0.973	4.67 ± 0.24
0.04 mol ℓ^{-1} NaOH	1.00	5.55 ± 0.56
	Present Work	
0.001 mol ℓ^{-1} H_2SO_4	0.99994	0.180
0.003 mol ℓ^{-1} $HClO_4$	0.99989	0.277
0.005 mol ℓ^{-1} H_2SO_4	0.99968	0.186
0.01 mol ℓ^{-1} $HClO_4$	0.99963	0.199
0.01 mol ℓ^{-1} H_2SO_4	0.99935	0.087
0.1 mol ℓ^{-1} $HClO_4$	0.99660	0.00249
0.1 mol ℓ^{-1} H_2SO_4	0.99640	0.000249

and (ii) catalytic decomposition of the hydride by hydronium ions, as proposed by Salzberg (69), might occur before the former leaves the surface:

$$PbH_x + H_3O^+(aq) = \underset{metal}{Pb} + H_3O^+(aq) + \frac{x}{2}H_2(g) \qquad (4.8)$$

or

$$PbH_x + H_3O^+(aq) + e^- = \underset{metal}{Pb} + H_2O + (\frac{1 + x}{2})H_2(g) \qquad (4.9)$$

In dilute acid solutions the slopes of the disintegration rate versus the quantity of electricity discharged (see Table 11), do not seem to depend on $[H_3O^+]$. The best explanation of the similar slopes is that under these conditions there is little or no inhibition by hydronium ions of the formation of hydride.

The cathodic disintegration of lead at low c.d.'s occurs with higher rates in alkaline solutions than in acid solutions. The insertion of alkali metal into the lead lattice and production of an alkali metal lead alloy which subsequently is decomposed by water as proposed by Angerstein (74), Kabanov and coworkers (76-80), could probably enhance the disintegration rates in alkaline solutions compared with those in acid solutions In the present work, the information concerning the disintegration of lead in alkaline solutions is insufficient to prove the above suggestion.

Early work (104) indicated a negligible solubility for molecular hydrogen in lead at greater than room temperatures (ca. 530 K) but no information concerning the diffusion of electrolytically generated hydrogen in lead at room temperature is available from the literature

before 1970. The early findings of Deming and Hendricks (105) that molecular hydrogen permeated through lead at a rate of 1 μg h^{-1} cm^{-2} at 538 ± 15 K, is remarkable for the fact that no attention was paid by these workers to preparation of the lead surface. However, the solubility of hydrogen in molten lead has been measured by Opie and Grant (106), who obtained solubilities (expressed as atomic ratios) ranging from H/Pb = 1.8×10^{-5} at 973 K to 2.3×10^{-4} at 1173 K.

More recently, evidence that lead dissolves hydrogen has come from the gas phase studies of Wells, Roberts and Young (66,67), as mentioned earlier. From the slope of the hydrogen uptake vs time curve and the mass of the lead phase, they derived a formula of $PbH_{0.2}$ at 273 K ($PbH_{0.22}$ at 195 K) for the composition of a hydride which appears to be reasonably stable either in a hydrogen atmosphere or in a vacuum. This hydride only very slowly absorbs atomic hydrogen passed over it. At low temperatures, ca. 78 K, i.e. at higher surface coverages, the surface H atoms were removed by the combination with H atoms from the gas phase. However, at temperatures $\geq$ 273 K, i.e. at lower surface coverage, <u>the recombination of H atoms within the lattice leading to molecular desorption via the solid</u> was thought to become significant when the probability of recombination within the lattice is comparable to the probability of a hydrogen atom finding a stable lattice site. This occurs when one H atom is present per five lead lattice atoms, i.e. when the lead hydride has a composition $PbH_{0.2}$.

Ives and Smith (9,107) estimated, according to their hypothesis for overvoltage shifts with time, that upper and lower limits of

diffusivity of H atoms in lead are 10^{-6} and 2.5×10^{-11} cm^2s^{-1}. Their lower limit, 2.5×10^{-11} cm^2s^{-1}, was equated to the interstitial diffusivity of Au in lead. The upper limit, 10^{-6} cm^2s^{-1} was, however, based on the general property of metal atoms of diffusing faster in lead than in any other solid metal while H atoms in general diffuse much faster than metal atoms because of their smaller radius and low valency (107a). Barr (107a) has shown that there is a decreasing diffusivity in lead with increasing valence in the sequence: Ag, Cd, In.

The first measurements of the diffusivity of hydrogen in lead came from the work of Cadersky, Muju and Smith (49). They showed by the shape of current transients that permeation of electrolytically generated hydrogen through lead foils of 0.015 cm thickness does indeed occur. Their diffusivities for H in Pb at 298 K at cathodic c.d.'s of 10, 25 and 50 mA cm^{-2} were 1.2×10^{-7}, 2.9×10^{-7} and 7×10^{-7} cm^2s^{-1}, respectively. From the estimated bulk hydrogen concentration in lead of 10^{-6} g atom H cm^{-3}, they reported a most probable hydride composition of $PbH_{0.00002}$, much less hydrogen-rich than the $PbH_{0.2}$ of Wells, Roberts and Young (66,67). The higher bulk H concentration observed by these workers compared with that of Cadersky, Muju and Smith's work may be explained by the relatively superior experimental conditions, e.g. the high vacuum system used by Wells, Roberts and Young in their gas phase adsorption studies. The findings of Cadersky et al, i.e. the diffusion of hydrogen atoms through lead, was confirmed by Muju and Smith (46). These workers employed a technique using tritium in

an electrolytic hydrogen permeation study, because a radioactive tracer can be accurately assayed even at low concentrations.

With the confirmation of the reality of hydrogen atom diffusion through lead, an alternative mechanism of lead disintegration could be the diffusion of hydrogen atoms through the lead lattice followed by combination within the lattice to H_2, i.e.:

$$Pb - H_{ads} = Pb - H_{abs}$$

$$Pb - H_{abs} + H_{abs} - Pb = H_2 + Pb_{particles}$$

as suggested by Roberts and Young (67) to explain their observations of the interactions of gaseous hydrogen atoms with lead, exerting such pressures that particles of lead are ejected. This explanation is consistent with the discontinuous disintegration observed here which, we believe, occurs because of the gradual accumulation of atomic hydrogen in the metal, periodically reaching saturation proportions so that again lead particles are ejected to relieve the H_2 pressure. The evidence of Figure 20, with rapid bursts of Pb release (rapid rise of $[Pb^{2+}]$) followed by longer periods during which lead is deposited and $[Pb^{2+}]$ falls gradually, supports this view.

PART 2

HYDROGEN ADSORBED ON AND ABSORBED BY SILVER CATHODES IN ACID SOLUTIONS

Chapter 1

INTRODUCTION

The second part of this thesis is concerned with the subjects of

(a) diffusion of electrolytically generated hydrogen atoms through silver cathodes,

(b) hydrogen overvoltage measurements on silver cathodes, and

(c) electrode capacitance measurements on silver in aqueous perchloric acid solution specifically to determine the hydrogen pseudo-capacitance.

The absence of evidence for diffusion of hydrogen atoms, produced during electrolysis, through a silver cathode and the lack of hydrogen coverage measurements at a silver cathode in aqueous acid solution made it desirable to study the diffusion phenomenon as well as the hydrogen overvoltage. This work was later extended to obtain adsorption pseudocapacitance data from which the hydrogen coverage could be calculated. It is the aim of the second part of this thesis to study electrolytic hydrogen evolution and the related adsorption and absorption of atomic hydrogen by silver in perchloric acid under the cleanest attainable experimental conditions. Special attention was paid to stringent deoxygenation, for it is thought that only under such conditions can the phenomenon of hydrogen adsorption and absorption be properly studied.

In this chapter, surveys are given of previous work on three topics:

I. Diffusion of gas phase hydrogen through silver

II. Hydrogen overvoltage measurements on silver

III. Capacitance measurements on silver and adsorption of hydrogen by silver from aqueous solution.

I. Diffusion of Gas Phase Hydrogen Through Silver

The study of diffusion of hydrogen through metals has attracted much interest because of its relation to the problem of hydrogen embrittlement.

To date no completely successful study of hydrogen diffusion through silver in contact with an aqueous solution has been made.

The diffusion of hydrogen through silver from the gas phase at high temperatures ($\geq$ 673 K) was reported (108-113). In 1866, Graham (108) obtained an absorption of 1.8×10^{-5} g atom H cm^{-3} for silver wire, and 8.0×10^{-5} g atom H cm^{-3} for silver which had been reduced from the oxide. Baxter (109) found a smaller absorption of 4.5×10^{-5} g atom H cm^{-3} for silver which had been reduced from the oxide. In 1928, Steacie and Johnson (110), using a degasification technique, obtained a solubility of about 4.46×10^{-7} to 4.1×10^{-6} g atom H cm^{-3} over the temperature range 673 K to 1173 K. Below 673 K, the absorption of hydrogen by silver was extremely small, being undetectable at 473 K. Since the rate of diffusion of hydrogen through silver was proportional to $\sqrt{P_{H_2}}$, where P_{H_2} is the partial pressure of H_2, Steacie and Johnson proposed that the diffusion of hydrogen through silver takes place by movement of atomic, not molecular hydrogen. In 1957, Siegelin, Lieser and Witte (111), using a gasification process obtained a value of 1.92×10^{-7} g atom H cm^{-3} for the solubility of hydrogen in silver at 770 K. In 1958, Eichenauer, Künzig and Pebler (112) measured the diffusion coefficient and solubility of hydrogen in silver by following the degasification of silver as the rate of increase in pressure in a previously evacuated system. They

reported values of 2.1×10^{-5}, 2.87×10^{-5} and 3.74×10^{-5} $cm^2 s^{-1}$ for the diffusion coefficients and values of 1.96×10^{-7}, 2.4×10^{-7} and 3.2×10^{-7} g atom H cm^{-3} for solubilities of hydrogen in silver at temperatures of 773, 823 and 873 K, respectively. In 1967, Thomas (113), using a quick quench extraction technique with subsequent quantitative analysis by mass spectroscopy, obtained values of 4.7×10^{-8} and 4.8×10^{-7} g atom H cm^{-3} of silver for temperatures of 873 and 1173 K, respectively. These solubility values for hydrogen in silver are in considerable disagreement with the work of Steacie and Johnson (110) and others (111,112). Thomas claimed that his technique eliminated the errors present in other workers' methods.

II. Hydrogen Overvoltage Measurements on Silver

The hydrogen electrode reaction, $2H^+ + 2e^- = H_2$, is an example of heterogeneous catalysis in which an electrode material acts as catalyst. The electrochemical approach to heterogeneous catalysis provides many advantages in comparison with the usual chemical one.

In 1923, Knobel, Caplan and Eisemann (114) found a linear relationship between $-\eta$ and $\log_{10}(-i)$ over the cathodic c.d. range 10^{-4} to 10^{-2} A cm^{-2} for a silver electrode in 1 mol ℓ^{-1} H_2SO_4 using a slow technique (the electrode was polarised at constant c.d. until the potential became constant). A similar result was also found by Bowden and Rideal (40) and Hickling and Salt (115) with sulphuric and hydrochloric acid solutions, respectively.

In 1959, Antoniou and Wetmore (116) studied both single and polycrystalline electropolished silver electrodes in pre-electrolysed 1 mol ℓ^{-1} H_2SO_4. They found two Tafel slopes b = 59 and 116 mV for the cathodic c.d. range 0.03 μA cm^{-2} to 2 mA cm^{-2}. The lower and higher portions of the Tafel lines intersected at an overvoltage of 196 ± 20 mV. They also observed that at a constant charging current the overvoltage build-up was linear with time and then bent off smoothly to a constant overvoltage. In some experiments, in which O_2 was known to be present at the beginning of experiment, the initial part of the curve was sigmoid.

More recently, Gossner and Mansfeld (117) studied hydrogen overvoltage at silver foils (heated in H_2 at 723 K for 24 hours) in pre-electrolysed 1 mol ℓ^{-1} H_2SO_4 over the cathodic c.d. range 2 to 200 mA cm^{-2} and Kilimnik and Rotinian (118) recorded Tafel plots for

mechanically polished 99.99% silver electrodes in sulphuric acid solution over the cathodic c.d. range 10 μA cm^{-2} to 1 A cm^{-2}. Gossner et al observed that at the beginning of the experiment, $-\eta$ decreased with time (up to ca. 30 minutes) and reached an almost constant value on a fresh silver cathode. The relationship between $-\eta$ and time was studied for a maximum of 2 hours. A b value of 120 mV was observed by Gossner et al in their work. In the investigation of Kilimnik et al, the observed overvoltages were higher than those found by Gossner et al (possibly because of use of unpurified sulphuric acid by Kilimnik et al) and at a cathodic c.d. of 10 mA cm^{-2}, there was an overvoltage jump from 0.65 to ca. 1.2 V in the Tafel plot. Above the overvoltage jump, the slope of the Tafel line was reported to be 120 mV.

In 1950, a rapid technique of measuring $-\eta$ was used by Azzam, Bockris, Conway and Rosenberg (119) for silver cathodes in acid solutions. Reproducible results were obtained when solutions were adequately purified by pre-electrolysis. In 1952, Bockris and Azzam (120) measured hydrogen overvoltages on silver heated in a hydrogen atmosphere at 873 - 973 K, then chemically polished and studied in pre-electrolysed 5 mol ℓ^{-1} HCl. A linear Tafel plot was obtained with b value of 120 mV over the cathodic c.d.'s of 1 mA cm^{-2} to 100 A cm^{-2}. Bockris and Conway (121), however, found two Tafel slopes of 60 ± 5 and 130 ± 5 mV within the cathodic c.d. range 1 μA cm^{-2} to 100 mA cm^{-2}, in solutions of pre-electrolysed HCl of concentrations greater than 0.1 mol ℓ^{-1}. There was an inflection at an overvoltage of 190 mV at a cathodic c.d. ~ 5 mA cm^{-2} in, e.g. 1 mol ℓ^{-1} HCl. They also observed a rise of $-\eta$ at silver cathodes in hydrochloric acid

with addition of either potassium chloride or barium chloride. Later, Bockris, Ammar and Huq (122) examined the effect of purification of the electrolyte for the hydrogen evolution reaction on spectroscopically pure silver electrodes. At low levels of pre-electrolysis, results were complex. After pre-electrolysis of, e.g. 0.4 mol ℓ^{-1} HCl, has been increased to a cathodic c.d. of 10 mA cm^{-2} for 60 hours, further pre-electrolysis caused no change in Tafel lines, which had two slopes of 57 ± 2 and 101 ± 9 mV over the cathodic c.d. range of 0.1 μA cm^{-2} to 1 mA cm^{-2} in 0.4 mol ℓ^{-1} HCl. Conway (123) also confirmed the existence of two Tafel slopes at silver cathodes in pre-electrolysed 0.1 mol ℓ^{-1} HCl. The Tafel line was broken at $i \simeq -1$ mA cm^{-2} at an overvoltage of 230 mV and gave the values of b = 72 ± 7 and 125 ± 5 mV over the (-i) range 3 μA cm^{-2} to 10 mA cm^{-2}.

In 1967, Bystrov and Krishtalik (124) investigated the effect of the solution composition and pH on the overvoltage at a silver cathode in hydrochloric and sulphuric acid solutions. They observed two Tafel lines with gradients 110 ± 10 mV for the upper and 60 ± 1 mV for the lower portion of the Tafel plot for a complete cathodic c.d. range of 0.01 μA cm^{-2} to 30 μA cm^{-2} in 0.05 mol ℓ^{-1} H_2SO_4. The Tafel line was inflected at an overvoltage of 130 mV at $i \simeq -1$ μA cm^{-2}. The larger value of $-\eta$ (ca. 50 mV at $i \simeq -20$ μA cm^{-2}) in sulphuric acid solutions than hydrochloric acid solutions was interpreted as an effect of specific adsorption of anions on the silver surface.

Wetterholm (125) studied the effects of a wide range of surface-active organic substances on the overvoltage at silver cathodes in sulphuric acid plus sodium sulphate solutions. Addition of organic

compounds, e.g. ethanol or acetaldehyde, to 0.5 mol ℓ^{-1} H_2SO_4 + 0.35 mol ℓ^{-1} Na_2SO_4 caused higher values of $-\eta$ at a particular c.d. This was explained as due to adsorption of the organic compound on the most active part of the electrode surface. The Tafel equation was examined between $i = \sim -20\ \mu A\ cm^{-2}$ and 20 mA cm^{-2} without addition of organic compound, the slopes being b = 119 ± 1 mV, using doubly-distilled water, and 108 ± 14 mV, using singly-distilled water in preparation of electrolytes. Essentially similar conclusions to Wetterholm were reached by Hillson (126) who studied the hydrogen overvoltage at silver in solution of HCl and H_2SO_4 containing organic compounds. Addition of n-hexanol to acid solutions led to a large increase, ca. 200 mV, in $-\eta$ and a marked decrease in the capacitance.

Table 15 summarizes the results of the Tafel slopes and exchange current densities at silver electrodes in acid solutions found by the above and other investigators.

TABLE 15 SUMMARY OF THE RESULTS OF TAFEL SLOPES AND EXCHANGE CURRENT DENSITY ON SILVER IN ACID SOLUTIONS BY VARIOUS INVESTIGATORS.

Form	Pre-treatment	Solution	Pre-electrolysis	Temperature/K	Range of $\log_{10}(-i/A\ cm^{-2})$	$\log_{10}(i_o/A\ cm^{-2})$	Tafel Slopes/mV	Reference
Wire	Chem. polished	0.05 mol ℓ^{-1} H_2SO_4	Conducted	-	-4 ~ -2	-5.7*	110	(127)
-	-	0.05 mol ℓ^{-1} H_2SO_4	-	293	-7 ~ -3.5	-6.42*	119*	(128)
Single or poly-crystal	Electropolished held in hot H_2 for a few days, gently anodised	1 mol ℓ^{-1} H_2SO_4	Conducted	Room	-7.5 ~ -2.7	~-6*	59 116	(116)
Wire	Heated in H_2 at 450°C for 24 h.	1 mol ℓ^{-1} H_2SO_4	100 mA cm^{-2}, 2.16×10^4 C	Room	-2.3 ~ -1.3	-5.4	120	(129)
Wire	Alkali, HNO_3, polished with fine glass powder	0.1 mol ℓ^{-1} H_2SO_4	Conducted	298	-8 ~ -4.5	-7.2*	115*	(124)
Wire	Alkali, HNO_3, polished with fine glass powder	0.05 mol ℓ^{-1} H_2SO_4	Conducted	298	-7 ~ -4.5	-6.3*	135	(124)

TABLE 15 (cont'd)

Form	Pre-treatment	Solution	Pre-electrolysis	Temperature/K	Range of $\log_{10}(-i/A\ cm^{-2})$	$\log_{10}(i_o/A\ cm^{-2})$	Tafel Slopes/mV	Reference
Wire	Heated in H_2 at 700°C for 1 h. sealed into glass bulb	0.1 mol ℓ^{-1} HCl	100 mA cm^{-2}, 8.6×10^3 ~13×10^3 C	299 ± 1	-5.5 ~ -2	-6.1 ± 0.23 -4.8 ± 0.15	72 ± 7 125 ± 5	(123)
-	-	1 mol ℓ^{-1} HCl	1 A cm^{-2} 3.1×10^4 C	298	-6 ~ -1	-5.4 ± 0.4 -3.7 ± 0.4	60 ± 5 130 ± 5	(121)
Wire	Chem. polished heated in H_2 at 600°C for 2-3 h.	5 mol ℓ^{-1} HCl	1 A cm^{-2}, ~10^5 C	298	-3 ~ -1	-5.5*	120	(120)
Wire	Heated in H_2 at 700°C for 1 h. sealed into glass bulb	0.4 mol ℓ^{-1} HCl	10 mA cm^{-2}, ~2.2×10^3 C	296 ± 2	-7 ~ -3	-6.6 -5.35	57 ± 2 101 ± 9	(122)

* Values estimated from figures or from slopes.

III. Capacitance Measurements on Silver and Adsorption of Hydrogen by Silver in Aqueous Solutions.

The electrical double layer capacitance $C_{d.l.}$, is defined in equation (7), i.e. $C_{d.l.} = \left(\frac{\partial q}{\partial E}\right)_{\mu,T,P}$ is the rate of change of charge, q, on the metal per unit area with electrode potential, E, at constant chemical potential of the electrolyte, μ, temperature, T, and pressure, P.

Many studies of the electrical double layer capacitance of silver in aqueous solutions have been carried out. The agreement among the values of the capacitance observed in these studies is very poor. This is partly because of the use of different electrolytes over different concentration ranges. Differences in manner of electrode surface preparation and differing solution purities have probably been the major causes for the disagreements. Often, the surfaces have been mechanically polished or subjected to long and complicated chemical cleaning. The surface state was generally unknown and varied from worker to worker.

Electrochemical methods have shown the existence of adsorption of hydrogen at silver in aqueous solutions. A study of the behaviour of a silver electrode in alkaline solutions is complicated by the discharge of alkali metal cations, which occurs within a certain range of cathodic potentials and the simultaneous reduction of water molecules and formation of adsorbed hydrogen atoms. Measurements of the degree of coverage, θ_H, of a cathode with

adsorbed atomic hydrogen is a factor which is of fundamental importance from the electrochemical and metallurgical points of view. The diffusion of hydrogen atoms from the surface of a metal into its interior might be dependent on Θ_H. A knowledge of Θ_H might allow distinction to be made between various possible mechanisms of the hydrogen evolution reaction under the conditions concerned. There is no indication in the literature of previous measurements of Θ_H at silver cathodes in acid solutions, although the capacitance of silver electrodes in acid solutions has been reported.

In 1963, Rüetschi (130) using a pulse technique and in 1973, Gagnon (131) by the method of triangular voltage sweep, measured the double layer capacitance of silver electrodes in potassium hydroxide solutions. Rüetschi obtained a value of $C_{d.l.} = 70\ \mu F\ cm^{-2}$ for the region where the Tafel plot was linear, i.e. over the potential range -100 to -300 mV while Gagnon found a value of $C_{d.l.} \doteq 32 \pm 2\ \mu F\ cm^{-2}$ at a sweep rate of 56.6 mV sec^{-1}. Higher sweep rates in Gagnon's work gave spurious results. Gagnon also found that the capacitance of silver decreased with temperature.

In 1965, Ramaley and Enke (132) studied the electrical double layer capacitance of silver wires (electropolished in 60% $HClO_4$ for several minutes) in pre-electrolysed charcoal-cleaned 1 mol ℓ^{-1} $NaClO_4$ plus $HClO_4$ (to adjust the pH over a wide range) using a small amplitude sinusoidal potential superimposed on a fast linear potential sweep. They found a value of $C_{d.l.} = 50$ to $65\ \mu F\ cm^{-2}$ in the potential range 0 to -200 mV in 1 mol ℓ^{-1} $NaClO_4 + HClO_4$ at pH = 4. Their

results and later those of Dagaeva, Leikis and Sevast'yanov (133) suggested that the double layer structure on silver and mercury may be very similar.

In 1928, Bowden and Rideal (40), using a galvanometer, found a value of $C_{d.l.}$ = 100 to 310 μF cm^{-2} for silver in 0.05 mol ℓ^{-1} H_2SO_4, freed from Ag^+ ions and O_2, the exact value depending on the previous treatment of the silver electrode. Impedance measurements were made by Leikis and Aleksandrova (134), in 1967, to determine the adsorption pseudocapacitance and double layer capacitance of the silver electrode in the same acid solution as used by Bowden and Rideal. Measurements of impedance were conducted over the hydrogen overvoltage range, $-\eta$ = 180 to 250 mV where the Tafel plot was linear. They found a frequency dependent $C_{d.l.}$ = 36.6 μF cm^{-2} at 100 kHz at η = -250 mV The adsorption pseudocapacitance, C_{ps}, on silver varied, in different experiments, from 20 to 30 μF cm^{-2} and was attributed to the adsorption of hydrogen atoms on the silver surface. Later, Bystrov and Krishtalik (135) studied the behaviour of silver cathodes in 0.05 mol ℓ^{-1} H_2SO_4. The slopes of the overvoltage decay after the interruption of the cathodic current were used to measure the capacitances, all of which lay in the range 60 - 80 μF cm^{-2}. They considered that the electrode capacitance C_{expt} is the sum of an adsorption and a double layer capacitance, in which the low value of electrode capacitance indicates that the adsorption pseudocapacitance is extremely small, i.e. $\theta_H \ll 1$.

In alkaline solutions, other methods of studying hydrogen adsorbed on metals have been used. Because of the overlapping of the

potential corresponding to the oxidation of adsorbed hydrogen and the commencement of the next anodic process (e.g. oxide formation, oxygen evolution, dissolution of silver), the determination of the hydrogen adsorbed by silver by the galvanostatic method is rather difficult. Therefore, Devanathan, Bockris and Mehl (33), in 1959, used a method of double charging to find θ_H for silver in 0.1 mol ℓ^{-1} NaOH. The adsorbed hydrogen coverage increased with increasing cathodic hydrogen overvoltage, but even at high overvoltages (-η) of about 400 mV at a relatively small fraction of the total electrode surface, only 10%, was covered with atomic hydrogen. In 1966, using the potentiostatic method of triangular voltage pulses, Loodmaa, Past and Khaga (136) obtained a value of 25% of a monolayer at cathodic potentials of -200 to -300 mV in 0.5 mol ℓ^{-1} KOH, while Past, Tamm and Takhver (137) used the current interruption method and found an average θ_H of 0.27 ± 0.03 in the region of cathodic potentials of -200 to -500 mV in 0.3 to 0.5 mol ℓ^{-1} NaOH and KOH. Past et al found that θ_H is independent of the composition of solutions of alkali metal hydroxides.

In 1969, Bockris, Argade and Gileadi (138) and in 1973, Devanathan and Ramakrishnaiah (139) and more recently Vitanov et al (140,141) studied the structure of the electrical double layer on a silver electrode in very dilute, 10^{-3} mol ℓ^{-1}, $HClO_4$ (138), in charcoal-cleaned KNO_3, Na_2SO_4 (139) and in KF, KCl, KBr, ~~KI and $MgNO_3$~~ (140,141) by the a.c. method. Bockris et al found $C_{d.l.}$ = 20 - 21 μF cm^{-2}, deduced from the capacitance-potential curve, for an activated silver electrode, i.e. anodically and cathodically pulsed, in 0.001 mol ℓ^{-1}

$HClO_4$ in the cathodic potential range -100 to -150 mV. Devanathan et al obtained a value of $C_{d.l.}$ = 30 - 40 μF cm^{-2} (deduced from the capacitance-potential curve) in 1 mol ℓ^{-1} KNO_3 and 1 mol ℓ^{-1} Na_2SO_4 solutions. Using (100) and (111) faces of silver single crystals, Vitanov et al found a value of $C_{d.l.}^{(100)}$ = 30 ± 1 μF cm^{-2} and $C_{d.l.}^{(111)}$ = 20 ± 1 μF cm^{-2} in 6 mol ℓ^{-1} $AgNO_3$ at 318 K. In KF solutions, the point of zero charge on the capacitance-potential curve was independent of the concentration. This confirmed the conclusion drawn earlier (142) that there is no specific adsorption of the fluoride ions on single crystals of silver. In experiments with KCl, KBr and KI solution, Vitanov et al found that adsorption of Cl^-, Br^- and I^- on the (100) face of silver is markedly stronger than by coulombic forces alone. The earlier finding (143) of the specific adsorption of anions on silver i.e. in decreasing order $I^- > Br^- > Cl^- > SO_4^{2-} > OH^- > ClO_4^-$, was confirmed by Vitanov et al for halide ions. The strong adsorption of halide ions on silver caused the electrode not to respond to the a.c. fluctuations during the differential capacitance determination.

Chapter 2

EXPERIMENTAL METHODS AND PROCEDURE

In this chapter, the experimental techniques and procedure used for the study of the cathodic behaviour of silver and hydrogen adsorption and absorption by silver are described in two different sections (A and B).

A Experimental Methods and Procedure for Electrolytic Hydrogen Diffusion Through Silver and Hydrogen Overvoltage Measurements on Silver

I. Materials

Only materials which are not mentioned in Part 1 will be listed below.

Silver: Foils supplied by Goodfellow Metals (Ag 99.99+% pure; impurities: Au, 10 ppm; Fe, 8 ppm; Pd, 3 ppm) of thickness 0.125 mm and (Ag 99.97% pure; impurities: Fe, 60 ppm; Pb, 40 ppm; Ca, 40 ppm; Cr, Cu and Si, 20 ppm each; Au, 8 ppm) of thickness 0.10 mm were used.

Potassium hydroxide: BDH reagent grade (maximum impurities PO_4^{3-}, 0.0005%; SiO_2, 0.005%; SO_4^{2-}, 0.003%; Al, 0.002%; Ca, 0.0025%; Fe, 0.005%; Ni, 0.001%; Zn 0.0015%) was used without purification.

Sodium perchlorate: BDH reagent grade ($NaClO_4 \cdot H_2O$, 99.0%; $HClO_4$, 0.005%; Cl^-, 0.002%; SiO_2, 0.001%; SO_4^{2-}, 0.002%; heavy metals e.g. Pb, 0.0005%; K, 0.005%) was used without purification.

Charcoal: Charcoal was prepared from sugar (Fisher Scientific Co.) and concentrated sulphuric acid. After washing with distilled water and filtration, the charcoal was dried in an oven at 333 - 343 K for several hours. Then the charcoal was oxidised by electrically heating it to a dull redness in air in a silica test tube. Charcoal oxidised

in this manner was purified by repeated washing with refluxing ethanol in an all-glass Soxhlet extractor for two days followed by repeated washing with boiling triple distilled water in a Soxhlet extractor for at least six weeks (the water being changed each week). Before use, the charcoal was reactivated by electrically heating it to dull redness in a silica test tube with nitrogen streaming over its surface.

Platinum: Platinum foils and gauze were used for reference and counter electrodes, respectively. All platinum parts were cleaned with boiling HNO_3, washed with triple distilled water and steamed with steam from triple distilled water. For use as reference hydrogen electrodes, they were platinized (82) in 2% chloroplatinic acid solution at 100-200 mA cm^{-2} for 2-3 minutes. Reference electrodes were washed with distilled water, steamed with steam from triple distilled water and stored in triple distilled water before use. Reference electrodes were freshly prepared for each experiment.

Glassware: Pyrex was used throughout. All glassware was cleaned first with sodium hydroxide, washed with distilled water, then cleaned with hot nitric acid, washed with distilled water and finally with triple distilled water. After a final cleaning with steam from triple distilled water, most of the apparatus was dried in a stainless steel oven reserved for clean glassware and then assembled by glass working.

Wash-bottle: A Pyrex wash-bottle was used to contain triple distilled water.

Gases: Hydrogen from two sources were used. Elhygen ultra-pure H_2 (< 10 ppb impurity), electrolytically generated and diffused through a Pd-Ag alloy cathode, was passed through copper and Pyrex

tubing, a liquid N_2-cooled trap and a triple distilled water-filled presaturator to the counter electrode on the cathodic side of the cell. Identical ultra-pure H_2 was supplied to a gas lift pump on the diffusion side of the cell. Swagelok connectors were used to join copper pipes together while stainless steel bellows with a Kovar insert joined copper to Pyrex. The pre-electrolysis cell (see Section II of this Chapter) was similarly supplied from a third Elhygen generator.

Reference electrodes were supplied with Matheson ultra-high purity hydrogen (H_2 99.999%; O_2 < 2 ppm; N_2 < 2 ppm), deoxygenated further as described in Chapter 2 of Part 1, divided into separate streams by greased (Dow Corning silicone high vacuum grease) taps in experiments A1 to A7 and later by grease-free Teflon and Pyrex high vacuum stopcocks followed in all cases by a liquid nitrogen-cooled trap and a presaturator, as described in Chapter 2 of Part 1.

Matheson ultra-high purity nitrogen (N_2 99.999%; O_2 < 2 ppm; H_2 < 2 ppm) was used to supply the counter electrode on the diffusion side of the cell. The nitrogen was further purified by the same purification train as for ultra-high purity hydrogen except that the liquid nitrogen-cooled trap was replaced by a solid carbon dioxide-ethanol-cooled trap.

II. Purification of Solutions

(a) Pre-electrolytic Purification

Pre-electrolytic purification was used to deposit impurities on the cathode under a hydrogen atmosphere for a sufficiently long time that impurities were essentially eliminated.

Pre-electrolysis of $HClO_4$ was not carried out in the first three experiments (A1 to A3) but was carried out in all later experiments. Pre-electrolysis in pure hydrogen-saturated solutions was conducted in a 2 litre reservior cell, shown in diagrammatic form in Figure 33. The anode and cathode were both attached to glass plungers moving in ground-glass sleeves so that one or both could be removed from the solution. A rectangular silver foil cathode (total area $\simeq 1.2\ cm^2$, exposed area $\simeq 0.8\ cm^2$), shown in Figure 33, was contacted with a fine Pt wire, protected from the solution by heat-shrinkable Teflon tubing, fitting tightly over the silver and the Pyrex tubing enclosing the wire. A large Pt gauze anode (total area $\simeq 50\ cm^2$, exposed area $\simeq 35\ cm^2$), shown in Figure 33, made contact with a fine Pt wire and was supported by glass hooks and by the glass tubing enclosing the wire. It was supplied with ultra-pure hydrogen, the reactions being presumed to be molecular hydrogen ionisation at the platinum anode and hydrogen ion discharge on the silver cathode.. All cup-cones, sockets and gas taps were water sealed. The perchloric acid was deaerated by bubbling hydrogen gas for about 20 hours, pre-electrolysis being carried out at $i = -10$ to $-30\ mA\ cm^{-2}$ (area $\simeq 0.8\ cm^2$) for 3 to 4 days. This current was supplied by a custom-built galvanostat. The

Fig. 33.
PRE- ELECTROLYSIS CELL

1. Reservoir Cell (2 Litres)
2. Plungers
3. Silver Cathode
4. Platinum Anode
5. Gas-Solution Control Taps; Water Sealed
6. Heat Shrinkable Teflon

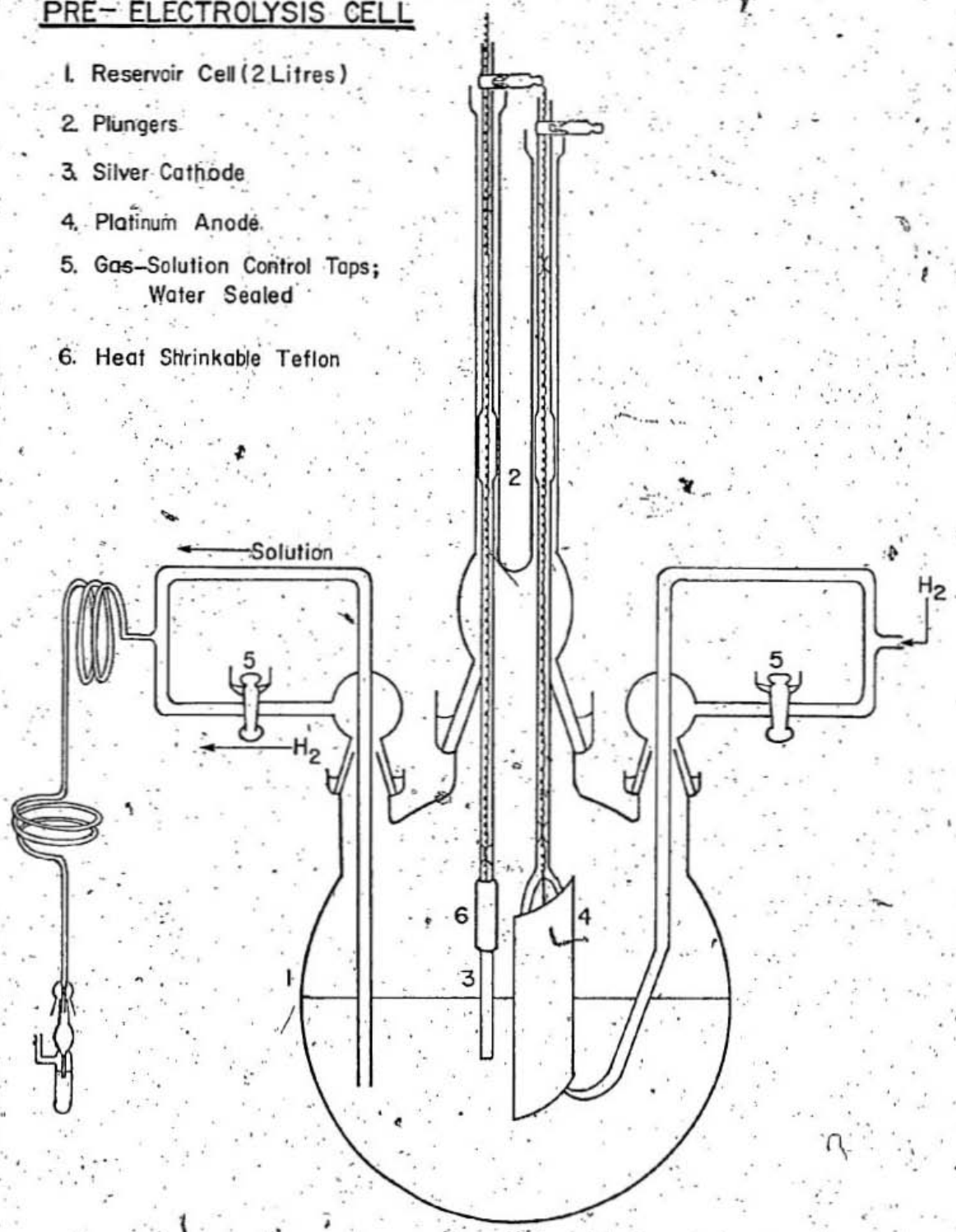

pre-electrolysis cell was temporarily attached to the main cell (see Fig. 34) by means of a flexible glass spiral and Quickfit B7 joint (cup-cone and socket), when it was desired to pass solution from the reservoir into the cell. The first portion of the solution, used for washing out the tubing between the pre-electrolysis cell and the main cell of Figure 34, was discarded. The pre-electrolysis current was not interrupted during transfer of pre-electrolysed solution to the main cell.

(b) Adsorptive Purification

Cathodic polarisation is ineffective in removing surface-active non-electrolytes, because such substances are unlikely to be adsorbed at a strongly polarised electrode, as normally used in pre-electrolysis. It is, therefore, useful to supplement pre-electrolysis by use of some unpolarised adsorbing medium. This can be achieved by means of adsorptive cleaning of the cell solution with activated charcoal (144,145) as was done by Ives and Smith (9,107) and by Rao (61) in their experiments. Whereas the adsorption of uncharged molecules occurs on all charcoals, the adsorption of electrolytes depends on the charcoal composition and its pre-treatment. Thus, according to Bikerman (146), charcoal, after heating in air, carries a negative surface charge in water, whereas heating of charcoal in the absence of air at 1173 - 1273 K causes the surface to be positively charged on subsequent immersion. The latter type of charcoal was used in this work.

III. Apparatus

The Pyrex apparatus used in this work is shown diagrammatically in Figure 34. It consisted of two cells terminating in flat flanges. Each flange carried a Parafilm gasket on the side facing the silver foil. With aluminum clamps secured, Parafilm gaskets can produce seals which will hold 10^{-5} torr after heating with hot air (147). The cell above the silver foil (cathodic side) consisted of two compartments (counter-electrode and reference) each fitted with presaturators and copper and glass gas-supply lines as described in Section I of this Chapter. A large platinum gauze (area ~ 100 cm^2) counter electrode was supplied with H_2 from an Elhygen generator via the purification train (see Section I of this Chapter). The reference electrode compartment contained two platinized Pt hydrogen electrodes (82), each having an area of ca. 8 cm^2. The tip of the Luggin capillary from the reference electrode compartment was situated very close to the silver cathode surface. The reference electrode was supplied with Matheson ultra-high purity cylinder hydrogen with purification as mentioned in Section I of this Chapter. High vacuum outflow stopcocks were used to facilitate the removal of electropolishing and washing solutions.

The cell below the silver foil (diffusion side) consisted of the main compartment, a counter-electrode compartment and a reference electrode compartment connected, respectively, to the main compartment by a gas-lift pump and by a Luggin capillary, as Figure 34 indicates. The tips of the gas-lift pump and the Luggin capillary were situated

Fig. 34. Main Cell
1. Cathodic Side
2. Diffusion Side
3. Counter-Electrode Compartments.
4. Reference Electrode Compartments.
5. Luggin Capillaries
6. Gas Lift Pump
7. High Vacuum Outflow Stopcocks.
8. Solution Delivery Tubes.
9. Parafilms.

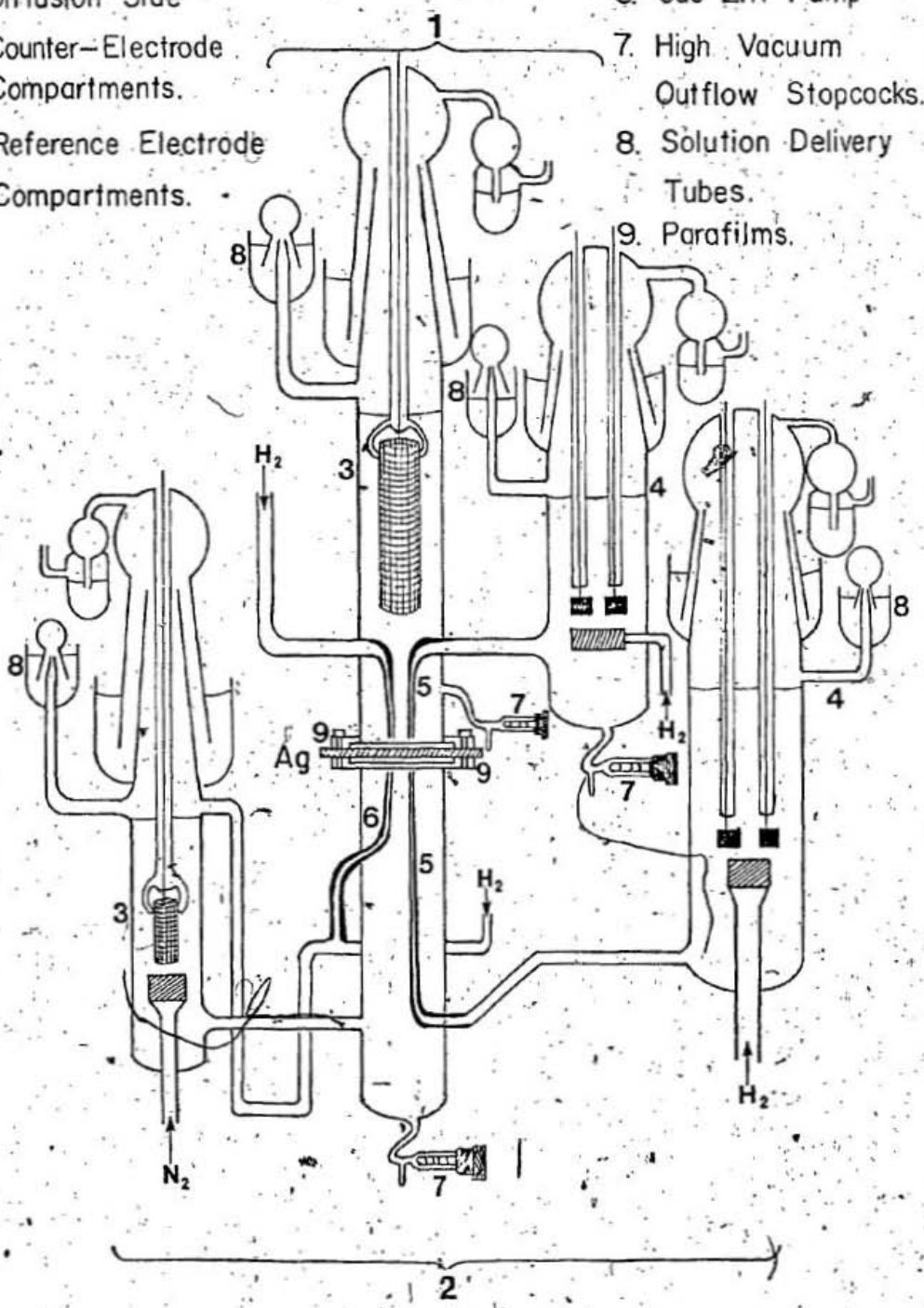

very close to the silver anode surface. The platinum counter electrode of 30 cm^2 area was supplied with purified N_2 via the purification train as described in Section I of this Chapter. The reference electrode for this cell was similar to that for the upper cell. The gas-lift pump capillary was supplied with hydrogen from an Elhygen generator and was used to facilitate removal of air or hydrogen bubbles below the silver foil.

Leakage of air through the taps was retarded by maintaining a positive pressure of hydrogen and/or nitrogen in the cell. All cup-cones and sockets were water sealed.

IV. Procedure and Instrumentation

Silver foils were initially degreased in refluxing xylene for 8-12 hours. They were then washed with ethanol, triple distilled water and then subjected to chemical polishing and electropolishing. After initial cleaning but before electropolishing, electrodes were chemically polished for 3 minutes in 60% $HClO_4$ in contact with a platinum gauze (area ca. 20 cm^2), washed with triple distilled water and then subjected to electropolishing. In experiments A2 to A4, after initial cleaning, chemical polishing and washing, the silver foils were mounted in the cell (see Fig. 34) and then electropolished in situ in unpurified 1 mol ℓ^{-1} $HClO_4$ (experiments A2 and A3) or in pre-electrolysed 1 mol ℓ^{-1} $HClO_4$ (experiment A4) at i = +500 mA cm^{-2} (area = 0.865 cm^2) for 27 ± 3 seconds with a PAR Model 371 Galvanostat-Potentiostat as a power source. In these experiments, after electropolishing the electrodes were thoroughly washed with unpurified 1 mol ℓ^{-1} $HClO_4$ (experiments A2 and A3) or with pre-electrolysed 1 mol ℓ^{-1} $HClO_4$ (experiment A4).

In later experiments, after initial cleaning and chemical polishing, the electrodes were thoroughly washed with triple distilled water and transferred to a separate cell (Fig. 35) for electropolishing. This electropolishing cell consisted of two halves terminating in flat flanges. Each flange carried a Parafilm gasket on the side facing the silver foil, the whole being sealed by screwing up aluminum clamps. A Pt counter electrode (area ~ 20 cm^2) was used in each half of the cell. Where necessary, each side of the silver foil was electro-

Fig. 35.

SECTIONAL DRAWING OF ELECTROPOLISHING CELL.

1. SILVER FOIL ANODE.
2. PLATINUM CATHODES.
3. THIN PLATINUM WIRE FOR ELECTRICAL CONTACT.

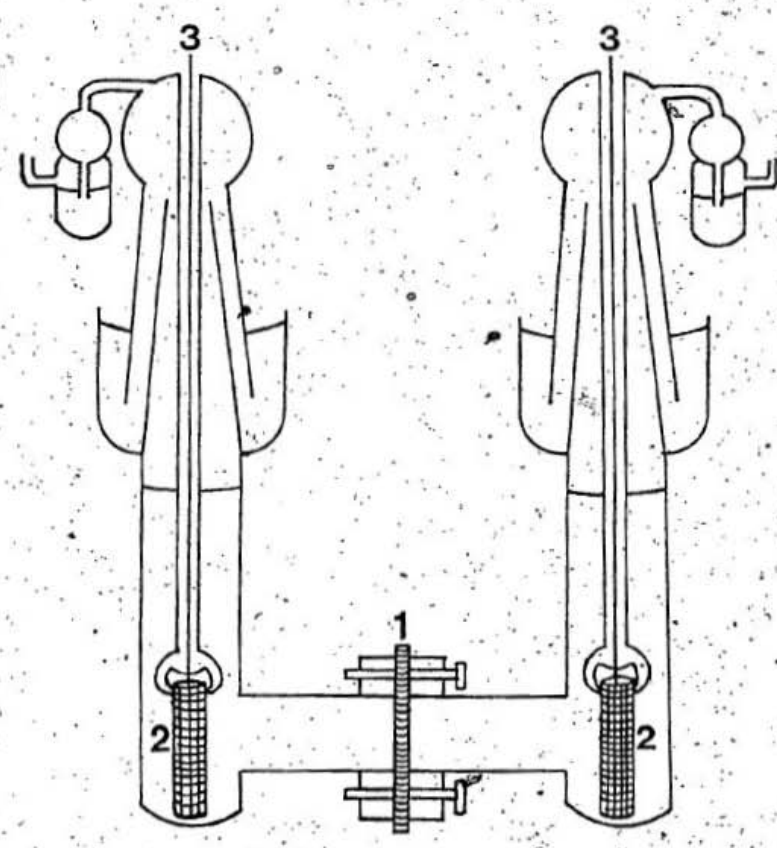

polished in unpurified 1 mol ℓ^{-1} $HClO_4$ at i = 1A anodic (area = 0.865 cm^2) for 15 ± 3 seconds. In experiments A5 to A7 both sides, but in later experiments only one side, of the silver foil was electropolished. In electropolishing of silver for these experiments a custom glavanostat, based on a Hewlett Packard 6824A amplifier was used as the current source. After electropolishing, the mirror-bright electrode was thoroughly washed with about one litre of nitrogen-saturated triple distilled water and mounted in the cell (see Fig. 34) as quickly as possible. The foil was then kept under hydrogen atmosphere in order to wash the silver foil and upper half (cathodic side) of the apparatus with the pre-electrolysed acid solution. Finally, upper and lower halves of the cells (Fig. 34) were filled with hydrogen saturated pre-electrolysed acid solution (the way for transferring pre-electrolysed solution into the cell was discussed in Section II of this Chapter) and unpurified 0.2 mol ℓ^{-1} $NaClO_4$ + $HClO_4$ to pH = 4, respectively. For experiments A8 onwards, only the cathodic side of the silver foil was polarised in acid solution, the diffusion side of the cell remaining empty.

In experiment A10, activated charcoal was used for further cleaning of the pre-electrolysed solution during its delivery to the cell. A charcoal container with a volume of ca. 30 ml (not shown in Fig. 34) was attached to the solution delivery tube for the upper half of the cell (cathodic side of Fig. 34) and to the flexible glass spiral delivery tube from the pre-electrolysis cell (Fig. 33) by means of a Quickfit cup-cone and socket joint. The activated charcoal was supported by a fine sintered filter disc (145-175 µm porosity).

Silver electrodes were cathodised galvanostatically on the cathodic side using a Keithley 225 current source and the overvoltage variation with time was observed using, for experiments A1 to A9, a Keithley 662 Differential Voltmeter (±0.01% limit of error) and for the remaining experiments a Fairchild Digital Multimeter Model 7050 (0.1% accuracy). Currents were measured with a Keithley 160 Digital Multimeter.

The diffusion side of the silver foil was potentiostated at a positive potential versus a hydrogen reference electrode. Measurements of current flow between the silver electrode and the counter electrode on the diffusion side were made with a Keithley 150B Microvolt Ammeter (accuracy ±3% of the full scale on all ranges), the output of this instrument being fed into a Keithley 370 recorder (accuracy ±1% of full scale). A block diagram of the experimental set-up using the cell of Figure 34 is shown in Figure 36.

All experiments were carried out at room temperature within an earthed copper cage to diminish the effects of a.c. pick up.

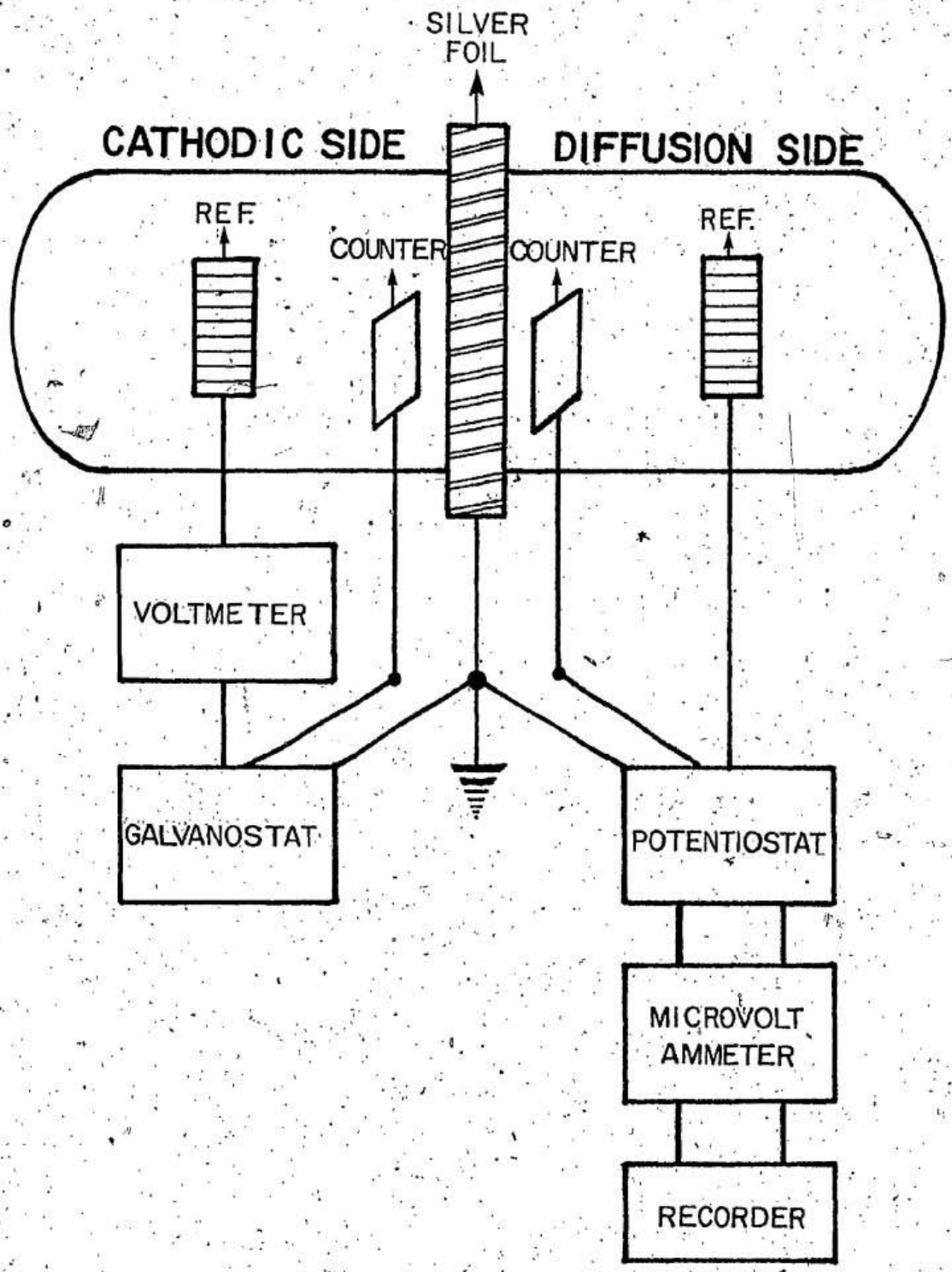

FIG. 36. THE ELECTRICAL CIRCUIT

B Experimental Methods and Procedure for Capacitance Measurements

Cell, materials, gas purification, methods of preparation of solutions and of electrodes and other experimental conditions, unless stated otherwise, were similar to those described in previous sections.

Capacitance measurements were made by observing the rapid open-circuit decay on an oscilloscope, a standard technique (38), which has been improved (148). The method used was similar to that used by Rao (61) in capacitance measurements on lead cathodes in acid solutions. The voltage decay and its derivative were measured with a microswitch (Fig. 37) in combination with a differentiating circuit (Fig. 38).

The microswitch used was similar to that of Hammerli, Mislan and Olmstead (149). It operates in a current range up to 800 mA and voltage range up to 60 V and is switched by a single pulse. The theoretical frequency response of the switch is 250 MHz, which corresponds to a break of 4 nanoseconds. The practical response was about 200 nanoseconds. Operation of the circuit depends on the fact that one state of the bistable or flip-flop circuit, consisting of the two 220 pF capacitors, the diodes D_9, D_{10} and micrologic element B_1 (type MC 914G), turns on the transistors, Q_1 and Q_2 (type 2N2219) and the other state of the bistable circuit turns them off. When the transistors are conducting, the current source is short-circuited to ground, but diodes D_1-D_8, since they will then be back-biased, prevent the cell from also being short-circuited. When the transistors are not conducting, current readily flows through the cell because diodes D_1-D_8 are then